High Energy Radiation Effects in Optical Elements.

A Thesis Submitted for the Degree

of

Master of Philosophy of the University of London

by

Sean Christian Giddens Dodd

Department of Physics and Astronomy

University College London

University of London

2003

ProQuest LLC
789 East Eisenhower Parkway
P.O. Box 1346
Ann Arbor, MI 48106-1346

Abstract

The detrimental effect of radiation has been a noted problem since its discovery by Becquerel. This thesis has studied the effect of radiation on components used in optical systems that have, or may be used, in instrumentation lofted on satellite platforms. Particular emphasis has been placed on the effects of radiation observed in materials associated with vacuum ultraviolet observations. The main parameter studied is transmission, though reference is made to methods of studying changes in dispersion.

The results have been analysed and show that a number of factors can affect the influence of ionising radiation on a chosen medium. These results are used to see if these effects can be approximated by simple mathematical functions.

Acknowledgements

First and foremost, I would like to thank my supervisor John Fordham for his input and help. In particular, thank you for your patience over the years and for getting the extension.

To Keith, Bob and Trevor in the MAPS workshop and drawing office: For the amount of work that went into building the sample holders for the Harwell work, and the (many) 11^{th} hour alterations that were needed. Thank you.

This project was the result of support from the Engineering & Physical Sciences Research Council, and the Department of Trade and Industry as part of the Postgraduate Training Partnership.

Finally, thank you to my wife Jo, and daughter Imogen, for their patience with me while I completed this work.

I look to the hills, for I know where my strength comes from.

Contents

List Of Tables

List Of Figures

1 Introduction

The development of radiation damage as a field of study was brought about by the technological revolution that occurred during the Second World War. [1] The scientific projects initiated during this time have touched virtually every area of science and engineering, extending our knowledge in many areas and highlighting areas where we knew very little at the fundamental level.

Solid-state physics was hardly considered a separate field before 1945, but the development of modern technology has changed this outlook. In particular the increased demand on our knowledge of matter and our ability to be able to manipulate matter has stimulated a great deal of research into the subject area.

As research developed in this new area of physics, materials were required that combined more and more unusual and unlikely combinations of physical properties. Nuclear technology, for example, required low neutron capture cross-sections with great tensile strength for structural components. This and other such demands led to a complete re-examination of materials and their associated properties. As more research in materials science looked at radiation and radioactivity, the field of *Radiation Damage Research* came into being.

1.1 Historical Background

As early as 1815, Wollaston and Berzelius observed that the dark mineral gadolinite behaved unusually when heated to incandescence. This curiosity was engaged further with the concurrent discoveries of x-rays and natural radioactivity by Roentgen and Becquerel in 1895. What followed was groundbreaking work by physicists, including the classic experiments of Rutherford, Mosely, Bragg, Debye and Von Laue. All this laid the groundwork for modern studies into atomic and nuclear physics, and crystal lattice theory.

However, this work was limited in that only natural sources were available. All this changed with the development of the first nuclear pile in 1943. Overnight, the focus of research changed from an interest in the effects of these interactions on the actual radiation to the actual media undergoing irradiation.

Prior to 1943, interest lay in phenomena such as scattering and diffraction and how the observed interactions could be used to infer information on the structure of both atoms and crystals, which was the focus of much attention at this time. After 1943, research into the more permanent effects of radiation on matter came to the fore.

This focus changed again in October 1957 when the launch of Sputnik heralded the dawn of satellites and ultimately space exploration. At first it was only simple satellites that were lofted into orbit. Rapidly, the pressure was on to launch more and more complex equipment and finally animals and humans into orbit.

However, space is filled with many natural phenomena of radioactivity. These include both high energy photons such as gamma and x-rays, and particles such as solar protons or cosmic rays. With every project that put equipment into orbit, or in the case of Voyager launched into deep space, new materials were used, and in turn they had to be assessed to understand what the effect of this natural radiation would be, and indeed to see if they were even suitable.

In turn, the project related to this thesis was driven by the need to quantify the radiation damage to a number of selected optical materials to help facilitate choice of components for a specific space-based project, the XMM-Newton Observatory.

1.2 XMM-Newton

In the early-1990s saw development of a new space-based astronomical observatory called X-Ray Multi-Mirror Mission, or XMM, as part of the ESA Horizon 2000 Science Program. This was later renamed XMM-Newton. Its design includes both x-ray and optical telescopes. The intended lifetime of the Observatory is 10 years. The details in the following sections are taken from Much, *et al* [2] unless otherwise stated.

1.2.1 The X-ray Telescope

This telescope contains three independent mirror modules, each 70 cm in diameter and each comprising of nested mirror shells. The three mirror approach is to allow the mission to have a collecting area of 1475 cm^2 for 1.5 keV x-rays and 580 cm^2 for 8 keV x-rays. The x-rays are analysed by two spectroscopic cameras, EPIC (0.35 - 2.5 keV) and RGS (0.1 - 15 keV).

1.2.2 The Optical Monitor

The Optical Monitor (XMM-OM) is a stand-alone instrument that is aligned with the main x-ray telescope. The XMM-OM was incorporated to allow observations in the optical/UV region to be made simultaneously with the x-ray observations. It provides the capability of detecting sources with a sensitivity limit of magnitude 24 in its 17 arcmin field of view with a spatial resolution of 1 arcsec. The XMM-OM incorporates two cameras; the blue detector for imaging in the UV (160 nm to 550 nm and is equipped with broadband filters to allow colour discrimination [3]) and the red detector for imaging the 500 nm to 1100 nm region [4]. The input beam is imaged on to the two cameras via a dichroic beam splitter.

The red detector is a conventional CCD camera; the blue detector is a photon counting detector where the MIC photon counter was selected for incorporation. [5] This type of detector was chosen as it would provide the required UV response.

A block diagram of the MIC detector head is shown in Figure 1 (taken from [2]). The Suprasil entrance window is figured to flatten the focal plane and has a S20 photocathode deposited on its underside. Input photons are initially detected by the photocathode and the resultant photoelectrons are amplified by the three-stage microchannel plate (MCP) image intensifier operating at ≈ 8.8 kV. The photoelectrons are amplified at a photon gain of 5×10^6 by the MCPs and result in scintillations on the output phosphor. These scintillations are then imaged via a fibre optic taper on to a fast scanning CCD camera.

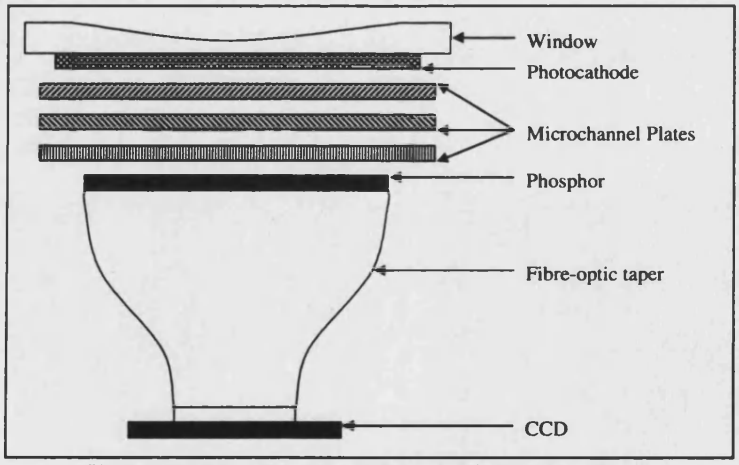

Figure 1 Block diagram of the MIC detector head.

The input window of the image intensifier has three purposes:

- The photocathode, which defines the sensitivity range of the camera, is deposited on its inner surface.
- Its perimeter provides a vacuum seal for the intensifier.
- It is figured as a field flattening lens.

The optical properties of the input window constrain the operating wavelength of the detector and the material used must allow transmission over the desired 160 to 550 nm range. My project was associated with the choice of materials for this window and was related to radiation damage to potential candidate materials.

1.2.3 The Space Radiation Environment

The space environment is both extreme and hostile. The form and level of radiation that affects a space-borne instrument is a function of both the duration and orbit of the platform. The main hazard for radiation damage comes from the charged particles trapped in the Van Allen Belts. In the main these are highly energetic electrons and protons. Additionally, cosmic rays stream throughout the space environment. Cosmic rays consist of various energetic particles differing in mass and charge. They can include alpha particles and heavy particle nuclei. In addition, SAMPEX, the *Solar Anomalous Particle Explorer*, a German-US mission launched in 1992, identified a new belt sitting between the two Van Allen belts. [6] This third belt stores energetic oxygen, nitrogen and neon ions.

Further to the particle aspect, high-energy photons such as x- and gamma rays are present. Although not as numerous as the particle radiation, they can become significant over the long durations that current missions now demand.

The Van Allen belts are split into inner and outer belts. In the inner belt, the majority of the particles are trapped protons stripped from the solar wind. This is a stream of charged particles emitted by the Sun. The majority of the outer belt is composed of trapped electrons, again stripped from the near-Earth environment. These particles are trapped by the geomagnetic field of the Earth and held in orbit. The energy and intensity of both of the belts are closely linked to solar activity. As the solar cycle follows an 11-year cycle, it is conceivable that a long-term mission will have to operate through the increased radiation of a solar maximum.

Currently, manned operations tend to operate at altitudes below 550 km where the Van Allen belts begin. In the case of the Apollo missions, it was noted that the most dangerous part of the mission was passing through the belts. However, since it would only take a short while to pass through, the exposure to the astronauts would be at a minimum. [7] Another factor would be related to high solar activity. Even so, although no one was in space at the time, NASA used particle data from the solar event of August 1972 to assess the risk to an Apollo craft should one have been in orbit at that time. They concluded that within the shielded Command Module, the astronauts would have received a dose of 3.6 Gy to their skin, and 0.35 Gy to their blood forming organs. The gray (Gy) is the SI unit of absorbed dose and is discussed later in 3.5.2. This dose would not be enough to incapacitate the members of the crew, but would place them in an area of high risk. Bailey [7] then notes that had they been caught outside of the Command Module, either during a spacewalk or in the lightly shielded Lunar Module, the consequences would have been far more serious.

The detrimental effects of exposure to the space environment can be seen in the operation of instruments used there. The main manifestations are spurious signals and, over the long term, degradation of systems in orbit. Different orbits have different hazards, and these must be carefully addressed in the early planning stages.

A low Earth orbit environment, typically 400 km or so, is significantly different to that of higher orbits. These higher orbits, in turn, are completely different to those found around other planets or associated with deep space missions. From a radiation damage viewpoint, the dominant source of the problem is duration rather the dose rate.

The original plans for the NASA Space Station Freedom would have placed the vehicle in a 350 to 440 km altitude for a thirty-year lifetime. This substantial lifetime has highlighted a number of problems. First was the lack of suitable data to calculate the effects of this length of exposure. Unlike the nuclear reactor, where the dose can be controlled and calculated, the space environment is far more unpredictable. A number of factors are responsible for this.

This unpredictable nature can also be influenced by human activity. Not all of the particles in the Van Allen belts are there from natural processes. Operation Starfish, an American high level nuclear test carried out in the 1950s introduced a belt of highly energetic particles went it detonated a 1.4 megaton device at 400 km. These particles are decaying with time. The combination of these particles and the variation in the solar wind mean that the space environment is difficult to model over a long time period. [8]

This is compounded further by the inability to be able to service instrumentation once in orbit. This leads to stringent testing and qualification making up the majority of pre-flight work for the space agencies. [9] Estimates for a 12.5-year mission based upon extensive tests have concluded that in certain orbits a total dose of 10^7 Gy is not unrealistic. [10] It will require the completion and analysis of several long-term missions before the space radiation environment is more readily estimated.

1.2.4 The XMM Radiation Environment

For XMM-Newton, the orbit was defined by the scientific demands of the project. [11] The orbit had to achieve a maximum of time in an undisturbed environment away from a near earth orbit to maximise scientific observation time. The project was to observe the soft x-ray emissions, and so would need to be located away from the near earth orbit or the Van Allen belts to enable clean signals to be analysed.

At the same time, the orbit would have to maximise ground coverage to allow real-time data acquisition. This would then minimise the requirements for on-board data storage. The orbit had to be stable for just over the 10 years specified as the ideal extended length of the mission. Finally, the solar budget had to ensure that there was enough sunlight to enable power to be maintained both via direct solar power and from batteries.

The analysis of these requirements led to the choice of a highly elliptical geosynchronous orbit. The elliptical nature of the orbit allows a maximum of time above the Van Allen belts, and takes 47.86 hours to complete. Additionally, this time is approximately a multiple of 24 hours and gives an optimal coverage for the ground stations.

Eight days after the launch in December 1999, the operational XMM-Newton orbit had the following parameters:

- Perigee altitude of 7,000 km
- Apogee altitude of 114,000 km
- Inclination of 40 deg

Over time, these parameters will evolve as the mission progresses. For example, the perigee altitude will vary between 7,000 km and 22,000 km, while the apogee altitude will vary between 115,000 km and 100,000 km. [11]

From the analysis of the XMM-Newton orbit the expected total radiation exposure of the mission as a function of aluminium was calculated. [12] Part of this is reproduced in Table 1.

In the initial technical specification the XMM-OM was budgeted with 4 mm of aluminium shielding and it was expected that the spacecraft structure would provide a further 2 mm of equivalent shielding. [4] Further, it was stipulated that the devices within the XMM-OM should have tolerance to at least 50 krad of radiation and ideally to 100 krad.

Aluminium Absorber Thickness (mm)	Total Dose (krad)	Geomagnetically Trapped Particle Dose			
		Electrons (krad)	Bremsstrahlung (krad)	Trapped Protons (krad)	Solar Protons (krad)
0.05	114,000	83,600	46	29,900	538
0.1	55,200	49,300	35	5,540	344
0.5	8,070	7,850	13	104	103
1	2,720	2,640	7	19	54
4	114	101	2	1	11
6	23	15	1.5	0.2	6.3
10	4.1	0.1	1.0	0.1	2.8
20	1.54	0.00	0.67	0.01	0.86

Table 1. Dose in krad as a function of aluminium spherical shell shielding thickness [12] showing the variation of total dose by shield thickness, and the relative composition of the finals dose from solar protons, and from geomagnetically trapped electrons, protons and bremsstrahlung.

1.3 Initial Project Outline

From the technical specifications of the XMM-OM structure and the MIC it was possible to specify an initial structure for the core of this project.

Firstly, it was necessary to identify materials capable of transmitting light over a range from 160 nm to above 550 nm as a minimum. Next it was necessary to look at the various forms of natural and man-made radioactivity and then to understand the basic processes of radiation damage. From this it was possible to draw up an experiment to analyse the effects of radiation on suitable samples, and then to analyse the results of this experiment.

2 Optical Materials

The ultraviolet or UV can be considered as the region from 10 nm to 400 nm. The shorter wavelength from 10 nm to 200 nm is sometimes called the *vacuum ultraviolet* or VUV.

Some research delimits the UV range as *extreme ultraviolet* (10 nm — 100 nm), *far ultraviolet* (100 nm — 200 nm), *middle ultraviolet* (200 nm — 300 nm) and *near ultraviolet* (300 nm — 400 nm). Other groups delimit UV as the commonly known *UVA* (400 nm — 315 nm), *UVB* (315 nm — 280 nm) and *UVC* (280 nm — 100 nm).

As can be seen, these delineations are slightly subjective and often linked to the history and interest of a particular science community. For example, material scientists looking at the behaviour of polymers in a space environment may well prefer to use the extreme or far UV divisions reflecting their area of interest. In contrasts biologists studying carcinoma may prefer to use UVA/B etc. which is more familiar to the general public.

The UV region was of little interest to science until fairly recently. Since the atmosphere absorbs the majority of the UV radiation, any work was initially limited to experiments involving discharge lamps. Any astronomical research was out of the question until balloons, high altitude aircraft and rockets were developed that allowed observations to be made. This was later supplemented by space-borne platforms.

As each of these platforms was developed, the subsequent analysis of UV radiation pushed the boundaries of our knowledge further, uncovering more questions. This in turn led to greater demand for UV research.

In particular, astronomy benefited from these new observations. For example, the Lyman alpha (Lyα) emission feature for hydrogen occurs at 121.6 nm. As hydrogen is the most abundant element, it is one of the most important emission lines in cosmological studies. Similarly, the analysis of spectra of the Lyman absorption series is of great importance for the study of neutral hydrogen in the intergalactic medium. Some satellites (such as the groundbreaking International Ultraviolet Explorer) were specifically designed to observe deep into the UV.

2.1 Material Selection

The initial choice of optical material would be limited by the wavelength range specified for the XMM-OM. The specific range from 160 nm to above 550 nm was seen as a minimum. However, a simple selection of materials capable of transmitting UV light would have produced a range of materials too numerous to cover within the limited bounds of this project. For example, Table 2 has seven crystals capable of transmission below 160 nm, and additionally there are fused silica and quartz materials that have been used in similar projects.

In the end it was decided that the project would concentrate on the more widely used materials. In particular, sapphire and magnesium fluoride had previously been suggested as possible materials for optical components in XMM-OM and so these were selected.

Material	Cut-off Wavelength (nm)	Material	Cut-off Wavelength (nm)	Material	Cut-off Wavelength (nm)
Sapphire Al_2O_3	150	Caesium Iodide CsI	250	Magnesium fluoride MgF_2	110
Barium Fluoride BaF_2	150	Potassium Bromide KBr	230	Sodium chloride NaCl	200
Calcium Fluoride CaF_2	130	Potassium Chloride KCl	210	Sodium fluoride NaF	150
Caesium Bromide CsBr	220	Lithium Fluoride LiF	120	Strontium fluoride SrF_2	150

Table 2. The cut-off wavelength for a small selection of crystals. The listed crystals are all suitable for use as optical materials though some require careful handling, and all transmit light into the UV.

In addition, and at the request of SIRA who were co-sponsoring this project, it was decided to include a number of glasses that are regularly used in optical systems. Although there are a large number available, the request was that we look at the more commonly used industrial glasses produced by the glass manufacturer, Schott.

The complete range of Schott glasses is too numerous to be included within the scope of this project. However, two particular groups of the Schott glasses are used quite extensively - the flint glass *F* range and the crown glass *BK* range. As a representation of these ranges, two particular samples were chosen, BK7 and F2.

Both of these glasses have radiation-hardened versions. This hardening is produced by the addition of cerium which increases their lower cut-off wavelength by approximately 100 nm. (See Figure 3) This effect greatly reduces their usefulness for the UV side of this project, but radiation hardened glasses are still dealt with because of their importance in optics used elsewhere in high radiation environment.

2.2 Magnesium fluoride

Magnesium fluoride (MgF_2) is frequently used in UV and VUV windows, lenses and polarisers. It is a positively birefringent crystal that can be grown in diameters of up to a hundred or so millimetres. Since it is often used in the UV great care has to be taken during its production. Generally, it has a transmission of ~40% at Lyα though this will vary from source to source due to external factors such as purity. As a material it is strong and rugged to both thermal and mechanical shock, characteristics that make it attractive to an engineer.

The natural form of magnesium fluoride is known as sellaite, with the Eastman Kodak company being the first to develop a hot pressed polycrystalline form which they named Irtran-1. The production of magnesium fluoride tends to be somewhat specialised, so cost can be a problem.

For this project, magnesium fluoride was sourced from three suppliers. The bulk of the material was Merck magnesium fluoride, but a smaller number of samples were sourced from Roynon Howes and from Carl Zeiss.

2.3 Sapphire

Sapphire is the crystallised form of aluminium oxide (Al_2O_3) and has a number of mechanical and optical properties that endear it to the engineer. [13] Its high strength, hardness and chemical stability allows it to be used in applications as diverse as high temperature and severe environment windows, through to watch glasses. Its infrared (IR) cut-off at 5.5 μm is the limit to its use as an IR optical component, though it can be used down to 150 nm, which is why it has been chosen for many UV uses. Sapphire maintains a transmission in excess of 70% to about 300 nm before the material begins to become opaque. Sapphire is also very slightly negatively birefringent. The transmission spectrum of sapphire is shown in Figure 2.

The more widespread use of sapphire has the advantage that its production is both widespread and economic, thus sapphire is a good economical choice. The majority of samples for magnesium fluoride were sourced from Merck with a smaller batch sourced from Union Carbide. In addition, high purity samples were obtained from CMS; these were the ultra-pure Hemex and high quality Hemlite.

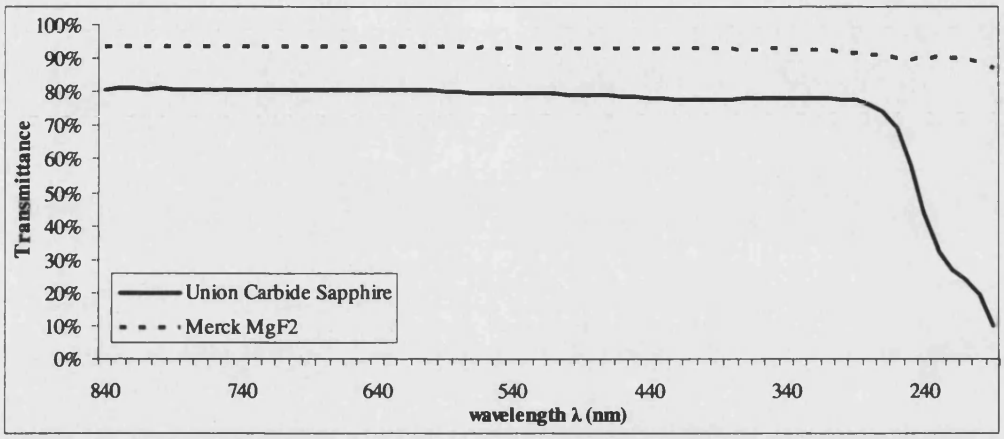

Figure 2. A comparison of the transmittance of sapphire and magnesium fluoride. The figure clearly shows the superiority of the magnesium fluoride across the 190 nm to 840 nm range of the graph. The figure also shows the cut off of the sapphire. The data is from the samples used in this project which were 10 mm thick.

2.4 Schott Glass F2-620 364

This Schott glass is a widely used industrial flint glass, so named as early glass was made with ground flint as the source of the silica. The coding after its number gives a few quick insights into its properties. There are 15 variants in the F group (F1 - F15). F2 has an internal code within this group of 620 364, this code relating to that material's optical properties.

The first part of the code is given by the refractive index (n_d), which is 1.620004, or 1.**620**.

The second part of the code is the dispersion ratio (ν_d) and is also called the Abbé factor. This is used to quantify the rate of change of the refractive index (i.e. the dispersion) of an optical material as a function of wavelength, with the smaller the value of ν_d, the greater the dispersion. This ratio is calculated by:

$$\nu_d = \frac{n_d - 1}{n_f - n_c} \approx 36.4 \qquad \text{Equation 1}$$

The difference $n_f - n_c$ is called the *principal dispersion.* In Equation 1, n_d is the index of refraction for the helium D line (587.6 nm), n_f is the index of refraction for the hydrogen F line (486.1 nm) and n_c is the index of refraction for the hydrogen C line (656.3 nm).

For F2 the value of v_d is 36.37, or **364** in its abbreviation to 3 significant figures. Both this number and the value of the dispersion are given for each particular type of glass in the Schott Optical Glass Catalogue. [14]

2.4.1 Schott Glass BK7-517 642

BK7 is a crown glass and is the last in its family of seven glasses. Crown glass is made without the addition of lead or iron. It used to be the main form of window glazing, but is now primarily used as an optical glass of low refractive index. It has a refractive index of $n_d = 1.51680$, and a dispersion ratio of $v_d = 64.17$. As a glass, the transmittance of BK7 is more useful at the blue end of the spectrum as its cut-off is at a lower wavelength. This is shown in Figure 3.

2.4.2 Schott Radiation Hardened Glass F2 G12-621 366

Before describing the characteristics of F2 G12, it is necessary to quickly introduce the rationale behind hardened glasses. Later, in Section 4.6, it will be seen that ionising radiation can liberate charge carriers in the form of electrons and holes. These can then be trapped to form defect centres. It is these defect centres that manifest themselves as "damage" to a material's optical properties. It has also been noted that doping with rare-earth elements can reduce this effect. However, as with many an advantage, there can be a price to be paid, and this is the case when using cerium.

The doping with cerium oxide affects the transmittance of the material in the blue region of the spectrum. Figure 3 shows this effect. Even before the glass is exposed to any radiation, the transmittance of the doped glass is less than that of the pure sample. To the eye, the material displays a characteristic yellow tint that is the most obvious external result of the doping.

Even though doping the glass reduces the range of transmission, it does improve the resilience of the glass to radiation damage. Although these hardened glasses would have limited use in UV work, we included them in this project with the rational that the glasses are widely used and it would be useful to compare these radiation resistant glasses against their unhardened counterparts. Exposing all of the glasses at a range of doses, the disadvantage of the distinctive yellow tint combined with the higher cost of the hardened glasses can be compared with the cheaper, but more susceptible standard glass samples. This would then allow a comparison on the trade-off between the harder, but less transparent glasses against their more economic, but susceptible, counterparts to see in any cost saving would actually be a false economy. Conversely it may also show that for certain projects, using hardened glasses may be an over-engineered and expensive solution.

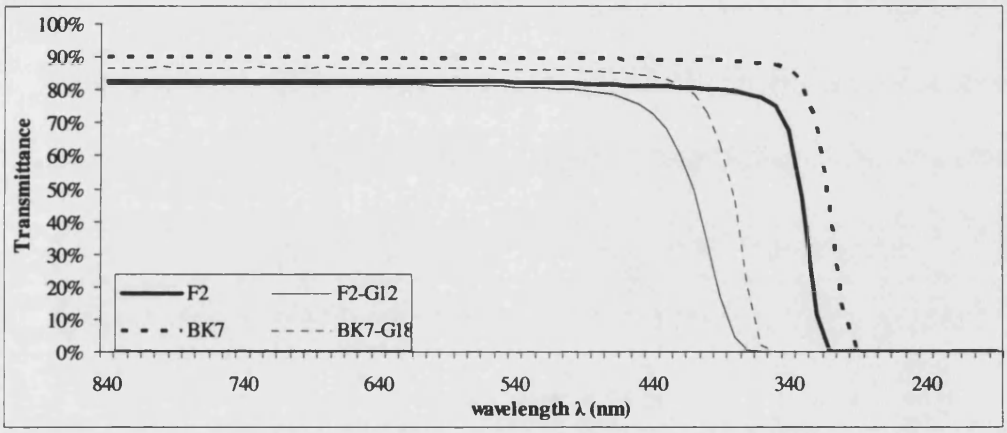

Figure 3. The transmittance of the Schott glasses. The figure shows that the addition of cerium oxide to the base glasses (F2 & BK7) increases the cut-off wavelength of the glass. The doped glasses are shown by the G12 and G18 suffix. The data is from the samples used in this project which were 10 mm thick.

Returning to F2 G12, with a refractive index of $n_d = 1.62072$ and a dispersion ratio of $\nu_d = 36.56$, the addition of 1.2% (**G12**) of cerium oxide seems to have a limited effect on the optical properties of the original F2 ($n_d = 1.620004$ and $\nu_d = 36.37$).

The effect of the addition of cerium oxide on the cut-off wavelength could mean that F2 G12 would be ruled out of some experiments or projects where F2 would be considered suitable.

2.4.3 Schott Radiation Hardened Glass BK7 G18-520 637

As with the F2 glass above, this glass has also been doped with cerium oxide, but this time to a level of 1.8%. Again, neither the refractive index or dispersion ratio are severely affected with values of $n_d = 1.51975$ and $\nu_d = 63.66$ (c.f. $n_d = 1.51680$ and $\nu_d = 64.17$).

Again the addition of cerium affects the transmittance before irradiation in comparison with its undoped counterpart.

3 Radioactivity

As early as 400 BC, the ancient Greeks were already discussing the possible existence of sub-atomic matter. In particular, the Greek philosopher Democritus developed an atomic theory of the universe – though it would be fanciful in the extreme to imagine him reaching a similar view to what we hold as our view of the sub-atomic world. (Similarly, it would be impossible for us to imagine what will be the standard view of the sub-atomic world in hundred years from now.)

Born in Abdera, Thrace, Democritus wrote extensively, but only fragments of his works remain. Fortunately, one of these works was his exposition of the atomic theory of matter. In this he stated a belief that every object was composed of minute, invisible, indestructible particles of pure matter. The word he chose for these particles was *atoma*, which meant "indivisibles".

These atoma were in a perpetual state of motion moving through infinite empty space (kenon, or "void"). Furthermore, these atoma were all made of the same material, differing only in shape, size, weight, and position. It was these slight differences that led us to observe different forms of matter on the macroscopic scale. It is this concept that could be held as the first example of atomic theory.

In the early 19^{th} century, John Dalton, a British chemist and physicist, developed his own atomic theory. Dalton advanced his theory in 1803, and it can be viewed as the cornerstone of all the modern physical sciences around us. As such, though Dalton wrote a number of works, it was his theory of matter that is generally held as his most important contribution to science.

In his theory, he proposed that matter is composed of atoms of differing weights and that these atoms combine in simple ratios of weight. In 1808, Dalton published "A New System of Chemical Philosophy." In this work, he listed the atomic weights of a number of known elements - an element is a compound made up of only one type of atom. For these elements, he gave their weight as relative to the hydrogen atom.

The basic premise of the atom is that it is the smallest amount of an element that can exist and still keep the same chemical characteristics. All chemical compounds are formed of atoms, the difference between any two compounds being linked to the difference between the nature and make-up of their constituent atoms.

Although these weights were of varying accuracy, this laid the foundation for the later work of Dmitri Mendeleyev. In 1869 he stated that "the properties of elements are in periodic dependence upon there atomic weight" rather than their atomic number and so the modern periodic table was formed. This is now found in all modern chemistry textbooks, and is the foundation stone of chemistry (see Appendix C for an example).

3.1 Atomic structure

Though both the Greeks and Dalton believed the atom to be the smallest particle of matter that could exist, we now know that the atom is not a fundamental particle. The atom is made up of further smaller particles, the *proton*, *neutrons* and *electrons*.

Proton (p^+): Positively charged sub-atomic particle with a mass, m_p of 1.67252×10^{-27} kg, equivalent to 938.3 MeV c^{-2}. This is slightly less than a neutron, but much greater than that of the electron. The proton has a mass of approximately one *atomic mass unit* that is 1.661×10^{-27} kg, and unit electrical charge.

Electron (e^-): The smallest of the three particles with unit electrical charge and a mass, m_e, of 9.109×10^{-31} kg, or 0.5110 MeV c^{-2}.

Neutron (n_0): A subatomic particle with neutral electrical charge believed to exist in small nuclei with an atomic number of greater than 1. Its mass, m_p, is very similar to that of the proton at 1.675×10^{-27} kg, or 939.6 MeV c^{-2}.

These values were taken from the CRC *Handbook of Chemistry and Physics.* [15]

The neutrons and protons make up the central core of the atom with the electrons surrounding it in specific orbits. These orbits are numbered with the first (n = 1) nearest the nucleus at the centre, the second is the next out (n = 2) and so on, with the electrons populating the lowest energy states first. However, not all of the electrons can occupy the lowest levels as a consequence of the Pauli Exclusion Principle ("In a multi-electron atom there can never be more than one electron in the same quantum state." [16]) In simple terms, this means that in the n^{th} orbit, only $2n^2$ electrons can exist at any one time. In the first orbit, n =1 so only two (2×1^2) electrons can exist. In the next orbit, eight (2×2^2) electrons can exist, next eighteen (2×3^2) electrons, then thirty-two (2×4^2), and so on.

As well as being numbered, the orbits are sometimes referred to as *shells*. The innermost orbit is called the *K shell*; the next is the *L shell*, with the *M* and the *N* after that. In Figure 4, the structure of zinc is illustrated. This has 30 electrons and protons. This means that the first 3 shells, K, L and M are full with 2 + 8 + 18 = 28 electrons. The two remaining electrons are in the N shell.

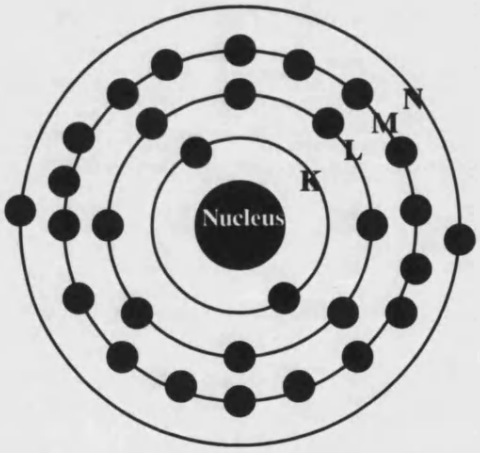

Figure 4. The atomic structure of zinc showing the electrons fully populating the K, L and M shells, with the remaining electrons in the N shell.

3.2 Mass Number, Atomic Number and Isotopes

The mass of the electron is insignificant compared to the proton and neutron. The number of protons can be added to the number of neutrons to give the *Mass Number* **A.**

For example, consider the mass number of zinc and helium shown in Table 3:

Zn	Mass		He	Mass
30 protons	30		2 protons	02
35 neutrons	35		2 neutrons	02
30 electrons	—		2 electrons	—
A =	65		A =	04

Table 3. Mass number of zinc and helium to illustrate the relation between atomic number, Z, and mass number, A.

The number of protons in an atomic nucleus gives the *Atomic Number* **Z** with zinc having Z = 30 and helium having Z = 2. This number determines which element the atom belongs to, so all atoms with an atomic number 30 are zinc, etc.

For an element X, the atomic and mass number Z and A can be shown in shorthand form ${}^{A}_{Z}X$. Thus helium can be written as ${}^{4}_{2}He$.

The heaviest naturally occurring element, uranium, has an atomic number of 92. Other elements can be produced with atomic numbers higher than this (e.g. Lawrencium with Z = 103) but these tend to be unstable and relatively short lived (see Section 3.3.3).

Although the atomic number defines which element an atom belongs to, an element can often be found to have a differing number of neutrons. For example consider phosphorus, P, with Z = 15. It can have a varying number of neutrons:

${}^{28}_{15}P$ 15 protons 13 neutrons

${}^{31}_{15}P$ 15 protons 16 neutrons

${}^{34}_{15}P$ 15 protons 19 neutrons

These variants are all chemically identical to one another and are known as *isotopes*. The different mass number is often used to label an individual variant, called a *nuclide*. For example, the nuclide ${}^{31}_{15}P$ is often called simply "phosphorus–31".

A final point to note is that apart from a handful of the light elements, all of the elements have more neutrons than protons, with this difference becoming greater with the heavier particles. For example, consider helium, phosphorus, zinc and uranium:

${}^{4}_{2}He$ 2 protons 2 neutrons

${}^{31}_{15}P$ 15 protons 16 neutrons

${}^{65}_{30}Zn$ 30 protons 35 neutrons

${}^{238}_{92}U$ 92 protons 146 neutrons

3.3 Natural and Induced Radioactivity

There are a number of texts that cover radioactivity. Two texts in particular, *An Introduction to Radiation Protection* [17] and *Radiation Protection* [18] were consulted during this project.

Shapiro [18] considered ionising radiation as being directly *ionising, indirectly ionising particles or a mixture of both.* Directly ionising radiation included electrically charged particles having sufficient kinetic energy to produce ionisation by collision. This included protons, electrons, alpha and beta particles, etc. In contrast, indirectly ionising radiation were the uncharged particles capable of either liberating directly ionising particles or able to initiate a nuclear transformation by creating instability. Thus it included neutrons, gamma rays, neutral mesons, etc.

Under certain circumstances, atomic nuclei can become unstable. This leads to the production of radioactivity as the nucleus attempts to stabilise itself by emitting radiation. It is this instability that explains the lack of naturally occurring elements with atomic numbers higher than uranium. Although produced by natural processes, over a geological or astronomical timescale, the vast majority of elements heavier than uranium have decayed to other more stable elements and now only remain in trace amounts.

3.3.1 Alpha, Beta and Gamma Radiation and Neutrons

As the nucleus attempts to stabilise, radioactive decay occurs as the nucleus breaks down and emits radiation in one of three varieties; *alpha, beta* and *gamma.* The other general form of radiation is the neutron.

- **Alpha radiation** is a particle consisting of two protons and two neutrons bound together. This binding is so strong that when emitted the particle behaves as one particle, not four. As such, it has the same nuclear arrangement as a naturally occurring helium nucleus. When moving, the alpha particle strongly ionises the medium it is traversing. However, being a strong ionisation source as well as a large particle, it will only traverse a few centimetres of air before being stopped.

The reason it ionises so powerfully is due to the massive size and weight of the particle. As it traverses any media, alpha particles can either collide with, or interact electronically with, any matter that they impinge on. In every collision or interaction, the particle will release its energy readily. This means that despite being a strong ionisation source, a sheet of paper will adequately shield an alpha source. The only time an alpha particle becomes a problem is if a source is ingested. In this case the body's tissues are extremely close to a strong ionising source. In this situation, the short-range powerful ionisation can be lethal. (See Section 3.5.2.)

- **Beta radiation** is a particle emitted from the nucleus that weighs 1/1837 the mass of a proton. The negatively charged beta particle, β^-, is identical to the electron. Similarly, the positively charged beta particle, β^+, is identical to the positron (e^+), the electron anti-particle. The emission of a β^- particle carries away excess electrical charge and to remain neutral, the nucleus transforms a neutron to a proton. The opposite of this occurs in the emission of a β^+, transforming a proton to a neutron. The beta particle does not exist within the nucleus itself; moreover it is formed when the decay occurs. It is then created and expelled from the atom.

It is possible to completely shield a beta source, but it needs more material than an alpha particle. However, absorbing fast electrons in a dense medium produces secondary x-rays, which is why plastic or aluminium is preferable to lead. The secondary x-rays produced in this manner are called *bremsstrahlung*, German for "braking radiation", a topic covered later in Section 3.6.2.

- **Gamma radiation** is electromagnetic radiation emitted from the nucleus of the atom. Originally they were called "nuclear x-rays", but they differ from normal x-rays in two ways. Firstly, they are of a much higher energy, generally in excess of 1 MeV. Secondly, their formation is fundamentally different. An electron filling a vacancy in the K-shell forms x-rays. The in-falling electron falls into the vacancy and to reach a minimum energy state emits a quantum of radiation. The surplus energy is expelled as an x-ray photon. With gamma rays, it is the nucleus rather than the shell that is rearranged. Again the surplus energy is expelled as a photon, but of a higher energy and this is the gamma ray.

Another method of producing a gamma ray is when a particle collides with an anti-particle. For example, when an electron and positron collide, the subsequent annihilation produces a gamma ray. This process is called annihilation and occurs when the two particles combine and release a photon. (The e^-:e^+ event is known as inverse pair-production and creates a 1.02 MeV gamma ray.) Being electromagnetic radiation, gamma photons travel at the speed of light. They can traverse a substantial amount of shielding before being stopped. The key to x-ray and gamma ray energy is the frequency of the emitted photon. For a photon, the energy is proportional to its frequency. Gamma rays have a much higher frequency than x-ray photons, and so are more energetic. The extra energy makes them more damaging.

- **Neutron radiation** has only been studied since the discovery and development of the nuclear reactor. The field of neutron bombardment has been of interest to scientists, and of particular interest to structural engineers designing power stations. Since the neutron is an uncharged particle, it does not undergo the same processes or interactions as either the alpha or the beta particle. It relies on collisions with atomic particles to absorb its momentum and reduce its speed. This makes the initial energy of the neutron a major factor in the subsequent effects it can induce.

  Neutrons tend to be grouped as either *thermal, intermediate* or *fast* according to their energy. The energy is linked to the speed of the neutron. Thermal neutrons are slowest and least energetic with energy values below 1 eV. In contrast, fast neutrons are those with energy values in excess of 100 keV.

  For the slower, thermal neutrons, the collisions tend to be elastic and direct momentum transfer displaces and ionises particles. With the faster, more energetic neutrons, particles are displaced so violently that secondary x- and gamma rays are emitted. This makes energetic neutrons about 20 times as dangerous as the same dose of gamma rays.

As can be seen above, the electron-volt, eV, is commonly used as a unit of energy. If an electron is accelerated by a potential of 10,000 volts, it acquires energy of 10,000 eV, or 10 keV. This is quite a trivial equation for beta particles, but the principle can still be applied to other particles.

For a particle of mass **m** travelling at a velocity **v**, where v is much less than light ($v \ll c$) then the kinetic energy of the particle is given by:

$$E_{ke} = \tfrac{1}{2}mv^2$$

If m is in kg, and v is in ms^{-1}, then E_{ke} is in joules, where $1.602 \times 10^{-19} J \equiv keV$.

For electromagnetic radiation of frequency ν, the energy is given by:

$$E = h\nu$$

where $h = 6.626 \times 10^{-34}\ J\ s^{-1}$ is Planck's constant.

3.3.2 Radioactive decay

The root cause of radioactive decay in naturally occurring elements is instability. As the atomic numbers of the elements increase, the difference between the numbers of protons and neutrons also increases. Again consider uranium-238 with its 92 protons and 146 neutrons. For this element, one method by which it may attempt to attain stability is by emitting an alpha particle. This reduces the number of protons to 90 and the number of neutrons to 144, converting it to the nuclide thorium-234. This decay may be written as:

$$^{238}_{92}U \rightarrow ^{4}_{2}\alpha + ^{234}_{90}Th$$

or alternatively,

$$^{238}_{92}U \xrightarrow{\alpha} ^{234}_{90}Th$$

Another example is the decay of polonium-218 to lead-214 by an alpha emission:

$$^{218}_{84}Po \xrightarrow{\alpha} ^{214}_{82}Pb$$

However, although the alpha emission reduces the number of protons and neutrons by 2, it does not address the overabundance of neutrons in the initial nucleus. For uranium-238, the proton to neutron ratio was originally 92:146 which is approximately 0.630. After the emission, the ratio is 90:142, or 0.634 to three decimal places. Thus, alpha emission produces neutron rich nuclei that are still inherently unstable. In this situation, since the nucleus cannot simply eject a neutron it converts a neutron to a proton and emits a high-speed electron, a beta particle. This can be written in a shorthand manner as:

$$^{1}_{0}n \rightarrow ^{1}_{1}p + \beta^{+}$$

This is beta emission. In the case of the uranium-238 alpha decay, it's daughter element, the thorium-234, decays by beta emission to protactinium-234. The full process can be written as:

$$^{238}_{92}U \xrightarrow{\alpha} {}^{234}_{90}Th \xrightarrow{\beta^-} {}^{234}_{91}Pr$$

Similarly, the decay for polonium-218 results in bismuth-214 by the process below:

$$^{218}_{84}Po \xrightarrow{\alpha} {}^{214}_{82}Pb \xrightarrow{\beta^-} {}^{214}_{83}Bi$$

Bismuth-214 is still unstable, so further emission will occur until a stable atom is created.

The high-speed electrons that are produced by the beta decay process have a continuous energy spectrum ranging from zero to maximum energy ($E_{max.}$) with the majority of the electrons emitted with energy of $\frac{1}{3}E_{max}$. This maximum energy is a characteristic of the decaying isotope and is often used to help identify unknown compounds.

Two other decay processes that are important in the modification of nuclei are *positron emission* and *electron capture.*

Positron emission is a variation of beta emission. In this process, a proton is converted to a neutron and a positron is ejected. This can be written as

$$^{1}_{1}p \rightarrow {}^{1}_{0}n + \beta^+$$

For example:

$$^{22}_{11}Na \xrightarrow{\beta^+} {}^{22}_{10}Ne$$

Electron capture is a process by which an electron is plucked from an orbit and converts a proton into a neutron. This can be shown as:

$$^{1}_{1}p + e^+ \rightarrow {}^{1}_{0}n$$

There is then a subsequent rearrangement of the electrons and x-rays are emitted as the vacancy created in the inner orbit is filled.

3.3.3 Natural Radioactivity, Induced Radioactivity, and Nuclides

There are four naturally occurring radioactive series. Three are currently abundant on Earth, but the fourth's half-life is so short in comparison with the others that it only occurs on Earth in trace amounts. The three still occurring in reasonable quantities are the thorium, uranium-radium and actinium series. The neptunium series is the fourth, but the half-life of its longest-lived member is approximately 10^6 years, which is very short compared with the current age of the Earth hence this element and the subsequent daughter elements have long since decayed to a stable state. Only a very small amount of material is left active.

These series are listed in Table 4, and are sometimes referred to as the heavy disintegration series.

Series	Final stable isotope	Longest lived member
Thorium	^{208}Pb	^{232}Th ($T_{½}$= 1.39×10^{10} years)
Uranium-Radium	^{206}Pb	^{238}U ($T_{½}$= 4.50×10^{9} years)
Actinium	^{207}Pb	^{235}U ($T_{½}$= 8.52×10^{8} years)
Neptunium	^{209}Bi	^{237}Np ($T_{½}$= 2.20×10^{6} years)

Table 4. Naturally occurring nuclear elements showing the four members of the heavy disintegration series. The final stable isotope and the longest lived isotope for each series are shown. As can be seen, the half-life of the longest lived member of the neptunium series is two to four orders of magnitude shorter than the other series.

3.3.4 Induced Radioactivity

As well as the naturally occurring radioactive elements, lighter elements can be made radioactive by bombarding them with radiation. One example of this is the production of cobalt-60.

The naturally occurring cobalt-59 is bombarded with neutrons from a nuclear reactor, and a number of neutron-gamma (n,γ) events occur.

In the first part of this reaction, a neutron is captured by the cobalt-59 nucleus. The nucleus then emits a Gamma ray and a new isotope, cobalt-60, is produced. The resulting atom is unstable due to the excess neutron and will decay by beta emission to nickel. This reaction and subsequent decay is shown below:

$$^{59}_{27}Co(n,\gamma)\rightarrow ^{60}_{27}Co \xrightarrow{\beta^-} ^{60}_{28}Ni$$

The first stage of this reaction, the (n,γ) event, is shown in brackets as it is a nuclear reaction rather than a radioactive decay.

Radioactive decay, both natural and induced is statistical in nature. The result is that in a time t, a given proportion of atoms will emit radiation. This results in radioactive decay being exponential in nature. The half-life ($T_{½}$) of a species is defined as the time in which half of the nuclei in the sample decay, that is the time at which $N=N_0/2$. For a radioactive sample:

$$N = N_0 \exp^{-\mu t} \quad \text{Equation 2}$$

where μ is the *radioactive decay constant.* It can be shown (see Appendix A.1) that

$$T_{½} = \frac{\ln 2}{\mu} = \frac{0.693}{\mu}$$

The activity (A) of a sample is directly linked to the number of unstable nuclei contained within that sample. This can be simply expressed by replacing N with A for activity in the equation above. This gives

$$A = A_0 \exp^{-\mu t}$$

3.4 Measurement Units

The half-life of a particular isotope is constant, and is one means of identifying an unknown radioactive substance. However, if one radioactive atom was isolated, the point in time that it will decay and emit radiation cannot be predicted. All we could say is that if the half-life was 1 hour, then in 1 hour, there is a 50:50 chance it will decay.

This statistical nature can be problematic as half-lives can vary from incredibly long, e.g. 10^{17} years for ^{209}Bi, to incredibly short, e.g. 10^{-14} years for ^{212}Po. The difference between these two nuclides is a factor of 10^{31}.

The nuclear disintegration usually involves the emission of one or more charged particles, either alpha or beta; sometimes there is also an emission of a gamma ray. Some nuclides decay by only emitting gamma or x-rays.

The becquerel (Bq) has now superseded the curie as the unit of activity. The becquerel (Bq) is defined as one nuclear disintegration per second. The following list compares the various units of Bq and disintegrations:

1 becquerel (Bq)		= 1 dis s^{-1}
1 Megabecquerel (MBq)	= 10^6 Bq	= 10^6 dis s^{-1}
1 Terabecquerel (TBq)	= 10^{12} Bq	= 10^{12} dis s^{-1}

In turn, these can be linked to the curie by:

1 μCi ≡ 37,000 Bq	and	1 Ci ≡ 3.7^{10} Bq
1 Bq ≡ 2.7^{-5} μCi	and	1 TBq ≡ 27 Ci

3.4.1 Nuclides

Over many years of work, a vast amount of information has been compiled about the various stable and unstable nuclides. These can be listed in a tabular form called a table of nuclides. The stable isotopes are often highlighted, and from these it is possible to see how different emissions or absorption will affect the nuclide. A portion of such a table is given in Figure 5.

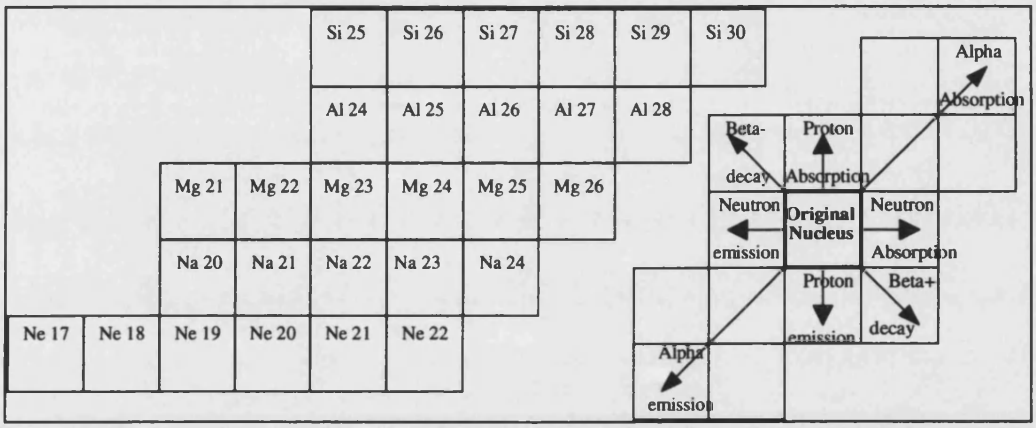

Figure 5. Excerpts from a table of nuclides showing how various elements and isotopes can be formed by nuclear decay and absorption.

Such a table can be used to give rapid information on an isotope. For example, a (n,γ) reaction with sodium-23 produces sodium-24. From sources such as the CRC handbook [15] it can be seen how sodium-24 decays. With a half-life of 15 hours, it emits beta particles with energy of 1.39 MeV and Gamma rays with energies of 2.75 MeV and 1.37 MeV. This decay transforms sodium-24 into the stable isotope magnesium-24.

3.4.2 Matter Penetration by Radiation

Charged particles such as alpha and beta particles lose energy by interacting with the atomic electrons of the medium they are traversing, causing these atomic electrons to be excited to a higher energy level, the process of *excitation.* If the transferred energy is high enough, electrons may be stripped from the nucleus, the process of *ionisation.*

If the particle is slowed down very rapidly by passing near a nucleus *bremsstrahlung* is emitted in the form of x-rays. This secondary radiation can be problematic, especially with beta particles in dense mediums. Section 3.6.2, covers this subject and recommends that beta shielding is made from aluminium or plastic, not lead.

For x-rays and gamma photons, the three most important interactions are the *photoelectric effect*, *Compton scattering* and *pair-production.*

In the photoelectric effect all of the photon's energy is transferred to an atomic electron that is then ejected from its parent atom. The photon is completely absorbed by this process. Although a certain amount of energy is needed to overcome the electrons initial bonding to the atom, gamma rays have more than this energy. The surplus energy is then transferred to the ejected electron as kinetic energy.

With Compton scattering, only part of the photon's energy is transferred to the electron. This means that the photon is then scattered with a reduced frequency.

If a gamma photon gets close to the intense electric field that is found near the atomic nucleus, it may be converted to an electron-positron (e^-:e^+) pair. This is pair production and requires that the photon energy is greater than 1.022 MeV, which is equivalent to the rest-mass energy of the two particles. Any energy in excess of 1.022 MeV is converted into the momentum of the e^-:e^+ pair.

Neutrons are uncharged and cause ionisation indirectly by colliding with particles and transferring their energy to charged particles. These charged particles can then cause damage by ionisation through the processes mentioned above. The neutron is a heavy particle, and since it is neutral the electric field near atoms does not affect it. This means that neutrons can penetrate deeply causing significant secondary emissions.

The larger charged particles such as alpha particles travel moderately slowly through any medium. This means that for low mass particles, energy is not proportional to mass. Therefore, since alpha particles have a high mass, their energy is proportional to their mass as well as their speed. This lower speed means that the chance of it interacting with atoms along the way is higher, explaining why ionising radiation like alpha particles have a very low range, but ionise very strongly along their path.

Beta particles are much smaller than alpha particles and travel much faster. In a unit length of media, a beta particle has fewer interactions than an alpha particle, thus they have a greater range in materials than alpha particles. This is reflected in the increased amount of shielding material that is needed to halt them.

For x- and gamma rays, the range is even greater. These photons only interact with atomic electrons and travel a great distance into any media. This makes total shielding very difficult, if not impossible. As can be seen in Section 3.6.2, the attenuation of gamma rays is exponential. Doubling the amount of shielding media only halves the dose, and so total shielding is impossible. In practice, it is usually more prudent to decide upon an acceptable dose limit and design the shielding around this level.

For neutrons, the interaction process depends on the initial neutron energy. Neutrons are a very penetrating form of radiation, with the unusual feature that thermal neutrons are absorbed by low Z elements more efficiently than high Z elements. Hence water (mainly hydrogen; Z = 1) is a better shield than lead. These properties are summarised in Table 5.

Type	Process	Consequence	Mass (u)	Charge	Range in air (m)
Alpha	Inelastic collisions with bound electrons	Leads to excitation ionisation	4	+2	0.03
Beta	1) Inelastic collisions with atomic electrons 2) Deceleration in the field of the nucleus	1) Leads to excitation and ionisation 2) Leads to emission of bremsstrahlung	1/1840	e^+ =+1 e^- =-1	3
X- and gamma rays	1) Photoelectric effect 2) Compton scattering 3) Pair-production	1) Photon absorbed. 2 & 3) Part of photon is absorbed	0	0	Very large
N^0	Elastic scattering Inelastic scattering Inelastic scattering	See Section 3.6	0	0	Very large

Table 5. A summary of the processes and consequences of interaction of alpha particles, beta particles, x- and gamma rays, and neutrons with matter.

3.5 Working With Radiation

The whole process by which radiation interacts with matter is a simple principle of energy absorption. Although the sources may vary, from isotopes to x-ray machines, the principle is the same. To visualise the principles behind shielding radiation, use the following simple analogy from Martin & Harbinson [17]

Consider the effect of heat on the body from a large open fire. As the warmth from the fire strikes the body, it heats the body up. If this gets too much, we can move behind a shade (shielding) or move further away from the source (distance) or try to minimise the time in front of the heat (time). These are the three basic processes which can be used to limit the effect of radiation.

With radioactivity, the principle is the same, but the actual processes involved are far removed from the open fire. For example, a lethal dose of gamma radiation would raise the temperature of a human body by about 1/1000th of 1 degree centigrade [17]. Hence, the human body is unable to detect even very high intensities of radiation. Nuclear radiation differs from normal radiation in that every particle or photon has enough energy to cause ionisation. This high-energy is due either to high velocity in particles or the short wavelength of the x- or gamma radiation.

3.5.1 Ionisation

The process of ionisation is the removal of an orbital electron from an atom. The removal of a negative particle means that the atom then has a net positive charge. The removed electron and the ionised atom are referred to as an ion pair.

When radiation passes through a medium, it loses energy by transferring energy to either the electrons or the nucleus. Thus radiation leaves a trail of ion pairs as the surrounding environment absorbs it, and the particle is slowed or the photon is degraded.

These tracks of ionised particles are used to detect radiation in devices such as ionisation chambers. The number of ion pairs produced is a function of both the radiation's speed and mass. For beta particles, many hundreds of ion pairs are produced per centimetre in air. For alpha particles, tens of thousands are produced per centimetre. In media such as water, ionisation can break down molecules.

In the human body, water is the main component and H_2O can be broken down and reformed into the free radicals H and OH. A free radical is an atom or group of atoms that remains in its host compound and remains unaltered during the host compounds ordinary chemical changes. These free radicals are particularly destructive in the human body where they form in cells and then interfere in the cell's operation. By staying chemically inert, the cell cannot function properly. Another chemical formed is hydrogen peroxide, H_2O_2, which is a strong oxidising agent and again harmful to the body's tissues.

3.5.2 Absorbed Dose and Equivalence

The ionisation of gas in chambers led to the first radiation unit, the *roentgen*, which was based on the ionising effect on air of x- and gamma rays. It was defined as the amount of radiation that would produce 1 electrostatic unit of ions per unit volume.

This had a number of limitations and was complemented by two further units, the *rad* and the *rem.* These have now been replaced by the SI units the *gray* and the *seivert.* These are the preferred units of the International Commission on Radiation Units (ICRU) and the International Commission on Radiological Protection (ICRP).

Absorbed dose measures the amount of energy deposited into a medium by ionising radiation, rather than the amount that has passed through the medium. The first unit of absorbed dose was the rad that was equivalent to 0.01 J kg^{-1}.

The SI unit, the gray (Gy), is the deposition of energy equivalent to 1 J kg^{-1}. By comparing these two definitions, it is easy to compare the rad and the gray as:

1 Gy ≡ 1 J kg^{-1} ≡ 100 rad*

The absorbing media is a deciding factor when calculating absorbed dose. As such, it is important to refer to the medium when referring to absorbed dose.

Although the concept of absorbed dose gives an idea of the energy transfer involved, different forms of radiation have different effects on different materials. This is especially true of the human body where 0.05 Gy (5 rad) of fast neutrons will do as much damage as 1 Gy (100 rad) of gamma radiation. The rad was originally corrected for this by attributing a quality factor, (Q), to a specific form of radiation. This gave a concept of *dose equivalent* radiation. The first unit to employ this idea was the rem (roentgen equivalent man). This was given by:

dose equivalent = absorbed dose x Quality factor

rem = rad x Q

The SI system has used this system and altered it with a further modifying factor, N. This takes account of things such as dose rate and any environmental factors. This project will be dealing with gamma rays, and so the Q factor is 1. The SI dose equivalent is termed the seivert (Sv) given by:

dose equivalent = absorbed dose x Quality factor x Modification

Sv = Gy x Q x (N = 1)

and since 1 Gy is equal to 100 rad, 1 Sv is equal to 100 rem.

---

* 1 Gy is normally enough to induce chronic radiation sickness. 2 Gy is sufficient to kill. With 3 Gy, the victim only has a 50% chance of surviving a month.

Type of Radiation	Q
x-rays, gamma rays and electrons	1
Thermal neutrons	5
Fast neutrons and protons	20
Alpha particles	20
Cosmic rays	20

Table 6. Quality factor (Q value) for radiation types.

The quality factor is linked to the density of the ionisation that takes place within the absorbing medium and reflects the extra damage that alpha particles, neutrons and cosmic rays can induce.

3.6 Radiation Hazards

Although radiation can be hazardous to matter, there are three ways in which damage can be limited: time, distance and shielding. Alpha particles are rarely seen as a risk due to the fact that virtually any substance will completely block them. From a biological point of view, alpha particles are only a risk when a source is ingested. Sources of alpha radiation are often considered as less dangerous than beta particles, x-rays, gamma rays and neutrons though no source should ever be underestimated.

3.6.1 Time and Distance

Since the dose accumulated by a target is limited by the dose rate, limiting the time of exposure is one method for minimising damage. This is of prime concern in areas where large constant radiation fields exist, for example near a nuclear reactor.

Assuming a point source, the dose rate is related to both the flux and the distance from the source by an inverse square law. If the intervening matter between the source and the target does not attenuate the radiation, or does so only slightly, an approximation can be made about dose *D* at a distance *r* from the source:

$$D \alpha \frac{1}{r^2} \text{ or } D = \frac{k}{r^2}$$

where k is a constant for a particular source. Furthermore, we can now consider how the dose will vary from two points away from the source. This gives:

$$D_1 r_1^2 = D_2 r_2^2 \text{ Equation 3}$$

A useful expression for calculating the approximate dose rate from a gamma source is given by [17]:

$$D = \frac{ME}{6r^2}\ \mu Sv\ hr^{-1}$$

where D is the dose rate in $\mu Sv\ hr^{-1}$, M is the activity in MBq, E is the gamma energy per disintegration in MeV, and r is the distance from the source in metres. From the earlier table, the Q value for gamma photons is unity; hence Sv and Gy are interchangeable.

These equations can be applied to a facility to test some experimental parameters. For example, consider a facility where the source is quoted as giving a dose rate of 23 Gy hr^{-1} at 1 m. The chamber that houses the source has a maximum distance of 6.5 m from the source.

Let us assume that for our experiment, we need a final dose of 10 kGy over a period of 12 hours. This infers a dose rate of $\frac{10\ kGy}{12\ hour} = 833\ Gy\ hr^{-1}$ so applying this to Equation 3:

$$D_1 r_1^2 = 23\,Gy\,hr^{-1}\ x\ 1^2$$

$$D_2 r_2^2 = 833\,Gy\,hr^{-1}\ x\ r_2^2$$

$$\text{hence } r_2^2 = 0.027\,m \Rightarrow r_2 = 0.166\,m$$

This assumes a 12-hour exposure. Over this time period, we can calculate the minimum dose received by an unshielded sample at the back wall.

$$\text{If } r_2^2 = (6.5\,m)^2 \Rightarrow 42.25$$

$$D_2 = \frac{23\,Gy\,hr^{-1}\ x\ 1\,m^2}{42.25\,m^2}$$

$$D_2 = 0.54\,Gy\,hr^{-1} \times 12\,hr$$

$$D_2 = 6.5\,Gy$$

This also allows us to calculate the activity of the source. Assuming the source is a cobalt-60 gamma source, emitting two photons per disintegration at 1.17 and 1.33 MeV [15]:

At 1 metre, the dose rate was 23 Gy hr^{-1}, or $23 \times 10^6\ \mu Gy\ hr^{-1}$

$$\Rightarrow 23 \times 10^6 = \frac{M \times (1.17 + 1.33)}{6 \times 1^2} \text{ thus } M = 55.2\ TBq$$

Cobalt-60 has a half-life of 5.52 years. [15] If this figure was given in 1992, then in the 5 years since then, the source will have reduced in activity to about 29 TBq.

3.6.2 Shielding: Alpha, Beta and Gamma

Often, time or distances are not viable options for reducing the effect of radiation. In these situations, the usual method is to place something between the source and the target to absorb at least some of the radiation, if not all of it. The amount and type of shielding is dependent upon the type of radiation involved.

Alpha particles: Despite being a powerful ionisation source, they are easily shielded by a thin layer of any material, for example a piece of paper.

Beta radiation: More penetrating than alpha particles, and for natural sources they normally occur in an energy range of 1-10 MeV requiring shielding of up to 10 mm for complete absorption. For artificially accelerated beams, the energy can be much higher, and so more shielding would be needed.

Shielding charged particles can produce secondary x-rays. These are the result of slowing down of the beta particles. This bremsstrahlung is a fraction of the beta energy re-appearing in electromagnetic form. The main method of production for bremsstrahlung is when an electron is deviated from its track by a strong electric field, such as the one found near the nucleus. For materials like lead with a high atomic number, it is more likely for an electron to be slowed by the nucleus and produce bremsstrahlung. This is why the amount of incident energy converted to secondary x-rays is proportional to the atomic number of the shield material. The result of this is that beta shields are best formed from aluminium or acrylic sheet but not lead.

Also, since the beta source emits a continuous spectrum with mean particle energy of $\sim\frac{1}{3}E_{max}$, by concentrating on removing the particles with energy less than the mean energy it is possible to obtain adequate shielding and reduce weight constraints – assuming that total shielding is not a primary requirement.

Gamma and X-rays: These rays are attenuated exponentially when passing through material. It is more a case of reducing them to an acceptable level than total shielding. The dose rate due to the irradiation emerging from a shield can be written as $D_t = D_0 \exp^{-\mu t}$ where D_t is the dose rate appearing from a shield of thickness t made of a material with a linear absorption coefficient of μ irradiated by a dose of D_0. The linear absorption coefficient is a function of both the material and the incident radiation energy. It has the dimensions of $(\text{length})^{-1}$.

3.6.3 Shielding: Neutron

As well as the nuclear reactor, there are a number of sources that produce relatively small amounts of neutrons. The most common sources are based on the $^{9}Be(\alpha,n)^{12}C$ reaction. The alpha particles are emitted from sources such as ^{241}Am or ^{226}Ra. For the $^{241}Am/^{9}Be$ sources, the emitted strength is ≈70 neutrons per MBq of ^{241}Am. The energy spectrum is not monoenergetic, but highly peaked over a range of 3 to 6 MeV, that is, it is a relatively fast source.

A second method is to use the photoneutron process, a (γ,n) reaction. This is usually formed with equal mixtures of antimony-124 and beryllium, ejecting relatively monoenergetic neutrons.

The shielding of neutrons is complex in that the wide range of neutron energies plays an important role in deciding which method to employ. The most important reactions are given below.

Elastic scatter: In these processes neutrons are scattered like snooker balls. During the collision, some energy is imparted to a nucleus in a transfer of momentum. Light elements are more susceptible to this process, and so materials with high hydrogen content are chosen to slow down neutrons by elastic scatter. Materials such as paraffin, water and concrete are suitable.

Inelastic scatter: This is similar to elastic scatter, but the transfer of momentum is not as efficient. In an inelastic collision some of the incident neutron's energy is transferred as momentum, the rest excites the nucleus. The target nuclei usually emit gamma radiation as they de-excite. This process is most important in interactions with the heavier nuclei.

Neutron capture: This form of shielding is related to a neutron being captured by a target nucleus, a photon or particle being subsequently emitted. This most commonly makes use of the $^{10}B(n,\alpha)^{7}Li$ reaction. The importance of this reaction being used for shielding is that the boron converts a penetrating neutron into an easily stopped alpha particle.

A less useful, but very common, neutron capture reaction involves the emission of a penetrating gamma ray and in particular the $^{58}Fe(n,\gamma)^{59}Fe$. This is common since steel is often used in structural supports in nuclear reactors. As such, it is necessary to use a high Z material in the shield design to capture the gamma rays produced by the steel support structure.

3.6.4 Half Value Thickness

The half value layer (HVL or $t_{½}$) or half value thickness is the thickness of material needed to attenuate a beam to half its intensity. Placing this into Equation 2 gives:

$$\frac{D_t}{D_0} = 0.5 = \exp(-\mu t_{\frac{1}{2}})$$

Thus:

$$t_{\frac{1}{2}} = \frac{0.693}{\mu}$$

This exponential equation is known as the Beer Lambert law. Similarly, the tenth-value layer, $t_{1/10}$ can be calculated as:

$$t_{\frac{1}{10}} = \frac{0.2303}{\mu}$$

(See Appendix A.3.)

Examples of some values of half- and tenth- value thickness are given in Table 7.

Gamma energy	mm of lead		mm of water	
(MeV)	$t_{½}$	$t_{1/10}$	$t_{½}$	$t_{1/10}$
0.5	4	12.5	150	500
1.0	11	35	190	625
1.5	15	50	200	700
2.0	19	60	225	750

Table 7. Approximate values of half- and tenth-value layers for lead and water for several energy ranges of gamma photons.

3.7 The Terrestrial Radiation Environments

In Section 1.2.3, the space radiation environment was discussed both in general and in relation to the XMM-Newton mission. Another environment that has driven the field of radiation damage research was the development of the nuclear reactor. Unlike the space environment, the nuclear reactor is comparatively easy to access to has some differences in terms of the dose rates and types of radiation found in that the majority of the radiation is in the form of energetic neutrons.

Work involving nuclear reactors continued studies first begun by the Manhattan Project. The primary concern in a reactor is the copious neutron flux generated in the core by the neutron chain reaction. Many sources use the term flux to describe the number of particles or photons passing through an area at a distance from a source. This should be referred to as the fluence rate (See appendix A.2). Additionally, the environment near to the actual core itself emits abundant gamma rays. Dose rate can vary between 10^{-5} and 1 Gy hr^{-1} depending upon the location during normal operation, and up to 10^4 Gy hr^{-1} during accidents.

Over a normal forty-year operation, a plant can expect certain hot areas to receive doses in the order of 10^1 to 10^6 Gy. Again the actual position relative to the core is important. A dose of approximately 10^6 Gy can be accumulated between the primary and secondary shield, whereas outside the secondary shielding, a dose of 10^4 Gy is more likely to be amassed [19]. Within the core itself, doses of 10^3 to 10^8 Gy hr^{-1} can be expected [20] but it is unlikely that much instrumentation would be designed to work in this environment, certainly not long term.

Although these are significant levels of radiation, systems can be designed to receive an exposure of the order of 10^7 Gy over an operational lifetime. Unfortunately, a nuclear accident after 40 years of operation could still give an instrument a total dose in excess of 10^8 Gy.

A possible area of future interest could be the development of fusion reactors. Experiments involving fusion test reactors so far have predicted that their nuclear environment could be as hostile as current reactors, with dose rates of up to 10^8 Gy hr^{-1} again, and neutron fluxes of 10^{14} n cm^{-2} s^{-1} have been suggested. [21] Since modern environmental standards are more rigorous than when the original fission reactors were developed, it is conceivable that there may well be a need for instrumentation to work close to the core to monitor the prototypes.

4 Radiation Effects in Materials

Once the general processes of radiation were understood next step was to address the effect of radiation on matter. Although the effect of radiation had been noted by earlier scientists, the Manhattan Project was the first scientific study that paid significant attention to radiation effects in materials. The Manhattan Project used optical devices to examine reactor components and found that over time the optics became dark, or *brown* due to exposure to radiation. The scientists on this project then found that the addition of *rare earth elements* to the lens materials reduced this effect. Rare earth elements are the 15 elements of the lanthanide series. This series ranges from lanthanum, with an atomic number of 57, to lutetium, with an atomic number of 71 (see Appendix C). In particular the element cerium which is used in the radiation hardened F2 and BK7 and several other hardened glasses is from this series and has an atomic number of 58.

This early work discovered that the radiation-induced discolouration in a sample of material occurred in small, individual sites. These could produce quite spectacular changes in the sample's colour and were named *colour centres.*

Study into the formation of these radiation induced colour centres continues today. The interest in these centres continued during the late 1950's and early 60's, but diminished during the mid-60's. Interest was revived by the need for materials to use in projects in the newly opening space environment. This included the glasses and crystals used in both optical components and solar cells and led researchers to study nuclear particle and photon-induced effects. Current research is stimulated by lasers, fibre optics, and radiation resistant detectors for high-energy physics.

Although there is a substantial body of knowledge available on radiation effects in optical materials, the majority of the literature is devoted to the identification of the colour centre sites rather then their actual formation. [22] Figure 6, (taken from [23]) shows an idealised spectrum for am alkali halide crystal showing the various colour centres associated with the material.

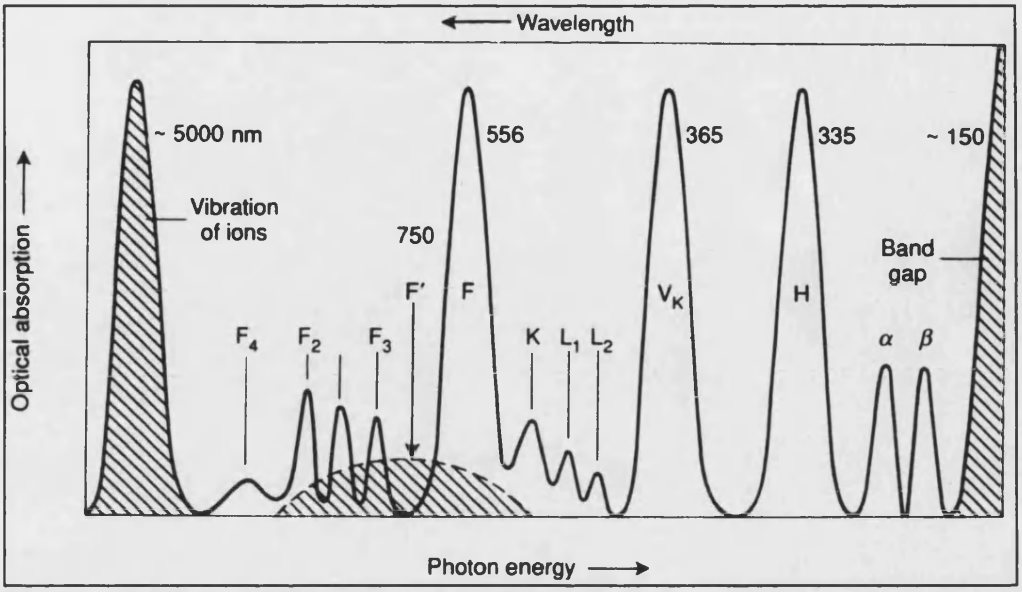

Figure 6. Optical absorption bands in alkali halide spectrum. A perfect crystal would have no absorption peaks between the shaded pair (band to band and vibrational absorptions.) As a result, the materials are transparent to the eye. On irradiation, the most obvious peak in the visible, the F centre, is produced and the crystal exhibits a *pure* colouration.

The previous chapter introduced information about the particles and photons that make up radiation. The following sections detail the intricate way in which matter and radiation interact.

4.1 Electromagnetic Radiation and Matter

As was discussed earlier in 3.4.2, there are several basic processes by which radiation interacts with matter. The Photoelectric Effect, Compton Effect and Pair Production involve the scattering and absorption of radiation in matter. In addition Pair Annihilation involves the production of radiation and exposure to gamma radiation involves Absorption and Luminescence. All these effects are discussed further in Appendix A. Further information on the quantum aspects is available in standard texts. [16]

4.2 Basic Damage Processes

There are three basic process by which radiation can effect matter. They are:

- Radiolytic Processes: ones that rely on purely electronic excitation mechanisms.

- Displacement Damage Processes: where momentum is transferred to the atomic structure.
- Electronic Rearrangement: usually associated with the presence of defects within the glass or crystal.

4.2.1 Radiolytic

These are processes where the atomic structure undergoes some form of rearrangement that is powered by the non-radiative recombination of electrons and holes. Radiolytic damage could be induced by any form of radiation or particle bombardment of sufficient energy to excite electrons across the forbidden gap, E_g, into the conduction band. For insulators the value of E_g typically lies in the range of 5 to 10 eV, with SiO_2 having a value of 9 eV. [24] Since 400 nm ≡ 3.15 eV (see Appendix A.4), E_g must be greater than 3.2 eV to allow UV light to pass through without absorption.

For glass E_g tends to be greater than the bond strengths of the atoms and tends to hamper the formation of a photon. Thus the recombination energy that is emitted must be channelled into nuclear motion. In the situation where all this energy is focused onto one atom, the production of a defect is quite likely. This resulting defect can be either stable or metastable, depending on the energies involved.

Again SiO_2 is a useful example. Here, the bond strength is ~4.5 eV, half the value of E_g. If a hole is formed at the top of the valence band, it is possible for a hole to form in the Si-O bonding orbital or at the level of the core. This results in even higher potential energies for defect formation. For example, typical values of the threshold energies are ~9 eV for an upper valence band hole, ~15 eV for a hole in a Si-O bond and ~30 eV for the O_{2s} core hole.

In the core level case, there is the possibility that an Auger electron may be produced. In this case, an electron falling from a higher energy level fills the hole in the inner shell. As it does so, it emits its extra energy either as a photon or by the emission of a secondary electron. This emission of an electron is the Auger process. Since the energy value of the inner shell varies from element to element, the Auger process is used in Auger electron spectroscopy to identify the chemical composition of the surface of the material.

4.2.2 Displacement

Displacement, or knock-on, damage is due to the direct transfer of momentum from an incident particle (or perhaps by a secondary particle such as a Compton electron) to an atom in the glass network or crystal structure. To break the bonds associated with glass networks, energies of at least 4 to 25 eV, the values of the bond strengths, must be transferred. The maximum energy that can be transferred per collision, T_m, is given by:

$$T_m = \frac{4mME}{(m+M)^2}\left(1+\frac{E}{2mc^2}\right)$$

where m and E are respectively the mass and energy of the incident particle, and M is the mass of the lattice ion. For example, if the incident particle were an electron

$$T_m = 2147.7\,E\left(\frac{E+1.022}{A}\right)$$

where E and T_m are in MeV, and A is the atomic mass of the recoil particle. For example, assuming that the minimum energy to displace an oxygen atom in glass is T_m = 10 eV, the threshold energy ($E_{th}(O)$) for the electron is $E_{th}(O)$ ~70 keV. To displace a silicon atom, an electron would have to overcome the entire cohesive force of the four bonds. This means that to overcome ~18.8 eV, the electron threshold energy becomes $E_{th}(Si)$ ~200 keV.

For high-energy photons such as Gamma rays, displacement damage can still occur through the action of secondary radiation such as Compton electrons. For a photon of energy hν, scattered through an angle θ, the resultant Compton electron will have energy of:

$$E = h\nu\left(1-\frac{m_0c^2}{h\nu(1-\cos\theta)+m_0c^2}\right)$$

where m_0 is the electron rest mass. For 1.5 MeV Gamma rays, with a head on collision ($\theta = \pi$), the maximum $E_{max(\gamma)}$ ~1.3 MeV. However, for 100 keV x-rays, E is a maximum of $E_{max(x\text{-}ray)}$ ~28 keV. Thus a cobalt-60 source with gamma rays of energy 1.17 and 1.33 MeV, could produce displacement damage in SiO_2 by displacing either O or Si atoms, whereas 100 keV x-rays could displace neither.

However, just because T_m exceeds the threshold value does not mean that displacement will occur. Heavy ions dissipate far more energy in electronic processes than in direct displacements. [25] As for which process is dominant, this is usually determined by experiment. For electron irradiated a-SiO_2, (amorphous silicon oxide), evidence suggests that an ionisation mechanism is the dominant source for producing E2' centres. [26,27]

4.2.3 Electron Rearrangement

Electron rearrangement generally occurs only when there are other types of defects present. In the scope of the Continuous Random Network model for glass, or CRN (see 4.6), it is believed that deviation from this idealised network (in the form of vacancies, non-bridging oxygen, impurities, etc.) serve as traps for the liberated charge carriers (the electrons and holes.) Thus, radiolytic or knock-on damage may sow the seeds for electronic rearrangement later.

However, it has often been suspected that the melt temperature of the glass may also be significant in the formation of defects. Glasses quenched from high temperature melts will have a high number of Frenkel defects (vacancy-interstitial pairs), the number being characteristic of the melt temperature.

If these existing faults were to act as the predominant charge traps for radiation induced charge carriers, then the resulting number of colour centres would saturate at some fixed number, say ~10^{18} cm^{-3} for glass. [28] If the centres were produced by radiolytic and displacement damage, the number of defects would be expected to saturate at a higher number, say ~10^{20} cm^{-3}. The limit on the latter number is the point at which the wave functions of the defects begin to overlap and annihilation occurs. It has also been noted that the saturating components show a dependence on the fictive temperature which supports the Frenkel defect concept for a-SiO_2. [19]

4.3 Particle Irradiation and Matter

From the basic principles of radiation and radioactivity, the specific characteristics of each of the main radiation types can be addressed.

4.3.1 Electrons

For electrons, this can refer to both natural radioactivity (beta particles) and simulated radiation (electrons and positrons) since they display similar characteristics. As an electron passes through crystal or glass, it interacts with the constituent electrons. If these interactions are strong enough, an electron-hole pair is produced. If not, then the electrons are excited to produce phonons. The phonon is the vibration or heat equivalent of a photon and results in the material is heated. In the case of crystals it usually requires energy of roughly two to three times the material's band gap to produce an ion pair.

Electrons can produce displacement damage but they have to be highly energetic. (See Section 4.2.2) and the displacement process is inefficient. When an electron is incident on a body, it loses energy, and the rate of energy lost per unit length is high. This means that the vast majority of impinging electrons will lose energy so rapidly that they will have insufficient energy to liberate a lattice atom.

4.3.2 Heavy Charged Particles

In working terms, this covers all particles with a mass greater than the electrons. Specifically, this includes protons, alpha particles and atomic ions. The way in which these particles undergo collisions is very similar to that of neutrons, with the majority of collisions being elastic rather than inelastic.

Since they are charged, they lose a substantial amount of energy due to ionisation processes. However, since they are heavier than electrons, the displacement process can be more significant.

The ratio of energy lost by transfer of momentum during collisions rather than by the ionisation of the electric fields depends upon particle mass, velocity and charge. Protons produce relatively few displacements and appreciable ionisation compared with energetic oxygen ions (such as those found in the third Van Allen belt) that produce a relatively high ratio of displacements to ionisation.

4.3.3 Fission Neutrons

The majority of neutron work has been focused on uranium-235 as it forms the central process in the generation of nuclear energy. The neutrons emitted by a fissioning fragment of uranium-235 are distributed with an energy spectrum ranging from ≈ 0.5 MeV to ≈ 10 MeV. The average energy is 1.5 MeV, and this is the value used in the majority of calculations for this source of neutrons.

Due to the copious neutron flux (up to 10^{17} n^0 cm^{-2} s^{-1}) the damage caused by neutrons to reactor materials is substantial and well documented. The general method by which a neutron affects a material is by displacement damage. Saying this, very little of the damage is due directly to the neutron, but to the particles it impacts against whilst driving through the material. Even though the neutron is uncharged, the fragments it produces usually are not. This results in charged particles ploughing through the material. The disrupted region is usually quite narrow and contains both vacancies and interstitial atoms and is often referred to as a displacement spike.

4.4 Factors Governing Radiation Damage

Now that the basic processes have been defined, it is possible to address the effects for glassy and crystalline structures. The majority of reference literature for crystals covers work on the alkali halide crystals where halides, or halogens, are the elements in column 7 of the periodic table. Although none of this project's samples were from this group, alkali halides have been extensively tested and magnesium fluoride is very similar in compound to the alkali halide lithium fluoride.

Before using an optical material in an environment containing ionising radiation, a number of choices can be made to minimise the effect of the radiation on the material. [29] They are:

Is a more suitable material available?

Can purifying or doping the material reduce effects?

Minimise surfaces, strains and line defects that can be reached by the radiation.

Can the operating or post-irradiation temperature be altered to minimise?

If the radiation is pulsed, does the material have any short-term behaviour?

Will post-irradiation exposure to light help or hinder recovery?

Since the behaviour of polycrystalline thin films can differ from that of bulk materials, will this be problematic?

Will ultraviolet light damage the selected materials?

4.4.1 Radiation Resistant Crystals

The simplest solution to the problem of avoiding radiation damage is to choose a resistant material in the first instance. Unfortunately, there is not always an obvious candidate that suits the requirements of the instrumentation design.

Certain crystals suffer displacement and radiolytic lattice damage described in Section 4.2. Others only suffer displacement damage within the lattice (where displacement damage is by momentum transfer).

The displacement and photochemical lattice damage prone crystals have a higher threshold for initial radiation damage. This is unusual since the threshold for photochemical damage is normally that of the material's band-gap. This is typically in the ≈5 to 12 eV range in most halide crystals. For knock-on displacement, the energy threshold tends to be much higher. This is usually of the order of ≈15 to 80 eV.

The threshold incident particle energy value is a function of the masses of the impinging particle and the struck atom. With the momentum requirements, the energy will need to be much higher since the heavier a particle is the more effectively it will plough its way through a medium.

Crystalline halides, especially fluorides, are useful materials for optical systems. Fluorides display two useful features: Firstly, they tend to have wide bandgaps and so can transmit light across a wide spectral range. Secondly they tend to have a quite high chemical resistance. Williams [29] covers this in detail for calcium fluoride.

However, others [22] believe that in radiation environments oxide crystals or glasses should be employed in preference to halide crystals. This is due to photochemical generation of lattice defects from electron-hole pairs, a process that seems to be almost exclusively found in the halides. These electron-hole pairs cause the movement of charge carriers as holes and electrons among existing traps and defects found in the initial crystal.

Even so, the displacement damage and charge transfer processes can occur in all materials. In a pure lattice structure, the photochemical damage is believed to be short-lived. To create a defect that will survive this process, it is necessary for the fluorine interstitial and the vacancy to diffuse apart under thermal activation. This has to occur before the electron can recombine. Even if the ion pair can separate, the defect would still not be permanent. It is quite possible that mobile fluorine interstitials would eventually find, and annihilate with, a fluorine vacancy. This assumes that no other fluorine traps exist. Hence, the final stage of photochemical radiation damage is a mechanism to trap, or stabilise, the diffusing components of the defect.

4.5 Purity and Doping Effects

Once a material has been chosen for a specific project, improved material purity generally improves the radiation resistance of the material. Even so, there is only a finite point to which this can be undertaken. Similarly, beyond a certain level of purity, the cost of further purification becomes exorbitant.

So although impurities are a problem, they are a problem that can be addressed. This raises more questions. For example, which impurity causes the greatest effects? How does the level of impurity affect the mechanical properties of the material? Is it worth hardening the material for small doses – for example the cerium added to the F2 and BK7 glass? Often, this means that the impurities are often expensive to address fully. To simplify matters, radiation effects caused by chemical impurities are often grouped into three categories: *Intrinsic, Extrinsic*, and the combination of the two.

4.5.1 F and V Centres

Literature about radiation induced defects centres often refer to F- and V-centres, where the simplest distinction is that an anion vacancy site forms the F centre, and a cation vacancy site forms a V centre.

From the early work in alkali halides and oxide crystals it was noted that the discolouration of optical windows was localised about one particular wavelength, hence the material would take a distinctive hue. For example, potassium chloride shows a distinctive peak in radiation-induced discolouration at 556 nm. This is why it displays such a strong purple tint after radiation. This is the F centre for this material. For this material, in the infrared (at wavelengths > 750 nm) other anion absorption bands produced in the same manner appear. These are denoted F_2, F_3, etc. Down toward the UV, at 365 nm an absorption band as deep as the F centre appears. This is a cation centre, a V centre.

4.5.2 Intrinsic Defects

Intrinsic radiation-induced defects are those produced in a crystal with a perfect lattice structure and of very high purity. These would include displaced ions in various charge states distributed at various sites within the lattice. Similarly, vacancies would exist with a widespread distribution.

However, spectra of defects in lithium fluoride [30] and magnesium fluoride [31,32,33] at room temperature that were attributed to F centres and their aggregates and were the only effects observed appear to be intrinsic in nature. VUV data [34] illustrates the beta absorption band, which is due to excitons being perturbed by the presence of a nearby F centre. It has been noted that virtually all defects induce a similar band that can be significant for deep VUV applications.

4.5.3 Extrinsic Defects

In contrast, extrinsic radiation-induced defects occur on an impurity atom. Effects such as a change in the position or charge state of the impurity atom can produce an observable effect in the optical properties of the material being irradiated. For example, irradiation can induce the ejection of an impurity atom into an interstitial site. Similarly, it can also induce either the aggregation or break up, of an impurity cluster. Since this damage is directly linked to impurities in the host crystal, it will decrease with increased purity. Indeed, the effect of radiation on these sites could be used as a guide to the level of purity of the sample.

4.5.4 Intrinsic and Extrinsic Defect Interaction

The final group is the rather loose category of both of the previously mentioned defect categories. In reality, materials used in projects will generally have a slightly imperfect structure and a small level of impurity. As such, radiation-induced damage has been observed that either occurs or is stabilised by some form of interaction between intrinsic defects and impurities.

With most halide crystals and some believe in silicon oxide, [35] it is believed that ionising radiation produces vacancy-interstitial pairs with very small lifetimes. These lifetimes are believed to be in the nanoseconds to microseconds range depending upon the temperature of the material. Indeed this may help partially explain the process of thermal annealing (see Section 4.5.7.)

Another example is that it is believed that in a perfectly pure crystal, any generated interstitial would simply fall back into the vacancy left at its original site. However, the presence of an impurity gives the generated interstitial another bond to connect with and thus the impurity allows the defect to be fixed into place, that is, we have an impurity-stabilised *intrinsic* damage centre. The problem lies in the identification of this site. The centre of the site, e.g. an F centre, may be of either an intrinsic or extrinsic origin.

An example of extrinsic radiation damage can be found in irradiated aluminium oxide. Damage in this material is commonly linked with two bands that coincide with 3.08 eV and 5.56 eV. The 5.56 eV band (227 nm) is due to Cr^{2+}. The natural form of this impurity is Cr^{3+}, and though only found in trace amounts, it is found almost universally in sapphire. When exposed to ionising radiation, it is transformed from Cr^{3+} to Cr^{2+}. In the process, a hole is released which can then be trapped at an aluminium vacancy (an intrinsic defect) forming a V^{2-} centre, or if an OH^- is near enough, this can replace one of the neighbouring oxygen ions giving a V_{OH} centre. Both of these bands absorb light at the 3.08 eV (410 nm). Ionising radiation impinging on these centres produces the ultraviolet absorption band at 227 nm and a similar blue band at 410 nm, the latter being observed as brown solarisation.

4.5.5 Intentional Doping

Although purity can often help reduce the response of a material to radiation, under certain circumstances, defects can actually help in stabilising damage. For example, the use of rare earth elements and most notably cerium is accepted as standard for some applications and is used in the glasses used in this project. Cerium forms the ion Ce^{3+} when added to glass. This ion competes with intrinsic defects to capture radiation-induced holes. When these holes are captured by the cerium, it creates an aggregate that is less disruptive than if the hole had been stabilised by an intrinsic defect. The trade-off comes about as cerium is itself a UV absorber, and this is generally the case for most chemicals used for doping.

A significant difference between glasses and crystals is observed in this area. For glasses with their high number of *intrinsic* defect sites, the inhibition of charge trapping by the doping is significant. However, for a high purity crystal of minimal physical deformity, doping could be counter-productive, so little research has been carried into doping for many crystals. One crystal that has been tested is magnesium fluoride. Sibley and Facey [36] found that the least pure crystal displayed a greater susceptibility to radiation induced colouring at lower doses, but at higher doses it demonstrated a lower saturation level.

4.5.6 Strain, Surfaces and Line Effects

Internal and external surfaces play a significant role in modifying the radiation damage within a sample. The surfaces and dislocations of the material act as a sink where mobile defects can be trapped and stabilised before they can re-combine. This has the effect of making the defect formation appear efficient. For example, by providing a sink for mobile interstitial atoms, internal surfaces improve the photosensitivity of silver and thallium halides. In comparison, a good single crystal of these materials is known to be relatively insensitive to ionising radiation.

Actually applying a mechanical stress to a material can also modify the response. Experiments on stressed potassium chloride have shown that, for this crystal, stress is an important factor. By applying stress to the material, vacancies are created. These vacancies can then go on to react with the material to help create defects. One study showed that in both pure and doped potassium chloride, plastic deformation can effect the radiation hardness of the material. [37]

However it was also shown that the pure material reacted less to the deformation. From this, it was inferred that the deformation allows the material to significantly react with impurities, and hence adjust the radiation hardness of the material. Yet it was also shown that heavy doping (around 60 ppm) with lead could reduce the radiation damage associated with deformation.

4.5.7 Thermal Annealing and Optical Bleaching

It has been observed that thermal cycling of post-irradiated material can annihilate many defects completely, and rearrange others into less optically offensive clusters. The method by which the annealing is achieved can significantly affect the behaviour of the material if it is irradiated later. If the thermal cycling merely redistributes the ions, then it will be more susceptible to radiation later as the damage sites are still intact. Recombination of vacancies and interstitials will restore the perfect crystal lattice, but the increased mobility of the defects can allow larger, more stable, agglomerations to form. F centres in alkali halides are highly mobile in the temperature range of 200° to 400°C. In magnesium fluoride it has been observed that F centres are annealed quite efficiently in the range 300° to 400°C. [38]

The effect of light on post-irradiation defects has also been noted, and it produces a number of effects. These effects are grouped under the term *bleaching*.

In electronic bleaching, photons with hν > photo-ionising energy of a defect are used to target a species of defect. The photons strip the defect of its electrons (or holes), but only works if there are sinks available to receive the liberated ions. This allows a given absorption band to be removed from the final spectra. However, the defects still remain, and if a small dose of ionising radiation is incident upon the material, this may free charge carriers to reinstate the absorption band.

Alkali halides, though, can have atomic defects mobilised by light of optical or UV wavelengths. For magnesium fluoride exposure to 254 nm light causes the F centres to be partly converted to F2 centres, which absorb at 380 nm. [33]

4.5.8 Radiation Damage In Thin Films

The effects of surfaces acting as sinks for mobile defects are significant. An extreme example of this is found with the effect of radiation on thin crystalline films. Even in a perfect epitaxial* film, there is a large surface to volume ratio. Typically, films tend to be non-epitaxial, and this means that there are substantial dislocation densities and large stresses induced by lattice mismatch, differential cooling, etc.

Being a crystalline substance, columnar or grainy growth is not unknown in the manufacture of such films. This results in two effects that can significantly alter the response of the film to radiation. Firstly the extraneous growth increases the surface area, and secondly, it is even more difficult to maintain a high level of purity. The very small thickness of some films means that ionising radiation with minimal penetrating power (such as alpha particles) may now play a significant role in the generation of defects.

However, this increased surface area combined with the fact that it is relatively close to any part of the film, means that defects can be stabilised relatively easily and quickly. This increased surface area also has the effect that defects or material impurities can be ejected, or evaporated. This occurs with halogens being ejected from alkali halides. [39]

Although thin films are more susceptible to radiation damage, a problem may not actually exist. For example, a 0.1 μm film with a density of defects of 5×10^{19} F centres cm^{-3} will only attenuate the light by removing 0.1% of the incident light. However, although this attenuation may not be a problem in itself, there is a possibility that under high power optical conditions, the amount of radiation energy being deposited could produce secondary obstacles. For example, one obstacle could be the production of a thin metallic surface coating that could significantly affect the reflectance properties of the film.

---

* An epitaxial crystal is one where the orientation of the crystal structure is determined by the underlying crystal it grew upon.

4.6 Irradiating Glasses

The early days of irradiation testing saw a lot of attention directed at glasses, since they were widely used. From this work, a model of the behaviour of glassy, amorphous systems was developed and was known as the continuous random network (CRN). [40] This is an idealised view of the real system, and so it should be expected that there would be deviations from this. In particular, amorphous silicon oxide was modelled via the CRN and has been particularly successful in explaining the radiation-induced behaviour of this material.

The mechanism by which damage occurs is believed to be due to short wavelength radiation interacting with the atomic cores and electrons that constitutes the various component elements of the glass. This interaction ionises the particles, and this in turn liberates charge carriers. It has also been noted that the composition of the glass can be equally important. In some glasses doses as low as 10 Gy can induce discoloration.

This theory of the damage process is based on the belief that the ionising radiation releases charge carriers. This in turn leads to an explanation of how rare earth elements can help to harden a glass to radiation damage.

Although based on similar work as that described in the previous crystal section, glass is quite a different substance to its crystal counterpart. The same basic processes still occur, but with dissimilar levels of effectiveness. For example, in alkali halides, the radiolytic production of the vacancy-interstitial F-H pair defect is highly efficient. By contrast, in ionic oxides such as magnesium oxide, calcium oxide or sapphire, radiolytic processes are quite ineffectual with displacement mechanisms of greater significance.

The effect of irradiation can be highly significant. Ehrt [41] showed the enormous changes that occurred within a glass structure when bombarded by fast electrons. After a brief irradiation by 100 keV electrons the lead ions in a lead silicate glass filament had been reduced to a metallic state with small spheres being deposited into the glass. Continued irradiation showed the small lead spheres combining into larger, more apparent spheres. Finally, after further irradiation, the metallic lead had evaporated completely, leaving behind a pockmarked glass skeleton.

4.6.1 Defect Centres and Absorption Bands

The primary interest of this project is the effect of the defects on the optical properties of the material. Generally speaking, the most common method of observing radiation effects is to measure the change in the transmission of a material.

One particularly well-known correlation is that between the E'_γ and the radiation-induced absorption band at 215 nm (5.8 eV). [43] Another band in the VUV is that at 160 nm (7.6 eV). [42] This has been linked to the superoxide radical $\equiv Si - O - O \bullet$. [43] Although this is a particularly strong correlation, there is still the possibility that it is not a true one, that there are other less obvious processes that are actually responsible for the production of the features. This would also explain why there is no similar correlation between the E′ centres and the 5.85 eV absorption band.

Pfeffer [26] shows plots of the 215 nm (5.85 eV) and 245 nm (5.0 eV) bands. The 5.85 eV band is that associated with the E′ centre and the 5.0 eV band is that associated with the B_2 centres. The graphs show results for both heavy ions and proton irradiation. For the lighter proton bombardment, the amplitude of the E′ band is much greater than either the B_2 band or for the heavy ion irradiation. For 1 MeV electron bombardment, there is virtually no B_2 band, so these results do confirm a correlation between displacement damage and the strength of the B_2 band. However, the doses given to the samples were designed to produce the same number of displacements per lattice atom. So if there is a dependency, it is not a simple one.

In a similar experiment, samples were exposed to heavy ions and then protons. This experiment found that the proton irradiation actually reduced the strength of the B_2 band. This has led to the supposition that there is some form of chemical annealing by the implanted protons. A similar double exposure using inert He^+ ions instead of protons produced a similar, but less dramatic, annealing effect. This suggests the possibility of a radiation annealing mechanism.

These results have led to the suggestion that the B_2 band is due to the existence of the (diamagnetic) neutral oxygen vacancy ($\equiv Si:Si \equiv$), the site that then goes on to develop into the E'_γ centre. Thus it is to be expected that the electron rearrangement caused by ionising radiation (including protons and helium ions) would create E′ centres at the expense of B_2 centres. It has also been noted that there is a correlation between the 173 nm (7.2 eV) band and the 245 nm (5.0 eV) B_2 band. This has led to the suggestion that these could be different optical transitions of the same defect.

4.6.2 Annealing

Generally, most radiation effects are due to competition between the rate of production of defects, and their rate of annealing. There are believed to be three main annealing processes; *thermal annealing, radiation annealing,* and *photobleaching.*

If thermal annealing were the only process at work, then under steady irradiation, the growth of defects would saturate at a value that is a function of both temperature and dose rate. Studies of a-SiO_2 at both high total dose and high dose rates have shown that a radiation annealing effect is apparent. This occurred at a dose rate in excess of 0.4 Mrad s^{-1} (0.4×10^4 Gy). [44]

Photobleaching has been observed in glasses for a number of years, but is really a primary interest in fibre optics. [45,46]

4.7 Previous Experiments on Radiation Effects in Optical Materials

Most of the papers mentioned so far deal with the basics of the damage mechanisms in optical crystals and glasses. This Section deals with previous research papers covering areas of interest to this project and is intended to outline the research and theories in these areas, and is not exhaustive.

Within the space environment, the effects of radiation exposure concerning the XMM-OM project have already been contemplated by Bellis. [47]. He anticipates an effect on both the transmission and refractive index of the fibre optic taper that it used for coupling the image intensifier to the CCD camera in the MIC detector (see Figure 1). Extrapolating work by Friebele, [46] he calculated the worst attenuation on the tapers to be no more than 12 dB.

The dose that an instrument will receive in space is highly dependent upon both its orbit and altitude. Using general orbit parameters, a number of groups have simulated the effect of the space environment.

Blue and Roberts [48] illustrated one interesting aspect of this research. During work on the NASA Long-Duration Exposure Facility (LDEF, deployed in orbit April 1984), they exposed nine narrowband, broadband and neutral density optical filters to the equivalent of six years in space. Overall, they found that the general transmittance was decreased in most filters. They also found that narrowband filters shielded by aluminium survived far better than those exposed directly to space radiation.

In narrowband filters exposed openly to radiation, they found that the narrow centre band was not only broadened, but that the centre frequency was shifted. They also found shielding mirrors to be beneficial. They also found that a shielded neutral density filter was virtually unaffected, but that an exposed filter showed an increase in transmission. Even so, the actual exposure levels were relatively low. For unshielded samples, the total dose was < 3 kGy. In orbit, this dose would be primarily made up of trapped geocoronal electrons, a few protons also being incident.

In another study, Nicoletta and Eubanks [49] based their results on a simulation of an 1100 km circular polar orbit with a one year duration. They measured the change in the properties of several optical materials over the range of 200 nm to 3400 nm (0.2 μm to 3.4 μm). To do this, they modelled the space environment by substituting the power spectrum of space electrons and protons with one made up from a reduced range of energies. The energy of the electrons used was 0.3, 0.5, 1.0 and 1.5 MeV, and that of the protons was 0.5, 1.5 and 2.0 MeV. To help simulate the environment, they also adjusted the fluence of the particles. For their work, the maximum electron fluence they used was 7.3×10^{12} e cm^{-2} with energy of 0.5 MeV. The maximum proton fluence used was 3.8×10^{11} p^+ cm^{-2} with energy of 0.5 MeV.

Grillot and Rosenberg [50] carried out a similar study. In their experiment, samples of Schott BG-39 and Hoya CM-500 blue-green filter glasses were subjected exclusively to proton irradiation. They chose to only use protons on the premise that there was a significant pool of information concerning the effects of gamma rays and electrons, but very little concerning protons.

They integrated the equivalent flux of three years exposure of protons using a range of energies from 0.5 MeV up to 400 MeV. The use of such highly energetic protons had two benefits. Firstly, they are energy levels that are rarely addressed in optical experiments. Secondly, they allow samples to be placed outside the proton facility, the energy being more than sufficient to pass through a thin aluminium sheet needed to maintain a vacuum. This second advantage allowed them to change the filters easily in an adjacent laboratory, rather than within the chamber.

They found that 2.7 MeV protons had a negligible effect in optical transmittance up to fluences of 5.2×10^{14} p^+ cm^{-2}. They also found that the different samples showed differing levels of radiation tolerance. When exposed to 63 MeV protons (with a fluence of 5.3×10^{12} p^+ cm^{-2}) the Hoya samples showed only a negligible loss in transmission, whereas the Schott filters showed a significant reduction in transmission.

One important point noted is that the sample thickness is of prime importance. The thicker the sample, the more energy will be deposited during its exposure to radiation and this could be significant.

The fluences that could be expected during a mission are linked to the choice of orbit. In his paper, Daly [51] runs through a justification of the XMM orbit, and through several different scenarios. He calculates the expected proton fluence to be in the range of 10^8 p^+ cm^{-2} over its 10 year mission lifetime. However, this paper highlights an inherent problem in these forms of calculations. Although it is possible to estimate the fluence, the solar proton flux is not a constant one. Daly suggests that the maximum proton fluence could be of the order of 48×10^6 p^+ cm^{-2} $year^{-1}$. However, even this figure could be very inaccurate. Estimates for the solar maximum at the peak of the 11 year cycle estimate a proton fluence of 195×10^6 p^+ cm^{-2} $(5\ year)^{-1}$. One reassuring conclusion from this report is that the charged particle fluences are at a maximum just after the launch. Over time, a number of factors such as the Solar activity cycle will cause the fluences to fall, reducing their adverse effects.

Cole Smith *et al.* [52] highlight another problem associated with proton irradiation. UV windows have been known to fluoresce due to impacting protons, and the paper quotes examples of fluorescence in the South Atlantic Anomaly (SAA).

This is a region to the east of the southern tip of the South American landmass at an altitude of about 250 miles. Cole Smith investigated this area, as the orbit of the Hubble Space Telescope (HST) would pass through this region. On board the HST, it had been proposed to use Digicon solid-state detectors. Cole Smith's paper reported on experiments using protons over the range of 2 MeV to 400 MeV, with a maximum fluence at 60 MeV to evaluate the response of the detector. Although this paper was primarily concerned with effects of proton irradiation on solid-state detectors, the physical process are the same as with optics.

Calculating the radiation levels associated with space orbits is not a straightforward matter. Danner [53] used a number of models in an attempt to determine the charged particle induced background expected on XMM. This analysis assumed that although there are a number of sources of charged particles in an Earth orbit, there are only three that are of major significance. These are:

- Trapped radiation (Van Allen) belts
- Solar protons
- Cosmic rays.

Most of the data used was drawn from the International Sun Earth Explorer (ISEE) satellites, ISEE 1 and ISEE 2.

The two ranges of data that were addresses were 10 keV electrons and 8 to 200 keV electrons. After considering the electron behaviour, the resulting count rate was calculated as 1.6×10^{-3} counts per arcmin^2 per second. However, even though the paper carried out a thorough investigation, the results were incomplete. It seems that the more research looks into this problem, the more it highlights how much information is missing.

A paper published by ESA [54] covers the generation of colour centres with respect to optical media. Primarily concerned with windows, lenses and coatings, it also overlaps into optical fibres. The path lengths it considers vary over a range of magnitudes, from a few μm in coatings through to a few centimetres in lenses. It translates the level at which radiation induced attenuation becomes significant into a number of absorption units. These are given in Table 8.

Induced Attenuation	Critical Value
Absorption	10%
	1 dB where $dB = 20\log\left(\frac{A_1}{A_2}\right)$
Loss Rate	1 dB mm^{-1} or 10^6 dB km^{-1}
Optical Density	0.1
Absorption Coefficient	0.2303 cm^{-1}
Transmission	90%
	Assuming 100% initially

Table 8. Critical values of absorption units for different media. [54]

This paper highlighted that radiation induced absorption is more significant at the blue end of the spectrum when compared with the red. For silicate glasses, the radiation-induced loss at 400 nm is generally 10 times that at 800 nm. This could have serious consequences for glasses that are used in systems requiring high transmission in the blue.

In the discussion on coatings, the ESA paper stated that the small optical path length in these components reduces the significance of absorption. Generally, it was felt that the performance of optical coatings would not be significantly degraded by nuclear and space environments.

One method of dealing with the problem of discoloration in glasses was to use the less susceptible radiation hardened glasses. [55] It has been observed that comparatively low doses (as little as 10 Gy) can damage unhardened glasses. Even with relatively low power gamma ray energies of 1.25 MeV, these doses are enough to detrimentally affect their properties.

Marker *et al.* [55] noted that the behaviour of the glass is very much composition dependent. They found that for a glass such as BK7 that has boron as a prime constituent, the high neutron capture cross-section makes it unsuitable for use in environments with a high neutron flux. Glasses with lead in their CRN will often have the problem of metallic lead forming unless the lead is well bonded. Overall, the paper concludes that a careful choice of glass is necessary, but straightforward, in these situations.

Another aspect of the effect of radiation is that in its rearrangement of the materials structure, the refractive index may be altered. In experiments with cobalt-60, Malitson *et al.* [56] noted this effect. The doses used were quite high at 10 kGy to 1 MGy (10^6 to 10^8 rad), but a change in refractive index was noted, with a change of $\Delta n = 0.0002$ being reported. Changes were also noted in glasses doped with cerium, but these changes were smaller. One very interesting aspect is that the change at the lower wavelength, 400 nm, was nearly four times the value quoted at 1.083 μm.

In another paper based around the effects of space radiation on the HST, Becher *et al.* [57] studied the effect on two halide crystals, lithium fluoride and magnesium fluoride. The main concern of this paper was the spectral degradation in transmittance. To investigate this, they employed a range of radiation tests.

For their proton irradiation, 45, 85 and 600 MeV energy levels were used. For the electron source, they used beta particles emitted from a strontium-90 source, since they are identical to electrons. The thickness of the samples ranged from 1 to 3 mm, and made use of a filter wheel to rotate samples under irradiation without breaking the vacuum. The highest proton fluence recorded was 4×10^3 p^+ cm^{-2}. They noticed that for protons in the 40 and 80 MeV energy range, scattering became important.

To compare different exposures, they gave a figure of energy absorbed per unit volume in MeV cm^{-3}. To test the transmittance of the crystals, three spectral bands were used. These were VUV at 105 to 200 nm, the UV at 200 to 300 nm, and a visible band at 300 to 700 nm. They found that the fluence of the protons was important as only a fluence above 1.1×10^{11} p^+ cm^{-2} caused degradation to the samples.

The paper also noted that protons and electrons also induced phosphorescence in the magnesium fluoride sample. They also noted that 15 days after the irradiation, the sample still displayed some phosphorescence, but much less so. In comparison, lithium fluoride displayed very little phosphorescence.

In a separate phosphorescence study, as well as magnesium fluoride and lithium fluoride, calcium fluoride, strontium fluoride and barium fluoride were used. In this set of experiments, 86, 208, 312 and 600 MeV protons were used. This also allowed them to investigate above and below the Cerenkov threshold. For magnesium fluoride this is at ~375 MeV, and for lithium fluoride it is at ~263 MeV.

They ran tests at a fluence of 10^4 p^+ cm^{-2} s^{-1}, to simulate the SAA. They concluded that there is a relationship of luminescence $\propto$ bombardment energy. They also found that lithium fluoride was more susceptible to luminescence than magnesium fluoride, and that in turn these were about fifty times less sensitive than the other samples.

Musikant and Malloy [9] highlighted another form of degradation. In their paper they considered the effect of a low Earth orbit ($\approx$400 km) on a space-borne system. Although they addressed some of the previously mentioned problems, they were more concerned with the effects that, for example electrostatic build-up, space debris and thermal cycling could introduce into the system.

One aspect of radiation damage they addressed was the effect of atomic oxygen from the earth's upper atmosphere on coatings, especially those such as diamond and magnesium fluoride. The paper also mentioned other coatings that are resistant and gave a good account of why the space environment can be so hostile.

Returning to radiation induced transmission loss in optical materials, Pellicori *et al.*, presented results for a number of materials. [13] They covered seven groups of optical materials; Clear glasses, blue filter glasses, red filter glasses, birefringent crystals, glass optical fibres, plastic optical fibres and silica optical fibres.

They subjected their samples to a range of total doses, and noted the resultant effects over a range of 400 to 900 nm. They used 10 MeV electrons with doses between 1 Gy and 10 kGy (10^2 and 10^6 rad), and cobalt-60 gamma rays with doses of 0.1 and 1 kGy (10^4 and 10^5 rad). They included both magnesium fluoride and sapphire in their experiments on birefringent crystals. For magnesium fluoride they found that gamma irradiation produced degradation in the transmittance, with the degradation $\propto$ dose.

However, they found that electron irradiation did not produce a measurable change in the chosen range. The electron irradiation did, however, produce absorption bands at 260 and 367 nm. The sapphire was only exposed to gamma irradiation, but it did show some spectral degradation, the magnitude of which was greater than for the magnesium fluoride at the same doses.

In summary, there appears to have been little research carried out on this subject area at the shorter wavelengths with the red and IR regions of the electromagnetic spectrum covered to a far greater degree than the VUV. The papers also highlight how we are still developing our knowledge about the environment that surrounds Earth and that the dose a material receives is very much dependent upon its orbit, shielding and lifetime.

5 Experimental Procedure

The combination of the XMM background of dose and materials and the review of radiation and radiation effects gave the project the parameters required to begin constructing an experiment to expose optical materials to ionising radiation.

5.1 Experimental Objectives

The objective of the experiment was to quantify the effect of radiation on the transmission of the selected materials (Section 2.1): sapphire, magnesium fluoride and two types of Schott glass, BK7 and F2. Although the XMM specification provided a maximum radiation dose of 100 krad and a range of 160 to 550 nm, it was decided that to extend the usefulness of the project irradiation up to 30 Mrad should be undertaken and spectra would be measured from 115 to 840 nm (using the full capability of the MSSL spectrophotometer.) Up to this level, it was decided that measurements should be made at 10 irradiation levels. These points were:

1, 3, 10, 30, 100 and 300 krad

1, 3, 10 and 30 Mrad

By shielding half the face of the samples with a HVL of lead (see 3.6.4), this effectively doubled the number of levels. Initially the samples for each material had to be prepared. This involved grinding and polishing each of the samples and techniques for carrying this out had to be developed and are described in Section 5.3.

By encompassing such a wide range, it was conceivable that the data could be applied more widely if future missions in the space environment became longer in duration, or were sent to more extreme areas (for example, near to Jupiter) the data would still be useful. It would also be in line with some of the previous work that had exposed work to the Mrad level. [13]

Prior to irradiation, initial baseline measurements on the transmission of each sample were to be made over the wavelength range from 115 nm to 840 nm. Irradiation then took place at Harwell and, in advance, a planned programme for this had to be developed. Initially, the radiation source had to be selected and it was decided that cobalt-60 should be employed. Gamma rays were chosen as irradiation could be carried out with relative ease using the facilities that were available, and by referring to the Q values (Section 3.5.2) this work could be related to other forms of radiation.

Gamma rays are the hardest form of radiation to stop, being exponentially attenuated as they pass through a medium and the experiment had to designed to accommodate this. At Harwell, the radiation sources were housed in isolated rooms (or cells) and the radiation dosage was dependent upon the distance of the sample from the source. Hence, with a cell full of samples, the distances of each sample from the source had to be calculated to arrive at the correct dosage. It was also decided that, during irradiation, dosimeters should be employed for confirming the radiation dose received by each sample.

With the experimental plan complete, holders for mounting the samples in the cell had to be designed and manufactured.

After irradiation the change in transmission for each sample was measured and then compared against the original value.

It should be mentioned here that, at the outset of the project, the intention had been to measure changes in refractive index as well as transmission. Although this component was not completed, the design of the experiment included facilities to measure such changes. It was assumed that each sample was, independently, of a uniform structure and a lead mask was manufactured that covered half of the face of each sample. This mask, manufactured of lead, was designed to halve the dose received by the covered area. Then the intention had been to measure refractive index change by using ratio of the changes in the unmasked and masked areas.

The following subsections go into the detail of the experimental procedures.

5.2 Material Selection

Sapphire (Al_2O_3) and magnesium fluoride (MgF_2) are relatively common materials, which helped in getting samples from a varied range of suppliers. The sapphire was relatively cheap to purchase. Magnesium fluoride is not so widely used, and so was sold at a premium. In comparison, the Schott BK7 and F2 are widely available.

It was possible to buy these materials cut and polished to order, but due to constraints in the amount of funds available to the project, the unpolished costs were obtained for in-house preparation.

5.3 Sample Preparation

To define what dimensions the samples would need, it was necessary to consider what was going to happen to them in the process of the project. The main parameter that was to be measured was the effect of radiation on the transmission of light. The next parameter was to be any change in refractive index due to radiation effects.

The first limitation was the transmission measurements. This work was due to be carried out on using a monochrometer on loan from the Mullard Space Science Laboratory. This unit contained both a deuterium and tungsten lamp for providing light all sealed in a vacuum unit. This source provided light down to below the Ly_α emission feature at 121.6 nm and provided a continuum from 115 to 370 nm with several distinct emission lines to allow accurate calibration of the data. Above this wavelength, a tungsten lamp can be used to provide light.

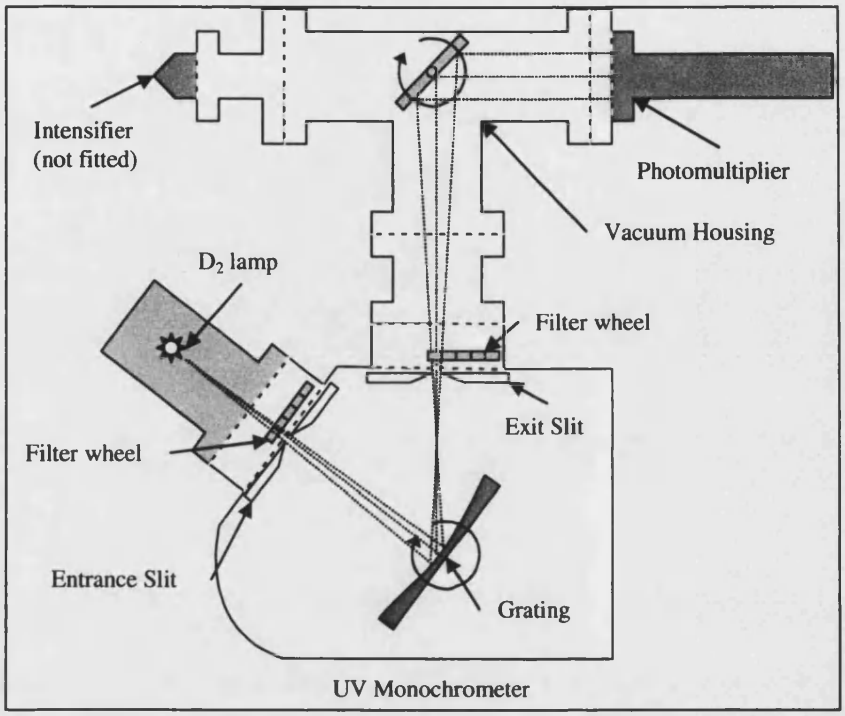

Figure 7. Schematic of UV monochrometer showing path from deuterium lamp to photomultiplier tube, with entrance and exit slits and filter wheels. The filter wheel on the exit slit was used to hold the samples.

The light from these two sources was collimated through a filter wheel before the entrance slit which held several filters to allow for wavelength calibration. The light was then directed toward a reflection grating and the subsequent reflected spectrum collimated toward a photomultiplier tube. The grating took the incident beam, and spread it out into a spectrum. By changing the angle of incidence from the UV beam to the grating, it was possible to alter the wavelength of reflected light incident on the exit slit. The light passing this slit was then collimated through the filter wheel on the exit slit held up to seven samples for pre- or post-irradiation measurement. The basic layout of the monochrometer is shown in Figure 7.

The apertures in each filter wheel were ≈13 mm diameter and just over 10 mm deep. To fit in this unit, the samples needed to be 12.5 mm diameter and 10 mm long. Another consideration was the surface finish of the samples. To allow us to measure the slightest change in transmission, the faces of the samples would need to be polished to a high finish.

The next stage was to have been refractive index work. SIRA had an industrial interferometer that could measure the index of a sample at the wavelength of its internal laser. However, to be able to measure this accurately, both faces of each sample would need to be nearly parallel. These two constraints on the faces being polished to a high finish and needing to be close to parallel increased the prices of the samples.

The Optical Science Laboratory (OSL) at UCL has facilities for polishing quite large pieces of glass. Dave Brooks was the group member who manufactured the OSL optical components, with a broad experience in creating and polishing mirrors, off-axis paraboloids and various other optical components.

When approached for advice on preparing the samples in-house, he was very positive about the idea. Although his area of experience and expertise was with large diameter samples, he was confident that they could be prepared in the OSL optical workshop.

Due to the financial constraints on the project, the decision was made to buy the samples unpolished and prepare them at UCL.

5.3.1 In-House Preparation

This area of the project began in March 1994 when the glass samples were used to test out the method for preparing small optical samples. These were the cheapest of the samples, and more importantly, the easiest to replace if something was to go wrong. The method adopted was in theory a fairly simple process. In practice it was not as straightforward as at first anticipated.

Rather than prepare each sample individually, the idea was to lock them into a single unit that could be prepare all the samples en masse. This first attempt involved using petroleum jelly to fix the samples to an optical flat (a 750 mm × 750 mm × 40 mm glass plate with a surface level to a very high tolerance). An aluminium ring was then turned down with a lathe to the 12.5 mm height of the samples and then set round these samples, and a mixture of plaster of Paris was poured into the ring. This was then left overnight to harden.

Once the samples were set in place, the whole unit could be ground and polished at once. Between each stage of the grinding, it was necessary to rinse and clean all the samples and the ring. To prevent the water from damaging the plaster, it was painted with a thin layer of shellac to make it watertight. A section through the edge of the first ring is shown in Figure 8.

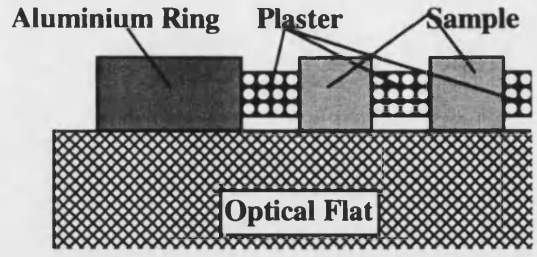

Figure 8. Sample preparation with aluminium ring only, with aluminium flush to the optical flat mounting.

The process of actually preparing the faces of the samples can be considered in two stages. The first stage is simply a grinding operation to smooth down the faces to an even flatness and course finish and prepare them for the second stage. This was done by using differing grades of carborundum powder. The second was the actual polishing using cerium oxide.

5.3.2 Preparing the Samples

At the beginning of the grinding stage, a very coarse grade of carborundum was used which quickly brought the surfaces down quite quickly. After being abraded by carborundum, the surface began to look like frosted glass. When the surface had an even texture, the samples' faces were all evenly finished and the unit was rinsed and washed down. The process was then repeated with finer grades of carborundum until the finest grade had been used. The initial grade of carborundum utilised was a very coarse 200 grade, rising through 400, 800, 1600 to the finest grade used, 3200.

However, this method did not even get to grade 400. The problem was that aluminium is a soft metal and the ring was worn down in preference to the glass samples. To get around this, the aluminium ring was turned down on a lathe to a reduced thickness and glass wasters were affixed to the ring. These wasters were small soda-glass squares about 2 mm thick and were used as they had a smaller total area in contact with the carborundum than the aluminium ring and were of a comparable hardness to the samples. In the process of removing the samples after grinding, it was found that the plaster had set so hard that three samples were damaged during extraction. To get around this, lime was added to soften the plaster mix to in an attempt to reduce the problem.

Another problem was that the samples were chipping around the edge during the grinding causing significant scratching. This was because the edge of the samples had been simply cut square by the suppliers. To overcome this, each sample was chamfered by hand with a diamond file. The chamfered samples and glass wasters are shown in Figure 9.

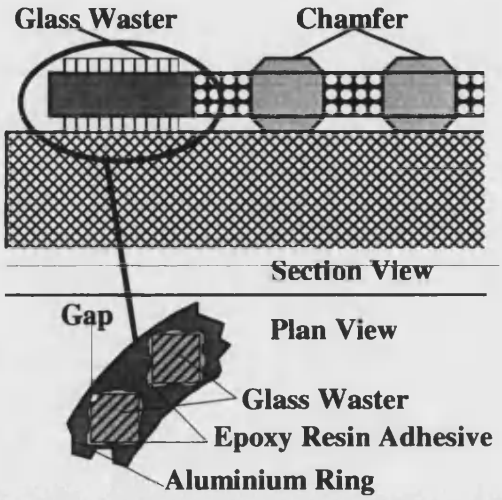

Figure 9. Sample preparation with aluminium ring and glass waster. This also shows the problem of a small air gap beneath a waster where carborundum could be trapped.

When the process of grinding the faces began a new problem was introduced by the wasters. These had to be stuck carefully to the ring so the adhesive would cover all the underside of the waster. However, occasionally a small gap could be formed between the lower surface of the waster and the aluminium ring. This problem initially manifested itself by trapping a coarse grade of carborundum and releasing it later when a finer grade was being used. These liberated coarse grains would scratch the surface and necessitated going back to the 200 grade carborundum and starting again.

A second problem related to incomplete epoxy cover. The possibility existed that if the epoxy did not completely cover the underside of the waster, an edge of glass could be left exposed. This small edge could break during the grinding or polishing and again scratch the samples and forcing the process to restart with coarse carborundum. Additionally the glue that was extruded around the edge had to be smoothed as surplus glue with a rough texture could also trap carborundum, though careful application overcame this issue.

The next problem addressed was the somewhat excessive enthusiasm of the plaster to hold the samples in place. To overcome this problem, a number of test mixes were made with differing compositions of plaster and lime. At the extreme, there is the hard option of 100% plaster and the soft, brittle, 100% lime.

The plaster used here was gypsum (plaster of Paris), a form of calcium sulphate. The lime used was hydrated (slaked) lime. This is calcium hydroxide which is made by reacting quicklime (calcium oxide) with water and is used in making mortar and fertiliser.

By experimenting with various ratios of plaster and lime it was found that a 1:1 plaster:lime mix provided reasonable strength whilst being easy to remove after submersion in warm water.

Petroleum jelly of uniform thickness was used to bond the samples to a large optical flat. This jelly was heated to a thick viscous fluid and poured into the ring to form a 1 mm layer. Over this, the 1:1 mix was poured to a depth of about 6.5 mm. When the samples were pushed in, the petroleum jelly they displaced pushed up the average depth to the desired 2 mm. This is shown in Figure 10.

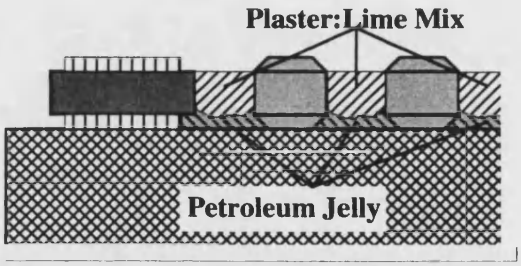

Figure 10. Using petroleum jelly to set samples in position and hold the plaster:lime mix away from the sample faces.

However, the displacement of the petroleum jelly caused a problem. The insertion of the samples forced petroleum jelly up the side of the aluminium ring and up between the samples. This weakened both the bond between compound and ring, and the structure of the central block of plaster. This is shown in Figure 11.

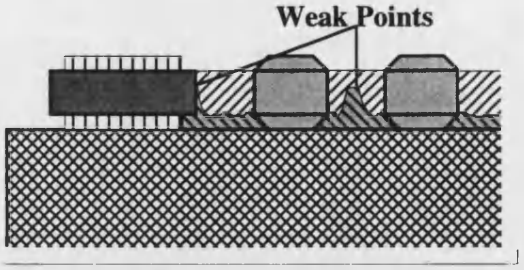

Figure 11. Weak points in compound mixes caused by extruded petroleum jelly. Weak spots between the plaster and the aluminium ring and could cause the whole central section to come away as one block and weak spots between samples could cause the plaster to fail and a smaller section to come loose.

To get around this, the setting was modified using make use of combination of warm and cool petroleum jelly. Initially, a thin layer (less than the thickness of the wasters) of cool petroleum jelly was smeared onto the flat. The ring was then pushed into this and a layer of molten petroleum jelly built up around the inside edge. A small paintbrush was used to help fill the gaps where the jelly could leak past the wasters. Care was taken to ensure that none of the petroleum jelly got onto the inside edge of the aluminium ring or weakening could occur.

Once this was completed, the samples were carefully pushed into the thin cool petroleum jelly layer to bond them to the flat. The molten petroleum jelly was then carefully poured around them trying to avoiding any single build up of petroleum jelly forming a weak spot.

Even so, there were still problems with weak spots and uneven petroleum jelly distribution. This led to the further, more labour intensive revision. To ensure that the rings and samples were free from petroleum jelly, white spirit was used to scrub them clean. Again the optical flat was prepared with a thin layer of petroleum jelly, and the ring set into this. Around the edge of the ring, a small layer of petroleum jelly was built up to form a seal. The samples were then pushed into the thin petroleum jelly layer and left while the jelly cooled. The compound was then poured in around the samples. Finally, a method that worked had been arrived at.

The petroleum jelly served three purposes. Firstly, it stopped the compound bonding with the optical flat. Secondly it made releasing the ring and samples easier once the plaster had set. Finally, it held the samples tight to the surfaces to stop them moving when the mix was poured in between them. This is shown in Figure 12.

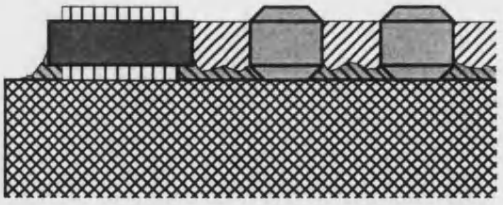

Figure 12. Final method of sample setting showing an even layer of plaster:lime mix.

Now another problem introduced itself: Although the optimum ratio of plaster to lime had been established, there was a question over how fluid the compound should be when poured? Too much water and it would settle and take days to solidify. Too thick and it would not flow around the samples and would leave gaps. Of the two options, it was better to err on the side of too much water. Over a period of hours, the compound separates with the excess water settling on top of the compound. This can then be removed with a paper towel. The compound then needs to be topped up. This extends the amounts of time it takes to prepare a set of samples, but is better than removing the ring only to find that the plaster had not set around all the samples.

However, once the mixture had set solid it was found that the problem of separation was worse than anticipated. Not only did the mixture shrink in height, it pulled away from the ring and samples. To fix this, the mixture had to be moistened and pushed down allowing the mixture to regain contact with the edge of the ring and bond to it.

This method seemed to work with the samples and ring being set into one unit. However, the price paid for this was the increase in effort after the mixture had set. As can be seen from Figure 12, the mixture was only held away from the optical flat by a thin layer of petroleum jelly. The unit could be released easily enough, but the mixture was now too near the faces of the samples. Before going any further, the mixture had to be scraped down with the end of a fine file, almost chiselling the mixture out.

Finally, the disk unit was ready. The mixture had been slowly worked away from the samples and was of a generally even thickness, about the same thickness as the aluminium ring. As before, to protect the mixture from water that would weaken it, it was painted with a thin layer of shellac. Left to dry overnight, next morning the unit was ready to be worked. An image of a large and small sample ring prior to the upper surface being scraped away is shown in Figure 13.

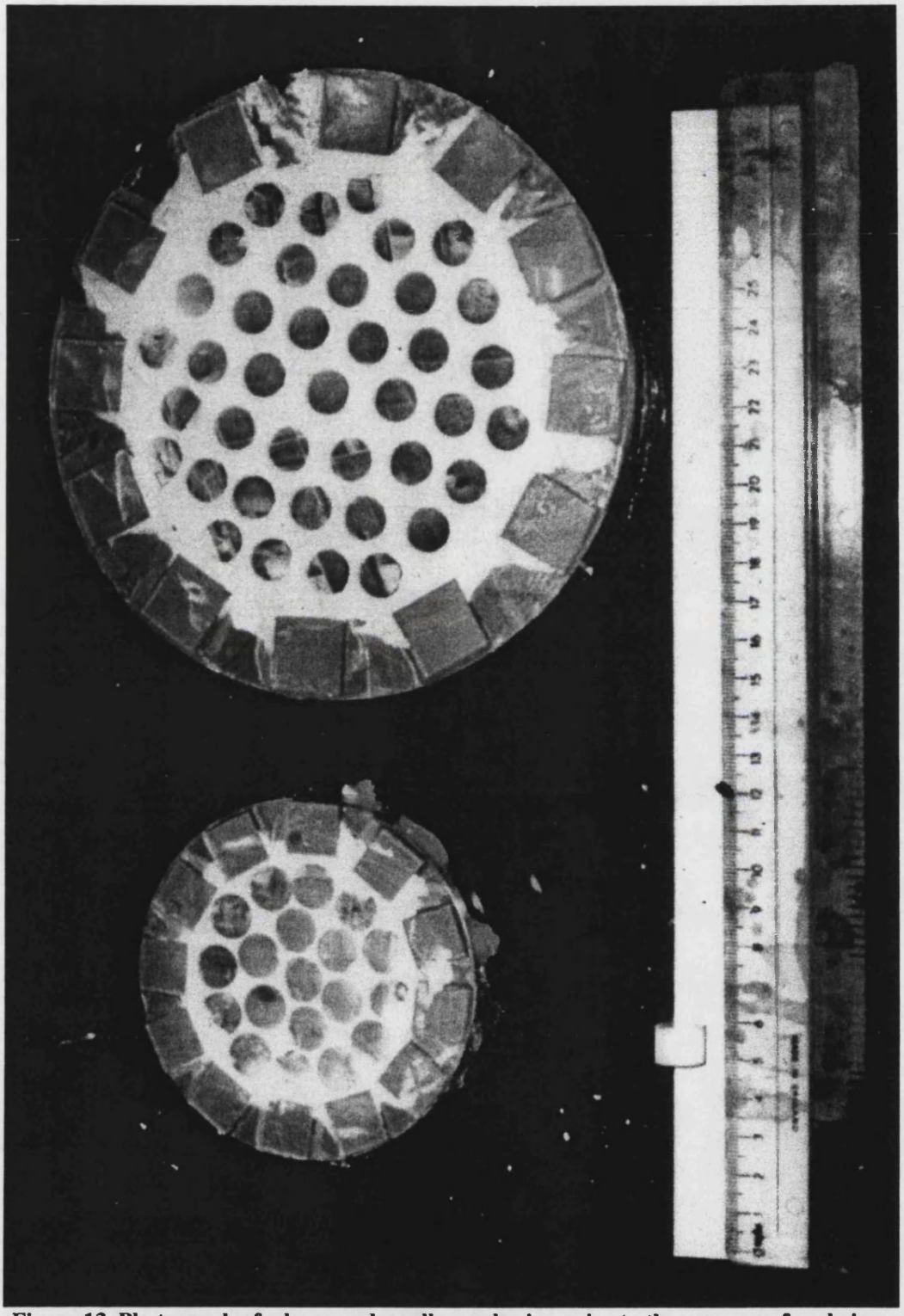

Figure 13. Photograph of a large and small sample ring prior to the upper surface being scoured away and coated with shellac. A single glass sample can be seen in the lower right of the image.

5.3.3 Grinding Down the Samples

Even though the sample unit was quite sturdy, there was still a chance that the area at the centre of the mixture could flex during the grinding process. To prevent this, and to make it easier to work, a Pyrex blank was found that had a similar diameter as the aluminium ring. The blank was warmed in a small laboratory oven and small pieces of beeswax were then sprinkled over it and melted to form a uniform layer. A small hair-drier was used to help keep the wax soft and the blank warm. The sample unit was then placed square on top, and pushed down to form a tight seal with the wax. The wax solidified quite quickly. Around the edge of the ring, warm wax was pushed in to form a seal. This was to help avoid any problems with trapped carborundum.

Now the samples could be worked against a large flat glass disk that was mounted on a turntable. The carborundum was kept in a powdered form, but was mixed with water before use to form a paste. This was then spread over the face of the large glass disk. To minimise the risk of contamination, each grade of carborundum was kept in a separate bag with its own container, brush and water bottle.

As the turntable revolved slowly, the mixture of carborundum and water was brushed over the surface of the glass disk. Only a small amount was needed to cover the surface. Still revolving, the blank with the samples was placed face down so the samples were now in contact with the glass disk. By slowly working the blank back and forth, and slowly rotating it, the faces of the samples were worked by the carborundum. This is shown in the Figure 14.

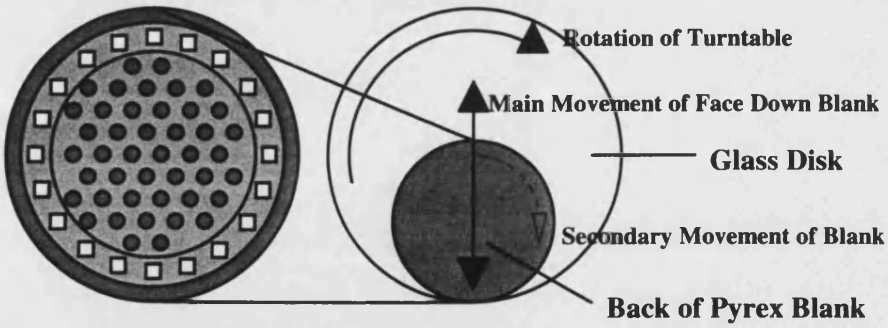

Figure 14. Grinding the samples on the flat glass disk showing the layout of the sample holder, and direction of rotation against a turntable.

After a few minutes, the surfaces of the samples were rinsed off and inspected. If all samples had an even texture then they had all been evenly abraded by the carborundum. If not, they needed to be worked further at that grade of carborundum. Only once all the samples had an even finish could the unit be rinsed off and the next grade of carborundum used.

The coarsest grade was 200 and was used initially to bring the surfaces to an even finish. Once all the samples did have an even texture, the blank had to be completely rinsed off. Whenever the unit was rinsed it was vital to remove all traces of the previous grade of carborundum. Once clean, the unit was put to one side and dried off. Next, the turntable was dismantled and rinsed thoroughly. Only once all traces of the carborundum were removed was it time to use the next grade.

Some of the subsequent grades were used for a relatively long time. The problem here was the carborundum drying out and it was necessary to add a small amount of water regularly as dry carborundum has little abrasive quality.

This process was repeated through the differing grades of carborundum until the finest grade had been used and it was time to begin polishing.

5.4 Polishing the Samples

Before polishing could begin, a pitch lap had to be prepared. This was a round disc with pitch mounted on its surface and was of similar dimensions to the sample unit. It had grooves cut into the surface to help in the polishing and to prepare it, it had to be flattened. This was done by compressing it against an optical flat and leaving it with some weight on it. To stop it locking to the flat glass, talc was dusted over its surface.

After about ten minutes, the flat and pitch lap were separated. The lap was placed on the turntable and cerium oxide (mixed with water) was poured onto it. The blank was then drawn back and forth, being slowly rotated, as the lap turned beneath it as is shown in Figure 15.

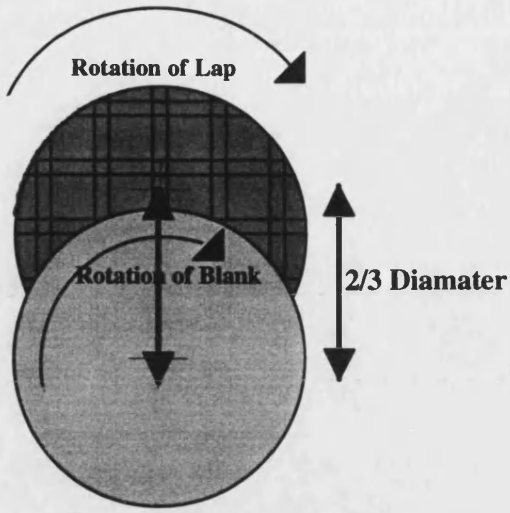

Figure 15. Polishing on the lap

After a short time, the lap would start to become convex and the samples concave. By swapping the lap and blank over every few minutes, this was levelled out. In effect, the samples were being made into a concave surface of infinite radius, i.e. flat.

To test the flatness of the samples, a sodium lamp and an optical flat were used to produce interference fringes. The flat was placed over the samples and the fringes could be easily seen across the samples. This gave a quick and ready guide to how the work was progressing, and if there were any areas that were not being worked. In addition, a spherometer was used to calculate the deviation of any problem areas. Typical fringes are shown in Figure 16. It was believed that for the study of the refractive index, it was necessary to have the surface flat to 1 fringe.

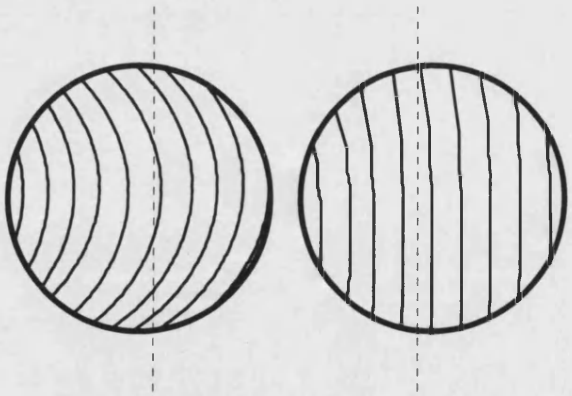

Surface accurate to 3 fringes **Surface accurate to within 1 fringe**

Figure 16. Testing flatness with fringes. The surface is said to be flat to 1 fringe if the interference bands produced by it are almost parallel.

The process of polishing involved continually removing the blank and testing the samples. The usual length of a polishing run was 5 to 15 minutes. At this point, the blank and lap were removed and cleaned. The lap was dusted with talc and pressed against the flat, and the samples were tested for flatness.

Although some limited success was obtained, the results were fairly poor in quality. They were still suitable for use, but it was decided that given the lack of time available the work should be contracted out to a professional company.

5.4.1 Outside Contract Work

After some negotiation, Merck Ltd. agreed to polish the remaining samples. This was fortunate since they had already been chamfered in preparation for our work.

The final cost of the outside work was £150 for each batch of approximately 35 samples of the same material. A 10% discount was negotiated, but even so, it was still quite expensive.

The batches sent to Merck were:

Material	Subgroup	Total
Glass	BK7	37
	BK7 G18	39
	F2	36
	F2 G12	39
Sapphire	Merck	36
Magnesium fluoride	Howes & Zeiss	15+20

Table 9. Samples sent for external polishing.

All the samples were returned parallel and flat to within 1 fringe.

5.5 Gamma Irradiation

Table 10 lists some of the properties of the more common sources used in commercial gamma irradiation facilities.

To expand on this, Table 11 lists the attenuation coefficients for 4 media over 4 magnitudes of photon energy.

A further table, Table 12, shows how much lead is required to attenuate a 1 Mrad dose to a minimal level.

The calculations used the exponential law quoted earlier assuming 1 MeV photons and the attenuation coefficient listed in Table 12.

Property	Beta-Gamma emitter		
of source	$^{125}_{53}I$	$^{131}_{53}I$	$^{60}_{27}Co$
Half-life	59.4 days	8.04 days	5.27 years
Beta energy			
Maximum	—	0.606	0.315
Average	0.020	0.188	0.094
Gamma energy			
	0.035	0.28	1.17
	(X-rays: 0.027-0.32)	0.36	1.33
		0.64	
For $^{60}_{27}Co$, each beta disintegration produces a pair of gamma rays			
All energies in MeV			
Gamma half-value layer			
Lead (cm)	0.0037	0.3	1.1
Water (cm)	2.3	5.8	19.0

Table 10. The half-life, beta particle energy, gamma energy and gamma half-value layer for the gamma sources iodine-125, iodine-131 and cobalt 60 used in commercial irradiation facilities.

Table 10 gives a HVL for lead for cobalt-60 as 1.1 cm which implies an absorption coefficient of $\mu = 0.63\ cm^{-1}$.

Gamma energy	$\mu\ cm^{-1}$			
MeV	Water	Iron	Lead	Concrete
0.01	4.99	1354	1453	62.3
0.1	0.168	2.69	59.4	0.400
1	0.071	0.469	0.776	0.150
10	0.022	0.235	0.549	0.054
100	0.017	0.340	1.056	0.055

Table 11. Linear attenuation coefficients for gamma rays over a range of energies.

Start dose (kGy)	End dose (Gy)	Lead (cm)	Start dose (Gy)	End dose (Gy)	Lead (cm)
10	5	12.1	400	5	7.0
7	5	11.5	100	5	4.8
4	5	10.6	70	5	4.2
1	5	8.4	40	5	3.3
0.7	5	7.8	10	5	1.1

Table 12. Maximum shielding requirements for a cobalt-60 gamma source with a linear absorption coefficient of 0.63 cm-1 for initial doses of the range 10 kGy to 40 Gy attenuated down to 5 Gy.

Since complete shielding of the samples for the gamma experiments was not feasible, the solution proposed was to apply a half-value layer of lead, 11 mm thick, and use the ratio of the two sides of the sample for the refractive index work. (Similar values were calculated for electron irradiation, and this is shown in Appendix A.11.)

5.5.1 Gamma Facilities

In many facilities, gamma irradiation is achieved by exposing material in proximity to a cobalt-60 isotope in isolated cells. Due to the restrictions imposed on the possession of radioactive materials, such isotopes are held at specialist facilities. Often these are research centres and have the ability to conduct experiments and to make their facilities available to outside organisations. The facility we approached was the Atomic Energy Authority (AEA) site at Harwell, Oxfordshire.

Within the research groups based at Harwell, the specific group contacted by this project was Harwell Dosimeters Ltd. This was the first branch of the AEA to be privatised. In addition to the irradiation facilities, another advantage of using Harwell was their wealth of experience in running radiation experiments.

The "cells" where the cobalt-60 was housed at Harwell consisted of bunkers built with thick, lead-lined concrete walls grouped around a shielded central pit where the sources were stored when not in use. They were stored below ground level to ensure that in the event of a fire there was no risk of the smoke containing radioactive particles. The sources were driven into and out of the cell by controls on the outside of the cell wall. The layout of the cell utilised is shown in Figure 17.

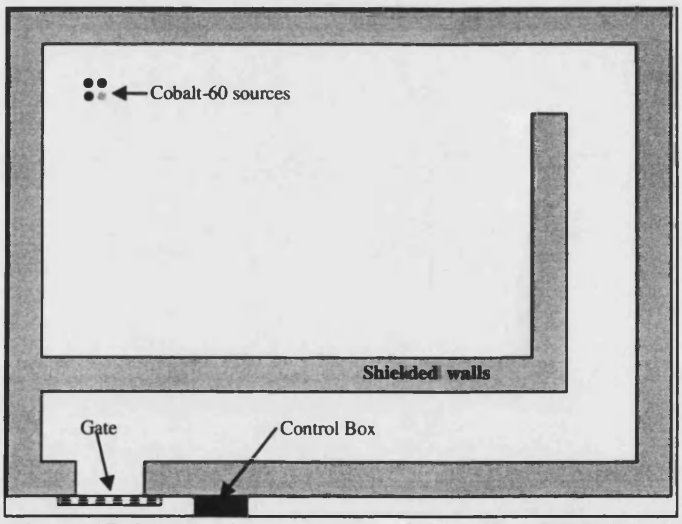

Figure 17. Schematic layout of the Harwell cobalt-60 cell.

The cobalt-60 was driven into the cell through 0.5" diameter metal tubes that ran from the central area to the cells. Each cell had four tubes running from the central pit into a corner of the cell. The isotopes were pulled along these tubes by chains within the tubing. Control panels on the outside of the cells controlled the movement of the sources in and out of the cells. From the control panel, it was possible to bring in up to four radioactive sources, each tube being numbered with a separate control on the panel. It took roughly 30 seconds to a minute for the radioactive sources to be either inserted or withdrawn from the cell. The panel itself was a very straightforward layout, with simple in/out buttons to drive the isotopes from their shielded locations into the cell.

There were strict procedures to ensure safety. The cell doors would not unlock while a source was in place and once a source was retracted, the doors could only be opened after removing a "key" from the control panel. After removal, the door could not be locked until the key was reinserted back in the panel. To ensure that the source had been with withdrawn, on entering the chamber a Geiger counter was held ahead of personnel as they moved toward the source. If the source was still in place, the counter would immediately issue an audible alert. When on-site, personnel had to wear individual dosimeters that were checked on a regular basis. For visiting personnel, the dosimeter was checked after they had finished their work and had left the site.

The particular cell used was *Cobalt Cell 1*, the working area of the floor of the cell was about 3 m by 4 m, the ceiling being around 2 m. Located in one corner of this cell were four 0.5" diameter tubes into which the radioactive sources could be inserted. Up to four sources could be placed in the cell at any one time, though for our experiment, only one was used. Harwell stated in a letter dated 6th April 1995 that the most active source available for that particular cell was a 51 TBq source, and that this level of activity was correct as of that date.

By using this value of activity, it was possible to calculate the dose rate for a sample at a distance from the source using the calculations shown in Section 3.6.1. From these calculations it was possible to find that the dose rate at 1 metre was 2125 rad per hour. To achieve the levels of exposure required (up to 300 kGy) the experiment would involve a lot of stopping and restarting as samples were removed for measuring as they reach the desired dose. The simple manner in which the radioactive sources could be injected or withdrawn from the cell was very useful.

Also at the site was a Pye Unicam 8800 Spectrophotometer. This had a typical range of 190 – 900 nm and was calibrated to a high standard by the staff at Harwell for their own work allowing allow accurate spectra (accurate to ±1 nm) to be obtained. This unit used quartz-halogen and deuterium sources illuminating a holographic grating and did not require a vacuum to operate. The output was recorded via a thermal printer, no electronic output was possible. (For further information, see Appendix A.12.)

For the exposure, it was envisioned that the samples would be grouped together by final dose, and placed into a holder. This sample holder would then be located for the correct time and distance and left to accumulate the required dose. The design of the sample holders is discussed in Section 5.8.

5.5.2 Dosimetry

As well as running the cobalt cells, Harwell Dosimeters also produced a range of disposable dosimeters for their own and for commercial use. These were rectangular strips of plastic 29.8 mm by 10.8 mm by 3.0 mm. To ensure their integrity, each dosimeter was sealed in a small plastic sleeve prior to use to keep it sterile.

There were three types of disposable dosimeter that Harwell Dosimeters produce. The irradiation range they were designed to cover are shown in Table 13.

Type	Range in Gray	Range in rad
Gammachrome Yellow	0.1—3 kGy	0.01—0.3 Mrad
Harwell Amber	1—30 kGy	0.1—3 Mrad
Harwell Red	5—50 kGy	0.5—5 Mrad

Table 13. Irradiation range of disposable dosimeters.

This led to a problem. In the proposed layout of the experiment, the range of doses was to be from 1 krad up to 30 Mrad. The Harwell disposable dosimeters provided full coverage from 10 krad to 5 Mrad, but could not measure directly outside this range.

To work around this issue, advantage was taken of the breaks that would occur when samples were removed samples. For example, it was anticipated that the 10 Mrad sample holder would receive a dose-rate of 160 krad per hour, or 80 krad per hour for the shielded side. This would mean that after approximately 30 hours, the accumulated dose would be approaching the 5 Mrad limit. However, since the longest the samples would be left was for 15 or so hours overnight, dosimeters could be removed before accumulated doses exceeded the dosimeter limits.

With the 30 Mrad unit things were more complex. With anticipated dose rates of 500 and 250 krad per hour, the 5 Mrad limit on the dosimeters would have occurred after 10 and 20 hours respectively. However, by breaking down the intervals into overnight and daytime sessions, this led to exposures with lengths of approximately 5, 17.5, 6, 17.25, 6 and 8.25 hours. Table 14 shows the doses anticipated for these exposure times.

Time	Unshielded Dose		Shielded Dose	
(hrs)	(kGy)	(Mrad)	(kGy)	(Mrad)
5	25	2.5	13	1.25
17.5	*88*	*8.75*	44	4.38
6	30	3.0	15	1.50
17.25	*87*	*8.65*	43	4.31
6	30	3.0	15	1.5
8.25	42	4.15	21	2.08

Table 14. Expected dosimeter exposures.

The italicised numbers are beyond the range of the dosimeters. Although breaking up the exposures made the experiment more complex, it did offer certain advantages. By changing the dosimeters regularly, a continuous record of the shielded dose was gained. By using these numbers to calibrate against the exposed dosimeters with sub-5 Mrad exposures, the exact level of attenuation gained by placing dosimeters behind the shields could be calculated. This would enable us to calculate the dose when the unshielded side is beyond the 5 Mrad limit but the shielded side stays below this limit.

At the other end of the scale, the problem with the 1, 3 and 10 krad units was that there wasn't enough radiation to measure. To overcome this, the dosimeters on these 3 low dose units were left in for the full 60 hours of the exposure in the same location as the exposure took place. It was anticipated that this would allow the holders to accumulate doses on the shielded dosimeters of 15, 18 and 12 krad - within the dosimeter range – and then by dividing the final dose by the total number of hours of exposure, the dose rate per hour could be calculated at the location of the samples. As long as we recorded how long each group of samples was in the cell, we could calculate the total dose for those samples.

5.6 Radiation Exposure Calculations

Once the basic outline of the irradiation plan had been conceived, it was then possible to begin the exact calculations and then design the physical units that would hold the actual samples during irradiation.

The overall plan was to group together the samples into batches that would all be exposed to the same level of radiation. For the lower dose samples, the positioning would be less critical. Based on the previous calculation, the cobalt source would effectively give an exposure of 2125 rad (or 2.125 krad) per hour at a distance of 1 metre. Our requirement was to achieve an integrated exposure of 30 Mrad over 3 days. To achieve this, it would be necessary to position the samples where they could receive a dose of 10 Mrad a day, equivalent to 417 krad per hour. Rearranging Equation 3 gives:

$$r_2 = \sqrt{\frac{D_1 r_1^2}{D_2}} = \sqrt{\frac{2.125\,\text{krad hr}^{-1} \times 1\,\text{m}^2}{417\,\text{krad hr}^{-1}}} = 0.07\,\text{m} \equiv 70\,\text{mm}$$

By assuming that $r_1 = 1$ and that $D_1 = 2.125$ and is constant for the duration of this experiment, if we assume that by careful preparation, we can obtain a placement of the holders to an accuracy of 1 mm, then by propagating the uncertainty on r_2 through this equation we can see that at a distance of 70 mm, the uncertainty on the dose rate σ_{D_2} is 12.391 krad hr^{-1}. (See Appendix B.)

Over a 3 day exposure this could result in an error of 890 krad, or about 3% for a 30 Mrad exposure, which highlights the critical nature of keeping the samples at an exact distance for the high dose exposures.

To expose the samples the project required ten sample holders, one for each of the dose levels listed above. Rather than leave all the samples in for the full 60 hours, it was decided to remove samples through the working day. This would allow the dosimeters on the high dose sample holders to be replaced, and allow the low dose samples to be measured on the Harwell spectrophotometer.

Holder	Final Dose	Time in Cell (hrs)	Dose rate (rad hr^{-1})	r		error for ± 1 mm		
				(m)	(mm)	(rad hr^{-1})	(rad)	(%)
1	30,000	60	500	0.07	65	15	920	3
2	10,000	60	167	0.11	113	3	177	2
3	3000	51.75	58.0	0.19	191	1	31.3	1
4	1000	48.75	20.5	0.32	322	0.1	6.2	0.6
5	300	45.75	6.56	0.57	569	0.02	1.05	0.4
6	100	28.5	3.51	0.78	778	0.01	0.26	0.3
7	30	25.5	1.18	1.34	1344	0.002	0.04	0.15
8	10	22.5	0.44	2.19	2187	0.0004	0.01	0.09
9	3	5	0.60	1.88	1882	0.001	0.003	0.11
10	1	2	0.50	2.06	2062	0.0005	0.001	0.10

Table 15. Dose rate, distance from source and error (assuming 1 mm error) on the dose rate and final dose for the sample holders used in the Harwell gamma cell.

A timetable was drawn up that would allow this process. Starting at 09:00 on day 1, all the sample holders were located in the cell. Two hours later, the 1 krad sample holder was removed, after 5 hours the 3 krad sample holder was removed and so on. This basic plan is shown in Table 15, along with the anticipated uncertainty on the final exposures.

A more detailed time line is shown in Table 16.

Day	Time	Total Hours		Action
		Day	Cumulative	
1	09:00	0:0	0:0	Move all holders into cell and prepare for irradiation
	09:15			Begin Irradiation
	12:00	2:45	2:45	Remove 1 krad samples, leave dosimeters
	12:15			Restart irradiation
	15:15	5:45	5:45	Remove 3 krad samples, leave dosimeters
				30 Mrad: Remove all dosimeters, replace shielded dosimeters
	15:30			Restart irradiation and leave overnight. Finish 08:15
2	09:00	22:30	22:30	Remove 10 krad samples, leave dosimeters
				10 Mrad: Replace all dosimeters and continue
				30 Mrad: Replace all dosimeters and continue
	09:15	0	22:30	Restart irradiation
	12:15	3	25:30	Remove 30 krad unit (unit is dosimeters and samples)
	12:30			Restart irradiation
	15:30	6	28:30	Remove 100 krad unit
				30 Mrad: Remove all dosimeters, replace shielded dosimeters
	15:45			Restart irradiation and leave overnight
3	09:00	23:15	45:45	Remove 300 krad unit
				10 Mrad: Replace all dosimeters and continue
				30 Mrad: Replace all dosimeters and continue
	09:15			Restart irradiation
	12:15	3	48:45	Remove 1 Mrad unit
	12:30			Restart irradiation
	15:30	6	51:45	Remove 3 Mrad unit
				30 Mrad: Replace dosimeters from unshielded side only
	15:45			Restart irradiation
	24:00	14:15	60	End All Irradiation
4	09:00			Remove 1 krad, 3 krad, 10 krad, 10 Mrad and 30 Mrad unit

Table 16. Detailed irradiation timeline for Harwell gamma cell.

5.7 AEA Harwell

The facility at Harwell had spectrophotometers on site. The main role of these machines was to measure transmission of small items used in experiments by the Harwell staff. By designing a small sample holder, it was possible to measure the transmission of the samples after irradiation.

For further work, this facility would be useful for measuring if samples recover exposure over time without any outside influence (see Section 4.5.7.)

5.8 Design of the Sample Holders

With the importance of the sample distance measurement shown above, it was important to design a specific unit capable of holding the samples at an accurate distance. For the lower dose samples, a basic holder could be used that was located with a tape measure. Another issue was that the Harwell spectrophotometer could not accept the samples in their cylindrical form, and so an adapter had to be designed that would allow the unit to accept the samples.

5.8.1 High Dose Sample Holder

In designing the sample holder for the high dose samples, it was critical to mount the samples at an accurate distance from the source. As was stated earlier, the isotopes are set inside 0.5" diameter tubes. Table 15 shows that the 1, 10 and 30 rad sample holders needed to be located within 20 cm of the source. A design was envisioned that used a sheet aluminium baseplate to hold these three sample holders at the correct distance.

Figure 18 shows a schematic of how a sample holder was held at a fixed distance using the aluminium baseplate. The samples were mounted on an aluminium sheet with a 0.5" diameter recess for the tube holding the isotope. The blocks holding the samples were then screwed to the plate at the correct distance.

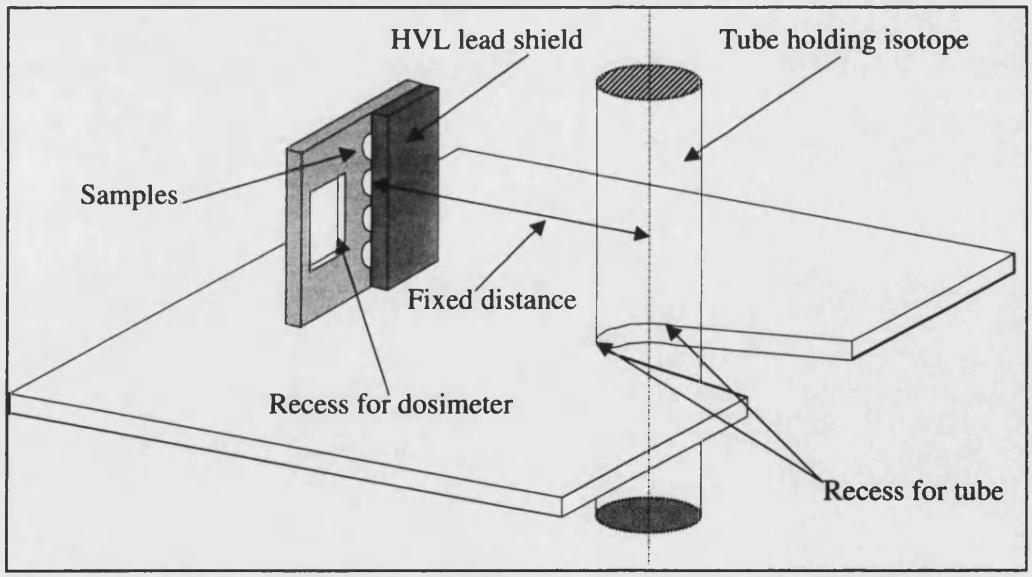

Figure 18. Schematic diagram of an aluminium footprint used to hold a high dose sample holder at the correct distance from an isotope source.

Figure 19 is a photograph showing a plan view of the holder. The 30 Mrad sample holder is fixed is located in the bottom right corner.

Figure 20 is a photograph of the same unit from a lower angle showing the face of the 30 rad sample holder. The spaces for five samples can be seen clearly in the centre of the sample holder.

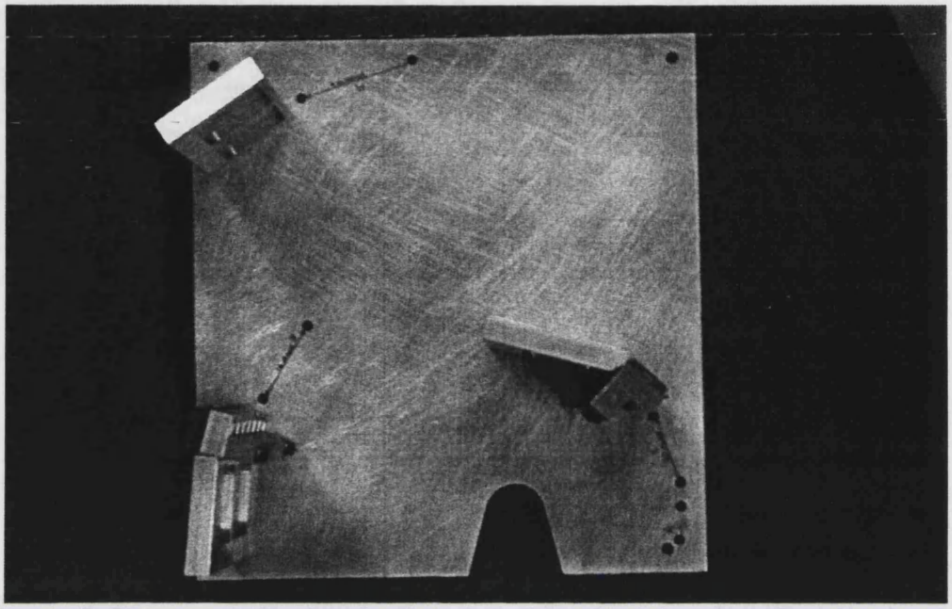

Figure 19. Photograph showing the plan view of the aluminium baseplate showing the location of the 1, 10 and 30 Mrad sample holders.

Half of the face of these units was blanked out with a HVL of lead. To the immediate left of the five holes can be seen a recessed aluminium plate designed to hold the Harwell dosimeters at the same distance as the samples.

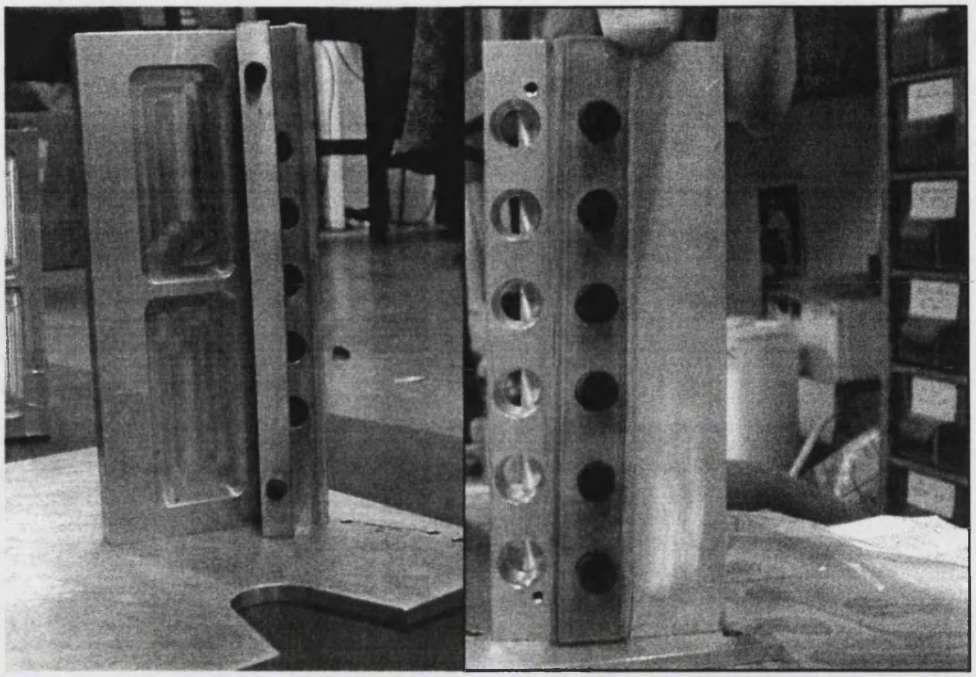

Figure 20. A close up view of the 30 Mrad sample holder. The photograph on the left is a face-on view of the sample holder showing the HVL lead shield across half the sample faces. The right hand photograph is the rear of the sample holder. Inside the sample holder, the recessed edge can be seen. At the rear of the holder is a Perspex strip with soft foam cylinders on to hold the samples in place.

5.8.2 Standard Sample Holder

For the remaining samples, their holders were of a generic design. The distances were not as critical and so were placed out with a steel tape measure. They share a number of similar features to the high dose sample holders in their overall design. Figure 21 is a photograph of two sample holders. The right hand holder shows the HVL shield in place covering 11 samples. The left hand holder shows the shield removed to show the recesses behind it where dosimeters could be located.

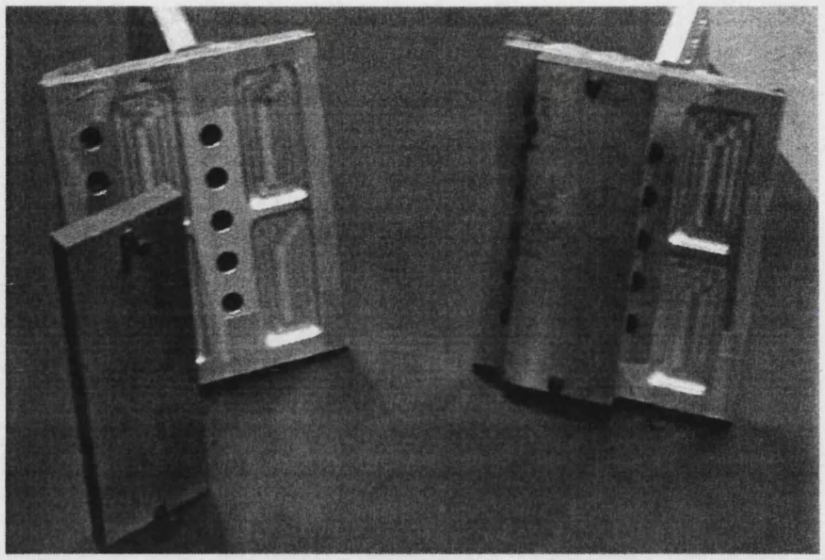

Figure 21. Photograph of two standard sample holders. Each unit was capable of holding up to eleven samples and four dosimeters.

5.8.3 Harwell Spectrophotometer Adapter

Figure 22 shows the holders designed to support the samples in the Harwell monochrometer. The sample is held in by a nylon bolt in the top of the holder

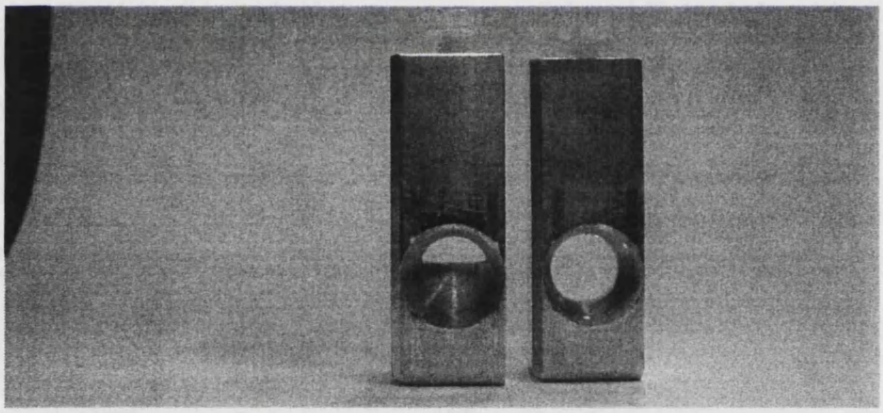

Figure 22. Photograph showing two sample holders for mountings samples for measurement in the Harwell spectrophotometer.

The right-hand holder was for unexposed samples. The left-hand one was for exposed samples so that each half of the face could be analysed. Figure 23 shows the distinct split across the face of a sample of magnesium fluoride exposed to 5 and 10 Mrad. Before the samples were loaded into the holders, the outer edge of the samples were marked to show the shielded and unshielded faces.

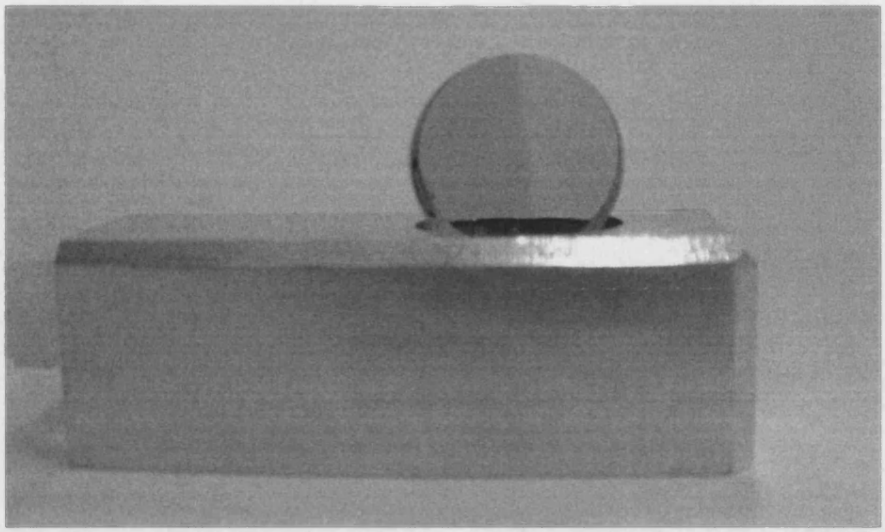

Figure 23. Close up of irradiated sample showing clear deliniation where the HVL shield has attenueted the dose.

5.9 Transmission Measurements

The initial transmission measurements of the samples were made using a vacuum spectrophotometer loaned from Mullard Space Science Laboratory. This was effectively a deuterium lamp emitting UV,

Internally, the grating could be moved through various angles by a software package. The samples could be placed in a wheel that rotated through the collimated beam before it reached the photomultiplier. The configuration of this wheel could again be controlled externally by a PC, and so up to seven samples could be measured without breaking the vacuum seal. This is shown in Figure 7.

The project plan called for the spectrophotometer to carry out multiple runs over the wavelength range of 115 nm to 840 nm to produce high definition spectra of the samples. The deuterium lamp was operated over its range of 115 to 370 nm; beyond this range a tungsten lamp was used. Due to the construction of the unit, it could only be used under vacuum conditions when operating the deuterium lamp. This meant that setting up a single run was a time intensive process.

Once the samples were placed in the necessary carriage and orientated so the light would pass through the irradiated face of the sample, it would be necessary to let the unit's vacuum pumps run overnight to take down the pressure to around 10^{-5} mbar. The next morning, the system could be fired up and exposures taken. In each run, one sample holder position would be left empty to allow the collimated beam to pass through for calibration purposes.

One benefit of carrying out multiple runs is that it would allow the deuterium lamp to settle down and over several runs the data could be combined. The downside was that the work rate meant that about 6 samples could be tested over a 2 day period.

Unfortunately, toward the start of the measurements it was found that the deuterium lamp began to become more and more unstable. In the end, we could no longer have confidence in the output of the lamp. With the amount of time then available, it was unfeasible to look as to whether it was the lamp or the system that was causing the erroneous signals. The reduced quality in the data forced a move away from the MSSL spectrophotometer and to a reliance on the initial data taken at Harwell. This can be seen in the data listed in the appendices, where some data is listed to 190 nm (MSSL monochrometer), some only to 330 nm (Harwell).

5.10 Data Acquisition

The program of exposure went smoothly and all samples were exposed as intended. The subsequent measurement was carried out, and the resulting data analysed. These results are discussed in more detail in the following chapters.

5.11 Refractive Index Changes

At about this point in the project, various constraints with the availability and suitability of the SIRA interferometer meant that the planned study of refractive index was put on hold. Unfortunately, this setback became permanent and no study was performed on this aspect of the materials response to irradiation.

6 Data Reduction and Analysis

Once the basic data was obtained, the next step was to take the raw output and produce meaningful information from it. The following sections detail the process by which the data was reduced into a dataset useful for predicting the behaviour of the selected materials to radiation.

Once the data had been normalised, the next stage was to analyse the response of each sample to the radiation it had received. The aim of the analysis was to quantify what effects, if any, had been produced by the irradiation. For the samples that did appear to show a response to irradiation, the subsequent analysis could be broken into a set of steps.

- To quantify any trend or pattern as a function of received dose.
- To attempt to describe the effect by a simple algorithm.
- To see if this algorithm could adequately describe the evolution of the feature as a function of the received dose.

Describing the evolution of any radiation induced features in the samples by a mathematical approximation would allow the effect to be estimated for any future work. The following sections describe the analysis of each sample group. This attempt to describe changes as a function of received dose has been fruitful for some samples, but limited for others.

6.1 Reduction and Basic Formatting

After exposure and subsequent measurement, the output from the spectrophotometer was printed on thermal paper. The first stage of any analysis was to transpose this from the paper format into some form of electronic file.

Initially, it was hoped that the paper output could be automatically scanned via a simple flatbed scanner and standard off-the-shelf OCR (optical character recognition) software. However, the quality of the scanner was unable to give a suitable contrast between the dull, reflective silver of the thermal paper and the black print. In the end, it was necessary to manually enter the data in to Excel, and save the data as basic comma delimited CSV files.

The first stage was to sense check the data for obvious mistakes. The commonest faults were typing errors such as dropped figures or numerals entered in the incorrect order. Generally, these were easy to spot and a simple check with the original data would soon allow an accurate value to be entered. Some were more subtle, and as such only began to drop out once the actual analysis was undertaken.

6.2 Data Normalisation

All the samples for any one material were closely matched physically and for all but one group of samples (Roynon Howes magnesium fluoride) had come from the same parent block. Hence it could be assumed that the transmission curve for one, unexposed, sample of a particular material would form a baseline against which the curves for irradiated samples could be compared.

The first step in carrying out this comparison was to normalise the transmission curves for each material. Then the intention was to model the absorption bands introduced by irradiation using simple mathematical functions.

With hindsight, it would have been beneficial to obtain multiple, high quality spectra for each sample before irradiation. Not only would this give an optimum before and after view, it would also have illustrated the homogeneity each sample set.

Unfortunately the unexposed samples were not among those at Harwell, since the Harwell spectrophotometer was to be used to produce a provisional data set, with more detailed spectra measured later. Since this subsequent, higher quality data set was not available (see Section 5.9), it was necessary to turn to the Harwell data set as the primary source. To surmount this oversight with the unexposed samples, the irradiated sample with the lowest dose for each group was used as the control sample.

To normalise the data, the first stage was to select a control sample to use as a baseline to compare the remaining samples of that group against. At first, it had been the intention to use unexposed samples for this task. With the reliance of the Harwell data, the next best option was to turn to the results for the 0.5 krad samples. The first step in the normalisation process was to divide each samples spectrum by that of the control sample. The transformation can be described by:

$$S_{N\lambda} = \frac{S_\lambda}{C_\lambda} \text{ where :}$$

$S_{N\lambda}$ is the part - normalised sample transmission at wavelength λ

S_λ is the original sample transmission at wavelength λ

C_λ is the control sample transmission at wavelength λ

By dividing each samples transmission by this, all the data was normalised relative to each other, but only for the actual shape of the spectra. Figure 24 illustrates this situation for the 30 Mrad data.

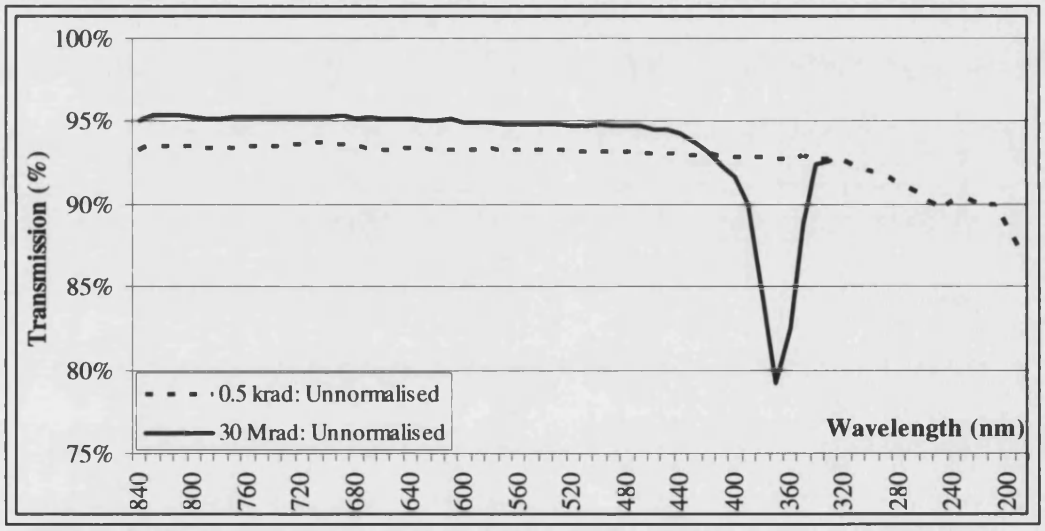

Figure 24. 30 Mrad spectrum compared with the 0.5 krad spectrum (unnormalised).

The sample chosen for exposure to 30 Mrad data had a higher transmission than the sample selected for the 0.5 krad exposure. Although the dimensions of both samples were very similar, differences in the preparation by the external supplier meant that the transmission of each sample was slightly different.

The result was that after the first part of normalisation, the 30 Mrad data had a transmission of 102% at 840 nm. To overcome this, the second step of the normalisation was to divide the sample spectra by their transmission at 840 nm. 840 nm was chosen as it was the furthest point from the absorption feature and was unaffected by irradiation.

By setting all the samples to have 100% transmission at this point, this was simulating the scenario where the pre-irradiation spectra of all the samples were identical. Overall, the normalisation process can be stated as:

$$S_{NT\lambda} = \frac{S_{N\lambda}}{S_{N840}} = \frac{S_\lambda \times C_{840}}{C_\lambda \times S_{840}} \text{ where:}$$

$S_{NT\lambda}$ is the fully normalised sample transmission at wavelength λ

S_{840} is the transmission of the original sample at 840 nm

C_{840} is the transmission of the control sample at 840 nm

$S_{N\lambda}$, S_λ and C_λ are as defined earlier.

The difference between part and full normalisation is shown in Table 17 and illustrated in Figure 25. In this example the Merck magnesium fluoride has been used to illustrate the process, but it was equally applied to sapphire and to the radiation hardened glasses. With the undoped glasses there was an effect across the whole wavelength range and so this process could not be used. This will be discussed later in the sections 6.13 and 6.16.

nm	840	830	820		390	380	370	360
0.5 krad: Unnormalised	93.3%	93.7%	93.5%	...	92.9%	92.8%	92.7%	92.8%
30 Mrad: Unnormalised	95.1%	95.3%	95.4%	...	90.0%	84.4%	79.2%	82.5%
30 Mrad: Divided by 0.5 krad	101.9%	101.8%	102.0%	...	96.9%	90.9%	85.4%	89.0%
30 Mrad: 100% at 840 nm	100.0%	99.9%	100.1%	...	95.1%	89.3%	83.8%	87.3%

Table 17. Illustration of the difference between original, part-normalised and fully normalised data for 30 Mrad Merck magnesium fluoride spectra.

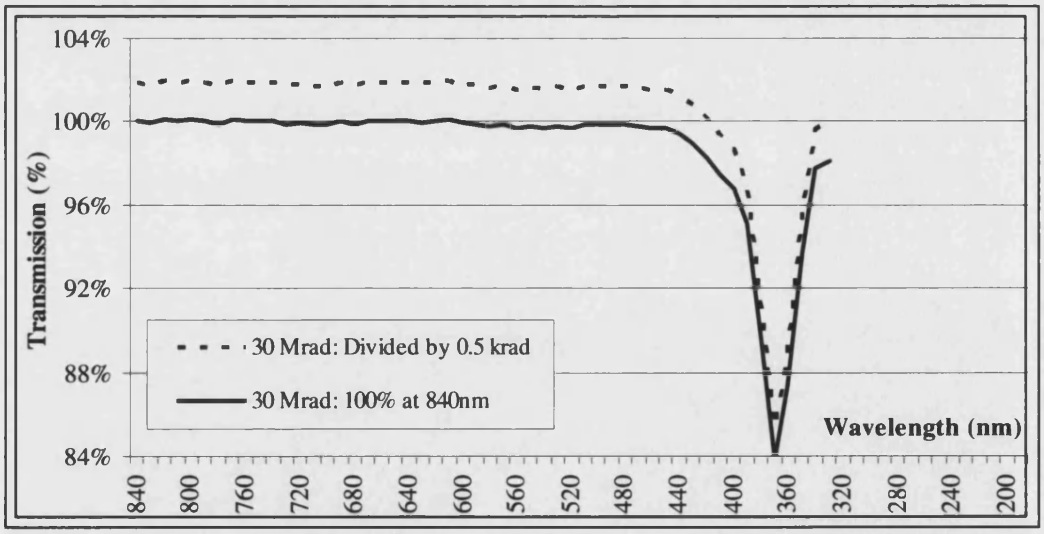

Figure 25. 30 Mrad data part and fully normalised by 0.5 krad spectra and transmission at 840 nm to return a transmission of 100% at 840 nm

By reversing the normalisation process detailed above, any subsequent fit can be superimposed on the data to test the accuracy of the fit and any subsequent approximation formulae.

6.3 Data Analysis Software

The primary package used for curve fitting was DataFit, [58] a data plotting, regression analysis and statistical analysis pack. In particular, the results were generated by the non-linear analysis of user defined formulae. Although DataFit does contain many generic equations, they tended to be of an unsuitable format that needed the user to redesign the equation or to enter a new one. For example, the Lorentzian fit used later in Section 6.6 was not listed and had to be entered by the user. However, it did provide a platform which allowed a large number of iterative runs to be carried out to fit differing equations against the data.

In particular, the package contained the functionality to integrate via DDE (dynamic data exchange) into the VBA interface of Excel. This allowed large numbers of runs to be pushed through, releasing the user to carry out other tasks. Another benefit of using the VBA interface was that once the Excel VBA project code had been set up and tested, the code could then sequentially run several fits across the results of several samples, record the subsequent data and reduce it before recording it to an Excel workbook. This reduced the scope for human error.

6.4 Curve Fitting Programme

The technical information about the operation and configuration of DataFit given in this section is taken from DataFit Help v8. [58] To initiate the fitting process it was necessary to define the actual equations to be fitted and the initial estimates for the variables in the equation. It was possible to build in several different versions of equations into one configuration file. However, the location for input data and output results, and parameters to govern the accuracy of the fit were defined for the file as a whole. These parameters were:

1. Regression Tolerance: For each iteration the calculation of the merit function was compared with the merit function calculated for the previous iteration. When the percentage difference was less than the Regression Tolerance specified, the iteration process was terminated.

2. Unchanged Iterations: If the merit function remained unchanged for the number specified by Unchanged Iterations, the iterative process was terminated. This did not mean that the solution was necessarily any good, but possibly as good as it could be for the initial estimates used
3. Max Iterations: This specified the maximum number of nonlinear iterations the solver would perform if the solution has failed to reach the Regression Tolerance specified above. Again, this did not mean the solution was good, but when the number of iterations exceeded this value, the iteration process was terminated to stop a model from running on indefinitely.
4. Derivatives: DataFit gave the option of using either Richardson's Extrapolation or the Central Difference method. Of the two, the slower Richardson's Extrapolation was used as generally it produces more accurate results.

An example of a macro configuration file is given in Appendix E.1. The example listed there employs three different sets of variables to the Gaussian equation to be fitted to the data. However, there was no limit on the number of variation that could be placed in the configuration file. One configuration file used to initially test the glass data had twelve variations on the variables used in the Gaussian and Lorentzian equations used.

The next step was to use VBA to call the DataFit program and point it toward the configuration file. DataFit provided examples of the code required to run the iterations (see Appendix E.3) which Excel can then call (see Appendix E.2).

A more detailed description of the Gaussian and Lorentzian equations fitted to the absorption features is given in Sections 6.5 and 6.6. Before presenting and discussing the results of fitting these functions using DataFit, it is beneficial to outline the methodology of applying the functions to the data and measuring the *goodness of fit* for the results generated. To calculate how good a fit is DataFit uses a merit function to minimise the nonlinear regression using:

$$\chi^2(a)=\sum_{i=1}^{N}\left[\frac{y_i-y(x_i;a)}{\sigma_i}\right]^2$$

where σ_i is the measurement error, or standard deviation of the i^{th} data point. As with linear regression, the program aims to minimise the sum of the squares of the distances between the actual data points and the regression line.

Once the iteration had terminated, if it had managed to produce a fit then it also produced the *Standard Error on the Estimate*, (SE), and this is the value used to define the *goodness of fit* for the results presented. The standard error on the estimate was the standard deviation on the residuals. The residuals are the vertical differences between an actual data point and the curve generated from the predicted values. Actual data above the curve results in a positive residual, negative if below. If the residual is zero, the actual data point lays on the predicted curve, hence the larger the residual, the further the data point lies from the curve.

For the data produced from the iterations, it was considered a "successful" iteration if the iteration produced values within the number of iterations defined by Max Iteration. The results were further winnowed down by observing the SE of the returned values. In some cases the SE was so high as to invalidate the data for that sample.

6.5 The Gaussian Function

The Gaussian shape is of the form:

$$y = A \times \exp\left[-\left(\frac{(x-B)^2}{(2\times C^2)}\right)\right]$$

where

A = Maximum value of the Gaussian peak

B = Centre of the Gaussian peak

C = Width of the Gaussian peak

An example of a Gaussian peak is shown in Figure 26 with the values of the maximum and centre both fixed. The maximum has been set at A = 3. This highest value occurs at the centre of the Gaussian peak at B = 5. The width, C, has been set to 1, 2 and 3 show the effect of this value in broadening the shape of the curve.

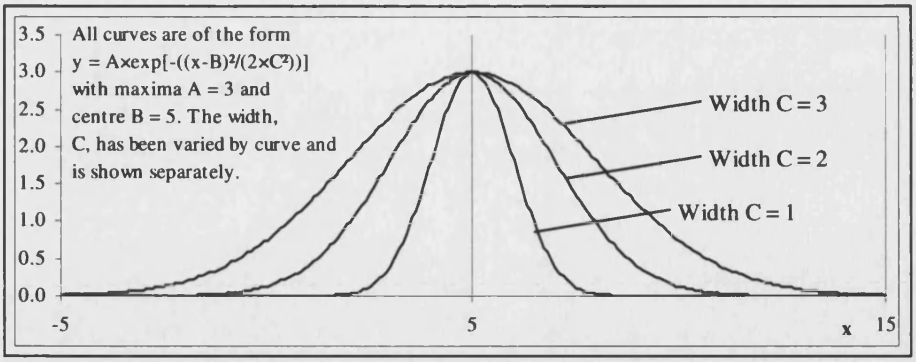

Figure 26. Gaussian peak of form y = A×exp[-((x-B)²/(2×C²))] with the maximum, A, set at 3 and the centre B set at 5. The width, C, has been shown for a range 1 – 3.

6.6 The Lorentzian Function

The Lorentzian is of the form:

$$y = A \times \frac{(B/2)^2}{(x-C)^2 + (B/2)^2}$$

where

A = Maximum value of the Lorentzian equation

B = Width of the Lorentzian peak

C = Centre of the Lorentzian peak

The width of the Lorentzian, B, is also known as the *Full Width Half Maximum* or FWHM. For the curve, the width given by variable B will be the width of the curve at half the maximum value.

For example, in Figure 27 consider the middle curve described by A = 3, B = 3 and C = 5. The peak value of y = 3 = A occurs at x = C = 5. The value of y is given by:

$$y = 3 \times ((3/2)^2) / ((x-5)^2 + (3/2)^2)$$

Thus for x = 3.5:

$$y = 3 \times ((3/2)^2) / ((3.5-5)^2 + (3/2)^2) = 1.5 = B/2.$$

Similarly, for x = 6.5:

$$y = 3 \times ((3/2)^2) / ((6.5-5)^2 + (3/2)^2) = 1.5 = B/2.$$

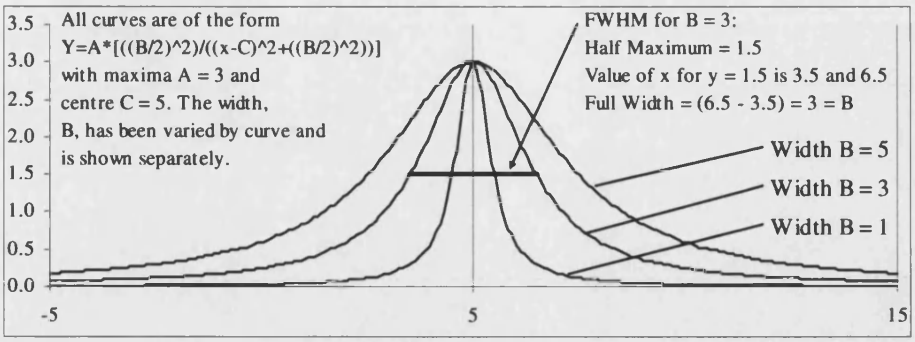

Figure 27. Lorentzian peak of form $y = A\times[((B/2)^2)/((x-C)^2+((B/2)^2))]$ with the maximum, A, set to 3 and the centre, B set to 5. The width, C, has been shown for a range 1 – 5.

6.7 Curve Fitting to the Merck Magnesium Fluoride

Being the most numerous group of samples, the Merck magnesium fluoride, samples provided the bulk of the data for analysis. Figure 28 shows a simple view of the spectra of selected irradiated samples over a wavelength range of 330 to 840 nm. The samples illustrated have been exposed to doses varying from 300 krad to 30 Mrad, the lower dose samples are excluded here for the sake of clarity. The response of the samples is quite flat from 840 to 450 nm and it is only below this level that any variation becomes apparent, in this case a deep, asymmetric, absorption feature.

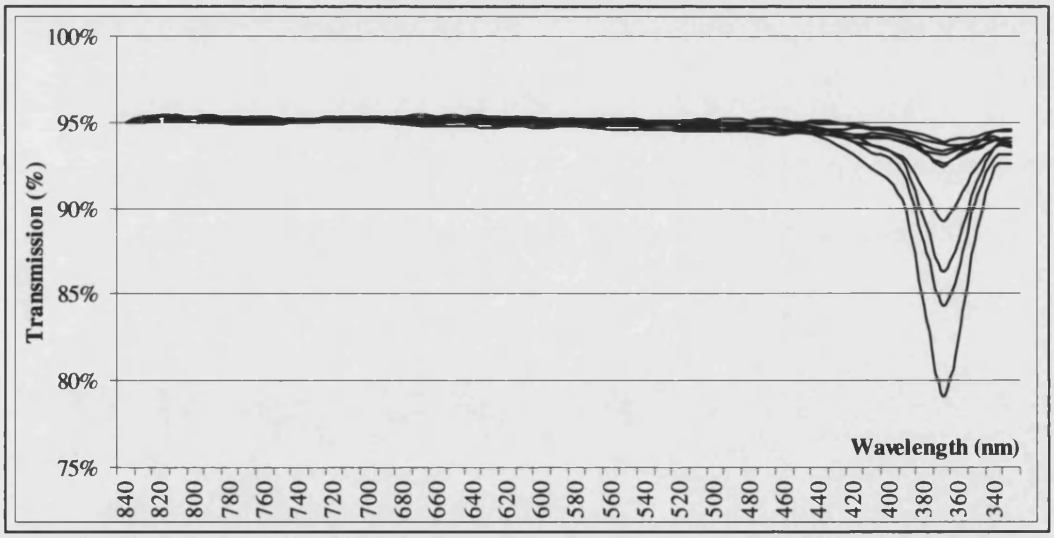

Figure 28. Transmission of Merck magnesium fluoride over 330 to 840 nm showing the concentration of radiation induced effects to below 450 nm.

Since this feature forms the only major change observed in the data, it forms the bulk of the analysis for this material.

6.7.1 Asymmetric Feature at 370 nm

To highlight this area of interest, Figure 29 is a close up of the feature focused around the 500 to 330 nm range. Clearly illustrated is the feature at ≈370 nm is asymmetric which implies that, though the absorption feature is centred about 370 nm, there may be another feature closer to 400 nm. This fits well with the work of Sibley and Facey. [36] In their work on M centres in magnesium fluoride, they found that the absorption bands associated with M centres centred around 370 and 400 nm.

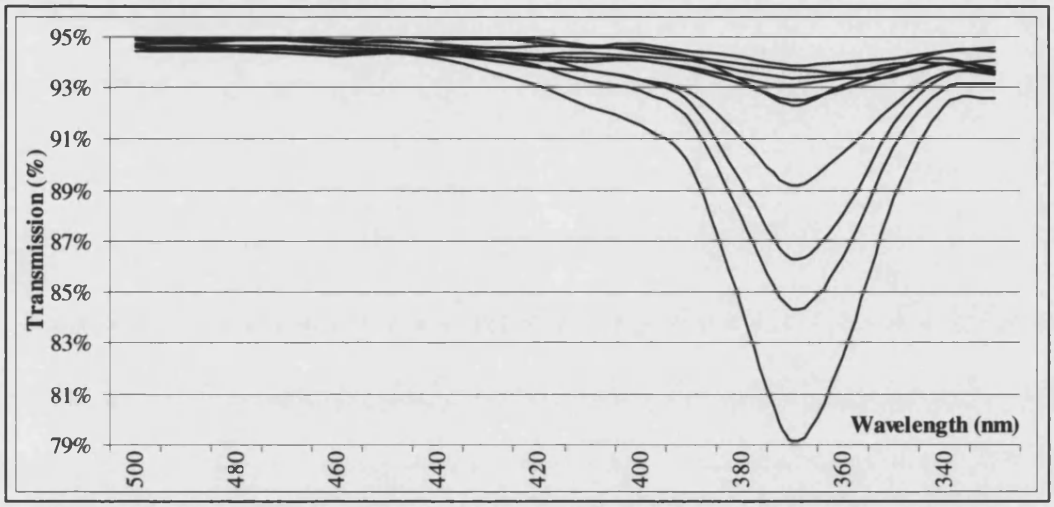

Figure 29. Transmission of Merck magnesium fluoride over 330 to 500 nm showing greater detail of the absorption feature at ≈370 nm. For clarity, the doses are not shown, but the depth of the 370 nm feature is proportional to total dose.

The initial step was to establish which mathematical functions would adequately describe the shape of the feature. Although there are many functions that could describe the feature, the Gaussian and Lorentzian were selected. The reasons for this were:

They are shapes that are easily described by 2 or 3 parameters, and as such can be analysed efficiently by a non-linear iterative approach.

They are both shapes that are commonly found in natural processes. The Gaussian shape follows a normalised distribution, and the Lorentzian shape is often used to describe natural phenomena such as the broadening of atomic line spectra. [59]

To plot the Gaussian profile as an absorption feature, the function $y = 1 - f(x)$ is applied to the data where $f(x)$ is the Gaussian equation shown above. There were three variations of the Gaussian function that were applied to the Merck magnesium fluoride data. These were:

- Freeform fits to the data
- Fixed Wavelength Fits

- Fixed Wavelength Difference Fits

The differences and reasoning behind these runs are discussed in the following sections with the results of all three runs presented and discussed afterwards.

6.7.2 Gaussian Fits

The first equation to be fitted was the Gaussian, with the variables modified into the three forms mentioned previously. The exact details of the fit were:

- Freeform fit: no constraint on the variables
- Fixed wavelength: the variable B was fixed to the values suggested by Sibley and Facey, but the remaining variables were free from constraint.
- Fixed wavelength difference: the wavelength B_2 was set as B_1+30 nm, but there was no constraint on B_1.

The results of these fits were compared to evaluate the most successful form of Gaussian.

6.7.2.1 Freeform Fits to the Data

Once the data had been normalised as detailed above, the data were pushed through DataFit. The work of Sibley and Facey [36] suggests two features centred on 370 and 400 nm. However, rather than assume that the feature seen in our data was centred at 370 nm, the first analysis was carried out with no constraint on the equations being fitted to the data. The form of equation applied to the data was:

$$y = 1 - (G_1 + G_2)$$

where

$$G_1 = A_1 \times \exp\left[-\left((x - B_1)^2 / (2 \times C_1^2)\right)\right]$$

and

$$G_2 = A_2 \times \exp\left[-\left((x - B_2)^2 / (2 \times C_2^2)\right)\right]$$

where the initial values of the variables were set at:

Variable	Initial Value	Variable	Initial Value
A_1	1	A_2	1
B_1	370	B_2	400
C_1	10	C_2	10

6.7.2.2 Fixed Wavelength Fits

The next form of Gaussian equation to be fitted was to assume centres at 370 and 400 nm and to repeat the iterations on the data. The form of equation applied was:

$$y = 1 - (G_1 + G_2)$$

where

$$G_1 = A_1 \times \exp\left[-\left((x - 370)^2 / (2 \times C_1^2)\right)\right]$$

and

$$G_2 = A_2 \times \exp\left[-\left((x - 400)^2 / (2 \times C_2^2)\right)\right]$$

where the initial values of the variables were set at:

Variable	Initial Value	Variable	Initial Value
A_1	1	A_2	1
C_1	10	C_2	10

6.7.2.3 Fixed Wavelength Difference Fits

An alternative was to assume that there were two features at 370 and 400 nm but to allow for inaccuracies in the data. The approach taken was to fit the curves with the difference between the centres set to 30 nm. The equations are of the form:

$$y = 1 - (G_1 + G_2)$$

where

$$G_1 = A_1 \times \exp\left[-\left((x - B_1)^2 / (2 \times C_1^2)\right)\right]$$

and

$$G_2 = A_2 \times \exp\left[-\left((x - (B_1 + 30))^2 / (2 \times C_2^2)\right)\right]$$

where the initial values of the variables were set at:

Variable	Initial Value	Variable	Initial Value
A_1	1	A_2	1
B_1	370		
C_1	10	C_2	10

6.7.2.4 Comparison of the Gaussian Fits

Table 18 shows the returned values for the variables used in the three Gaussian equations applied to the Merck data. It also reports the SE in both absolute terms and as a percentage. There are a number of points that should be noted. Firstly, the SEs for several of the variables reported for the first Gaussian equation (e.g. all of the 1 krad values) are denoted by '*'. For these variables the returned values were unreasonably large, in the order of 10^4 or greater, and as such they were discounted. This is a drawback with a simple iterative routine. Ideally, it should have returned values similar to those returned for the subsequent Gaussian fits. This is particularly disappointing for the 3 Mrad data. Generally, the higher the dose, the more pronounced the absorption feature and thus easier to fit. However, in this case the iterative routine has failed to return a meaningful result. Another anomaly was a *divide by zero error* which has been highlighted by '-'. This occurred for the percentage SE on variable A1 in the third Gaussian run. Here, the variable A1 returned a value of 0, and so the SE returns a divide by zero error.

To compare the data, it is useful to look at the evolution of the absorption feature as a function of dose. **Figure 30** shows as straight line fit of the form $y = mx$ to the Merck magnesium fluoride data. The absorption was calculated as $1-T_\lambda$ where T_λ is the transmission of the sample at 370 nm, the approximate location of the deepest part of the absorption feature. The absorption was plotted against the dose in Mrad and the least squares fit was forced to intercept through zero (since it is reasonable to expect that there would be no absorption at zero dose) and returns a reasonable straight line. With more analysis, a better fit could probably be obtained, but for the purposes of weighting data, over this range a straight line approximation was reasonable.

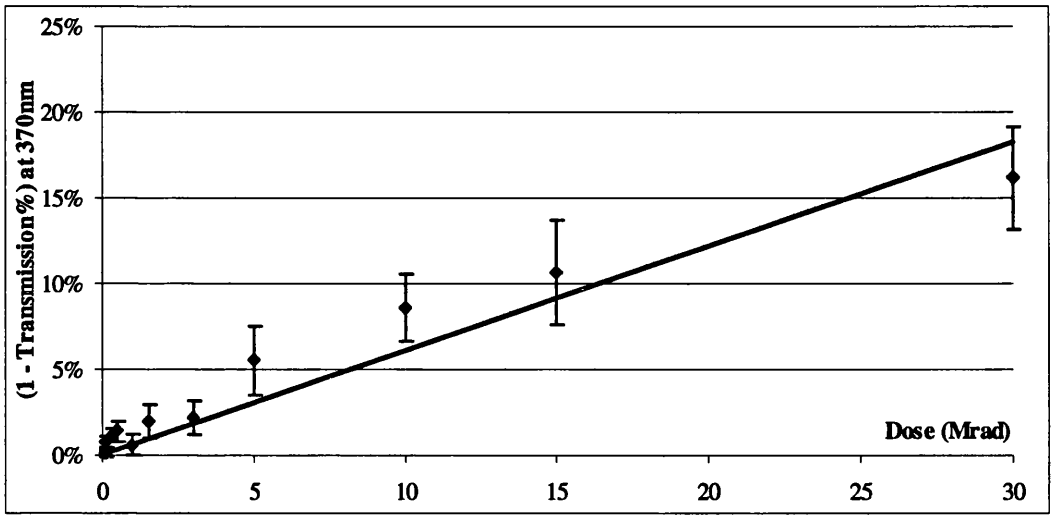

Figure 30. Linear relation between absorption at 370 nm as a function of dose for Merck magnesium fluoride.

Toward the higher doses, the data begins to drop below the straight line. This could imply that as the absorption feature grows, it does so rapidly to begin with, but as the dose increases the rate of growth of the feature starts to slow, and may well saturate at very high levels. Over the range of this project's data, this linear increase in the depth of the absorption feature as a function of dose allows the higher dose data to be weighted with more certainty over the lower dose samples. This in turn allowed the returned data for the first and third Gaussian fits to be compared where it was necessary to calculate a weighted mean for some of the variables.

	Dose	1 krad	5 krad	10 krad	15 krad	30 krad	50 krad	100 krad	150 krad	300 krad	500 krad	1 Mrad	1.5 Mrad	3
Gaussian 1: No constraint on wavelength	a1	0.717	0.003	0.004	0.009	0.007	0.007	0.004	0.009	0.007	0.009	0.007	0.016	0
	a2	-0.721	-0.003	-0.002	0.005	0.001	0.003	-0.003	0.011	0.005	0.005	-0.002	0.004	
	b1	420	365	370	346	360	355	369	362	367	366	365	368	
	b2	420	408	528	537	525	493	505	333	328	438	500	426	
	c1	216	14	16	-60	-30	-30	14	20	12	19	16	15	
	c2	215	151	137	187	243	89	170	3	110	162	197	144	
	SE(a1)	*	0.0007	0.0006	0.001	0.0005	0.0007	0.0008	0.0008	0.0008	0.0007	0.0008	0.0006	0.
	SE(a1)%	*	23%	15%	11%	7%	10%	20%	9%	11%	8%	11%	4%	
	SE(a2)	*	0.0003	0.0002	0.0003	0.0002	0.0003	0.0002	*	0.0006	0.0003	0.0002	0.0002	
	SE(a2)%	*	10%	10%	6%	20%	10%	7%	*	12%	6%	10%	5%	
	SE(b1)	*	3	3	10	3	3	3	6	2	1	2	1	
	SE(b1)%	*	1%	1%	3%	1%	1%	1%	2%	1%	0%	1%	0%	
	SE(b2)	*	25	18	30	84	15	28	*	17	21	45	21	
	SE(b2)%	*	6%	3%	6%	16%	3%	6%	*	5%	5%	9%	5%	
	SE(c1)	*	4	3	10	3	4	4	5	2	2	2	1	
	SE(c1)%	*	29%	19%	17%	10%	13%	29%	25%	17%	11%	13%	7%	
	SE(c2)	*	17	18	20	68	15	25	*	11	14	37	14	
	SE(c2)%	*	11%	13%	11%	28%	17%	15%	*	10%	9%	19%	10%	
Gaussian 2: Set to 370 and 400 nm	a1	0.001	0.003	0.005	0.006	0.006	0.005	0.005	0.011	0.008	0.008	0.007	0.015	0
	a2	-0.004	-0.003	-0.003	0.007	0.001	0.004	-0.003	-0.007	0.003	0.005	-0.002	0.004	-0
	c1	8	13	22	31	29	21	17	41	16	17	19	15	
	c2	173	153	198	219	281	163	210	-33	106	172	221	155	
	SE(a1)	0.0006	0.0007	0.0005	0.0008	0.0005	0.0006	0.0008	0.0011	0.0008	0.0007	0.0008	0.0006	0.
	SE(a1)%	60%	23%	10%	13%	8%	12%	16%	10%	10%	9%	11%	4%	
	SE(a2)	0.0002	0.0003	0.0002	0.0005	0.0003	0.0003	0.0003	0.0012	0.0004	0.0003	0.0003	0.0002	0.
	SE(a2)%	5%	10%	7%	7%	30%	8%	10%	17%	13%	6%	15%	5%	
	SE(c1)	4	3	3	6	3	4	3	5	2	2	2	1	
	SE(c1)%	50%	23%	14%	19%	10%	19%	18%	12%	13%	12%	11%	7%	
	SE(c2)	9	13	18	13	73	14	20	5	16	10	28	10	
	SE(c2)%	5%	8%	9%	6%	26%	9%	10%	15%	15%	6%	13%	6%	
Gaussian 3: Wavelength difference of 30 nm	a1	0	0.004	0.005	0.006	0.006	0.005	0.005	0.009	0.008	0.009	0.008	0.015	0
	a2	-0.004	-0.004	-0.003	0.007	0.001	0.004	-0.003	-0.001	0.003	0.005	-0.002	0.004	-0
	b1	414	365	368	367	361	359	369	352	364	367	365	368	
	c1	-19	14	22	31	28	23	17	32	17	17	18	14	
	c2	160	154	199	219	266	165	210	-275	104	172	226	154	-
	SE(a1)	0.0004	0.0007	0.0005	0.0008	0.0005	0.0006	0.0008	0.0005	0.0007	0.0007	0.0008	0.0005	0.
	SE(a1)%	-	18%	10%	13%	8%	12%	16%	6%	9%	8%	10%	3%	
	SE(a2)	0.0002	0.0003	0.0003	0.0005	0.0003	0.0003	0.0003	0.0003	0.0004	0.0003	0.0003	0.0002	0.
	SE(a2)%	5%	8%	10%	7%	30%	8%	10%	30%	13%	6%	15%	5%	
	SE(b1)	11	3	3	4	3	3	3	3	2	1	2	1	
	SE(b1)%	3%	1%	1%	1%	1%	1%	1%	1%	1%	0%	1%	0%	
	SE(c1)	41	3	3	6	3	4	3	4	2	2	2	1	
	SE(c1)%	216%	21%	14%	19%	11%	17%	18%	13%	12%	12%	11%	7%	
	SE(c2)	11	13	18	13	59	13	20	88	14	10	29	9	
	SE(c2)%	7%	8%	9%	6%	22%	8%	10%	32%	13%	6%	13%	6%	

Table 18. Results for the Gaussian fit to the Merck magnesium fluoride sample

6.7.3 Comparison of Results for the Gaussian Fits

From the form of the Gaussian, it was expected that the wavelength of the centre of the Gaussian peak (B_1 and B_2 in the equations above) would be constant, and that only the width and depth would change as a function of dose.

Figure 31 is a comparison on the returned values for all the Gaussian fits. For variables A and C, it was possible to compare the results for all three sets of fits, but for the central wavelength, B, only the first and third fits could be compared.

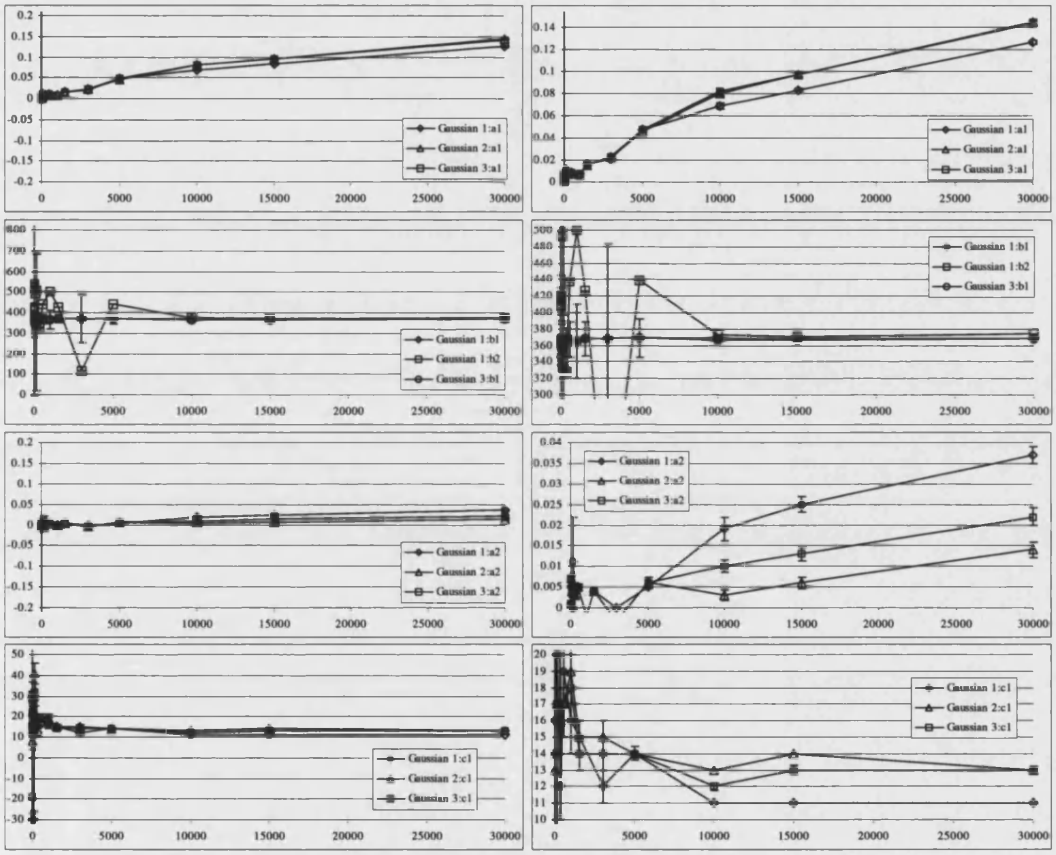

Figure 31. Series of graphs comparing the results of the Gaussian fits to Merck magnesium fluoride on the variables A, B and C. The left column shows the full range of data, the right shows the data in detail. The y-axis is the returned value for the variable, the x-axis is the total dose in rad.

From the fits, the weakest fit was the second fit with fixed wavelengths. Comparing the first and third fit, although the first fit produced a good value for B_1, the comparable value for the third fit is also good, with both standard deviations less than 0.3% of the actual value. However, the strength of the freeform fit of the first fit is diminished by the error on the second parameter, B_2. The uncertainty of this value is just under 7% of B_2 and overall it was concluded that the third Gaussian fit was the better of the three.

6.7.4 Lorentzian fits

The data was normalised as before (see Section 6.2) and a similar process was carried out as for the Gaussian fits, with free fit, fixed wavelength and fixed wavelength difference all being assessed. The results of these fits were compared to evaluate the most successful form of Lorentzian.

6.7.4.1 Freeform Fits to the Data

The form of equation applied to the data was:

$$y = 1-(G1+G2)$$

where

$$G1 = M_1 \times \left[(W_1/2)^2 / \left((x-L_1)^2 + (W_1/2)^2\right)\right]$$

and

$$G2 = M_2 \times \left[(W_2/2)^2 / \left((x-L_2)^2 + (W_2/2)^2\right)\right]$$

where the initial values of the variables were set at:

Variable	Initial Value	Variable	Initial Value
M_1	0.1	M_2	0.1
W_1	29	W_2	5
L_1	370	L_2	400

6.7.4.2 Fixed Wavelength Fits

The next form of Lorentzian fitted to the data was of the form:

$$y = 1-(G1+G2)$$

where

$$G1 = M_1 \times \left[(W_1/2)^2 / \left((x-370)^2 + (W_1/2)^2\right)\right]$$

and

$$G2 = M_2 \times \left[(W_2/2)^2 / \left((x-400)^2 + (W_2/2)^2\right)\right]$$

where the initial values of the variables were set at:

Variable	Initial Value	Variable	Initial Value
M_1	0.1	M_2	0.1
W_1	29	W_2	5

6.7.4.3 Fixed Wavelength Difference Fits

The final form of Lorentzian applied to the data was of the form:

$$y = 1 - (G1 + G2)$$

where

$$G1 = M_1 \times \left[(W_1/2)^2 / \left((x - L_1)^2 + (W_1/2)^2 \right) \right]$$

and

$$G2 = M_2 \times \left[(W_2/2)^2 / \left((x - (L_1 + 30))^2 + (W_2/2)^2 \right) \right]$$

where the initial values of the variables were set at:

Variable	Initial Value	Variable	Initial Value
M_1	0.1	M_2	0.1
W_1	29	W_2	5
L_1	370		

6.7.4.4 Comparison of the Lorentzian Fits

Table 19 shows the returned values from the three Lorentzian functions applied to the Merck magnesium fluoride along with there associated SE. Again '*' denotes SE values of 10^4 or greater that have been discounted. Another anomaly is that some of the iterations failed to return results before the number of iterations exceeded the Max Iterations limit (e.g. 5 Mrad samples for the second Lorentzian run.)

As with the Gaussian fits, the SE results were used to compare the first and second Lorentzian equations, with the central wavelength of the absorption feature used to compare the first and third run.

	Dose	1 krad	5 krad	10 krad	15 krad	30 krad	50 krad	100 krad	150 krad	300 krad	500 krad	1 Mrad	1.5 Mrad	3 Mrad	
Lorentzian 1: No constraint on wavelength	I1	421	*	372	567	392	408	375	353	390	366	365	368	369	
	I2	421	455	*	359	392	408	540	458	390	505	473	508	422	
	m1	-2.060	*	0.004	0.005	4.210	9.134	894	0.010	6.600	0.012	0.008	0.019	0.026	
	m2	2.060	-0.004	-0.001	0.011	-4.210	-9.131	-0.003	-0.002	-6.600	0.004	-0.002	0.003	-0.005	
	w1	-746	*	17	357	102	121	0	77	67	53	34	36	29	
	w2	-747	340	*	121	102	-121	321	-384	67	-238	411	-166	-232	
	SE(I1)	58	*	4	27	187	138	1	3	79	1	2	1	1	
	SE(%)	14%	*	1%	5%	48%	34%	0%	1%	20%	0%	1%	0%	0%	
	SE(I2)	58	17	*	4	187	138	20	83	78	14	48	8	22	
	SE(%)	14%	4%	*	1%	48%	34%	4%	18%	20%	3%	10%	2%	5%	
	SE(m1)	*	*	0.002	0.001	*	*	*	0.001	*	0.001	0.001	0.001	0.001	
	SE(%)	*	*	43%	10%	*	*	*	10%	*	6%	13%	3%	5%	
	SE(m2)	*	0	0	0	*	*	0	0	*	0	0	0	0	
	SE(%)	*	10%	10%	6%	*	*	10%	30%	*	8%	17%	6%	15%	
	SE(w1)	907	*	10	60	293	644	*	16	201	6	8	2	3	
	SE(%)	122%	*	59%	17%	287%	532%	*	21%	300%	11%	24%	6%	10%	
	SE(w2)	911	83	*	23	294	644	60	114	201	36	94	23	34	
	SE(%)	122%	24%	*	19%	288%	532%	19%	30%	300%	15%	23%	14%	15%	
Lorentzian 2: Set to 370 and 400 nm	m1	0.010	0.004	0.005	0.006	0.009	0.005	0.006	0.018	0.011	0.011	0.009	0.018	0.027	
	m2	-0.013	-0.005	-0.003	0.007	-0.004	0.003	-0.004	-0.012	-0.005	-0.005	-0.003	-0.004	-0.006	
	w1	-974	37	55	-67	105	48	-40	142	96	181	44	57	32	
	w2	712	224	361	-440	-59	-354	406	167	-28	22	363	17	218	
	SE(m1)	0.002	0.001	0.001	0.001	0.001	0.001	0.001	0.002	0.001	0.001	0.001	0.001	0.001	
	SE(%)	24%	18%	13%	17%	11%	15%	18%	12%	7%	7%	10%	5%	4%	
	SE(m2)	0	0	0	0	0	0	0	0	0	0	0	0	0	
	SE(%)	18%	13%	18%	14%	24%	19%	16%	20%	19%	29%	18%	38%	13%	
	SE(w1)	138	13	13	24	12	14	13	22	8	15	9	5	2	
	SE(%)	14%	35%	24%	36%	11%	29%	33%	15%	8%	8%	20%	9%	6%	
	SE(w2)	86	31	60	59	24	65	71	18	9	10	74	11	29	
	SE(%)	12%	14%	17%	13%	41%	18%	17%	11%	32%	45%	20%	65%	13%	
Lorentzian 3: Wavelength difference of 30 nm	I1	429	367	370	409	376		371	353	372	394	365	371	369	
	m1	-0.002	0.005	0.005	0.019	0.010		0.006	0.011	0.011	0.015	0.009	0.018	0.027	
	m2	-0.002	-0.005	-0.003	-0.011	-0.005		-0.004	-0.004	-0.005	-0.009	-0.003	-0.005	-0.005	
	w1	274	38	55	258	118		-39	96	98	184	41	60	31	
	w2	307	230	362	-132	-71		406	284	30	81	390	-20	-236	
	SE(I1)	*	4	3	7	5		3	3	2	4	2	2	1	
	SE(%)	*	1%	1%	2%	1%		1%	1%	1%	1%	1%	1%	0%	
	SE(m1)	-	0.001	0.001	0.002	0.001		0.001	0.002	0.001	0.001	0.001	0.001	0.001	
	SE(%)	-	18%	13%	12%	11%		18%	13%	7%	10%	10%	6%	4%	
	SE(m2)	-	0.001	0.001	0.002	0.001		0.001	0.002	0.001	0.001	0.001	0.002	0.001	
	SE(%)	-	13%	18%	18%	27%		16%	54%	20%	16%	19%	42%	13%	
	SE(w1)	*	13	14	14	15		13	22	8	11	8	6	2	
	SE(%)	*	34%	25%	5%	13%		33%	23%	8%	6%	20%	10%	6%	
	SE(w2)	*	33	62	26	21		73	82	10	18	79	11	33	
	SE(%)	*	14%	17%	20%	30%		18%	29%	33%	22%	20%	55%	14%	

Table 19. Results for the Lorentzian fit to the Merck magnesium fluoride sampl

6.7.5 Comparison of Results for the Lorentzian Fits

Figure 32 is a comparison on the returned values for all the Lorentzian fits.

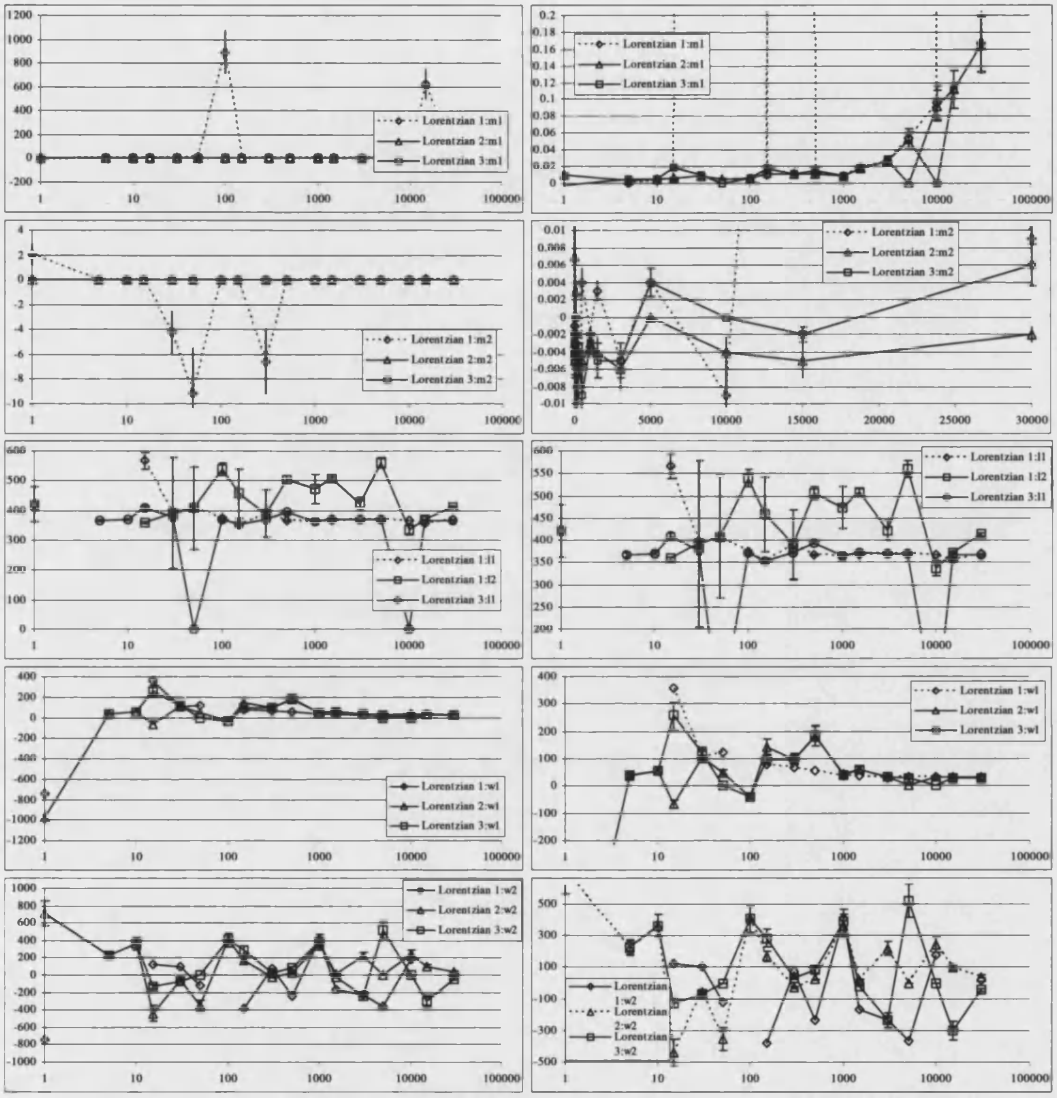

Figure 32. Series of graphs comparing the results of the Lorentzian fits to Merck magnesium fluoride on the variables L, W and M. The left column shows the full range of data, the right shows the data in detail. The y-axis is the returned value for the variable, the x-axis is the total dose in rad.

Since the central wavelengths (L) were fixed for the two Lorentzian equations used in the second run, only the first and third fit could be compared directly for L. Overall, the values were consistent with the 370 and 400 nm M centres identified by Sibley and Facey, the lowest uncertainty was found with the third Lorentzian fit. The L_1 term of the first Lorentzian was also quite accurate, but was let down by the error on the L2 term. However, the Lorentzian fits were finding the second absorption centre mentioned by Sibley and Facey on a more consistent basis. For example, the 30 Mrad sample showed 369 and 413 nm as the centre for its two curves.

6.8 Curve Fitting to the Roynon Howes Magnesium Fluoride

With the work completed on the Merck samples, it was then necessary to turn to the remaining sample groups; Roynon Howes and Carl Zeiss. The procedure of normalisation, fitting and analysis was the same as listed in detail in the preceding sections and so only the results will be discussed in the following sections.

The Roynon Howes material made up a small subsection of the magnesium fluoride samples. Originally, four samples were exposed to 0.5, 1, 15, 30 and 500 krad and to 1, 15 and 30 Mrad. The normalised transmission of the samples is shown in Figure 33 and shows that no clear feature can be distinguished.

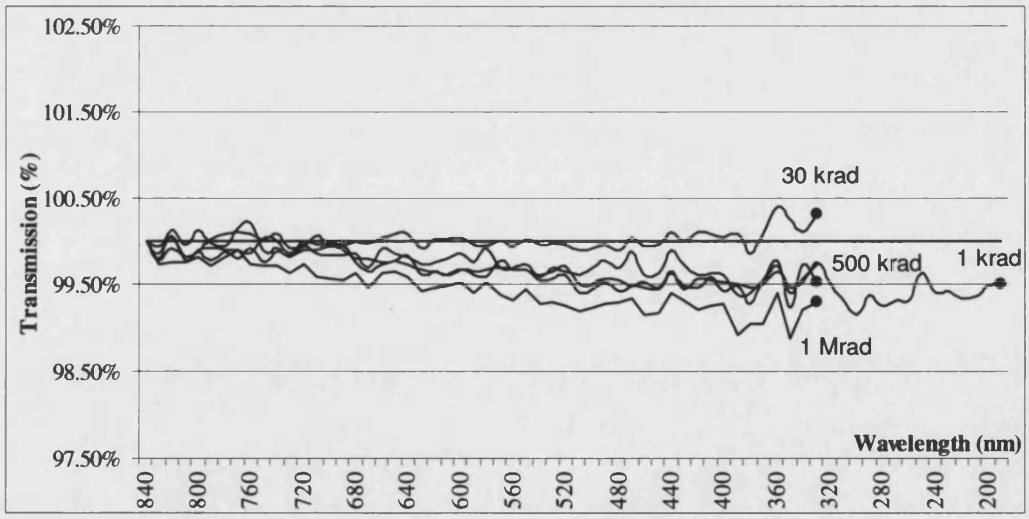

Figure 33. Transmission of Roynon Howes magnesium fluoride over a 330 to 840 nm range. No clear response to radiation is visible due to the lack of any sample exposed above 1 Mrad.

The main limitation to this set of data was the lack of spectra for samples exposed to 15 and 30 Mrad. This was due to the unexpected response of one of the samples. The sample selected to receive the maximum doses of 15 and 30 Mrad failed. Upon retrieving the samples from cell, it was found that this particular sample was completely darkened, more so than some of the glass exposed to similar levels.

At the time, it proved impossible to obtain any transmission spectra from it. When held up to the Sun a slight purple hue could be discerned, but this level of intensity was beyond the ability of any spectrophotometers available to this project. To this date the actual material that forms the sample remains unknown though it is probably not magnesium fluoride, unless it has been heavily contaminated.

The data was fitted with the Gaussian and Lorentzian equations mentioned earlier and the results of this are shown in Table 20.

	Gaussian						Lorentzian					
	Dose	1 krad	15 krad	30 krad	500 krad	1 Mrad	Dose	1 krad	15 krad	30 krad	500 krad	1 Mrad
Run 1: No constraint on wavelength	a1	0.003	*	0.004	0.004	0.004	l1	472	458	356	545	535
	a2	0.003	0.005	-0.003	0.003	0.007	l2	472	346	*	368	366
	b1	557	217	379	362	361	m1	6	0.01	0.00	0.00	0.01
	b2	379	439	357	533	496	m2	-6	700	0.00	0.00	0.01
	c1	143	20	6	41	37	w1	212	275	17	-188	295
	c2	85	157	33	114	174	w2	212	0	*	-108	-118
	SE(a1)	0.001	*	0.001	0.001	0.001	SE(l1)	35	9	2	17	17
	%	37%	*	23%	20%	20%	%	7%	2%	1%	3%	3%
	SE(a2)	0.003	0.000	0.001	0.000	0.000	SE(l2)	35	4	*	7	6
	%	83%	4%	17%	10%	4%	%	7%	1%	*	2%	2%
	SE(b1)	99	7	2	7	7	SE(m1)	*	0.00	0.00	0.00	0.00
	%	18%	3%	1%	2%	2%	%	*	5%	29%	14%	9%
	SE(b2)	17	12	9	27	17	SE(m2)	*	*	6.75	0.00	0.00
	%	4%	3%	3%	5%	3%	%	*	*	*	11%	12%
	SE(c1)	46	35	2	11	9	SE(w1)	270	25	7	50	34
	%	32%	175%	33%	27%	24%	%	127%	9%	41%	27%	12%
	SE(c2)	35	11	8	24	12	SE(w2)	270	*	*	33	34
	%	41%	7%	24%	21%	7%	%	127%	*	*	31%	29%
Run 2: Set to 370 and 400 nm	a1				-0.003		m1	-0.018	-0.014	-0.007	0.002	-0.034
	a2				0.007		m2	0.023	0.020	0.006	0.004	0.042
	c1				287		w1	1020	-810	-230	65	1124
	c2				211		w2	801	623	240	368	-880
	SE(a1)				0.003		SE(m1)	0.003	0.003	0.003	0.001	0.006
	%				87%		%	17%	19%	36%	50%	16%
	SE(a2)				0.003		SE(m2)	0.003	0.003	0.003	0.001	0.005
	%				36%		%	13%	14%	45%	23%	13%
	SE(c1)				79		SE(w1)	119	124	69	63	114
	%				28%		%	12%	15%	30%	97%	10%
	SE(c2)				30		SE(w2)	84	77	63	79	84
	%				14%		%	10%	12%	26%	21%	10%
Run 3: Set to 370 and 400 nm	A1	0.001		-0.005	0.003	0.001	l1			326	414	442
	A2	0.004		0.002	0.004	0.007	m1			-0.004	0.007	0.011
	B1	424		290	385	418	m2			-0.015	-0.004	-0.004
	C1	-58		-88	8	104	w1			12	252	325
	C2	183		117	174	195	w2			5	-78	105
	SE(a1)	0.001		0.003	0.001	0.003	SE(l1)			1	7	10
	%	60%		52%	33%	330%	%			0%	2%	2%
	SE(a2)	0.001		0.003	0.000	0.003	SE(m1)			0.004	0.001	0.002
	%	15%		165%	8%	49%	%			80%	16%	15%
	SE(b1)	12		65	3	18	SE(m2)			0.102	0.001	0.002
	%	3%		22%	1%	4%	%			667%	25%	49%
	SE(c1)	48		19	3	169	SE(w1)			14	25	29
	%	83%		22%	38%	163%	%			117%	10%	9%
	SE(c2)	12		64	14	25	SE(w2)			20	30	59
	%	7%		55%	8%	13%	%			400%	38%	56%

Table 20. Results for Gaussian and the Lorentzian to the Roynon Howes magnesium fluoride samples.

For Gaussian fits, the second fit with fixed wavelength only returned one set of results, and the SE on these results are significantly higher than for the freeform run. As such these results were of no use and were not considered further.

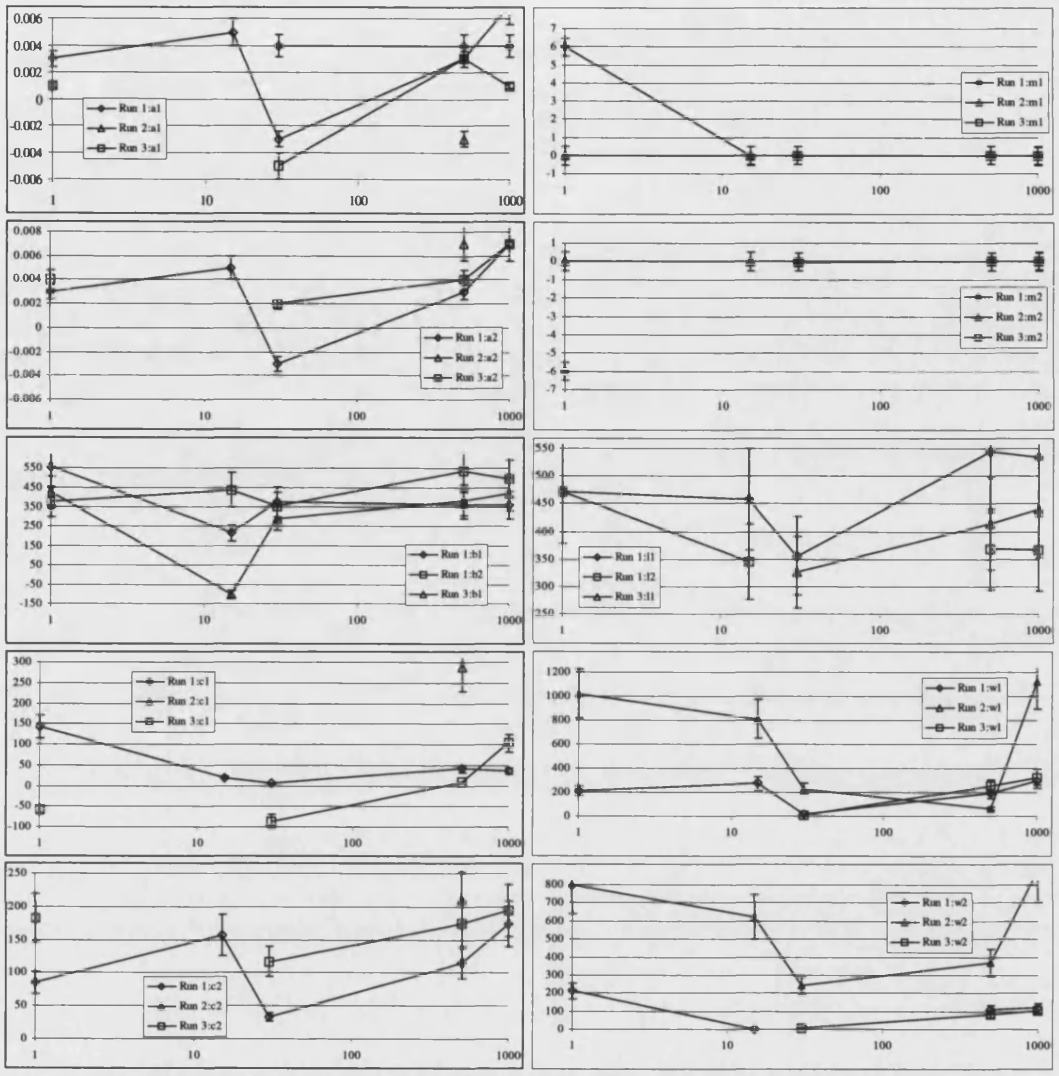

Figure 34. Series of graphs comparing the results of the Gaussian and Lorentzian fits to Roynon Howes magnesium fluoride. The left column shows the variables returned from the Gaussian fits data, the right shows the data for the variables returned for the Lorentzian. The y-axis is the returned value for the variable, the x-axis is the total dose in rad.

For the first and third Gaussian fits, the results were more complete though both fits struggled with the 15 krad sample. The first fit produced poor quality results, but the third run did not return any values. Overall the third Lorentzian fit produced the better results of the three fits, but of varying quality. The freeform fit returned values for each sample, but several of the SE were of such a high level that they were discounted. The second run with fixed wavelengths produced relatively good results, but the 500 krad sample was its weakest set of results. The fixed wavelength fit failed to return values for the first two data sets.

The returned values for the first and third runs show that the first run is the stronger. With both more returned values and generally better SE, but is still of a fairly low quality.

Overall, the Lorentzian data was of a disappointing quality, and could not be used to add to the previous results from the Merck magnesium fluoride. The lack of any real feature around the 370 nm region meant that the iterations were prone to finding spurious minima and there is little clarity to the results for the Roynon Howes samples.

6.9 Curve Fitting to the Carl Zeiss Magnesium Fluoride

The final batch of magnesium fluoride samples were supplied by the Carl Zeiss Company. As with the Roynon Howes samples, four samples were exposed to 0.5, 1, 15, 30 and 500 krad and to 1, 15 and 30 Mrad. The normalised transmission of the samples is shown in Figure 35 and shows a clear feature for the 15 and 30 Mrad data. Figure 36 shows the spectra over the 330 to 500 nm to show the absorption feature in more detail.

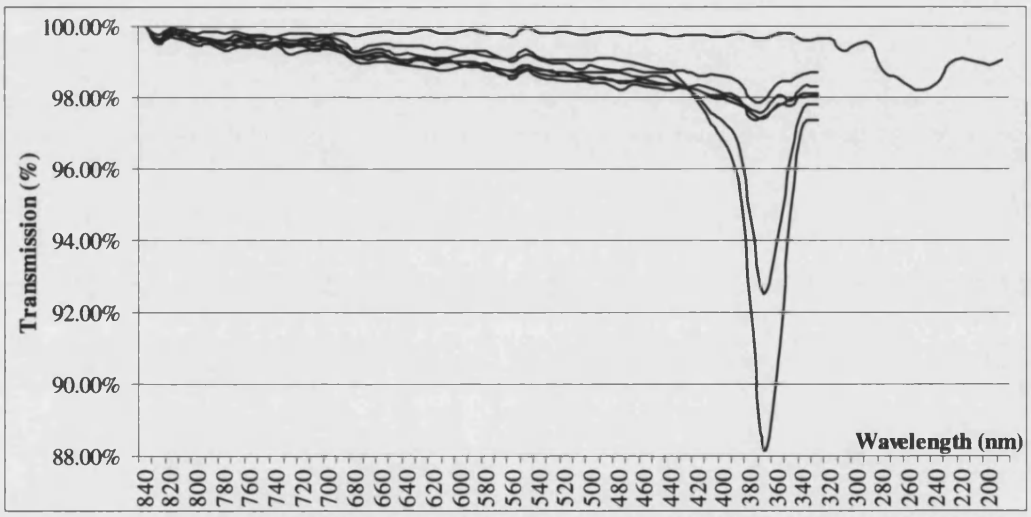

Figure 35. Transmission of Carl Zeiss magnesium fluoride over a 330 to 840 nm range. A response to radiation is visible around the 370 nm wavelength for the 15 and 30 Mrad samples. See following graph for details of total dose.

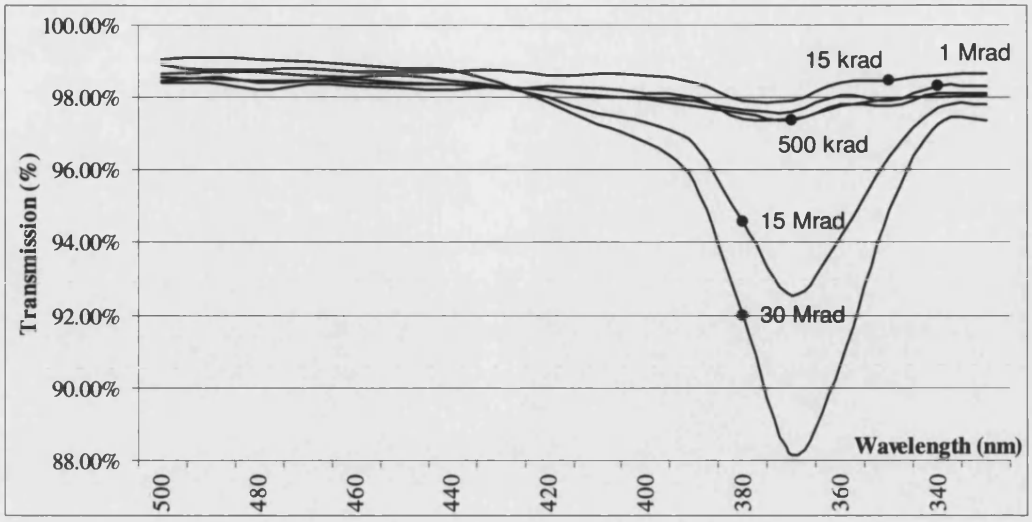

Figure 36. Transmission of Carl Zeiss magnesium fluoride over 330 to 500 nm showing greater detail of the absorption feature at ≈370 nm.

The data was fitted with Gaussian and Lorentzian equations and the results of this are shown in Table 21. The 'x' in certain cells is where the percentage error is exceptionally high where a very small value has a large error. (For example, the value for A_2 from the first run was 0.001 with an SE of 2 which gave a percentage error of 200,000%.)

For the Gaussian fits the freeform fit failed to return values for the 30 Mrad sample, the only Gaussian fit not to return data for this group of samples. Another interesting feature was how the returned values for the second and third runs converged for the 15 and 30 Mrad curves. Overall, the first run was more accurate than the third, with most variables having a lower SE, but a weighted average of the central wavelength was more accurate for the third run, mainly due to the presence of a value for 30 Mrad.

		Gaussian							Lorentzian				
	Dose	1 krad	15 krad	30 krad	500 krad	1 Mrad	15 Mrad	30 Mrad	Dose	1 krad	15 krad	30 krad	500 kra
Run 1: No constraint on wavelength	a1	-0.002	-12	0.013	-24	0.011	0.055		l1				
	a2	0.003	12	0.014	24	0.014	0.016		l2				
	b1	71	480	361	487	368	369		m1				
	b2	366	480	488	487	498	442		m2				
	c1	81	122	-43	-128	47	15		w1				
	c2	327	122	168	128	161	184		w2				
	SE(a1)	0.001	*	0.001	7000	0.001	0.002		SE(l1)				
	%	45%	*	9%	x	11%	3%		%				
	SE(a2)	0.000	*	0.001	7000	0.000	0.001		SE(l2)				
	%	7%	*	4%	x	3%	4%		%				
	SE(b1)	47	49	4	9	3	1		SE(m1)				
	%	66%	10%	1%	2%	1%	0%		%				
	SE(b2)	103	49	14	9	13	13		SE(m2)				
	%	28%	10%	3%	2%	3%	3%		%				
	SE(c1)	91	64	5	9	5	1		SE(w1)				
	%	112%	52%	12%	7%	11%	7%		%				
	SE(c2)	72	64	9	9	8	9		SE(w2)				
	%	22%	52%	5%	7%	5%	5%		%				
Run 2: Set to 370 and 400 nm	a1	-0.109	0.007	0.008	0.007	0.005	0.054	0.097	m1	0.001	0.017	0.022	0.024
	a2	0.111	0.014	0.017	0.019	0.018	0.017	0.015	m2	0.002	-0.003	-0.003	-0.002
	c1	-1247	13	20	19	19	14	14	w1	116	340	324	359
	c2	1085	187	189	198	188	188	164	w2	-598	16	-30	-87
	SE(a1)	0.280	0.001	0.001	0.002	0.001	0.002	0.003	SE(m1)	0.001	0.001	0.002	0.006
	%	257%	17%	16%	21%	26%	4%	3%	%	140%	6%	8%	25%
	SE(a2)	0.280	0.000	0.001	0.001	0.001	0.001	0.001	SE(m2)	0.001	0.002	0.003	0.005
	%	252%	3%	4%	4%	3%	4%	7%	%	35%	96%	82%	248%
	SE(c1)	1638	3	4	5	6	1	0	SE(w1)	338	25	24	49
	%	131%	23%	20%	26%	32%	7%	0%	%	291%	7%	7%	14%
	SE(c2)	1416	6	6	7	6	8	12	SE(w2)	171	26	46	267
	%	131%	3%	3%	4%	3%	4%	7%	%	29%	163%	153%	307%
Run 3: Set to 370 and 400 nm	a1	0.001	0.008	0.008	0.006	0.006	0.054	0.097	l1	502	375	374	431
	a2	0.001	0.014	0.017	0.018	0.017	0.017	0.016	m1	0.005	0.011	0.009	0.030
	b1	477	376	374	384	387	369	369	m2	-0.003	0.014	0.018	-0.013
	c1	234	10	19	24	27	14	14	w1	403	-13	-28	293
	c2	240	185	188	196	187	188	160	w2	-182	355	360	-115
	SE(a1)	2	0.001	0.001	0.001	0.001	0.002	0.003	SE(l1)	15	1	3	7
	%	x	16%	16%	22%	17%	4%	3%	%	3%	0%	1%	2%
	SE(a2)	2	0.000	0.001	0.001	0.001	0.001	0.001	SE(m1)	0.001	0.007	0.002	0.003
	%	x	3%	4%	4%	4%	4%	6%	%	24%	64%	25%	11%
	SE(b1)	*	2	3	4	4	1	0	SE(m2)	0.001	0.001	0.001	0.003
	%	*	1%	1%	1%	1%	0%	0%	%	38%	5%	6%	25%
	SE(c1)	6544	2	4	7	6	1	0	SE(w1)	44	11	13	16
	%	2797%	20%	21%	29%	22%	7%	0%	%	11%	85%	46%	5%
	SE(c2)	5210	6	6	7	6	8	11	SE(w2)	64	23	26	32
	%	2171%	3%	3%	4%	3%	4%	7%	%	35%	6%	7%	28%

Table 21. Results for Gaussian and the Lorentzian to the Carl Zeiss magnesium fluoride

Figure 37 is a comparison on the returned values for all the Lorentzian fits.

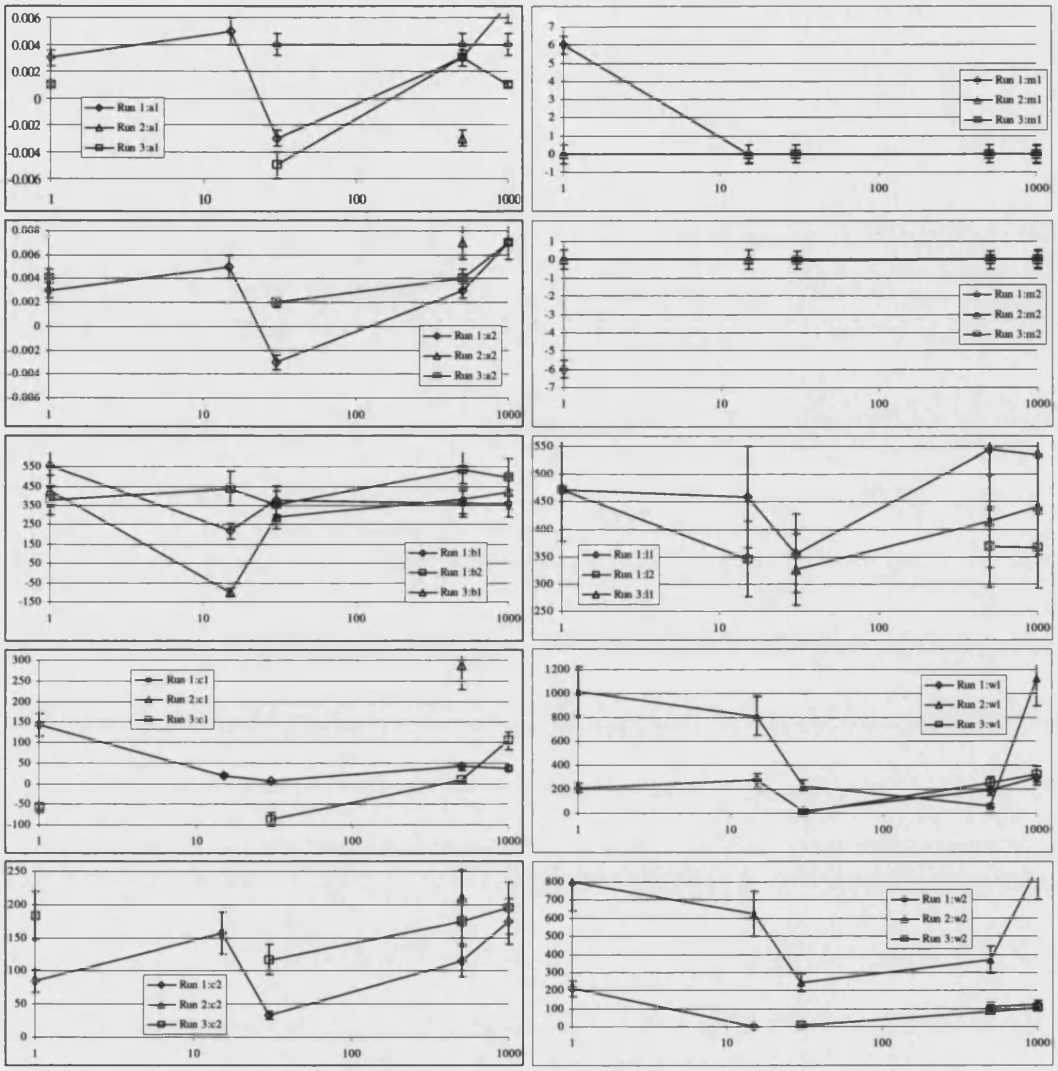

Figure 37. Series of graphs comparing the results of the Gaussian and Lorentzian fits to Carl Zeiss magnesium fluoride. The left column shows the variables returned from the Gaussian fits data, the right shows the data for the variables returned for the Lorentz fits. The y-axis is the returned value for the variable, the x-axis is the total dose in rad.

For the Lorentzian fits, the freeform fit only returned values for the two highest dose samples, though these had reasonable SE. In comparison, the fixed wavelength Lorentzian fit returned values for all the samples, but with very high SE for several of the samples. Overall, the presence of a deeper feature observed in the Carl Zeiss data led to better results from the iterative fits, however, the main growth of the feature is observed in the data for the two highest dose samples, 15 and 30 Mrad, and from these, the best fit was for the fixed wavelength difference equations

6.10 Summary: Magnesium Fluoride

Since the Merck samples made up the majority of the results, they formed the backbone of the iterative analysis. From these runs, the both the Gaussian and Lorentzian equations produced reasonable fits for the higher dose data, particularly for the fixed wavelength difference fits. Indeed, from the Merck data there is little to separate the two equations, though in both cases it is the fixed wavelength form which comes out best.

It is difficult to use the Roynon Howes and Carl Zeiss data to add to this comparison. In particular, the absence of any real feature in the Roynon Howes data due to the loss of the high dose sample limits the use of this particular group. However, the Carl Zeiss group did produce a range of data, and for the fixed wavelength difference run, the SE on the central wavelength of the Lorentzian fit was better across all the samples than for the Gaussian.

From this slight advantage, it was decided that the Lorentzian fit would be the one to apply to the task of approximating the 370 nm feature in Chapter 7.

6.11 Sapphire

Sapphire made up the second group of crystals for this study. As has been noted earlier, it is resilient to radiation but does show some reaction to high doses. In particular, the exposure of sapphire to electrons by Pellicori *et al* [13] showed the formation of absorption bands at 260 and 367 nm. Although the gamma rays are a different process, this work by Pellicori shows that the material does have a susceptibility to develop a feature at these wavelengths. Similarly, Griscom [35] notes that sapphire is susceptible to the formation of absorption bands at these two wavelengths.

Again, the samples provided by Merck formed the core of the study group for this material and where used for the majority of the analysis. As Figure 38 shows, the Merck samples did begin to develop a feature, but the total doses were not high enough to form a very deep feature.

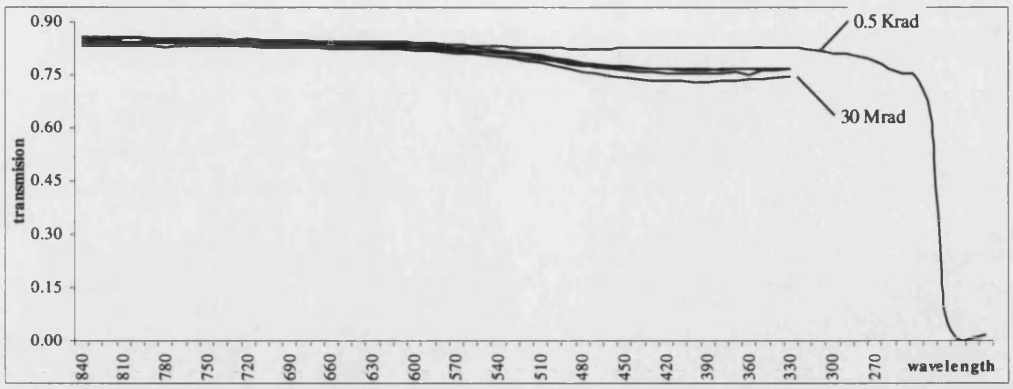

Figure 38. Transmission of Merck sapphire over 330 to 840 nm. The 0.5 krad to 30 Mrad spectra have been highlighted.

The region 330 to 600 nm is shown in detail in Figure 39. Both this figure and the one before are using data normalised in the same manner as the magnesium fluoride spectra (see Section 6.2.)

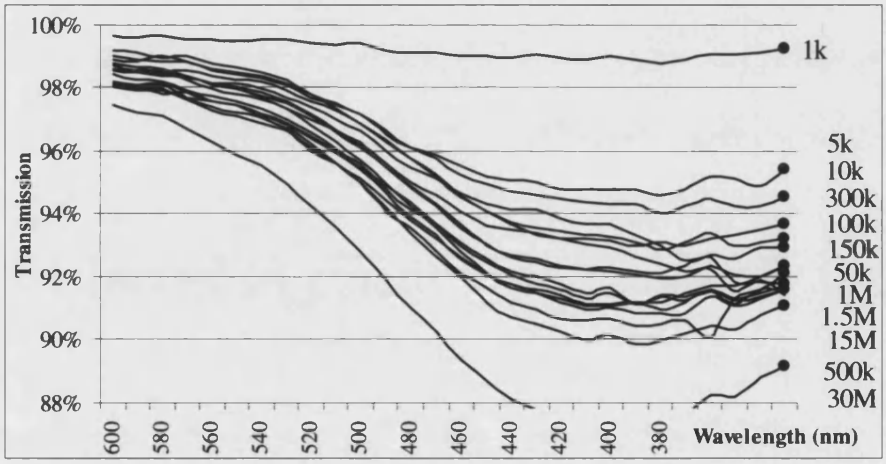

Figure 39. Transmission of Merck sapphire over 330 to 600 nm showing greater detail of the materials response to irradiation. The total dose is shown along the right side.

Although the sapphire does indeed show degradation, it is not spatially uniform. For example, although the data shows a decrease in transmission around the 400 nm range with increasing dose, the evolution of this feature in not smooth. This is further compounded that a significant portion of the radiation induced shape is truncated by the lower wavelength range.

Although it may well be possible to analyse and approximate this feature, since the current data does not capture the whole shape any proposed fit would be speculative. Based on the separate work Griscom and Pellicori *et al*, it was decided to approach the analysis by four routes:

Run 1: Lorentzian fit with wavelength fixed to 260 and 367 nm.

Run 2: Lorentzian fit with wavelength delta fixed to 107 nm.

Run 3: Lorentzian fit with wavelength fixed to 367 and 410 nm

Run 4: Lorentzian fit, 2 curves with no fixed wavelength.

Since the complete absorption feature was truncated by the lack of data at the lower wavelength, it was difficult to decide what shape to fit to the spectra. Since this would be a speculative approach, it was decided to fit the Lorentzian feature used for the magnesium fluoride data.

All the fits were undertaken in the manner described earlier for magnesium fluoride, the results are shown in Table 22 and Table 23. In these tables values that have been discounted from analysis have been shown by several marks;'*' denotes values above 10^4, '-' denotes divide by zero errors and '+' denotes percentage values greater than 10^5 %.

It was difficult to compare the results from these fits as they had diverse numbers of variables. However, it was possible to compare Run 1 with Run 3 (both have two curves with fixed wavelengths) and then to compare Run 2 with Run 4 (no fixed wavelength.)

In order to compare the runs across the dose range, it was necessary to see if there was a similar dependency between dose and absorption as seen in the magnesium fluoride samples. To establish whether such a relationship did exist, the wavelength of the lowest transmission was noted over the 330 to 600 nm range for each dose of the sapphire samples. These results are shown in Table 24.

	Dose	1 krad	5 krad	10 krad	15 krad	30 krad	50 krad	100 krad	150 krad	300 krad	500 krad	1 Mrad	1.5 Mrad	3 M
Lorentz 1: wavelength set to 260 and 367 nm	m1	0.013	0.074	0.085	0.12	0.13	0.12	0.10	0.11	0.099	0.14	-0.1	0.11	0.
	m2	12	0.0	0.0	0.0	0.0	0.0	0.0	0.0	397	0.0	0.19	71	0
	w1	-420	347	316	326	344	333	322	340	323	336	471	295	3
	w2	0	-23	-15	-18	-21	-16	15	-19	0	-17	-303	0	-
	SE(m1)	0	0.0100	0.0100	0.012	0.014	0.015	0.0100	0.013	0.0090	0.016	0.0090	0.0070	0.(
	%	7.7%	14%	12%	10%	11%	12%	9.9%	12%	9.1%	11%	8.3%	6.1%	9.
	SE(m2)	*	0.0080	0.011	0.013	0.013	0.018	0.012	0.013	*	0.018	0.0070	*	0.0
	%	*	200%	550%	433%	260%	450%	600%	433%	*	600%	3.7%	*	30
	SE(w1)	39	36	30	28	31	34	26	33	28	32	28	18	2
	%	9.3%	10%	9.5%	8.6%	9.0%	10%	8.1%	9.7%	8.7%	9.5%	5.9%	6.1%	7.
	SE(w2)	*	98	151	148	98	147	161	146	*	173	9.0	*	1
	%	-	426%	1007%	822%	467%	919%	1073%	768%	-	1018%	3.0%	-	61
Lorentz 2: wavelength difference set to 107 nm	I1	220	329	279	324	322	320	323	321	318	320	388	333	3
	m1	0.19	0.035	0.076	0.061	0.058	0.058	0.055	0.052	0.051	0.065	0.100	0.067	0.(
	m2	0	0.038	25	0.053	0.065	0.069	0.042	0.057	0.049	0.076	0.0080	0.042	0.(
	w1	-112	164	316	169	166	158	181	172	171	161	203	122	1
	w2	-67	-152	0	145	164	141	-140	147	135	-151	82	-161	1
	SE(I1)	96	6.0	7.0	5.0	7.0	4.0	5.0	6.0	5.0	6.0	3.0	3.0	4
	%	44%	1.8%	2.5%	1.5%	2.2%	1.3%	1.5%	1.9%	1.6%	1.9%	0.77%	0.90%	1.
	SE(m1)	5.9	0.0040	0.0070	0.0050	0.0080	0.0050	0.0050	0.0070	0.0050	0.0080	0.0020	0	0.0
	%	3168%	11%	9.2%	8.2%	14%	8.6%	9.1%	13%	9.8%	12%	2.0%	1.5%	3.(
	SE(m2)	0.24	0.0060	*	0.0090	0.012	0.0090	0.0070	0.0100	0.0080	0.012	0.0040	0.0020	0.0
	%	813%	16%	*	17%	18%	13%	17%	18%	16%	16%	50%	4.8%	6.
	SE(w1)	1718	38	24	31	46	38	29	46	37	43	11	7.0	9
	%	1534%	23%	7.6%	18%	28%	24%	16%	27%	22%	27%	5.4%	5.7%	6.
	SE(w2)	108	14	2844	15	16	12	17	17	16	14	69	6.0	6
	%	161%	9.2%	-	10%	9.8%	8.5%	12%	12%	12%	9.3%	84%	3.7%	3.(

Table 22. Results for the first and second Lorentzian fit to the Merck sapphire sam

	Dose	1 krad	5 krad	10 krad	15 krad	30 krad	50 krad	100 krad	150 krad	300 krad	500 krad	1 Mrad	1.5 Mrad	3 M
Lorentz 3: wavelength set to 367 and 410 nm	m1	0.050	0.023	0.035	0.053	0.050	0.042	0.050	0.040	0.043	0.052	0.042	0.082	0.(
	m2	0.027	0.036	0.031	0.036	0.049	0.058	0.027	0.047	0.035	0.060	0.063	0	(
	w1	209	204	191	208	215	193	209	205	195	198	199	221	2
	w2	-177	-195	-179	-184	-196	173	-177	-181	166	-183	-199	41	3
	SE(m1)	0.0090	0.0090	0.0100	0.012	0.014	0.011	0.0090	0.011	0.0090	0.014	0.013	0.0030	0.0
	%	18%	39%	29%	23%	28%	26%	18%	28%	21%	27%	31%	3.7%	2.
	SE(m2)	0.0100	0.0090	0.0100	0.012	0.014	0.012	0.0100	0.012	0.0090	0.015	0.014	0.0030	0.0
	%	37%	25%	32%	33%	29%	21%	37%	26%	26%	25%	22%	30%	6
	SE(w1)	36	79	57	45	57	55	36	57	40	54	64	6.0	7
	%	17%	39%	30%	22%	27%	28%	17%	28%	21%	27%	32%	2.7%	3.(
	SE(w2)	49	30	39	44	38	26	49	32	33	29	24	26	3
	%	28%	15%	22%	24%	19%	15%	28%	18%	20%	16%	12%	63%	10
Lorentz 4: no constraint on wavelength	L1	385	396	391	387	390	392	385	391	389	343	398	332	3
	L2	385	396	391	387	390	392	385	391	389	433	398	442	4
	M1	5.0	4.0	6.0	6.0	6.0	7.0	5.0	6.0	5.0	0	4.0	0.070	0.(
	M2	-5	-4	-6	-6	-6	-7	-5	-6	-5	0	-4	0.040	0.(
	W1	125	126	114	125	133	116	125	123	115	139	128	130	1
	W2	124	125	-113	-123	-131	115	124	122	-113	150	-126	158	-1
	SE(l1)	69	5.0	46	26	5.0	23	69	18	19	6.0	28	5.0	6
	%	18%	1.3%	12%	6.7%	1.3%	5.9%	18%	4.6%	4.9%	1.7%	7.0%	1.5%	1.
	SE(l2)	71	5.0	45	27	6.0	23	71	17	19	8.0	28	7.0	7
	%	18%	1.3%	12%	7.0%	1.5%	5.9%	18%	4.3%	4.9%	1.8%	7.0%	1.6%	1.(
	SE(m1)	*	10000	*	*	10000	*	*	*	*	0.0100	5000	0.0100	0.0
	%	*	+	*	*	+	*	*	*	*	-	+	14%	1
	SE(m2)	*	10000	*	*	10000	*	*	*	*	0.020	5000	0.0100	0.0
	%	*	+	*	*	+	*	*	*	*	-	+	25%	2
	SE(w1)	3686	1672	2244	1720	1633	1388	3686	1747	3063	49	1141	31	3
	%	2949%	1327%	1968%	1376%	1228%	1197%	2949%	1420%	2663%	35%	891%	24%	2
	SE(w2)	3713	1683	2253	1732	1648	1398	3713	1761	3084	16	1156	16	2
	%	2994%	1346%	1994%	1408%	1258%	1216%	2994%	1443%	2729%	11%	917%	10%	1

Table 23. Results for the third and fourth Lorentzian fit to the Merck sapphire sam

Dose (rad)	1k	5k	10k	15k	30k	50k	100k	150k	300k	500k	1M	1.5M	3M
λ_{min}	380	380	380	380	380	400	380	380	390	390	360	330	330
	Mean	374	SD	20									
Trans(380)	98.8%	94.6%	94.1%	91.9%	90.9%	91.2%	92.9%	92.1%	93.1%	90.0%	90.5%	93.0%	92.4%
Trans(370)	98.9%	94.8%	94.3%	92.0%	91.2%	91.5%	93.1%	92.3%	93.0%	90.2%	90.6%	92.5%	92.2%
Absorp(374)	1.14%	5.30%	5.84%	8.03%	8.93%	8.68%	7.03%	7.77%	6.97%	9.91%	9.47%	7.24%	7.71%

Table 24. Wavelength of lowest transmission for Merck sapphire in the 300 to 600 nm range. The absorptio lowest wavelength of 374 nm.

Table 24 shows that the wavelength of the lowest transmission (λ_{min}) varies from 330 to 400 nm, with an average value of 374 ±20 nm. A simple linear interpolation was taken for each sample to calculate the absorption (absorption = 1-transmission) at 374 nm and this value is plotted as a function of dose in Figure 40.

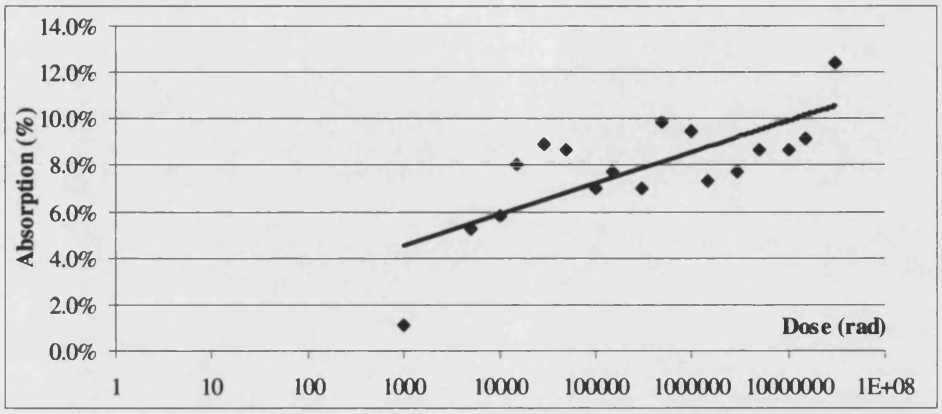

Figure 40. Log relation between absorption at 374 nm as a function of dose for Merck sapphire.

Over the range of the samples in this project, the growth of the absorption appears to be directly proportional to the Ln(Dose in rads). From this, it was decide to use this relation to weight the results for sapphire.

Figure 42 compares the variables returned from the Lorentzian fits to the Merck sapphire data. From these, it can be seen that of the runs based around the 260 and 367 nm wavelengths, Run 2 was superior to Run 1 for all samples.

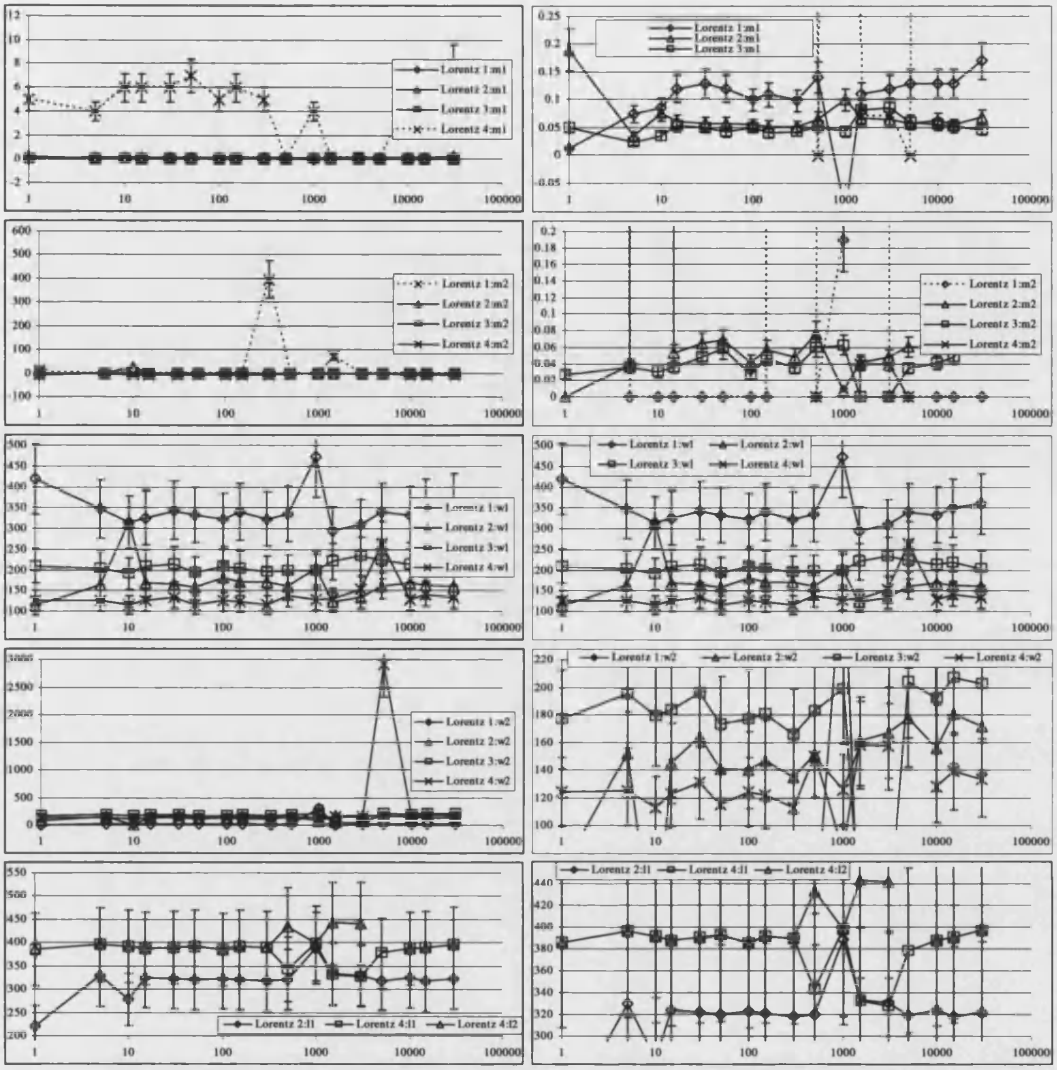

Figure 41. Series of graphs comparing the results of the Lorentzian fits to Merck sapphire on the variables L, W and M. The left column shows the full range of data, the right shows the data in detail. The y-axis is the returned value for the variable, the x-axis is the total dose in rad.

Similarly, Run 3 was stronger than both Run 4 and Run 2 which suggests that the best fit to this projects data for Merck Sapphire was obtained with a Lorentzian fixed to 260 and 367 nm.

6.12 Union Carbide, Hemex and Hemlite

In addition to the Merck sapphire, additional material was sourced from Union Carbide. This was their standard sapphire, their purer Hemlite and ultra-pure Hemex. In a similar manner as the magnesium fluoride, these secondary samples were spread over a wide range.

The Hemlite and Hemex showed virtually no response to irradiation, and the standard material showed less response than the Merck material. A comparison of the spectra of the 30 Mrad samples is shown in Figure 42, the material from Union Carbide showed a similar response as to the Merck. For fitting or approximation, the lack of response to irradiation from the Hemex and Hemlite meant they were of no use for this purpose.

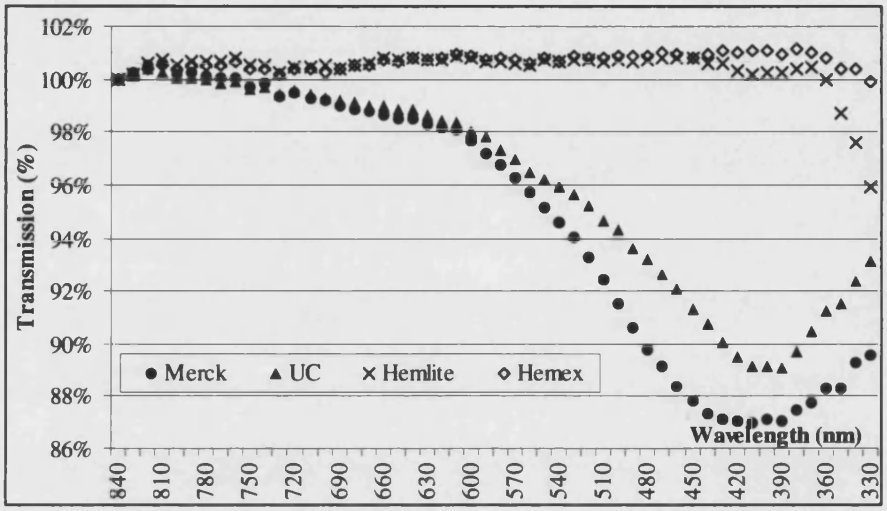

Figure 42. Comparison of transmission 30 Mrad samples of Merck, Union Carbide, Hemex and Hemlite samples over 330 to 840 nm.

6.13 Summary: Sapphire

The Merck samples made up the majority of the samples for the analysis of this material and from them it was found that a Lorentzian fit with the central wavelengths held to 367 and 410 nm was the most satisfactory.

However, the major weakness here was the lack of data at lower wavelengths. Unlike the magnesium fluoride fits where the majority of the 370 nm feature was captured, the width of the sapphire feature was such that there may well have been a significant proportion of the feature below the range of the data. Indeed, it may well be that if the data was present at lower wavelengths the first run (260 and 367 nm) may have been more significant.

The low level of confidence in the certainty of the fit meant that sapphire was not considered for the approximation process in Chapter 7.

6.14 F2

That the unhardened glass samples would be adversely affected by irradiation was of little doubt given that the "browning" of glass was amongst the first radiation effects noted. Figure 43 shows the transmission for several F2 samples over a range of total doses. As can be seen, the greatest change is over the 10 to 100 krad range. Beyond this, the damage starts to saturate and the rate of increase begins to slow. Indeed, there s little difference between the transmission spectra for the 10 and 30 Mrad samples.

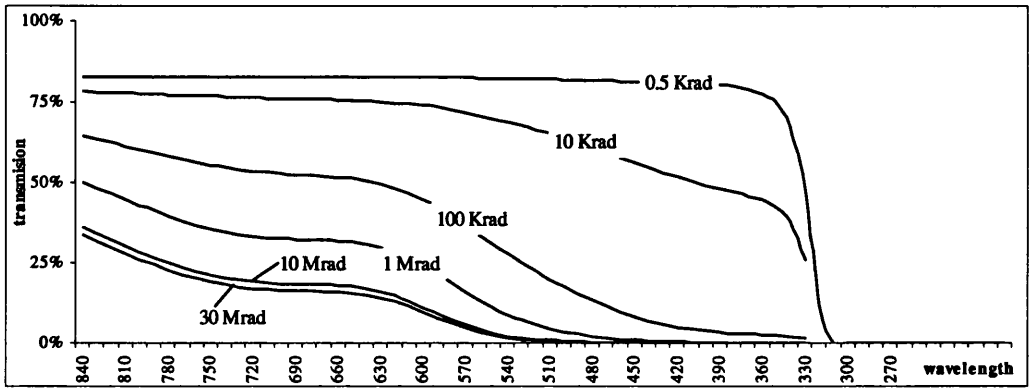

Figure 43. Response of F2 Samples to 0.5 krad to 30 Mrad gamma irradiation.

The process of normalisation for the F2 samples was slightly different to the magnesium fluoride and sapphire process mentioned earlier. Although the first step was same in that the spectra were divided by the lowest exposed sample, there was no justification for setting the transmission to unity at any particular point.

As can be seen from Figure 43, at 840 nm the spectra is affected by irradiation and so the normalisation of the F2 samples was of the form:

$$S_{N\lambda} = \frac{S_\lambda}{C_\lambda} \text{ where:}$$

$S_{N\lambda}$ is the part - normalised sample transmission at wavelength λ

S_λ is the original sample transmission at wavelength λ

C_λ is the control sample transmission at wavelength λ

The approach to fitting curves was slightly different as well. The main driver was to reduce the data to a point where the radiation induced attenuation could be modelled accurately. As such, the shape of the data was important in deciding how many fits would be necessary to accurately capture the shape and evolution of the absorption features.

6.14.1 Gauss vs. Lorentz; 2 runs vs. 3 vs. 5

The approach here was to attack the data with a large number of iterative runs. The underlying equations fitted were:

Gaussian:

2 Gauss curves, no fixed wavelength

3 Gauss curves, no fixed wavelength

3 Gauss curves, wavelength fixed to 395, 510 and 735 nm.

4 Gauss curves, wavelength fixed to 345, 395, 510 and 735 nm.

Lorentz:

2 Lorentz curves, no fixed wavelength

3 Lorentz curves, no fixed wavelength

3 Lorentz curves, wavelength fixed to 395, 510 and 735 nm.

4 Lorentz curves, wavelength fixed to 345, 395, 510 and 735 nm.

As was to be expected with such a wide net, the success rate varied across the equations, with some not fitting at all. This was a speculative pursuit to see if any particular combination came out in preference to the rest.

The fixed wavelengths used were taken from the average of the successful speculative free fit results. The process was to set of a multiple run with up to five wavelength centres in them. For each run that returned successful values, those values were stacked into a table. This process yielded 120 values for central wavelengths over the range 275 to 800 nm. These values were than sorted into 5 nm bins and their frequency ranked.

Rank	Bin (nm)	Members
1	735	24
2	510	15
3	395	14
4	345	9
5	705	7

Table 25. Frequency of five most common wavelengths for F2 iterative runs.

These values then formed the core for Lorentzian of Gaussian fit requiring a fixed wavelength. Of the multiple tests, the three Lorentzian fit with free wavelength proved to be more consistent and more accurate than the rest.

6.14.2 Selection of 3 Lorentz Fits

By comparing all the results from the various runs, the 3 Lorentz fits emerged as the most successful by some way. This is shown in Table 26.

Run	< 500	500 iterations	Failed runs
3 Gaussian – no fixed wavelengths	6	8	3
3 Gaussian - fixed wavelengths	7	0	10
3 Lorentzian – no fixed wavelengths	14	3	0
3 Lorentzian - fixed wavelengths	14	1	2

Table 26. Results of the three Lorentzian fit to the F2 data.

The form of the Lorentzian equation that proved most successful was:

$$y = 1 - (G1 + G2 + G3)$$

where

$$G1 = M_1 \times \left[(W_1/2)^2 / \left((x - L_1)^2 + (W_1/2)^2 \right) \right]$$

$$G2 = M_2 \times \left[(W_2/2)^2 / \left((x - L_2)^2 + (W_2/2)^2 \right) \right]$$

and

$$G3 = M_3 \times \left[(W_3/2)^2 / \left((x - L_3)^2 + (W_3/2)^2 \right) \right]$$

The results for the 3 Lorentzian with no fixed wavelengths are shown in Table 27.

Dose	1 krad	5 krad	10 krad	15 krad	30 krad	50 krad	100 krad	150 krad	300 krad	500 krad	1 Mrad	1.5 Mrad	3 Mrad
l1			310	317	316	321	323	325	330	330	335	335	
l2			416	425	437	452	481	497	519	511	519	529	
l3			769	753	754	750	753	752	755	749	751	754	
m1			0.31	0.37	0.55	0.66	0.79	0.84	0.89	0.87	0.89	0.91	
m2			0.22	0.25	0.36	0.41	0.41	0.4	0.32	0.36	0.32	0.27	
m3			0.03	0.02	0.06	0.07	0.16	0.22	0.31	0.27	0.31	0.35	
w1			194	190	222	241	326	375	480	428	465	540	
w2			-243	227	243	238	243	235	217	218	208	200	
w3			232	-142	178	160	222	232	265	237	252	267	
SE(l1)			10	6	6	5	7	8	9	8	9	10	
%			3%	2%	2%	2%	2%	2%	3%	2%	3%	3%	
SE(l2)			18	15	17	14	11	7	3	4	3	2	
%			4%	4%	4%	3%	2%	1%	1%	1%	1%	0%	
SE(l3)			4	4	3	3	2	2	2	2	2	2	
%			1%	1%	0%	0%	0%	0%	0%	0%	0%	0%	
SE(m1)			0.12	0.1	0.16	0.15	0.15	0.12	0.07	0.08	0.07	0.06	
%			39%	27%	29%	23%	19%	14%	8%	9%	8%	7%	
SE(m2)			0.12	0.11	0.19	0.19	0.23	0.2	0.14	0.16	0.14	0.12	
%			55%	44%	53%	46%	56%	50%	44%	44%	44%	44%	
SE(m3)			0	0	0.01	0.01	0.03	0.04	0.07	0.06	0.07	0.09	
%			0%	0%	17%	14%	19%	18%	23%	22%	23%	26%	
SE(w1)			104	78	101	93	124	128	132	125	121	138	
%			54%	41%	45%	39%	38%	34%	28%	29%	26%	26%	
SE(w2)			27	25	34	35	50	46	41	42	40	39	
%			11%	11%	14%	15%	21%	20%	19%	19%	19%	20%	
SE(w3)			23	23	22	22	28	29	33	31	31	36	
%			10%	16%	12%	14%	13%	13%	12%	13%	12%	13%	

Table 27. Returned values for Lorentzian fit with three free wavelengths with the actual and percen

The calculations of the central wavelengths L_1, L_2 and L_3 are also shown and can be calculated as:

$$L_1, = 327 \pm 8 \text{ nm}, L_2 = 496 \pm 45 \text{ nm}, L_3 = 755 \pm 5 \text{ nm}$$

6.14.3 Weighting

For any calculations that may require weighting, it was necessary to look at the growth of the radiation induced absorption. The value at 840 nm was chosen as the data had not saturated, and so would show the growth across the full range of dose. These values are shown in Table 29.

Dose (rad)	Absorption (%) at 840 nm.
1000	0%
1500	1%
3000	0%
5000	1%
10000	5%
15000	4%
30000	9%
50000	10%
100000	22%
150000	28%
300000	42%
500000	34%
1000000	40%
1500000	48%
3000000	50%
5000000	55%
10000000	56%
15000000	57%
30000000	59%

Table 28. Growth of absorption for F2 glass at 840 nm.

These values are shown in Figure 45 and show a log growth for the data. Thus for weighting, a log of the total dose would be suitable.

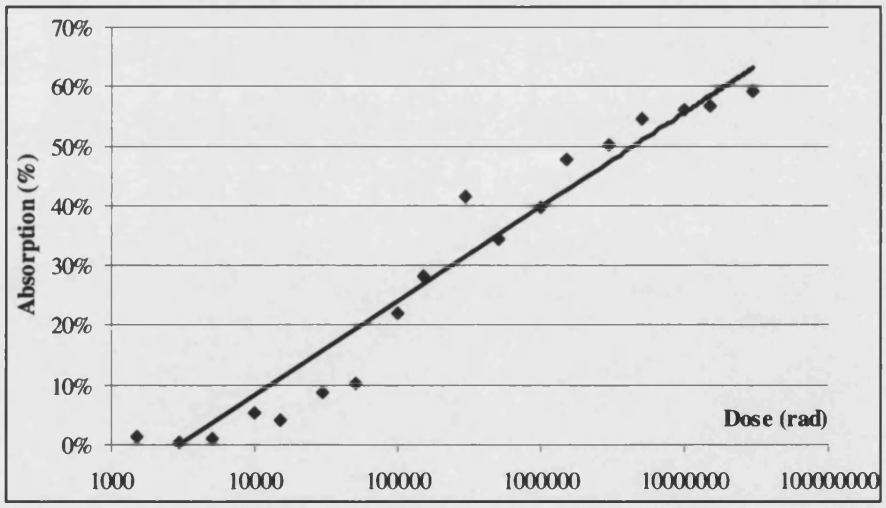

Figure 44. Growth of absorption in F2 glass at 840 nm.

6.15 Radiation Hardened F2 G12

As would be expected, the response of the hardened counterpart of F2 was far less significant. As is shown in Figure 45, there is very little change in the spectra above 480 nm. Below this point, there is a response which is proportional to the total dose, but is quite limited compared to the unhardened counterpart.

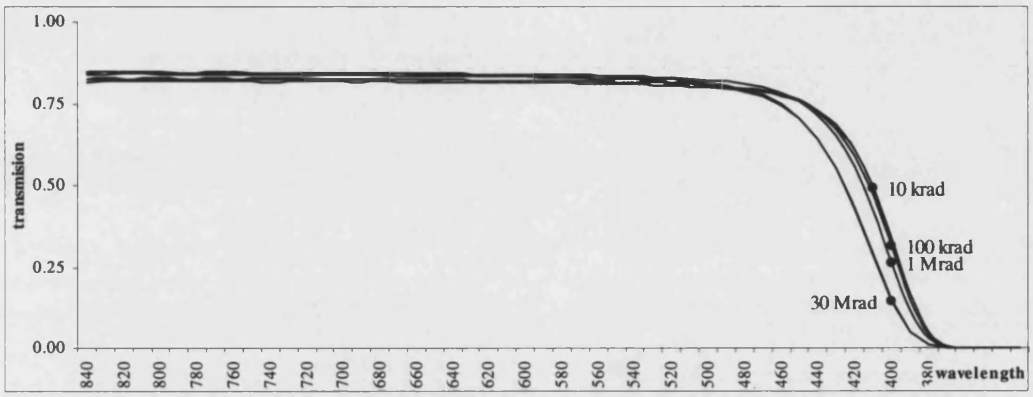

Figure 45. Transmission of F2 G12 over 1 krad to 30 Mrad total dose.

Figure 46 shows the spectra of several samples exposed to 0.01 to 30 Mrad normalised to the 0.5 krad spectra. This figure shows the development of a feature centred around 380 nm, the 5 nm steps in the data don't give enough detail to investigate the feature fully.

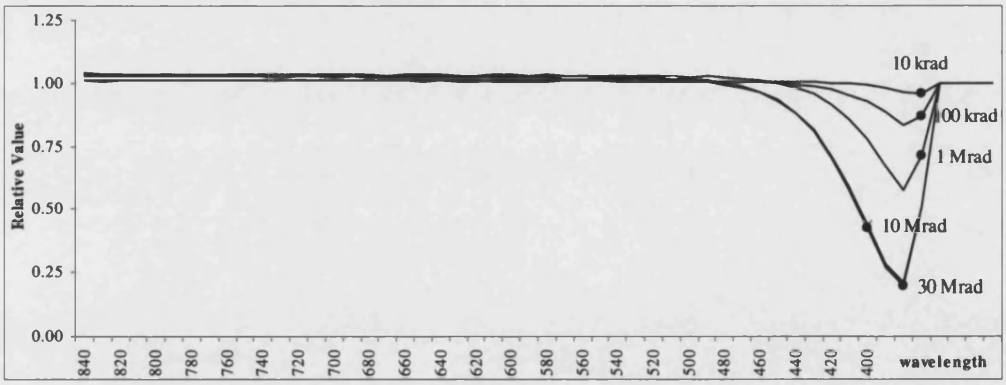

Figure 46. Relative transmission of F2 G12 10 krad to 30 Mrad samples relative to 0.5 krad spectra

Although similar in shape to the magnesium fluoride asymmetric feature investigated earlier, the difference is that at 380 nm, the samples are all approaching their natural cut off in transmission. This means that the values below 380 nm become very sensitive to any errors in the raw data. Another issue is that the feature is contained below 470 nm. If any instrument was to be designed to work below the wavelengths in a radioactive environment, then other materials such as sapphire and magnesium fluoride would be more suitable.

As such, it was decided that it would not be beneficial to investigate this feature further at this time.

6.16 BK7

As with the F2 samples it was of little surprise that the BK7 samples displayed a strong response to their irradiation. Although it was generally less susceptible than the F2, it was still strongly affected and shared the same propensity as F2 to suffer the majority of the attenuation at lower wavelengths.

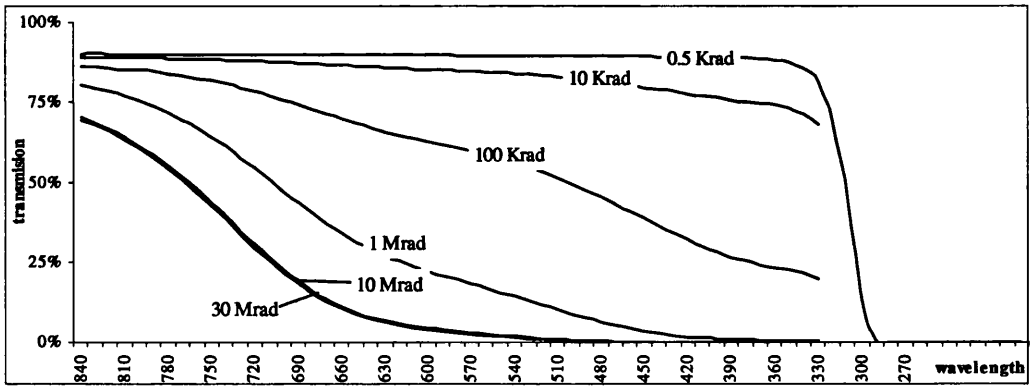

Figure 47. Response of Selected BK7 Samples to Gamma Radiation

Another difference was that where F2 had a slight plateau in its spectra around 600 nm for very high total doses, BK7 suffered a consistent fall in its transmission. However, into the infra-red even heavily irradiated BK7 was still able to transmit over 50% of light incident through the sample.

6.16.1 Selecting and Fitting a Curve

In a manner similar to that described earlier for F2, the first step in the analysis of the BK7 data was to attack it with multiple runs. Again, a combination of Gaussian and Lorentzian curves was fitted to see how they well they would respond.

The data was normalised in the manner described for F2 and then an attempt was made to fit the data with curves composed of 2, 3, 4, 5, 6 and 7 Gaussian and Lorentzian curves. A summary of the results is show below:

Run	Successful	Stopped at 500 iterations	Failed runs
2 Gaussian, no fixed wavelengths	17	2	0
2 Lorentzian, no fixed wavelengths	7	11	1
3 Gaussian, no fixed wavelengths	4	11	4
3 Lorentzian, no fixed wavelengths	5	14	0
4 Gaussian, no fixed wavelengths	1	6	12
4 Lorentzian, no fixed wavelengths	7	8	4
5 Gaussian, no fixed wavelengths	0	14	5
5 Lorentzian, no fixed wavelengths	2	13	4
6 Gaussian, no fixed wavelengths	0	12	7
6 Lorentzian, no fixed wavelengths	0	17	2
7 Gaussian, no fixed wavelengths	0	1	18
7 Lorentzian, no fixed wavelengths	3	14	2

Figure 48. Results of 2 to 7 Curve Fits to BK7 data

As can be seen, the clear frontrunner was the 2 Gaussian fit with no fixed wavelengths. This was of the form:

$$y = 1 - (G1 + G2)$$

where

$$G1 = A_1 \times \exp\left[-\left((x - B_1)^2 / \left(2 \times C_1^{\,2}\right)\right)\right]$$

and

$$G1 = A_2 \times \exp\left[-\left((x - B_2)^2 / \left(2 \times C_2^{\,2}\right)\right)\right]$$

The results of this function are shown in Table 27.

Dose	1 krad	1.5 krad	3 krad	5 krad	10 krad	15 krad	30 krad	50 krad	100 krad	150 krad	300 krad	500 krad	1 Mrad	1.5 Mrad	3 Mrad
A1	3.92	0.01	0.06	0.02	0.28	0.20	0.28	0.52	0.71	0.87	0.97	0.99	1.00	1.01	1.01
A2	-0.05	-0.01	0.00	0.85	0.01	0.06	0.14	0.12	0.26	0.13	0.12	0.18	0.21	0.30	0.37
B1	*	346	170	374	48	323	320	330	330	330	355	373	380	383	382
B2	840	794	*	*	*	555	486	604	579	644	645	642	642	646	650
C1	*	99	221	56	281	102	94	122	115	178	217	204	211	221	216
C2	1000	105	*	639	*	-125	176	98	123	72	60	73	78	89	94
SE(A1)	*	0.000	0.008	0.006	0.063	0.005	0.029	0.002	0.021	0.002	0.001	0.002	0.002	0.003	0.004
%	*	0%	14%	38%	23%	2%	10%	0%	3%	0%	0%	0%	0%	0%	0%
SE(A2)	4.532	0.000	0.003	2.450	*	0.004	0.013	0.005	0.023	0.007	0.002	0.007	0.010	0.019	0.031
%	*	0.0%	100%	290%	*	7.0%	9.0%	4.1%	8.9%	5.3%	1.7%	3.9%	4.9%	6.4%	8.4%
SE(B1)	*	9	54	16	93	2	3	2	3	2	1	2	3	5	6
%	*	2.6%	31.8%	4.3%	193.8%	0.6%	0.9%	0.6%	0.9%	0.6%	0.3%	0.5%	0.8%	1.3%	1.6%
SE(B2)	*	14	*	*	*	15	28	5	16	1	1	1	2	2	2
%	*	1.8%	*	*	*	2.7%	5.8%	0.8%	2.8%	0.2%	0.2%	0.2%	0.3%	0.3%	0.3%
SE(C1)	*	7	24	13	37	4	5	3	7	3	1	2	2	4	6
%	*	7.1%	10.9%	23.2%	13.2%	3.9%	5.3%	2.5%	6.1%	1.7%	0.5%	1.0%	0.9%	1.8%	2.8%
SE(C2)	*	13	*	258	*	6	12	2	7	2	1	2	3	4	4
%	*	12.4%	*	40.4%	*	4.8%	6.8%	2.0%	5.7%	2.8%	1.7%	2.7%	3.8%	4.5%	4.3%

Table 29. Returned values for Gaussian fit with three free wavelengths with the actual and percent

From these values, the centre of the two Gaussian curves was calculated as:

B1 = 359 ± 26 nm, B2 = 635 ± 66 nm

6.16.2 Weighting

For any calculations that may require weighting, it was necessary to look at the growth of the radiation induced absorption. The value at 840 nm was chosen as the data had not saturated, and so would show the growth across the full range of dose. These values are shown in Table 30.

Dose (rad)	Absorption (%) at 840 nm.
1000	0%
1500	-1%
3000	0%
5000	1%
10000	1%
15000	1%
30000	3%
50000	1%
100000	4%
150000	2%
300000	8%
500000	8%
1000000	11%
1500000	16%
3000000	17%
5000000	22%
10000000	22%
15000000	21%
30000000	23%

Table 30. Growth of absorption for BK7 glass at 840 nm.

These values are shown in Figure 49 and show a log growth for the data. Thus for weighting, a log of the total dose would be suitable.

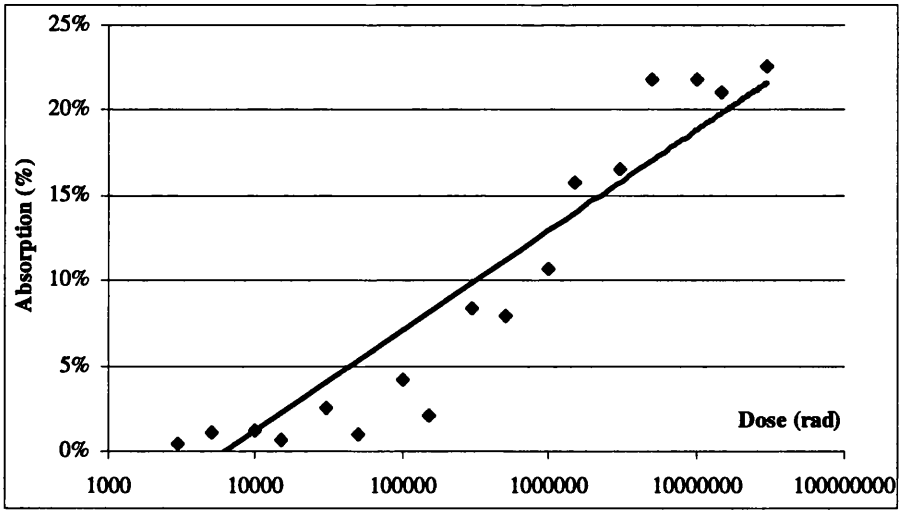

Figure 49. Growth of absorption in BK7 glass at 840 nm.

6.17 Radiation Hardened BK7 G18

As with the F2 glass, it was not anticipated that the radiation hardened BK7 would display much response to irradiation. As can be seen in Figure 50, the deterioration is virtually non-existent. Indeed, the variation evident in the spectra above 500 nm makes it very difficult to quantify the response of the material at these dose levels.

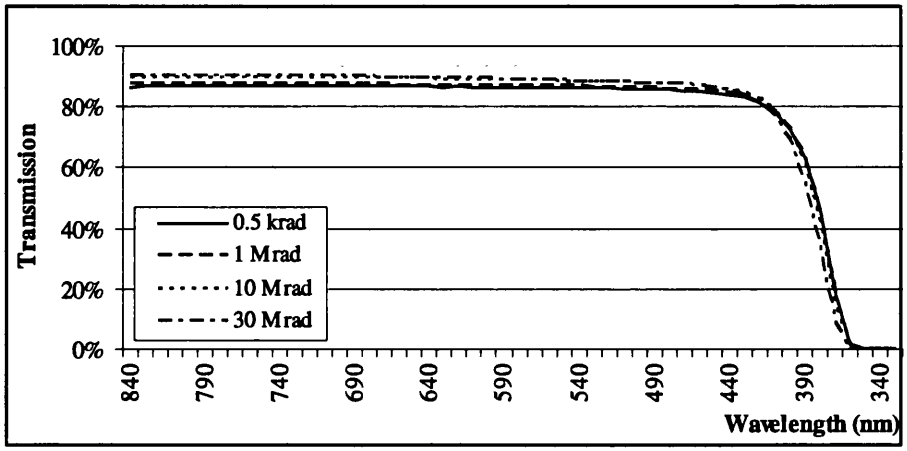

Figure 50. Transmission of BK7 G18 over 1 krad to 30 Mrad Total Dose

This lack of attenuation makes any analysis of the decline in transmission due to irradiation even more difficult. As Figure 50 demonstrates, there is little to analyse as the proximity of the feature to the materials cut-off requires data with more accuracy than this project has provided.

6.18 Summary: F2 and BK7

The unhardened glasses showed a strong response to irradiation. Lorentzian and Gaussian fits were successfully applied and will be considered further in Chapter 7. The lack of response from the hardened glasses meant no further analysis was possible.

7 Approximating Radiation Induced Absorption Features

From the results and analysis of chapter 6, the next step was to see if the iterative fits could be expanded upon to allow some form of approximation of the radiation induced features associated with each material. As was noted earlier, this approach was only viable for magnesium fluoride, F2 and BK7.

The approach taken was to investigate how each term in the Gaussian or Lorentzian equation developed as a function of dose. If the development of each parameter could be predicted, then the overall shape could predicted for a given dose and hence the radiation induced absorption for each material could be approximated as a function of total dose.

7.1 Magnesium Fluoride

As was noted in section 6.7, the best result was obtained with the Lorentzian fit with one unconstrained wavelength with a second feature 30 nm from it.

The form of the equation fitted was:

$$y = 1 - (G1 + G2)$$

where

$$G1 = M_1 \times \left[(W_1/2)^2 / \left((x - L_1)^2 + (W_1/2)^2 \right) \right]$$

and

$$G2 = M_2 \times \left[(W_2/2)^2 / \left((x - (L_1 + 30))^2 + (W_2/2)^2 \right) \right]$$

7.1.1 Determination of Parameters

The following sections seek to obtain the best values of M_1, M_2, L_1, W_1 and W_2 to best approximate this feature.

7.1.1.1 Wavelength: L_1

For this run, it was only necessary to calculate the value of one wavelength variable, L_1, as $L_2 = (L_1 + 30$ nm.)

The value of L_1 was derived from a weighted mean of the results of iterative fits. The derivation of the variable is shown in Table 31. The weighting for this variable was the total dose in krads.

Dose (rad)	L_1 (nm)
5	367
10	370
15	409
30	376
100	371
150	353
300	372
500	394
1000	365
1500	371
3000	369
5000	369
15000	368
30000	368

Table 31. Weighted mean for L1 for Merck magnesium fluoride.

The weighted mean from this data was:

$$L1 = 368 \pm 3 \text{ nm}$$

7.1.1.2 Centre: M_1 & M_2

Figure 51 illustrates that the growth of M_1 varies as the total dose increases. For M_2, it is not quite as obvious, but the same form of equation is applied to both sets of data. As M_1 had the stronger correlation, this was investigated first to see if a suitable fit could be found, and then to see if the same equation would fit M_2.

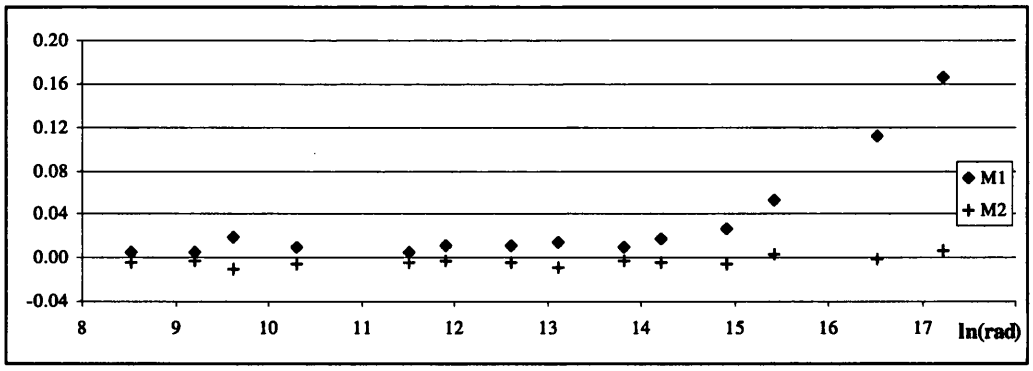

Figure 51 Values of M_1 and M_2 for Merck magnesium fluoride as a function of ln(total dose in rads)

The values of M1 and M2 are shown in Table 32.

Dose	M_1	M_2
1 krad	-0.0018	-0.0021
5 krad	0.0045	-0.0047
10 krad	0.0054	-0.0033
15 krad	0.0191	-0.0113
30 krad	0.0099	-0.0052
100 krad	0.0055	-0.0037
150 krad	0.0114	-0.0035
300 krad	0.0106	-0.0051
500 krad	0.0146	-0.0088
1 Mrad	0.0088	-0.0031
1.5 Mrad	0.0176	-0.0045
3 Mrad	0.0266	-0.0052
5 Mrad	0.0523	0.0038
15 Mrad	0.1120	-0.0020
30 Mrad	0.1652	0.0059

Table 32. Values of M_1 and M_2 for Merck magnesium fluoride.

For M_1, the equation:

$$Y = a \times \exp[b \times x]$$

was found to provide a good fit to the data. Using DataFit, it was found that the best fit occurred for:

$$a = 1.48E\text{-}06 \pm 1.20E\text{-}06$$

$$b = 0.68 \pm 0.05$$

This fit is shown in Figure 52.

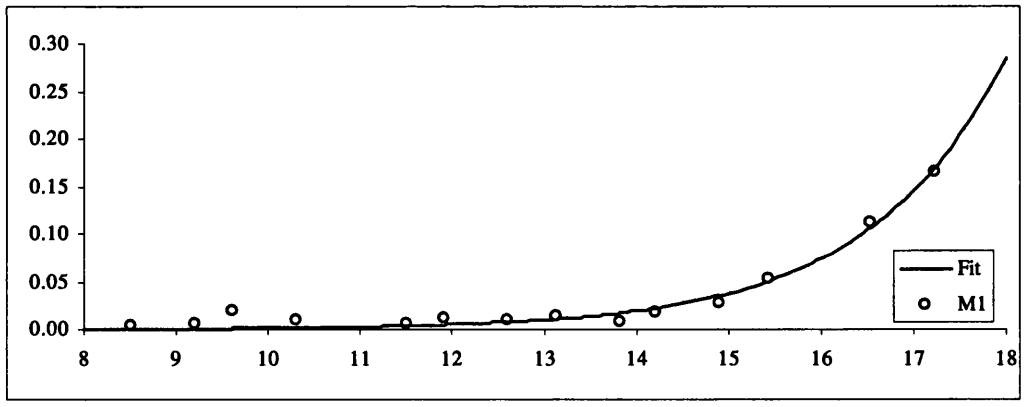

Figure 52 Fit of $Y = a \times \exp[b \times x]$ to M_1 for Merck magnesium fluoride samples.

For M_2, the equation $Y = a \times \exp[b \times x]$ was applied to the data and from an iterative approach, it was found that a suitable fit occurred with variables with values:

$$a = 8.13E\text{-}05 \pm 1.94E\text{-}05$$

$$b = 0.249 \pm 0.014$$

The presence of negative values for the width of the absorption is unrealistic, and so no further analysis could be completed on this variable.

7.1.1.3 Width: W_1 & W_2

In this group of samples, the presence of negative values was less contentious. Since the value is squared ($(W/2)^2$), the final shape is unaffected by the polarity of W. Unfortunately, DataFit was unable to receive a command to force all values of W_N to be positive, so only the absolute values of W were used.

These values are shown in Figure 53.

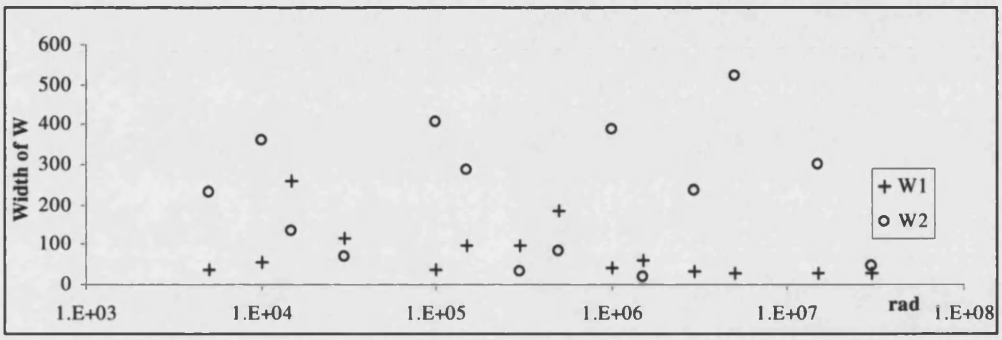

Figure 53 Values of W_1 and W_2 for Merck Magnesium Fluoride as a Function of Total Dose in rads

For W_1 it was difficult to discern any particular shape to the data. The simplest option was to look for a weighted average, but without any obvious growth, it was difficult to use dose as the weighting. For this variable, it was decided to use the SE returned from the iterative runs that produced the value of W_1 in the first place. The weighting for this variable was set as the inverse of the square of the SE. These are shown in Table 33. The values marked with '*' were originally negative.

Dose	W_1	(SE)	weight	W_2	(SE)	weight
5 krad	38	13.4	0.07	230	33.3	0.030
10 krad	55	13.6	0.07	362	61.7	0.016
15 krad	258	14.0	0.07	132*	26.2	0.038
30 krad	118	14.5	0.07	71*	20.7	0.048
100 krad	39*	13.0	0.08	406	72.5	0.014
150 krad	96	22.1	0.05	284	82.2	0.012
300 krad	98	8.21	0.12	30	9.84	0.102
500 krad	184	11.5	0.09	81	18.2	0.055
1 Mrad	41	8.11	0.12	390	78.9	0.013
1.5 Mrad	60	6.28	0.16	20*	11.1	0.090
3 Mrad	31	2.11	0.47	236*	32.5	0.031
5 Mrad	28	1.08	0.92	522	82.9	0.012
15 Mrad	29	0.61	1.64	301*	123	0.008
30 Mrad	28	0.60	1.66	46*	19.5	0.051

Table 33. Weighted fit for W_1 for Merck magnesium fluoride.

From these values, it was found that the weighted average was:

$$W1 = 29 \pm 10$$

$$W2 = 65 \pm 79$$

This error is quite significant, and will be discussed later in Section 7.1.2.

7.1.1.4 Summary of Results

The values of the L_N, M_N and W_N parameters are given in Table 34.

Variable	Value
L_1	372 ± 12 nm
M_1	$a = 1.48 \times 10^{-6} \pm 1.20 \times 10^{-6}$; $b = 0.68 \pm 0.05$ $M_1 = (1.48 \times 10^{-6}) \times \exp[0.68 \times \ln(\text{Dose in rad})]$
M_2	$a = 8.13\times 10^{-5} \pm 1.94\times 10^{-5}$; $b = 0.249 \pm 0.014$ $M_2 = (8.13 \times 10^{-5}) \times \exp[0.249 \times \ln(\text{Dose in rad})]$
W_1	29 ± 10
W_2	65 ± 79

Table 34. Parameters for approximating magnesium fluoride

Thus the Merck magnesium fluoride data may be approximated as:

$$y = 1 - (G1 + G2)$$

where

$$G1 = \left((1.48\times10^{-6})\times\exp[0.68\times\ln(\text{Dose in rad})]\right)\times\left[(29/2)^2/\left((x-372)^2+(29/2)^2\right)\right]$$

and

$$G2 = \left((8.13\times10^{-5})\times\exp[0.249\times\ln(\text{Dose in rad})]\right)\times\left[(65/2)^2/\left((x-402)^2+(65/2)^2\right)\right]$$

With the parameters established, the next stage was to test them against the data.

7.1.2 Approximating the Absorption Feature.

When an approximation was attempted on the data, the significance of the error on W_2 came to light. The initial approximation took the shape of the absorption feature, but was not particularly accurate. Upon reducing W_2, since this had the largest uncertainty on the figure, the approximation immediately improved in both shape and accuracy. The approximation against the 30 Mrad data is shown in Figure 54 for W2 = 65 and 0.

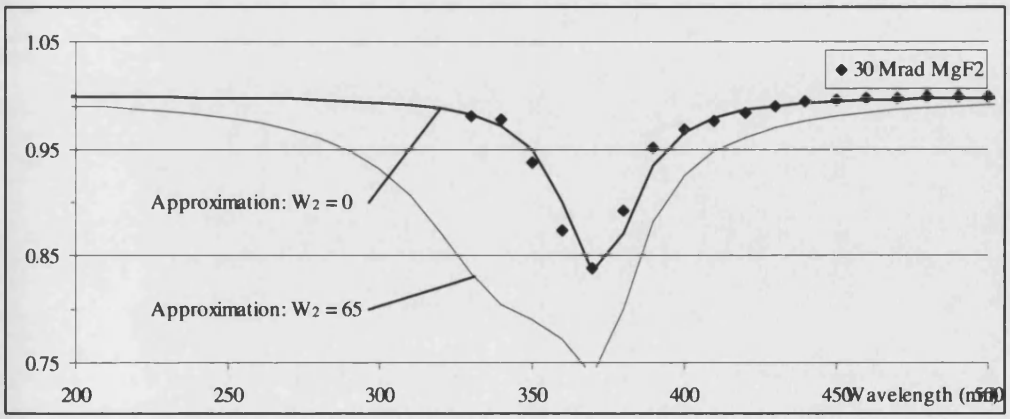

Figure 54: Approximation for 30 Mrad Merck magnesium fluoride, W_2 = 0 and 65.

Setting W_2 to zero removed the second Lorentzian term. Applying a single Lorentzian to the data, the approximation was still very good, and is shown in Figure 55.

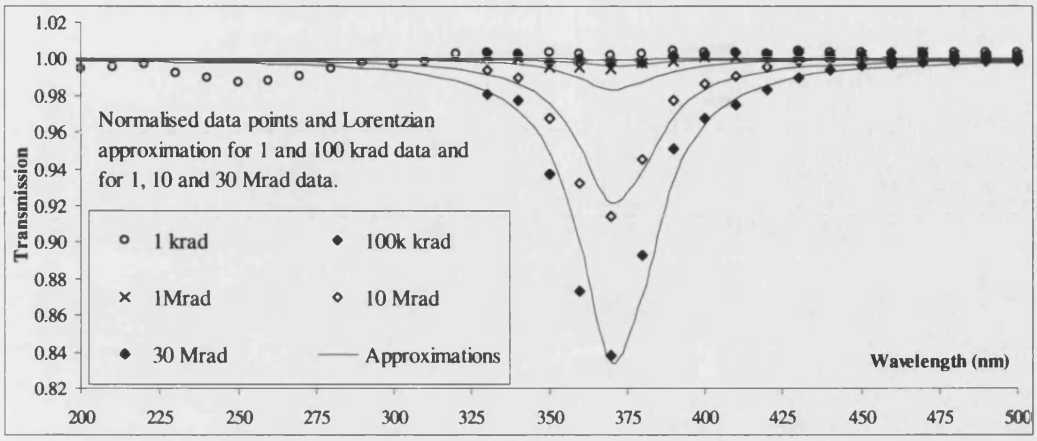

Figure 55: Comparison of Merck magnesium fluoride data with Lorentz approximation for 1 and 100 krad, and for 1, 10 and 30 Mrad.

Comparing the approximation with the other sources of material proved to be quite difficult. In the case of the Roynon Howes material, the lack of high dose data meant that the data did not show enough of a feature for and approximation to be measured against.

Although the Carl Zeiss data was better than the Roynon Howes, there was still a problem of the samples not being uniform enough for the approximation to be exact. For the approximation to be accurate, the spectra of the control sample that has been used to normalise the exposed samples should be the same as the spectra of the sample before they were exposed. With the Carl Zeiss samples, away from the 370 nm feature all the spectra should have been flat and of the same level. This wasn't the case, and this lack of uniformity with the samples meant that it was difficult to quantify how good the approximation is for although it catches the shape of the feature well, the magnitude is questionable.

The approximation is shown in Figure 56.

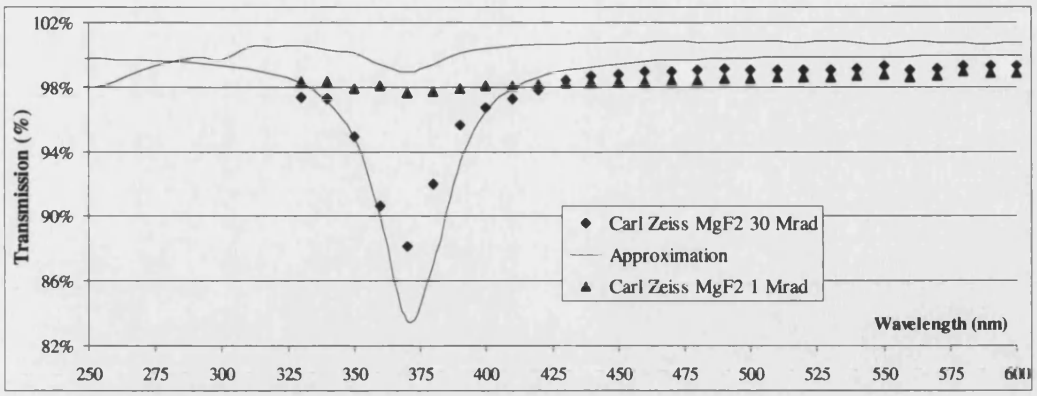

Figure 56: Comparison of Carl Zeiss magnesium fluoride data with Lorentz approximation for 1 and 30 Mrad.

7.1.3 Summary

Overall, the approximation catches the shape reasonably well, but the problem with the W_2 parameter hinders the work.

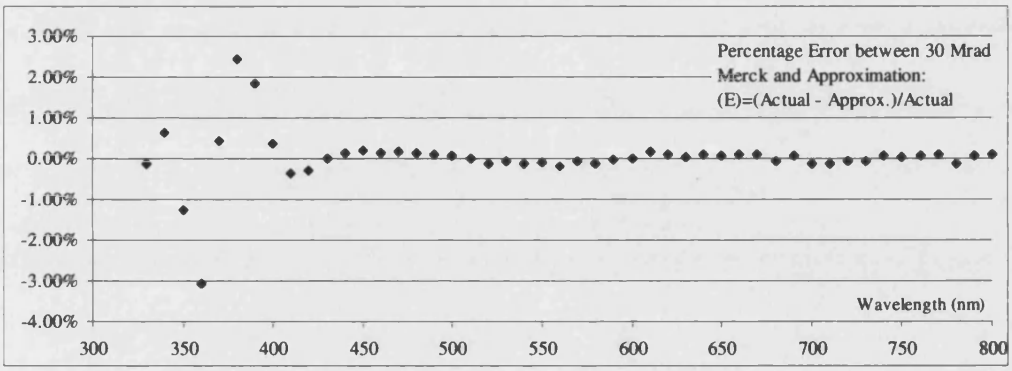

Figure 57: Percentage error between 30 Mrad Merck magnesium fluoride and approximation.

As Figure 57 shows, the approximation is good to within about 3% of the actual data, but the approximation could be improved. This will be discussed further in Section 8.2.

7.2 Sapphire

As was noted earlier, a significant portion of the radiation induced feature and one of the central wavelengths was found outside the wavelength range of this projects data. As such, the data would not produce results with high enough confidence levels to warrant any attempt to approximate it numerically.

7.3 BK7

As noted in Section 6.16, the best fit to the BK7 data was given by the equation:

$$y = 1 - (G1 + G2)$$

where

$$G1 = A_1 \times \exp\left[-\left((x - B_1)^2 / (2 \times C_1^{\,2})\right)\right]$$

and

$$G2 = A_2 \times \exp\left[-\left((x - B_2)^2 / (2 \times C_2^{\,2})\right)\right]$$

7.3.1 Determination of Parameters

The following section seeks to determine the best values of A_1, A_2, B_1, B_2, C_1 and C_2 to use to approximate the response of the glass.

7.3.1.1 Wavelength: B1 & B2

The method of determining the centre of the bands was to use a weighted mean. The values used to calculate the mean are shown in Table 35

Dose (rad)	weight (ln dose)	B_1	B_2
1500	0.4	346	794
30000	3.4	320	486
50000	3.9	330	604
100000	4.6	330	579
150000	5.0	330	644
300000	5.7	355	645
500000	6.2	373	642
1000000	6.9	380	642
1500000	7.3	383	646
3000000	8.0	382	650
5000000	8.5	384	658
10000000	9.2	384	658
15000000	9.6	383	658
30000000	10.3	384	659

Table 35. Weighted mean for B_1 and B_2 for BK7.

From these values, the weighted means were calculated as:

$$B_1 = 370 \pm 22$$

$$B_2 = 640 \pm 38$$

7.3.1.2 Maxima: A_1 & A_2

A brief investigation of the A_1 and A_2 values showed a pick-up proportional to the dose, before reaching a saturation value. This is shown in Figure 58.

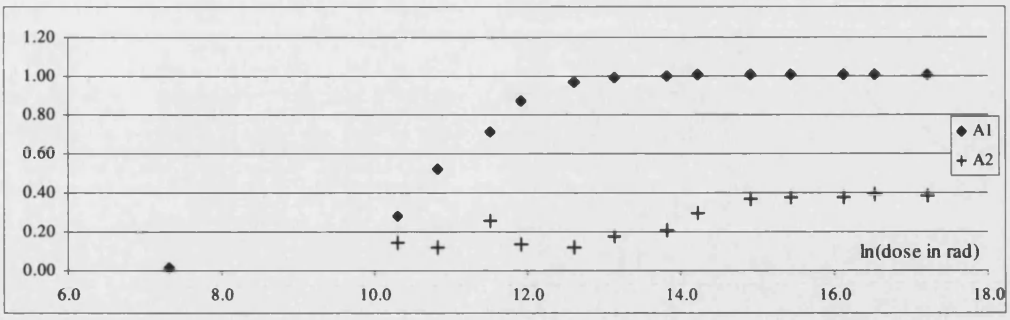

Figure 58 Centres A_1 and A_2 as a function of ln(total dose in rads)

A brief examination found that the shape of the A_1 curve could be described by:

$$y = a \times \exp[-\exp[b - cx]]$$

From an iterative approach, it was found that a suitable fit occurred with variables with values:

$$a = 1.014 \pm 0.008$$

$$b = 13.2 \pm 0.7$$

$$c = 1.25 \pm 0.07$$

This fit is shown in Figure 59.

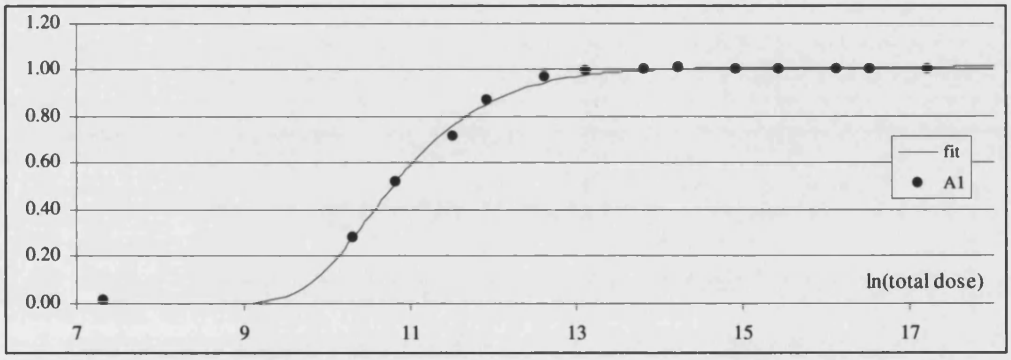

Figure 59: Fit of $y = a \times \exp[-\exp[b - cx]]$ to A_1 for Schott BK7

Applying the same formula to A_2, it was found that a suitable fit occurred with variables with values:

$$a = 0.77 \pm 0.68$$

$$b = 2.48 \pm 1.17$$

$$c = 0.17 \pm 0.15$$

This fit is shown in

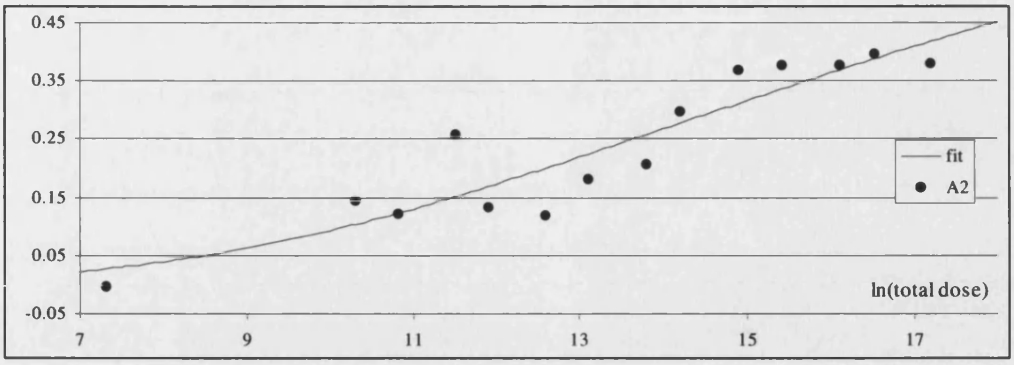

Figure 60: Fit of y = a × exp[-exp[b - cx]] to A_2 for Schott BK7

Both of these fits are satisfactory.

7.3.1.3 Width: C_1 & C_2

As the polarity of C does not affect the shape of the Gaussian the decision was made to only use absolute values. An initial evaluation of the data showed that a linear fit may be possible.

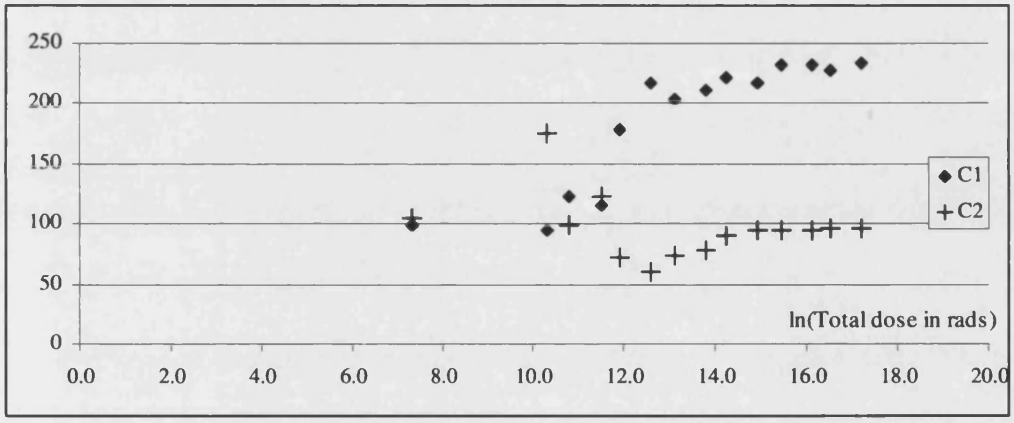

Figure 61: C_1 and C_2 as a function of ln(total dose in rads)

The first test was to carry out a quick straight line fit to the data points to see what statistics came out. For C_1 the error on the slope was 15%, and 78% in the intercept. For C_2, the error was 86% on the slope and 27% on the intercept.

The next test was to see what the value would be if the line was forced to pass through zero, i.e., no intercept.

For both parameters the results were better with a 4% error for C_1 and 11% for C_2.

For C_1 using an equation of the form y = mx, a least squares fit produced the following results:

$$m = 14.13 \pm 0.51$$

This is shown in Figure 62.

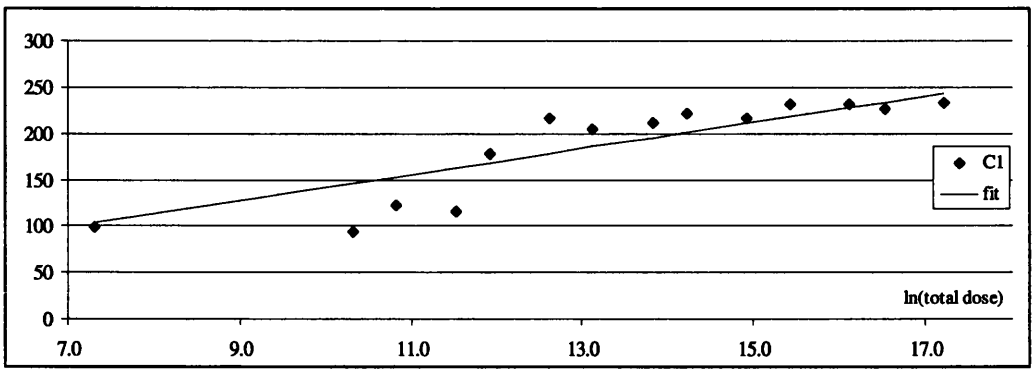

Figure 62: Fit of y = mx to C_1 for Schott BK7

Applying the same form to C_2, a least squares fit produced the following results:

$$m = 6.87 \pm 0.76$$

This is shown in Figure 63.

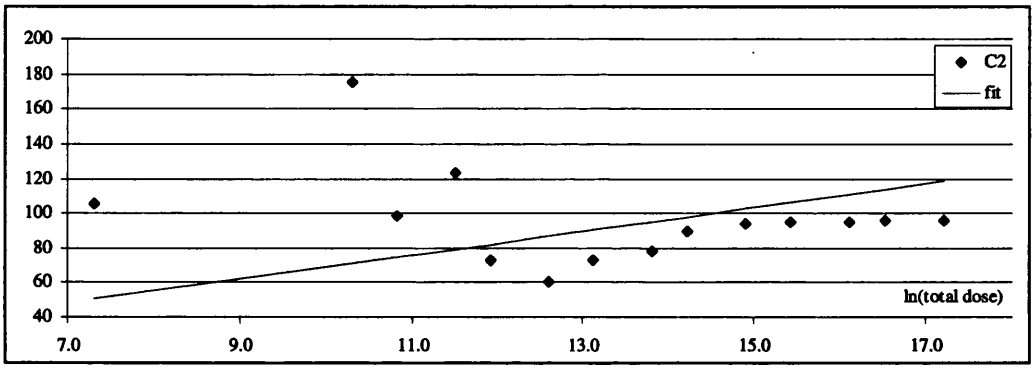

Figure 63: Fit of y = mx to C_2 for Schott BK7

7.3.1.4 Summary of Results

The values of parameters A_N, B_N and C_N are given in Table 36.

Variable	Value
A_1	$a = 1.014 \pm 0.008$; $b = 13.2 \pm 0.7$; $c = 1.25 \pm 0.07$ $A_1 = 1.014 \times \exp[-\exp[13.2 - (1.25 \times \ln(\text{Dose in rad}))]]$
A_2	$a = 0.77 \pm 0.68$; $b = 2.48 \pm 1.17$; $c = 0.17 \pm 0.15$ $A_2 = 0.77 \times \exp[-\exp[2.48 - (0.17 \times \ln(\text{Dose in rad}))]]$
B_1	370 ± 22 nm
B_2	640 ± 38 nm
C_1	$m = 14.13 \pm 0.51$ $C_1 = 14.13 \times \ln(\text{Dose in rad})$
C_2	$m = 6.87 \pm 0.76$ $C_2 = 6.87 \times \ln(\text{Dose in rad})$

Table 36. Parameters for approximating BK7.

Thus, the reduction in the transmission of Schott BK7 can be approximated by:

$$y = 1 - (G1 + G2)$$

where

$$G1 = (1.014 \times \exp[-\exp[13.2 - (1.25 \times \ln(\text{Dose in rad}))]]) \times \exp[-((x - 370)^2 / (2 \times 14.13 \times \ln(\text{Dose in rad})^2))]$$

and

$$G2 = (0.77 \times \exp[-\exp[2.48 - (0.17 \times \ln(\text{Dose in rad}))]]) \times \exp[-((x - 640)^2 / (2 \times 6.87 \times \ln(\text{Dose in rad})^2))]$$

7.3.2 Approximation the Absorption Feature

When tested against the actual data, initially the approximation held. Figure 64 compares the normalised spectra of four BK7 samples over a range of total dose with the value given by the approximation.

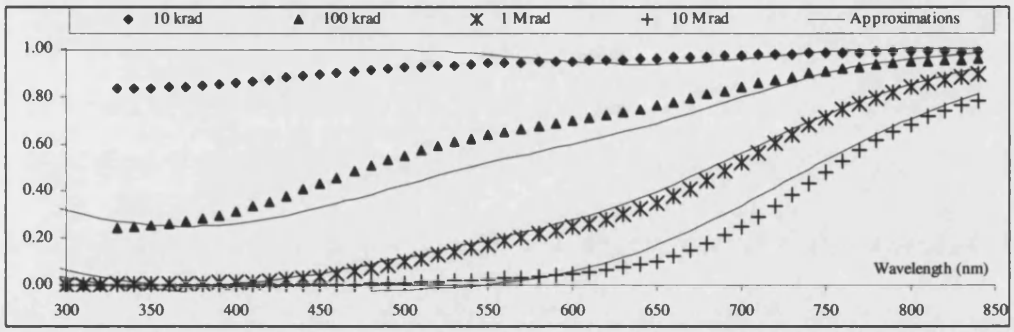

Figure 64: Approximations for 10 and 100 krad and 1, 10 and 30 Mrad Schott BK7

Although not a perfect match, it does follow the evolution of the spectra over the complete range of dose. The main caveat to the data is that below 350 nm, the approximation reach its minima and will begin to increase in value to approach 1, and so a manual correction will be required to hold the value down. This is only a slight problem as in reality as the cut-off of the material is around the 300 nm level. A simple linear correction was been applied to the 1 Mrad approximations and is shown in Figure 65.

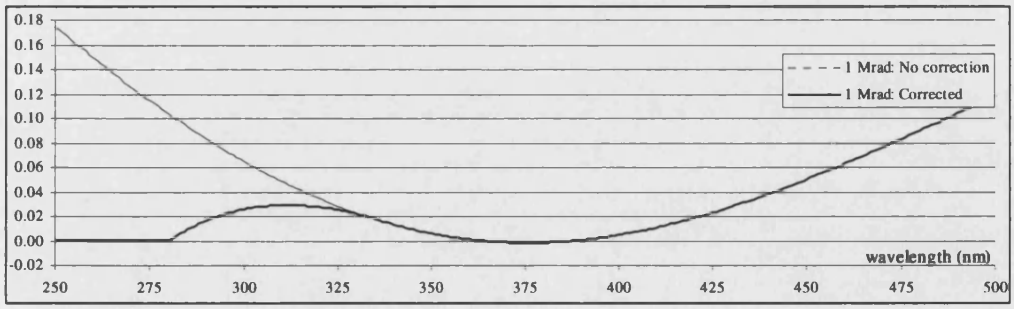

Figure 65: Approximations for 1 Mrad BK7 with and without cut-off correction

7.3.3 Summary

Overall the approximation gives a good guide to the magnitude of the radiation affected spectra, but further work is required to get a better approximation of the evolution of the shape.

7.4 F2

As was noted earlier in Section 6.14, the equation:

$$y = 1 - (G1 + G2 + G3)$$

where

$$G1 = M_1 \times \left[(W_1/2)^2 / \left((x - L_1)^2 + (W_1/2)^2\right)\right]$$

$$G2 = M_2 \times \left[(W_2/2)^2 / \left((x - L_2)^2 + (W_2/2)^2\right)\right]$$

and

$$G3 = M_3 \times \left[(W_3/2)^2 / \left((x - L_3)^2 + (W_3/2)^2\right)\right]$$

was deemed to give the best returns of iteration against the F2 data.

7.4.1 Determination of Parameters

The following section seeks to determine the best values of L_1, L_2, L_3, W_1, W_2, W_3, M_1, M_2 and M_3 to approximate the response of the glass.

7.4.1.1 Wavelength: L_1, L_2, & L_3

Again, a weighted mean approach was used. The values used to calculate the mean are shown in Table 37.

Dose	weight w	L_1	L_2	L_3
Rad	= ln(dose)			
10,000	9.2	310	416	769
15,000	9.6	317	425	753
30,000	10.3	316	437	754
50,000	10.8	321	452	750
100,000	11.5	323	481	753
150,000	11.9	325	497	752
300,000	12.6	330	519	755
500,000	13.1	330	511	749
1,000,000	13.8	335	519	751
1,500,000	14.2	335	529	754
5,000,000	15.4	334	536	758
10,000,000	16.1	334	538	758
15,000,000	16.5	333	539	758
30,000,000	17.2	333	541	759

Table 37. Weighted mean for L_1, L_2 and L_3 for F2.

From these values, the weighted means were calculated as:

$$L_1 = 328 \pm 7$$

$$L_2 = 504 \pm 41$$

$$L_3 = 755 \pm 5$$

7.4.1.2 Width: W_1, W_2 & W_3

A brief investigation of W_1, W_2 and W_3 showed a linear relationship. This was further reinforced when negative values were replaced with positive ones, since the Lorentzian equation makes use of term $(W/2)^2$ and so the polarity was unimportant.

This linear relation is shown in Figure 66.

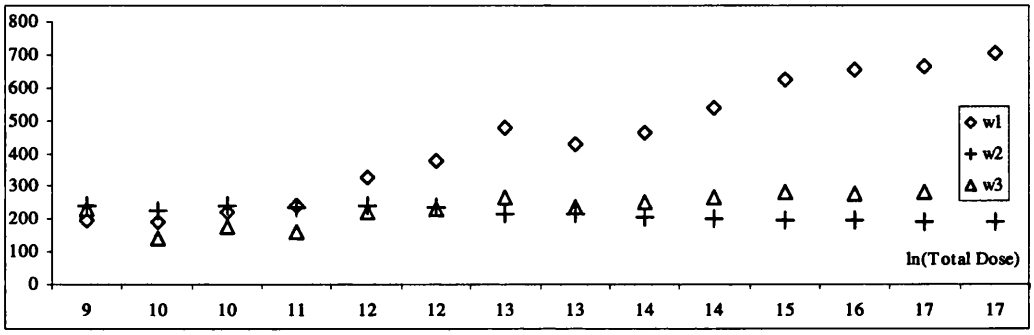

Figure 66: Width of W_1, W_2 and W_3 as a function of ln(total dose in rads).

From the assumption of a linear fit of:

$$y = mx + c$$

best described the shape and evolution of the width factors, a least squares analysis of W_1 found that the best fit occurred with:

$$m = 69 \pm 3$$

$$c = 469 \pm 42$$

which is shown in Figure 67.

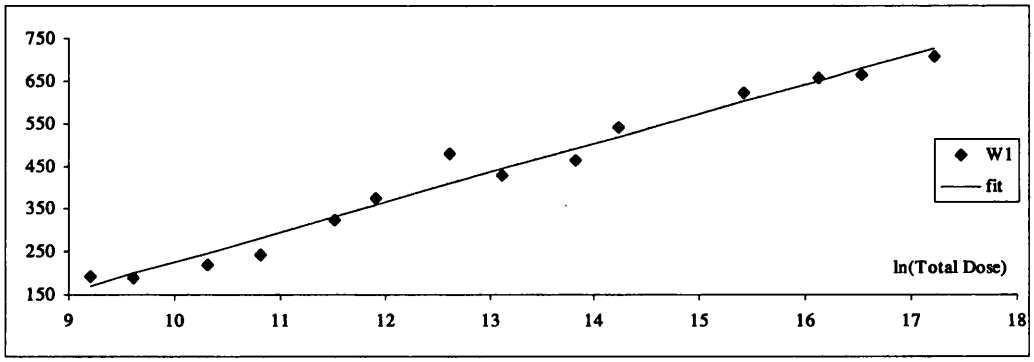

Figure 67: Fit of y = mx + c to W_1 for Schott F2

Repeating this for W_2, it was found that a least squares fit occurred with variables with values:

$$m = -7.3 \pm 0.8$$

$$c = 312 \pm 11$$

which is shown in Figure 68.

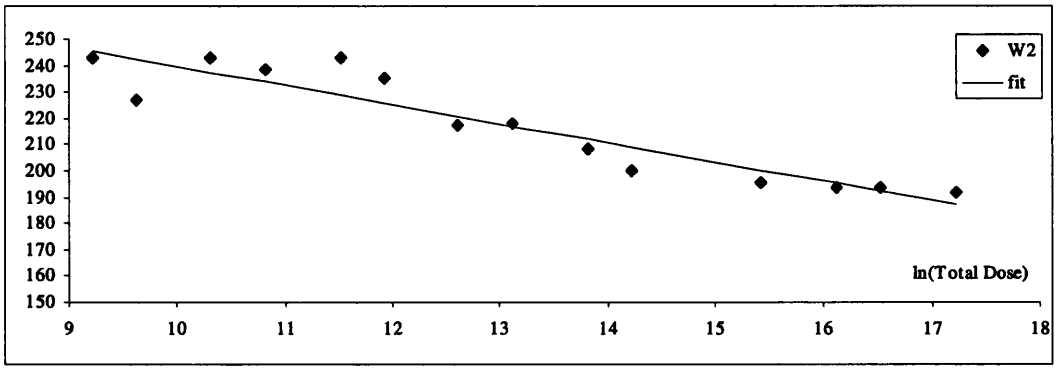

Figure 68: Fit of y = mx + c to W_2 for Schott F2

Repeating this again for W_3, it was found that a least squares fit occurred with variables with values:

$$m = 14.8 \pm 2.8$$

$$c = 43 \pm 38$$

which is shown in Figure 69.

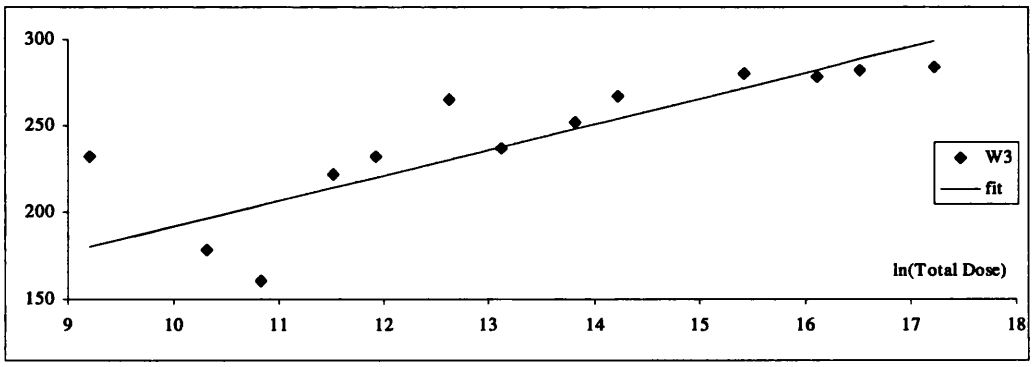

Figure 69: Fit of y = mx + c to W_2 for Schott F2

7.4.1.3 Maxima: M_1, M_2 & M_3.

A brief analysis of the maxima data showed the components starting of with a low value, before increasing to a point where the saturate and then level out again. This is shown in Figure 70.

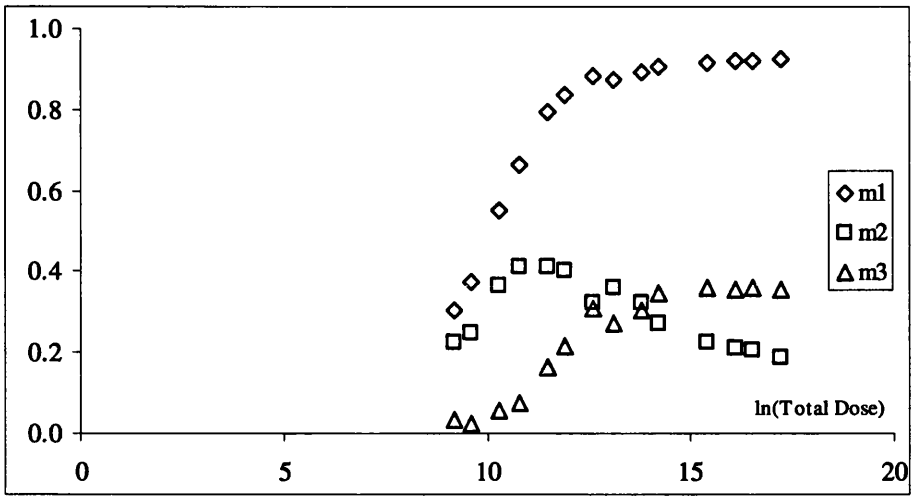

Figure 70: M_1, M_2 and M_3 as a function of ln(total dose in rads)

For M_1 a brief examination found that the curve:

$$y = a \times \exp[-\exp[b - (c \times x)]]$$

described the shape shown in Figure 70. For M_1, an iterative approach found that a suitable fit occurred with:

$$a = 0.927 \pm 0.008$$

$$b = 7.84 \pm 0.4$$

$$c = 0.83 \pm 0.04$$

which is shown in Figure 71.

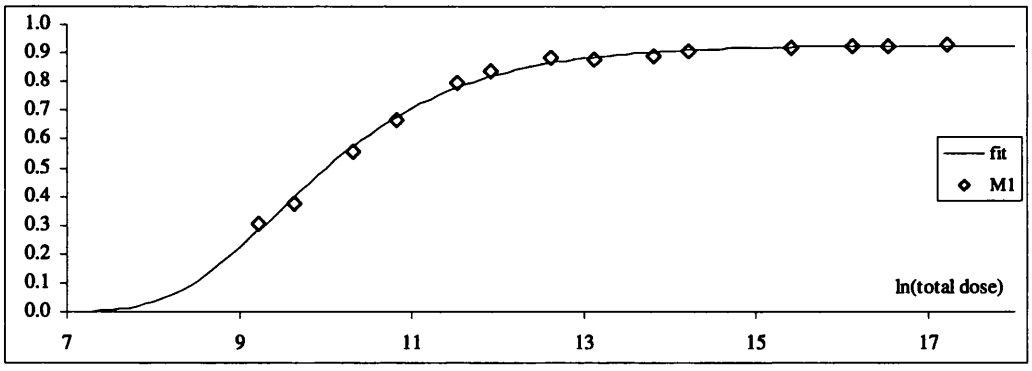

Figure 71: Fit of $y = a \times \exp[-\exp[b - (c \times x)]]$ to M_1 for Schott F2

The next step was to reapply the equation to M_2. It was found that a suitable fit occurred with:

$$a = 0.31 \pm 0.02$$

$$b = 29 \pm 76$$

$$c = 3 \pm 8$$

which is shown in Figure 72.

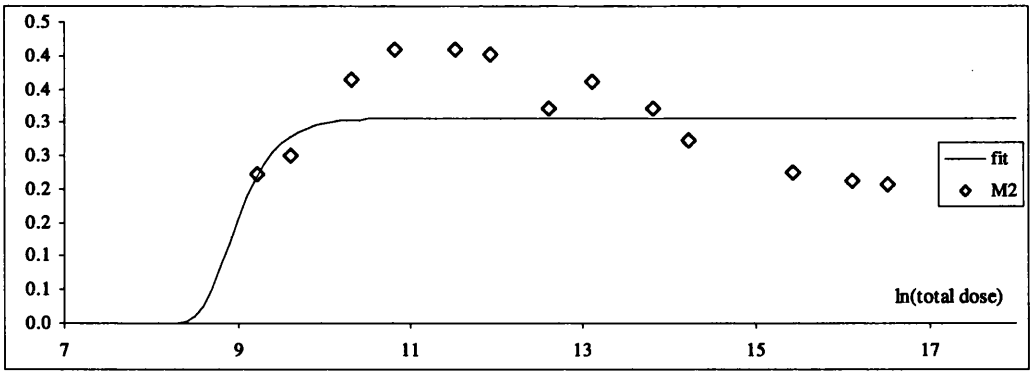

Figure 72: Fit of $y = a \times \exp[-\exp[b - (c \times x)]]$ to M_2 for Schott F2

Finally the process was applied to M_3 and it was found that a suitable fit occurred with:

$$a = 0.363 \pm 0.011$$

$$b = 9.2 \pm 1.2$$

$$c = 0.82 \pm 0.11$$

which is shown in Figure 73

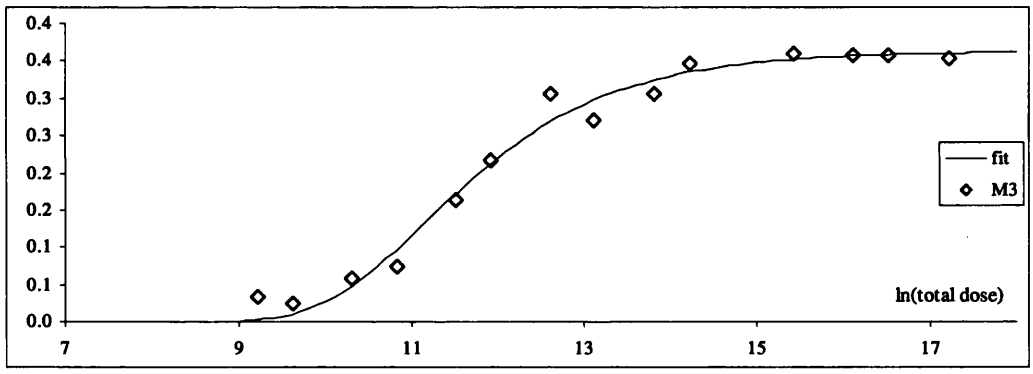

Figure 73 Fit of $y = a \times \exp[-\exp[b - (c \times x)]]$ to M_3 for Schott F2

7.4.1.4 Summary of Results

The values of parameters L_N, W_N and M_N are given in Table 38.

Variable	Value
L_1	328 ± 7 nm
L_2	504 ± 41 nm
L_3	755 ± 5 nm
W_1	m = 69 ± 3, c = 469 ± 42 W_1 = 69 × ln(Dose in rad) + 469
W_2	m = -7.3 ± 0.8; c = 312 ± 11 W_2 = 312 - 7.3 × ln(Dose in rad)
W_3	m = 14.8 ± 2.8; c = 43 ± 38 y = 14.8 × ln(Dose in rad) + 43
M_1	a = 0.927 ± 0.008; b = 7.84 ± 0.4; c = 0.83 ± 0.04 M_1 = 0.927 × exp[-exp[7.84 – (0.83 × ln(Dose in rad))]]
M_2	a = 0.31 ± 0.02; b = 29 ± 76; c = 3 ± 8 M_2 = 0.31 × exp[-exp[29 – (3 × ln(Dose in rad))]]
M_3	a = 0.36 ± 0.01; b = 9.2 ± 1.2; c = 0.82 ± 0.11 M_3 = 0.36 × exp[-exp[9.2 – (0.82 × ln(Dose in rad))]]

Table 38. Parameters for approximating F2.

7.4.1.5 Approximation of Radiation Absorption: F2

The reduction in the transmission of Schott F2 can be approximated by:

$$y = 1 - (G1 + G2 + G3)$$

where

$$G1 = \left(0.927 \times \exp\left[-\exp\left[7.84 - (0.83 \times \ln(\text{rad}))\right]\right]\right) \times \left[\left((69 \times \ln(\text{rad}) + 469)/2\right)^2 / \left((x - 328)^2 + \left((69 \times \ln(\text{rad}) - 469)/2\right)^2\right)\right]$$

$$G2 = \left(0.31 \times \exp\left[-\exp\left[29 - (3 \times \ln(\text{rad}))\right]\right]\right) \times \left[\left((312 - 7.3 \times \ln(\text{rad}))/2\right)^2 / \left((x - 504)^2 + \left((7.3 \times \ln(\text{rad}) + 312)/2\right)^2\right)\right]$$

and

$$G3 = \left(0.36 \times \exp\left[-\exp\left[9.2 - (0.82 \times \ln(\text{rad}))\right]\right]\right) \times \left[\left((14.8 \times \ln(\text{rad}) + 43)/2\right)^2 / \left((x - 755)^2 + \left((14.8 \times \ln(\text{rad}) + 43)/2\right)^2\right)\right]$$

7.4.2 Testing the Approximation

The test of the parameters presented in Table 38. The following subsection assesses the accuracy of the approximation against real data. The initial approximation is shown in Figure 74.

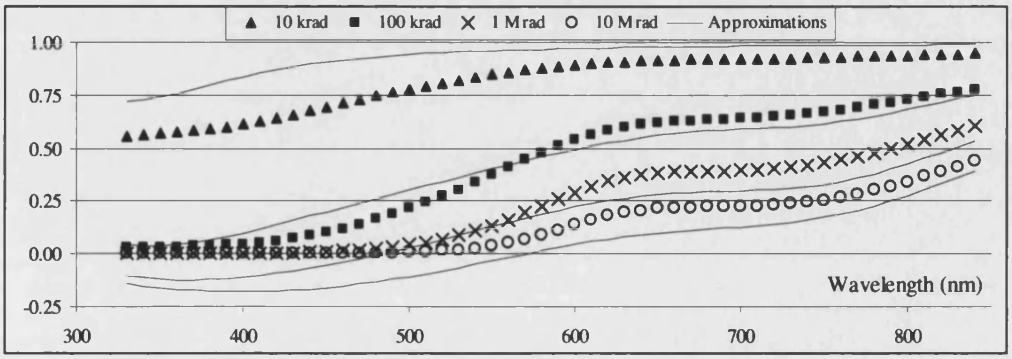

Figure 74 Approximations for 10 and 100 krad and 1 and 10 Mrad Schott F2

Although the curves are generally following the trend of the data, it is only a moderately accurate fit. Two aspects in particular need to be addressed. Firstly, the approximations drop below zero. This was easily modified by placing a floor of 0 in the function. Secondly, the approximations are reliant on a poor quality parameter in M_2. Assuming the later values, which are based on higher doses and have more pronounced features, are more accurate then a better fit is:

$$M_2 = 0.19 \times \exp[-\exp[35-(4 \times \ln(\text{rad}))]]$$

Both of these changes were built into a second function. The results of this function are shown in Figure 75.

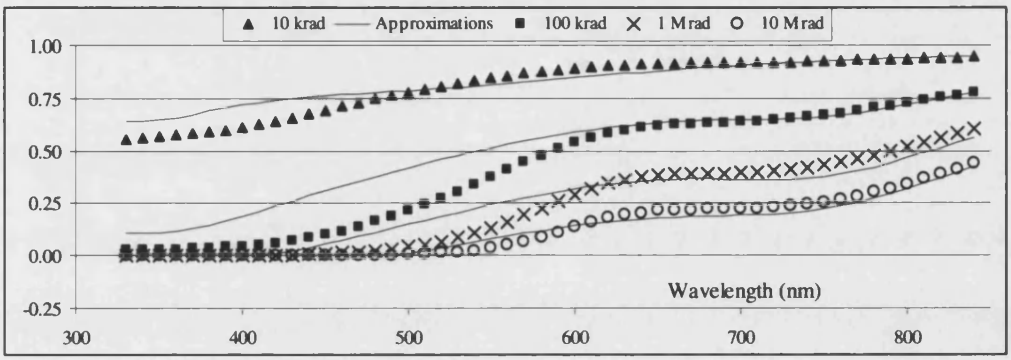

Figure 75: Approximations for 10 and 100 krad and 1 and 10 Mrad Schott F2: Corrected Function

7.4.3 Summary

Overall, the attempts to approximate the shape and magnitude of the radiation induced spectra have been successful given the quality of the initial data.

The work has shown that it is possible to numerically produce synthetic spectra, but that the quality of the initial data is vital in setting accurate parameters.

8 Conclusions

The aim of this project was to evaluate the response of several materials to high levels of radiation. From the initial parameters set by the XMM-Newton mission and expanded by the input from SIRA, samples of magnesium fluoride, sapphire and glass were exposed to a wide range of gamma radiation and subsequently analysed.

During the development of the experiment, a number of complications were addressed including the preparation of large batches of samples for polishing, overcome. A novel approach was developed for locating the high dose samples close to the isotope source with very tight tolerance on the distance from the source.

The results from this exposure were successfully analysed, and it was found that exposure to high levels of gamma radiation created a number of responses for the materials.

Magnesium Fluoride	Merck	A pronounced absorption feature was created at around 370 nm. Above 400 nm, the samples showed very response to irradiation
	Roynon Howes	Loss of 30 Mrad sample meant little data available for analysis.
	Carl Zeiss	Very similar in response to Merck magnesium fluoride.
Sapphire	Merck	Very robust material, but exposure to high doses induced attenuation around the 370 nm region.
	Union Carbide	Overall, a similar level of reaction as the Merck samples.
	Hemex & Hemlite	Very little response at all.
Glass	BK7	As expected, very marked response to irradiation
	BK7 G18	Very little response at all.
	F2	As expected, very marked response to irradiation
	F2 G12	Very little response at all.

Table 39. Summary of material response to gamma irradiation

The results were then fitted with Gaussian and Lorentzian equations, and it was found that the response of the magnesium fluoride, BK7 and F2 could be approximated by these functions. The following sections draw together some of the main conclusions and points drawn from the project.

8.1 Sapphire

It was expected that this material would be highly resilient to irradiation, and this was supported by the results. Looking at the 30 Mrad samples, none were too greatly affected by their exposure.

An interesting point is that the high purity samples of Hemex and Hemlite were the least affected of the groups. This supports the belief that purity is way of reducing the susceptibility of a material to radiation induced damage.

Overall, sapphire has proved to be a robust and reliable sample for materials to be used in a radiation environment.

That sapphire was so resilient reduced its feasibility for the second part of the project, that of approximating the spectra by a numerical approach. The truncated profile meant that any attempt to fit the data was speculative, but overall the results were positive in that the radiation response as recorded by this project could be fitted. Although this project did not pursue this any further, with data at a lower wavelength, the work could be successfully continued.

8.2 Magnesium Fluoride

Magnesium fluoride's ability to transmit light at levels down to below 200 nm makes it an attractive material for research at the wavelengths. In contrast to sapphire, magnesium fluoride displayed a distinct response to irradiation. The main feature was the development of an asymmetric feature around 370 nm with a growth $\propto$ total dose over the exposure range of this project. Even with the development of the 370 nm feature, at 370 nm magnesium fluoride was at least as transparent as sapphire, and nearly always better and as such, remained an excellent material for use, but the degradation of the transmission around 370 nm as a function of total dose would have to be addressed in any project using light at these wavelengths. Whether this was by a formal modelling of the growth of the feature, by a simulation of the anticipated environment to gain an empirical algorithm, or even taking a calibration spectra on a regular basis to track the degradation is a moot point. The issue is that it would need to be addressed if the project was to make use of magnesium fluoride in a radioactive environment.

The asymmetric feature at 370 nm was the focus for the approximation analysiss and it was found that the growth could be approximated by two Lorentzian curves. Overall, the approximation was quite successful at catching the approximate growth and shape of the feature.

It was also shown that the calculation of accurate spectra is critical to the success of this approach. In particular, the uncertainty over the value of a particular parameter (W_2) was seen to adversely affect the quality of the final approximation.

However, that the asymmetric feature could be approximated for both Carl Zeiss and Merck samples shows that the approximation does have merit and may warrant further work (and future work may prove the Gaussian to be the more suitable function.)

8.3 BK Group

Although there was a cost in both a reduced transmission and lower wavelength cut-off, the doped BK7-G18 proved to be very resistant to even very high doses of radiation. The higher doses did start to show an effect on the glass by slowly pushing the cut-off wavelength back. However, this effect was too minor to easily quantify and so no approximation could be attempted.

In contrast, BK7 showed a distinct response to radiation, with the spectra showing discernible effects from only a few krad of gamma rays. Although this would rule the material out for use in a radioactive environment, it did allow for approximations to be successfully carried out.

The BK7 approximation work looked at attempting to cover the whole 300 to 850 nm range of data. It was found that two Gaussian curves approximated the data well. The work on BK7 also highlighted a problem with using symmetric equations such as the Gaussians and Lorentzian. With the BK7 approximation, it was found that below about 375 nm, the approximated spectra began to increase in value. However, as simple correction factor was introduced into the function that would multiply the approximation by a correcting factor that fell steadily from 1 to 0 over a predefined range. In the work of this project, a simple linear correction was applied, however a more complex fit, for example of the form $y = a \times \exp[-\exp[b - c \times x]]$, could be utilized for a smoother correction.

8.4 F2 Group

As with its equivalent, the doped BK7-G18, the F2-G12 acquitted itself well hardly showing any response to irradiation. Again, the doping exacted a price with a reduction in the transmission spectra and short wavelength cut-off, but the doping proved its ability to allow the material to survive in a high dose environment.

As with the standard BK7, the F2 began to show a response to irradiation after only a few krad of exposure. Again, this was a material that was never really a candidate for a radioactive environment, but was considered due to its wide use in many commercial operations that may want to consider the impact of radiation on their system

As with BK7, the wide ranging effect of the radiation meant that the approximation sought to cover the full 330 to 850 nm range. For this sample group, it was found that the best approximation was found with 3 Lorentzian curves.

Again, the approximation highlighted that the imperative need for accuracy of the underlying parameters. Again, an initially weak approximation was vastly improved with a manual correction to one of the parameters. In this case, the data for fitting parameter M_2 was quite noisy. A manual correction by increasing the confidence on the higher dose data produced a better shape.

Another issue to a numerical approximation was the possibility that such an approach may produce a negative transmission. This was corrected by a simple function to limit the function to a floor of zero.

However, the only real issue with the data was the shape of the data prior to the manual correction of M_2. That is then produced a good approximation supported the choice of the underlying equations.

8.5 Further Issues

Overall, the project has highlighted the need for high resolution data to investigate the radiation induced features. Although the Harwell spectrophotometer was not our first choice, the data was good enough to allow a good investigation into the response of several groups of samples to radiation.

The approximations themselves generally caught the shape of the data, but highlighted the need for greater accuracy in the data for the production of numerical approximations.

A final point to note is that the samples were all 10 mm in length, a legacy of the original intention to investigate the effect of radiation on refractive index. This means that irradiation induced effects have a longer than normal path length compared to some optical components.

If the data was used to calculate attenuation figures, this would have to be addressed as often the figures are quoted per mm, for example dB mm^{-1}.

8.6 Suggestions for future work

In addition to the points above, here are some general suggestions for consideration of future work.

Sapphire: Although the material is radiation tolerant, it does show a response to irradiation. Future work may want to consider focusing on very high doses to see if any further features appear and to measure spectra to a lower wavelength to capture the full shape of any response.

Another issue with sapphire is the effect of purity on the sample. From the data presented, the Merck and Union Carbide data showed an effect, the Hemex and Hemlite did not. Similarly, any work may want to start their analysis at higher doses to ensure a greater response from the material.

Magnesium Fluoride: Overall a very good material. The main effect appears to be the growth of an M centre manifesting in the growth of curves at 370 and 400 nm. Future work may want to consider focusing on this area in some detail. Whether for empirical measurements, to help build a formal model, the material presents a good response given the research something to address in detail.

An issue with the magnesium fluoride work was the effect of the quality of the input data in building the parameters. As such, any work may want to look at using more samples over a wider range of doses to produce better fits.

Glass: Both the BK7 and F2 samples showed a strong response to irradiation. As such, any further work may wish to concentrate a sub-500 krad doses. Also, any study of the radiation hardened glasses will require very high doses. As it stands, the only response is at the point where the glass is approaching its natural cut-off and so any project that is looking for a material to operate in this region would probably not choose this material.

Other Experiments: Another area to consider would be the effect of dose rate vs. total dose. Another issue is the effect of irradiation by charged and heavy particles to doses comparable with this project.

Finally, future work may wish to address the effect of irradiation on other optical parameters such as reflectance, and of course refractive index

Appendix

A Expansion of Earlier Notes

The following sections contain more in-depth calculations or notes which are included for completeness only.

A.1 Derivation of Half-Life

If the original number of unstable atoms is known, along with the half-life of that isotope, then it is possible to calculate the number of nuclei present at any one time. This can be expressed as:

$$N = N_0 \exp^{-\mu t}$$

where N_0 is the number of nuclei present at time t = 0, N is the number remaining after time t, for a substance with a radioactive decay constant of μ. The half-life ($T_{½}$) of a species is defined as the time in which half of the nuclei in the sample decay, that is the time at which $N=N_0/2$:

$$N = \frac{N_0}{2} = N_0 \exp^{-\mu t} = N_0 \exp^{-\mu T_{½}}$$

Dividing across by N_0 and taking logs gives:

$$\ln\left(\frac{1}{2}\right) = -\mu T_{½}$$

where $\ln(½) = -\ln(2)$, hence we can derive the half-life of a sample as:

$$T_{½} = \frac{\ln 2}{\mu} = \frac{0.693}{\mu}$$

A.2 Rate and Flux

Although the gray and seivert units express the amount of radiation a body receives, a particular dose can be received over quite different rates of time. This is where the principal of dose rate is employed. Both dose equivalent rates (e.g. $Sv\ hr^{-1}$) and absorbed dose rates (e.g. $Gy\ r^{-1}$) can be used to give a final dose in a sample. To compare between the two, the dose rate is simply linked to the final dose by:

dose = dose rate × time

In some experiments, the amount of a particular type of radiation is expressed as the number of particles or photons crossing an area of 1 square metre in 1 second. Strictly speaking, this should be referred to as a fluence rate, but is more commonly referred to as the radiation *flux* Φ. This is best illustrated by considering a point source emitting P particles per second. At a distance of r, the number of particles passing through an area of 1 m^2 is the value of the flux. Assuming that the particle emission is uniform in all directions, the flux will fall off by the inverse square law. So at distance r, the area is $4\pi r^2$ to give a flux Φ of:

$$\Phi = \frac{P}{4\pi r^2} \text{ particles per square metre per second } (p\ m^{-2}s^{-1})$$

A.3 Half- & Tenth-Value Layer

The half value layer (HVL or $t_{½}$) or half value thickness is the thickness of material needed to attenuate a beam to half its intensity. Placing this into the equation for gamma attenuation gives:

$$\frac{D_t}{D_0} = 0.5 = \exp(-\mu t_{\frac{1}{2}})$$

Taking natural logs gives:

$$\ln 0.5 = -\mu t_{\frac{1}{2}}$$

$$\text{thus } -0.693 = -\mu t_{\frac{1}{2}}$$

$$\text{thus } t_{\frac{1}{2}} = \frac{0.693}{\mu}$$

One HVL reduces the intensity by one half, two HVLs reduce it to one quarter, etc. Another similar concept is the tenth-value layer, $t_{1/10}$. This can be calculated by a similar manner as before giving:

$$t_{\frac{1}{10}} = \frac{\ln 0.1}{-\mu} = \frac{0.2303}{\mu}$$

A.4 Photoelectric Effect

In 1886 and 1887, Heinrich Hertz confirmed the existence of the electromagnetic (EM) waves predicted by Maxwell's theory of light propagation. Amongst the effects he noted, Hertz discovered that an electrical discharge occurred far more readily between two electrodes when they where illuminated by UV light than when illuminated by normal lighting. Later work found that a greater number of electrons where emitted from the cathode's surface under the illumination of UV radiation. This ejection of electrons from the surface is the *photoelectric effect*. Further, below a certain frequency of illuminating light, no electron emission occurred. This is the cut-off frequency. Finally, there was no time delay between illumination and the effect. These three effects contradicted classical wave theory, but the experiment did prove the existence of EM waves and was hailed as a success.

In 1905, Einstein addressed this peculiar effect, and used it to question the classical theory of light and propose a new one of his own. He cited that with his new theory, he could correctly explain the photoelectric effect, and hence provide validity for his theory. In producing his theory, Einstein used this effect to contradict other aspects of the classical EM theory. In doing this he produced solid evidence of the quantum nature of EM radiation.

Einstein's rationale was as follows. From a radiant source (e.g. the UV lamp in the photoelectric effect) which emitted waves at frequency ν, the energy contained in the waves could be 0, or $h\nu$, or $nh\nu$, thus in going from state $nh\nu$ to $(n-1)h\nu$, a discrete amount of energy would be emitted, with an energy of $h\nu$. He then assumed that the energy content of each bundle was related to its frequency, ν, by the equation:

$$E = h\nu$$

He also assumed that in the photoelectric effect, energy was also absorbed discretely. Thus when the electron is emitted from the surface, the kinetic energy, K, will be given by:

$$K = h\nu - \phi$$

where ϕ is the work required to remove the electron from the metal. This work was believed to be the energy necessary for the electron to overcome the attractive forces that tie it to the metal atom.

Einstein's postulate completely addressed the three objections from the original photoelectric effect experiment raised. Whereas in 1905, this quantisation of energy was seen as a mathematical simplification, today the photon nature of light is completely accepted. The photoelectric effect applies photons of all energies, but for photons at wavelengths of the order of centimetres or more, the energy is far too low to emit photoelectrons.

An alternate view of this process is that the photoelectric process absorbs photons. This requires that electrons be bound to atoms as a free electron would not absorb a photon, merely deflect it. At higher photon energies the photoelectric equations still remain valid. Again, an electron is emitted, but with such energy that the original nucleus is also moved via the conservation of momentum.

The photoelectric effect is an important form of photon absorption up to, and including, x-ray energies. Beyond this energy, other processes become more significant, but this process still occurs.

A.5 Compton Effect

Compton further confirmed the particle-like nature of light in 1923. In his experiment a beam of x-rays, with a very narrow energy range (i.e. a narrow wavelength range), were made to strike graphite targets. For each target, the intensity of the scattered x-rays was measured as a function of their wavelength. He observed that for each wavelength range λ that entered the graphite; two peaks appeared in the scattered x-rays. The primary peak was of the same λ as the incident x-rays, but a second peak was observed at a longer wavelength λ', the difference $\Delta\lambda$ is called the *Compton shift*, where:

$$\Delta\lambda = \lambda' - \lambda$$

It is interesting to compare this with Rayleigh scattering, the process where photons are scattered without losing energy. As part of Compton's experiment, he still observed x-rays with an unaltered wavelength. A quantum explanation of this is that these are the x-rays that were scattered by the nucleus rather than the free electrons. The mass of a graphite (carbon) atom is some 20,000 times larger than the electrons. If one calculates the Compton shift from the x-rays striking the nucleus a Compton shift is still predicted. However, the shift predicted for a carbon atom in Compton's original experiment is some one-millionth of an angstrom, i.e. immeasurably small, but shows the universality of the effect.

A.6 Pair Production

Besides the photoelectric and Compton processes, there is a further mechanism by which photons can lose energy by interacting with matter, *pair production.* In this process, a high-energy photon passes near to or collides with a heavy nucleus. The nucleus acts as a catalyst for the process and remains unchanged by the whole event. The photon disappears and is replaced by an electron (e^-) and it's antiparticle, the positron (e^+).

This can only occur when the photon has energy in excess of the rest mass of the two particles. Given that $m_0 = Mass_{electron} = Mass_{positron} = 9x10^{-31}$ kg then from $E = m_0 c^2$

$$\gamma_{min} = \frac{2\times(9\times10^{-31}\text{kg})\times(3\times10^{8}\,\text{m s}^{-1})^2}{1.6\times10^{-19}\text{C}} = 1.02\,\text{MeV}$$

where the factor $1.6x10^{-19}$ C converts the energy to electron-volts. Thus, for pair production to take place, the photon must be a gamma ray with energy in excess of 1.02 MeV. The interaction occurs within the atomic nucleus, and the result is that the photon is completely absorbed.

If the gamma ray only has energy of 1.02 MeV, then the two particles will have no kinetic energy to separate from each other, will recombine and annihilate each another to reform a photon. For any energy the photon has in excess of this threshold, the particles will gain kinetic energy equivalent to that extra energy. If a 2 MeV photon is the source, there will be 0.98 MeV of surplus energy. This is split 50:50 between the 2 particles as kinetic energy. Since the pair are created and ejected from opposite sides of the atom, their angle of separation is often used in experiments to give the angle of the incident photon.

A.7 Pair Annihilation

Pair annihilation is the reverse process of pair production and occurs when a positron and electron collide. When the two particles meet, they return to a photon state. To conserve linear momentum, a pair of photons is created which propagate in opposite directions. If the original particles were the result of a 2 MeV photon, then this photon has effectively been degraded to two 1 MeV photons. If the particles had lost any momentum in the time between creation and annihilation, then the photon will have been degraded even further.

A.8 Absorption

While only a thin layer is necessary to stop ionising alpha and beta radiation, the higher energy photons require a few centimetres of lead to reduce their effects. Generally, for primary gamma radiation, the exponential absorption law holds and is discussed in Section 3.6.4. The equation uses an absorption coefficient μ which accounts for the Compton, pair production and photoelectric effects within the material being used.

A.9 Luminescence

Luminescence is the emission of EM radiation from a substance due to non-thermal process. If radiation is emitted due to a thermal process such as when a light bulb filament is heated to emit light, it is referred to as incandescence.

Luminescence is produced when atoms are excited and then fall back to the lowest vacancy available in any of the shells. In doing so, the extra energy the electron had is released as a photon. Some materials are naturally luminescent due to internal processes such as the decay of radioactive isotopes or impurities within them.

For materials in which luminescence only occurs after irradiation by an external source, if the luminescence stops within 10^{-8} seconds of the energy source being removed, it is referred to as *fluorescence*. If the luminescence persists after this time it is referred to as *phosphorescence*.

In certain solids, the excited electrons created by ionising radiation can be trapped at defects (see Section 4.5). If the solid is subsequently heated (though not to the point when the material actually becomes incandescent) the electrons are liberated and fall back to ground state, emitting a form of luminescence known as *thermoluminescence*. This has developed into the field of thermoluminescence dosimetry that is used to monitor radiation, and for archaeological and geological dating.

Luminescence can also be induced by friction (triboluminescence) and chemical reaction (chemiluminescence).

A.10 Conversion of Energy to Wavelength

To convert from energy to wavelength, use the relation $\lambda=hc/E$ where h is the Planck constant, c is the velocity of light and E is the energy in joules. From this, as h and c are constant, the wavelength is inversely proportionate to E.

Thus for 1 eV $\rightarrow$ $\lambda \approx (6.6\text{x}10\text{-}34\ \text{Js} \times 2.99\text{x}108\ \text{ms}^{-1})/(1.6\text{x}10^{-19}\ \text{J}) = 1.2\text{x}10^{-6}\ \text{m} \equiv 1.2\ \mu\text{m}$.

For a quick estimate, (λ in nm) = 1260/(E in eV.)

A.11 Experimental Considerations for Electron Irradiation

As can be seen from the table below, beta particles differ from gamma photons in that their penetration is limited to a maximum range. With beta particles, once the source is placed behind a certain amount a material, the source is completely shielded.

Beta particle sources and properties

Property	Beta emitter				
	^{3}H	^{14}C	^{45}Ca	^{32}P	^{90}Sr
Half-life	12.3 yrs	5730 yrs	163 days	14.3 days	28.1 yrs
Maximum Beta energy (MeV)	0.0186	0.156	0.257	1.71	2.27
Average Beta energy (MeV)	0.006	0.049	0.077	0.070	1.13
Range in Air (ft)	0.02	1	2	20	29
Range in unit density material (cm)	0.00052	0.029	0.06	0.8	1.1

In this area of experimentation, it is quite conceivable that electrons will be used with a much higher energy than listed above. A useful "rule of thumb" given by Shapiro [18] is that the maximum range for a beta particle (or accelerated electrons) is given by:

$$\text{Range in Centimetres} = \frac{\text{Energy in MeV}}{2}$$

As this range is in a shield of unit density, replacing this with a denser material will reduce the range further. If aluminium was used, this is about 2.7 times denser and so the range would be reduced by 2.5. For a sample that is being heavily irradiated, lead may be used. Although such a dense shield will produce secondary x-rays, the dose they add may be negligible in comparison to the initial irradiation. However, most experiments and isotopes produce quite energetic electrons, as do most particle accelerators so lead must chosen with caution.

The table below shows the effect of the density of the shield material.

Variations in electron penetration with particle energy

Medium	Shield depth	
	50 MeV	10 MeV
Water	25 cm	5 cm
Al $\rho = 2.7$ g cc^{-1} $Z = 13$	9.3 cm	1.9 cm
Pb $\rho = 11$ g cc^{-1} $Z = 82$	2.3 cm	0.5 cm

If total shielding is beyond the scope of the project, it is possible to calculate the HVL. The HVL for beta particles is a function of the particle energy in MeV. For unit density material, the HVL is given by:

$$\text{HVL in cm} = 0.041(\text{Energy in MeV})^{1.14}$$

This is an approximate formula. If this method had to be employed, it would need experimental data to calibrate it.

A.12 Pye Unicam 8800 Spectrophotometer

The following details are from the PU880 user manual and are provided to give further information to the reader. They are not exhaustive, but give a flavour of the key aspects of the unit's typical performance:

Wavelength accuracy	within 0.3nm	
Wavelength reproducibility	within 0.1nm	
Photometric accuracy	± 0.0015 at 1A, ± 0.003 at 2A, ± 0.005 at 3A, ± 0.2%T relative to filters traceable to National Physical Laboratories standards.	
Photometric reproducibility	0.0001 at 0A with no integration, 0.0001 at 1A with 2s integration, 0.0002 at 2A with 5s integration, 0.0010 at 3A with 5s integration measured at 546nm, 2nm bandwidth	
Baseline flatness	within ± 0.001A, 190-850nm at 2nm bandwidth, 5nm/s and 2s response.	
Baseline stability	better than 0.0001A/hr after warm-up	
Wavelength range	190 to 900nm	
Bandwidths	0.1, 0.2, 0.5, 1, 2nm and HE (High Energy)	
Display Ranges	Absorbance Transmission EHT	-0.3000 to 6.000A (3 to 6A by reference Addition Mode 00.00 to 199.9%T 00.00 to 2000 (Volts)
Integration times	00 to 99s	
Cycle Times	00.00 (continuous) to 99s	
# of cycles	001 to 999	
Sample #	000 (infinite) and 1 to 999	
Scan speeds	0.01, 0.02, 0.05, 0.1, 0.2, 0.5, 1, 2, 5, 10nm/s fixed speeds or, in AUTO varied according to slope of spectrum within the range of 0.1 to 5 nm/s	
λ setting speed	600nm/min (automatic) and push button forward/reverse at 0 – 150 (ramped) nm/min	
Program storage	Capacity Titles	10 programs operator-defined, up to 20 characters in length
Wavelength selection	Step λ Minimum step Selected λ	measurement at λ intervals between start and stop λ 0.1nm measurement at up to 10 λs with 'bubble' sorting

B Propagation of Errors

Consider the function $u = f(x,y,z)$. For random errors, the uncertainty on u can be calculated as:

$$(du)^2 = \left(\frac{\partial u}{\partial x}\right)^2_{y,z} dx^2 + \left(\frac{\partial u}{\partial y}\right)^2_{x,z} dy^2 + \left(\frac{\partial u}{\partial z}\right)^2_{x,y} dz^2$$
$$+ 2\left(\frac{\partial u}{\partial x}\right)_{y,z}\left(\frac{\partial u}{\partial y}\right)_{x,z} dxdy + 2\left(\frac{\partial u}{\partial y}\right)_{x,z}\left(\frac{\partial u}{\partial z}\right)_{x,y} dydz + 2\left(\frac{\partial u}{\partial x}\right)_{y,z}\left(\frac{\partial u}{\partial z}\right)_{x,y} dxdz$$

If variables are independent (i.e. no correlation) then cross terms average zero, that is:

$$dxdy = 0, dydz = 0, dxdz = 0$$

Hence,

$$du = \sqrt{(du)^2}$$
$$= \sqrt{\left(\frac{\partial u}{\partial x}\right)^2_{y,z} dx^2 + \left(\frac{\partial u}{\partial y}\right)^2_{x,z} dy^2 + \left(\frac{\partial u}{\partial z}\right)^2_{x,y} dz^2}$$

Set the standard deviation as the integral to obtain standard error propagation formula:

$$s_u = du, s_x = dx, s_y = dy \text{ and } s_z = dz$$
$$s_u = \sqrt{\left(\frac{\partial u}{\partial x}\right)^2_{y,z} s_x^2 + \left(\frac{\partial u}{\partial y}\right)^2_{x,z} s_y^2 + \left(\frac{\partial u}{\partial z}\right)^2_{x,y} s_z^2}$$

Rearranging Equation 3 gives: $D_2 = \frac{D_1 r_1^2}{r_2^2}$ With $r_1 = 1$ and $D_1 = 2.125$ and both constant for the duration of this experiment, for a sample at 65 mm ± 1 mm (0.065 m ± 0.001 m), the uncertainty on the dose rate σ_{D_2} is given by:

$$\sigma^2_{D_2} = \sigma^2_{r_2}\left(\frac{\partial}{\partial r} D_2\right)^2 \text{ now substitute } D_2 = \frac{D_1}{r_2^2}$$
$$= \sigma^2_{r_2}\left(\frac{\partial}{\partial r}\frac{D_1}{r_2^2}\right)^2 = \sigma^2_{r_2}\left(\frac{-2D_1}{r_2^3}\right)^2 = (0.001)^2\left(\frac{-2\times 2.125}{0.065^3}\right)^2$$
$$\sigma_{D_2} = 12.391 \text{ krad hr}^{-1}$$

This sample is exposed to a dose of 500 rad hr^{-1} for 60 hours to achieve a total dose of 30 Mrad. Thus the dose rate at 0.65m is 500 ± 12 krad hr^{-1}. For the final dose, this propagates to 30 ± 0.9 Mrad, or an error of 3%.

C Periodic Table of the Elements

D Weighted Average Calculations

For observed value x with weighting w, the mean, variance and standard deviation can be calculated by:

$$\text{Mean } \mu_w = \frac{\sum wx}{N} \text{ where } N = \sum w$$

$$\text{Variance } \sigma^2 = \frac{\sum wx^2 - N\mu_w^2}{N}$$

$$\text{Standard Deviation} = \sigma$$

For example, consider the data in the table below:

observed value (x)	weight (w)	wxx	x^2	wxx^2
506	99	50094	256036	25347564
499	88	43912	249001	21912088
505	88	44440	255025	22442200
498	90	44820	248004	22320360
506	76	38456	256036	19458736
511	67	34237	261121	17495107
494	1	494	244036	244036
490	45	22050	240100	10804500
510	43	21930	260100	11184300
495	46	22770	245025	11271150
501	65	32565	251001	16315065
488	6	2928	238144	1428864
506	25	12650	256036	6400900
507	34	17238	257049	8739666
501	35	17535	251001	8785035
Totals	808	406119		204149571

Thus:

$$\text{Mean } \mu_w = \frac{\sum wx}{N} = \frac{406119}{808} = 502.63$$

$$\text{Variance } \sigma^2 = \frac{\sum wx^2 - N\mu_w^2}{N} = \frac{25013.87}{808} = 30.96$$

$$\text{Standard Deviation} = \sigma = \sqrt{30.96} = 5.56$$

From this it can be reported that the average value of x is 502 ± 6

A more rigorous treatment of uncertainty on data can be found in standard texts such as Kohler.*

* Kohler, H., *Statistics for Business and Economics*, Scott, Foresman and Company, 2nd edition, 1988

E DataFit

E.1 Macro File for DataFit for Magnesium Fluoride.

The following is an example of the macro configuration file. It defines the equation to be fitted, its initial estimates for the variables and parameters to govern the fit.

```
B_MACRO
    Comment = This macro file is for MgF2 data
    Comment = It calls 3 versions of the gauss fit
    Comment = Call 1
    Comment = 2 Gaussian curves, with no constraint on the wavelength
    Comment = Call 2
    Comment = 2 Gaussian curves, wavelength constrained to 370 & 400nm
    Comment = Call 3
    Comment = 2 Gaussian curves, 1 unconstrained wavelength, 1 constrained
    Comment = with the 2nd wavelength =  wavelength 1 + 30nm
    HandShake = UseDDE, ShowProgress
    RegressionTolerance = 0.0000000001
    UnchangedIterations = 10
    MaxIterations = 5000
    Derivatives = Richardson
    DataFile = C:\Sean\Thesis - Working Directory\DataFit\inp1.csv
    IndependentVariables = 1
    Weighted = False
    ColumnOrder = Default
    InputDelimit = Comma
    OverrideDecimal = False
    OutputFile = C:\Sean\Thesis - Working Directory\DataFit\out1.csv
    OutputFormat = Spreadsheet
    LogFile = test
    LogSummaryOnly = False
    OutputDelimit = comma
    TableOutput = DataFile, CalcData, ErrorData
    SortKey = RSS
    OutputFitInfo = True
    B_MODEL
        ID = 2 gauss - no fixed wavelengths
        F1 = (A1*exp(-((x-B1)^2)/(2*C1^2)))
        F2 = (A2*exp(-((x-B2)^2)/(2*C2^2)))
        Y = 1-(F1+F2)
        Assign A1 = 0.12, Operator = Value, Fit = True, Derivative = Numerical
        Assign A2 = 0.03, Operator = Value, Fit = True, Derivative = Numerical
        Assign B1 = 370, Operator = Value, Fit = True, Derivative = Numerical
        Assign B2 = 400, Operator = Value, Fit = True, Derivative = Numerical
        Assign C1 = 10, Operator = Value, Fit = True, Derivative = Numerical
        Assign C2 = 35, Operator = Value, Fit = True, Derivative = Numerical
    E_MODEL
    B_MODEL
        ID = 2 gauss - fixed wavelengths
        F1 = (A1*exp(-((x-370)^2)/(2*C1^2)))
        F2 = (A2*exp(-((x-400)^2)/(2*C2^2)))
        Y = 1-(F1+F2)
        Assign A1 = 0.12, Operator = Value, Fit = True, Derivative = Numerical
        Assign A2 = 0.03, Operator = Value, Fit = True, Derivative = Numerical
        Assign C1 = 10, Operator = Value, Fit = True, Derivative = Numerical
        Assign C2 = 35, Operator = Value, Fit = True, Derivative = Numerical
    E_MODEL

    B_MODEL
        ID = 2 gauss - fixed wavelength delta
        F1 = (A1*exp(-((x-B1)^2)/(2*C1^2)))
        F2 = (A2*exp(-((x-(B1+30))^2)/(2*C2^2)))
        Y = 1-(F1+F2)
        Assign A1 = 0.12, Operator = Value, Fit = True, Derivative = Numerical
        Assign A2 = 0.03, Operator = Value, Fit = True, Derivative = Numerical
        Assign B1 = 370, Operator = Value, Fit = True, Derivative = Numerical
        Assign C1 = 10, Operator = Value, Fit = True, Derivative = Numerical
        Assign C2 = 35, Operator = Value, Fit = True, Derivative = Numerical
    E_MODEL
E_MACRO
```

E.2 Example of VBA Code to Run DataFit from Excel

The following is a copy of the VBA code used to call the DataFit interface code and to search, format and sort the resulting data.

```
Option Explicit
```

```
Option Base 0

Dim SheetNames(3), CSVinputfile, CSVoutputfile As String
    'Declare the values used in the Dfit call
        'ExePath is the path to DataFit.exe. This should be the full path
        'to datafit.exe, for example "c:\program files\datafit\datafit.exe".
        Const dFitPath As String = "c:\program files\datafit\datafit.exe"
        'MacroPath is the path to the macro file. This should be the full
        'path to the macro file, for example "c:\macros\mymacro.cfg".
        Const macroPath As String = "C:\Sean\Thesis - Working Directory\DataFit\macro\"
    'the following are specific to material and fit
    'and need to be edited as required
       'declare the macro to use
        'Const dmacro As String = "MgF2 2 Lorentz.cfg"
        'Const dmacro As String = "MgF2 2 Gauss.cfg"
        Const dmacro As String = "MgF2 2 fits.cfg"

        'then declare the 2 search strings
        'these are the ID lines used in the code
        Const sst1 As String = "2 lorentz - no fixed wavelengths"
        Const sst2 As String = "2 lorentz - fixed wavelengths"
        Const sst3 As String = "2 lorentz - fixed wavelength delta"
        Const sst4 As String = "2 gauss - no fixed wavelengths"
        Const sst5 As String = "2 gauss - fixed wavelengths"
        Const sst6 As String = "2 gauss - fixed wavelength delta"


Sub SplitData()
        Dim sTime, eTime As Date
        sTime = Now()
    'define the macro name and path
        Dim mPath As String
        mPath = macroPath & dmacro
    'set the variables for the input files
        CSVinputfile = "inp1.csv"
        CSVoutputfile = "out1.csv"
    'set the variables used in this subroutine
        Dim i, j, k, nCols, nRows, nmVal() As Integer
        Dim dose As String
        Dim yVal() As Double
    'declare the sheets to use
    SheetNames(0) = "Input Data"
    SheetNames(1) = "Macro Export"
    SheetNames(2) = "Macro Import"
    SheetNames(3) = "Results"

    'begin
    Application.ScreenUpdating = False
    'clear export data
    Sheets(SheetNames(1)).Select
    Range("A1").Select
    Selection.CurrentRegion.Delete
    'clear imported data
    Sheets(SheetNames(2)).Select
    Range("A1:AP10000").Select
    Selection.Delete
    'got to start of source data
    Sheets(SheetNames(0)).Select
    Range("A5").Select
    'quick error trap
    If ActiveCell.Value = "" Then
        MsgBox ("No data in cell A5")
        Exit Sub
    End If
    'calculate number of data sets
    Selection.CurrentRegion.Select
    nCols = Selection.Columns.Count - 1 'to remove nm
    nRows = Selection.Rows.Count - 1 'to remove header
    'set the size of the arrays
    ReDim nmVal(nRows)
    ReDim yVal(nRows)
    'Load X values
    Range("A5").Select
    For i = 0 To nRows - 1 'nrows-1 since aray starts at 0
        nmVal(i) = ActiveCell.Offset(i, 0).Range("A1").Value
    Next i
    'Load Y values
```

```
    For i = 0 To nCols - 1
        'get dose
        Range("A5").Offset(0, i + 1).Select
        dose = ActiveCell.Offset(-1, 0).Value
        For j = 0 To nRows - 1
            yVal(j) = ActiveCell.Offset(j, 0).Range("A1").Value
        Next j
        'paste data out
        Sheets(SheetNames(1)).Select
        Range("A1").Select
        For k = 0 To UBound(nmVal) - 1
            ActiveCell.Offset(k, 0).Range("A1").Value = nmVal(k)
            ActiveCell.Offset(k, 1).Range("A1").Value = yVal(k)
        Next k
        'write file
        WriteCSV (CSVinputfile)
        'call datafit
        Call RunDataFit(dFitPath, mPath)
        'save the data
        Call SaveOut(dose, i)
        'clear imported data
        Sheets(SheetNames(2)).Select
        Range("A1:AP10000").Select
        Selection.Delete
        'move to next data
        Sheets(SheetNames(0)).Select
    Next i
    eTime = Now()
    For i = 0 To UBound(SheetNames)
        Sheets(SheetNames(i)).Select
        If i = 0 Then
            Range("E1") = Format(sTime, "hh:mm:ss")
            Range("E2") = Format(eTime, "hh:mm:ss")
            Range("G1") = Format((eTime - sTime), "hh:mm:ss")
            Range("G2") = Format((eTime - sTime) / nCols, "hh:mm:ss")
        End If
        Range("A1").Select
    Next i
    Application.CutCopyMode = False
    Application.ScreenUpdating = True
End Sub

Sub WriteCSV(CSVfile)
    Dim isCSV As String
    ChDir "C:\Sean\Thesis - Working Directory\DataFit"
    isCSV = Dir("C:\Sean\Thesis - Working Directory\DataFit\inp1.csv")
    If isCSV <> "" Then _
            Kill "C:\Sean\Thesis - Working Directory\DataFit\inp1.csv"
    Sheets(SheetNames(1)).Select
    Sheets(SheetNames(1)).Copy
    ActiveWorkbook.SaveAs Filename:= _
        "C:\Sean\Thesis - Working Directory\DataFit\" & CSVinputfile, _
        FileFormat:=xlCSV, _
        CreateBackup:=False
    ActiveWorkbook.Saved = True
    ActiveWindow.Close
End Sub

Sub SaveOut(ds, run)
    Dim LastRow, NumIt As Integer
    Dim ThisBook As String
    Dim CellFind As Boolean
    ThisBook = ActiveWorkbook.Name
    Workbooks.Open Filename:= _
        "C:\Sean\Thesis - Working Directory\DataFit\out1.csv"

    Range(Cells(1, 1), Cells((ActiveCell.SpecialCells(xlLastCell).Row),
(ActiveCell.SpecialCells(xlLastCell).Column))).Copy
    Windows(ThisBook).Activate
    Sheets(SheetNames(2)).Select
    Range("A1").Select
    ActiveSheet.Paste
    Range("A1").Select
    Windows(CSVoutputfile).Activate
    Application.CutCopyMode = False
    ActiveWindow.Close
    'save the data
```

```
    Range("L3").Select
    ActiveCell.Value = ds

    'Lorentz
    'search for first term
    On Error Resume Next
    CellFind = False: NumIt = 0 'reset variables
    'attempt to find free wavelength data
    CellFind = Cells.Find(What:=sst1, _
        After:=ActiveCell, LookIn:=xlFormulas, LookAt:=xlPart, SearchOrder:=xlByColumns,
_
        SearchDirection:=xlNext, MatchCase:=False, SearchFormat:=False).Activate
    If CellFind <> True Then GoTo 1:
    Cells.Find(What:=sst1, _
        After:=ActiveCell, LookIn:=xlFormulas, LookAt:=xlPart, SearchOrder:=xlByColumns,
_
        SearchDirection:=xlNext, MatchCase:=False, SearchFormat:=False).Activate
    NumIt = ActiveCell.Offset(17, 0).Range("A1").Value 'number of iterations
    ActiveCell.Offset(6, -1).Range("A1:C6").Copy
    Range("K5").Select
    ActiveSheet.Paste
    ActiveCell.Offset(-1, 0).Value = NumIt
    GoTo 2 'step over error trap
1:  'error trap - no output found
    Range("L5").Select
    ActiveCell.Value = "RUN FAILED for " & sst1

2:  'data found, go to next term
    'attempt to find fixed wavelength data
    On Error Resume Next
    CellFind = False: NumIt = 0 'reset variables
    Range("A1").Select
    CellFind = Cells.Find(What:=sst2, _
        After:=ActiveCell, LookIn:=xlFormulas, LookAt:=xlPart, SearchOrder:=xlByColumns,
_
        SearchDirection:=xlNext, MatchCase:=False, SearchFormat:=False).Activate
    If CellFind <> True Then GoTo 3:
    Cells.Find(What:=sst2, _
        After:=ActiveCell, LookIn:=xlFormulas, LookAt:=xlPart, SearchOrder:=xlByColumns,
_
        SearchDirection:=xlNext, MatchCase:=False, SearchFormat:=False).Activate
    NumIt = ActiveCell.Offset(15, 0).Range("A1").Value 'number of iterations
    ActiveCell.Offset(6, -1).Range("A1:C4").Copy
    Range("K12").Select
    ActiveSheet.Paste
    ActiveCell.Offset(-1, 0).Value = NumIt
    GoTo 4 'step over error trap
3:  'error trap - no output found
    Range("L12").Select
    ActiveCell.Value = "RUN FAILED for " & sst2

4:  'data found, go to next term
    'attempt to find fixed wavelength delta data
    On Error Resume Next
    CellFind = False: NumIt = 0 'reset variables
    Range("A1").Select
    CellFind = Cells.Find(What:=sst3, _
        After:=ActiveCell, LookIn:=xlFormulas, LookAt:=xlPart, SearchOrder:=xlByColumns,
_
        SearchDirection:=xlNext, MatchCase:=False, SearchFormat:=False).Activate
    If CellFind <> True Then GoTo 5:
    Cells.Find(What:=sst3, _
        After:=ActiveCell, LookIn:=xlFormulas, LookAt:=xlPart, SearchOrder:=xlByColumns,
_
        SearchDirection:=xlNext, MatchCase:=False, SearchFormat:=False).Activate
    NumIt = ActiveCell.Offset(16, 0).Range("A1").Value 'number of iterations
    ActiveCell.Offset(6, -1).Range("A1:C5").Copy
    Range("K17").Select
    ActiveSheet.Paste
    ActiveCell.Offset(-1, 0).Value = NumIt
    GoTo 6 'step over error trap
5:  'error trap - no output found
    Range("L17").Select
    ActiveCell.Value = "RUN FAILED for " & sst3

    'Gauss
6:  'data found, go to next term
```

```
    'attempt to find fixed wavelength delta data
    On Error Resume Next
    CellFind = False: NumIt = 0 'reset variables
    Range("A1").Select
    CellFind = Cells.Find(What:=sst4, _
        After:=ActiveCell, LookIn:=xlFormulas, LookAt:=xlPart, SearchOrder:=xlByColumns,
_
        SearchDirection:=xlNext, MatchCase:=False, SearchFormat:=False).Activate
    If CellFind <> True Then GoTo 7:
    Cells.Find(What:=sst4, _
        After:=ActiveCell, LookIn:=xlFormulas, LookAt:=xlPart, SearchOrder:=xlByColumns,
_
        SearchDirection:=xlNext, MatchCase:=False, SearchFormat:=False).Activate
    NumIt = ActiveCell.Offset(17, 0).Range("A1").Value 'number of iterations
    ActiveCell.Offset(6, -1).Range("A1:C6").Copy
    Range("K23").Select
    ActiveSheet.Paste
    ActiveCell.Offset(-1, 0).Value = NumIt
    GoTo 8 'step over error trap
7:  'error trap - no output found
    Range("L23").Select
    ActiveCell.Value = "RUN FAILED for " & sst4

8:  'data found, go to next term
    'attempt to find fixed wavelength delta data
    On Error Resume Next:
    CellFind = False: NumIt = 0 'reset variables
    Range("A1").Select
    CellFind = Cells.Find(What:=sst5, _
        After:=ActiveCell, LookIn:=xlFormulas, LookAt:=xlPart, SearchOrder:=xlByColumns,
_
        SearchDirection:=xlNext, MatchCase:=False, SearchFormat:=False).Activate
    If CellFind <> True Then GoTo 9:
    Cells.Find(What:=sst5, _
        After:=ActiveCell, LookIn:=xlFormulas, LookAt:=xlPart, SearchOrder:=xlByColumns,
_
        SearchDirection:=xlNext, MatchCase:=False, SearchFormat:=False).Activate
    Stop
    NumIt = ActiveCell.Offset(17, 0).Range("A1").Value 'number of iterations
    ActiveCell.Offset(6, -1).Range("A1:C4").Copy
    Range("K30").Select
    ActiveSheet.Paste
    ActiveCell.Offset(-1, 0).Value = NumIt
    GoTo 10 'step over error trap
9:  'error trap - no output found
    Range("L30").Select
    ActiveCell.Value = "RUN FAILED for " & sst5

10:  'data found, go to next term
    'attempt to find fixed wavelength delta data
    On Error Resume Next
    CellFind = False: NumIt = 0 'reset variables
    Range("A1").Select
    CellFind = Cells.Find(What:=sst6, _
        After:=ActiveCell, LookIn:=xlFormulas, LookAt:=xlPart, SearchOrder:=xlByColumns,
_
        SearchDirection:=xlNext, MatchCase:=False, SearchFormat:=False).Activate
    If CellFind <> True Then GoTo 11:
    Cells.Find(What:=sst6, _
        After:=ActiveCell, LookIn:=xlFormulas, LookAt:=xlPart, SearchOrder:=xlByColumns,
_
        SearchDirection:=xlNext, MatchCase:=False, SearchFormat:=False).Activate
    NumIt = ActiveCell.Offset(16, 0).Range("A1").Value 'number of iterations
    ActiveCell.Offset(6, -1).Range("A1:C5").Copy
    Range("K35").Select
    ActiveSheet.Paste
    ActiveCell.Offset(-1, 0).Value = NumIt
    GoTo 12 'step over error trap
11:  'error trap - no output found
    Range("L17").Select
    ActiveCell.Value = "RUN FAILED for " & sst6

12:  'all run complete, reset error handler
    On Error GoTo 0
    'copy data out
    MakeData (ds)
    'select data
```

```
    Range("O2:P74").Copy

    Worksheets(SheetNames(3)).Select
    Range("A1").Select '(Cells(5, (3 * run) + 1)).Select
    ActiveCell.Offset(0, 3 * run).Select
    Selection.PasteSpecial Paste:=xlValues, operation:=xlNone, skipblanks:=False,
Transpose:=False
End Sub

Sub MakeData(krad)
    'common data
    Range("O2").Value = "Dose"
    Range("P2").Value = krad

    '2 Lorentz fits - fixed wavelength
    Range("O4").Value = sst2 & ": (" & Range("K11").Value & ")"
    Range("O5").FormulaR1C1 = "=R[7]C[-4]"
    Range("O5").AutoFill Destination:=Range("O5:O8"), _
        Type:=xlFillDefault
    Range("p5").FormulaR1C1 = "=R[7]C[-4]"
    Range("p5").AutoFill Destination:=Range("p5:p8"), _
        Type:=xlFillDefault
    Range("O9").FormulaR1C1 = "=""error on ""&R[-4]C"
    Range("O9").AutoFill Destination:=Range("O9:O12"), _
        Type:=xlFillDefault
    Range("P9").FormulaR1C1 = "=R[3]C[-3]"
    Range("P9").AutoFill Destination:=Range("P9:P12"), _
        Type:=xlFillDefault

    '2 Lorentz fits - floating wavelength
    Range("O14").Value = sst1 & ": (" & Range("K4").Value & ")"
    Range("O15").FormulaR1C1 = "=R[-10]C[-4]"
    Range("O15").AutoFill Destination:=Range("O15:O20"), _
        Type:=xlFillDefault
    Range("P15").FormulaR1C1 = "=R[-10]C[-4]"
    Range("P15").AutoFill Destination:=Range("P15:P20"), _
        Type:=xlFillDefault
    Range("O21").FormulaR1C1 = "=""error on ""&R[-6]C"
    Range("O21").AutoFill Destination:=Range("O21:O26"), _
        Type:=xlFillDefault
    Range("P21").FormulaR1C1 = "=R[-16]C[-3]"
    Range("P21").AutoFill Destination:=Range("P21:P26"), _
        Type:=xlFillDefault

    '2 Lorentz fits - fixed delta
    Range("O28").Value = sst3 & ": (" & Range("K16").Value & ")"
    Range("O29").FormulaR1C1 = "=R[-12]C[-4]"
    Range("O29").AutoFill Destination:=Range("O29:O33"), _
        Type:=xlFillDefault
    Range("P29").FormulaR1C1 = "=R[-12]C[-4]"
    Range("P29").AutoFill Destination:=Range("P29:P33"), _
        Type:=xlFillDefault
    Range("O34").FormulaR1C1 = "=""error on ""&R[-5]C"
    Range("O34").AutoFill Destination:=Range("O34:O38"), _
        Type:=xlFillDefault
    Range("P34").FormulaR1C1 = "=R[-17]C[-3]"
    Range("P34").AutoFill Destination:=Range("P34:P38"), _
        Type:=xlFillDefault

    '2 Gauss fits - fixed wavelength
    Range("O40").Value = sst5 & ": (" & Range("K22").Value & ")"
    Range("O41").FormulaR1C1 = "=R[-18]C[-4]"
    Range("O41").AutoFill Destination:=Range("O41:O46"), _
        Type:=xlFillDefault
    Range("p41").FormulaR1C1 = "=R[-18]C[-4]"
    Range("p41").AutoFill Destination:=Range("p41:p46"), _
        Type:=xlFillDefault
    Range("O47").FormulaR1C1 = "=""error on ""&R[-6]C"
    Range("O47").AutoFill Destination:=Range("O47:O52"), _
        Type:=xlFillDefault
    Range("P47").FormulaR1C1 = "=R[-24]C[-3]"
    Range("P47").AutoFill Destination:=Range("P47:P52"), _
        Type:=xlFillDefault

    '2 gauss fits - floating wavelength
    Range("O54").Value = sst4 & ": (" & Range("K29").Value & ")"
    Range("O55").FormulaR1C1 = "=R[-25]C[-4]"
```

```
    Range("O55").AutoFill Destination:=Range("O55:O58"), _
        Type:=xlFillDefault
    Range("P55").FormulaR1C1 = "=R[-25]C[-4]"
    Range("P55").AutoFill Destination:=Range("P55:P58"), _
        Type:=xlFillDefault
    Range("O59").FormulaR1C1 = "=""error on ""&R[-4]C"
    Range("O59").AutoFill Destination:=Range("O59:O62"), _
        Type:=xlFillDefault
    Range("P59").FormulaR1C1 = "=R[-29]C[-3]"
    Range("P59").AutoFill Destination:=Range("P59:P62"), _
        Type:=xlFillDefault

    '2 gauss fits - fixed delta
    Range("O64").Value = sst6 & ": (" & Range("K34").Value & ")"
    Range("O65").FormulaR1C1 = "=R[-30]C[-4]"
    Range("O65").AutoFill Destination:=Range("O65:O69"), _
        Type:=xlFillDefault
    Range("P65").FormulaR1C1 = "=R[-30]C[-4]"
    Range("P65").AutoFill Destination:=Range("P65:P69"), _
        Type:=xlFillDefault
    Range("O70").FormulaR1C1 = "=""error on ""&R[-5]C"
    Range("O70").AutoFill Destination:=Range("O70:O74"), _
        Type:=xlFillDefault
    Range("P70").FormulaR1C1 = "=R[-35]C[-3]"
    Range("P70").AutoFill Destination:=Range("P70:P74"), _
        Type:=xlFillDefault

End Sub
```

E.3 Interface Code as Provided by DataFit

The following is the code provided by DataFit to allow the DDE call between VBA and DataFit.

```
'Copyright (c) 1995-2002 Oakdale Engineering
Option Explicit

Private Declare Function WaitForSingleObject Lib "kernel32" (ByVal _
   hHandle As Long, ByVal dwMilliseconds As Long) As Long

Private Declare Function CreateProcessA Lib "kernel32" (ByVal _
   lpApplicationName As Long, ByVal lpCommandLine As String, ByVal _
   lpProcessAttributes As Long, ByVal lpThreadAttributes As Long, _
   ByVal bInheritHandles As Long, ByVal dwCreationFlags As Long, _
   ByVal lpEnvironment As Long, ByVal lpCurrentDirectory As Long, _
   lpStartupInfo As STARTUPINFO, lpProcessInformation As _
   PROCESS_INFORMATION) As Long

Private Declare Function CloseHandle Lib "kernel32" _
      (ByVal hObject As Long) As Long

Private Declare Function GetExitCodeProcess Lib "kernel32" _
   (ByVal hProcess As Long, lpExitCode As Long) As Long

Private Const NORMAL_PRIORITY_CLASS = &H20&
Private Const INFINITE = -1&

Private Type STARTUPINFO
      cb As Long
      lpReserved As String
      lpDesktop As String

      lpTitle As String
      dwX As Long
      dwY As Long
      dwXSize As Long
      dwYSize As Long
      dwXCountChars As Long
      dwYCountChars As Long
      dwFillAttribute As Long
      dwFlags As Long
      wShowWindow As Integer
      cbReserved2 As Integer
      lpReserved2 As Long
      hStdInput As Long
      hStdOutput As Long
      hStdError As Long
   End Type
```

```
Private Type PROCESS_INFORMATION
   hProcess As Long
   hThread As Long
   dwProcessID As Long

   dwThreadID As Long
End Type

Public Function CmdExecute(ByVal CmdLine As String, _
    ByRef ExitStatus As Long) As Boolean

    'This function launches DataFit as a shelled process. If the launch
    'is successful, this function returns TRUE, otherwise it returns FALSE.
    'The variable ExitStatus will hold the exit status returned by DataFit
    'on exit if the launch was successful. The calling routine can use the
    'exit status to determine if the DataFit run was successful.

    'The main difference between this method and using the Visual Basic Shell()

    'function is that the Shell() function runs the process in an asynchronous
    'mode (the shelled program continues to run independently of your application
    'until the user closes it). By using the method shown below, execution of the
    'calling program is suspended until the shelled process terminates.

    Dim proc As PROCESS_INFORMATION
    Dim start As STARTUPINFO
    Dim Success As Long
    Dim ret As Long

    'Initialize the STARTUPINFO structure

    start.cb = Len(start)

    'Start DataFit as a shelled process using the CreateProcess() API
    'function. The CreateProcess() function gives the calling program the
    'process handle of the shelled process through proc.hProcess.
    Success = CreateProcessA(0&, CmdLine$, 0&, 0&, 1&, _
        NORMAL_PRIORITY_CLASS, 0&, 0&, start, proc)

    'Wait for DataFit to finish. This is done by passing the handle of the process
    'returned in proc.hProcess to the WaitForSingleObject() API function. This causes

    'the suspension of this application until the shelled process terminates.
    ret = WaitForSingleObject(proc.hProcess, INFINITE)

    'Get the DataFit exit status. This is done by passing the handle of the process
    'in proc.hProcess to the GetExitCodeProcess() API function. The exit status is
    'returned in the variable ExitStatus.
    Call GetExitCodeProcess(proc.hProcess, ExitStatus)

    'Clean up
    Call CloseHandle(proc.hThread)
    Call CloseHandle(proc.hProcess)


    'Return results of CreatProcess function to calling routine.
    CmdExecute = Success

End Function

Public Sub RunDataFit(ExePath As String, macroPath As String)

    'This subroutine launches DataFit in non-graphical mode.
    'ExePath is the path to DataFit.exe. This should be the full path
    'to datafit.exe, for example "c:\program files\datafit\datafit.exe".
    'MacroPath is the path to the macro file. This should be the full
    'path to the macro file, for example "c:\macros\mymacro.cfg".

    'The cmdExecute function does not return until the shelled

    'process has completed.

    Dim CmdLine As String
    Dim retval As Long
    Dim ExitStatus As Long
    Dim strExitStatus As String
```

```
    CmdLine = ExePath & " -runcfg " & macroPath
    If CmdExecute(CmdLine, ExitStatus) = True Then
        'Launch was successful, check the exit status
        If ExitStatus = 0 Then
            'Solution process also was successful. Place code here to
            'read/process the results if desired.
            'ProcessSolution

        Else
            'Launch was successful, but the solution process failed.
            MsgBox "Solution process failed. Exit Status = " & CStr(ExitStatus)
        End If
    Else
        'Launch was not successful
        MsgBox "Could not launch DataFit"
    End If

End Sub
```

F User Defined Functions

In the approximations used in Chapter 7 the following User Defined Functions (UDF) were used in Excel to create the approximations. The benefit of this approach is that once the code has been accurately entered into a module, the user can call on it quickly and easily without the risk of mistyping the equations.

To call a UDF, the user enters the name as if it were a normal Excel Equation. For example, consider the UDF MgF2_Approx.

To call this, the user would enter the data in a spreadsheet as follows:

	A	B	C
1	Wavelength		30,000,000
2	nm	Sample Data	MgF2 Approximation UDF
3	490	0.99845	=MgF2_Approx(C1,$A3)
4	480	0.99835	
5	470	0.99815	
6	460	0.99699	
7	450	0.99646	
8	440	0.99415	
9	430	0.99004	

Upon hitting the enter key, the Excel would pass the values from C1 (Total Dose in rad) and $A3 (Wavelength in nm) to the function, which would return the approximate value. By copying the cell down, the two $ signs in C1 would ensure that this value is always used, where as the single $ in $A ensures that the column for the wavelength stays the same, but allows the value to change by row. The completed sheet would look like the following:

	A	B	C
1	Wavelength		30,000,000
2	nm	Sample Data	MgF2 Approximation UDF
3	490	0.99845	0.99750
4	480	0.99835	0.99702
5	470	0.99815	0.99639
6	460	0.99699	0.99555
7	450	0.99646	0.99438
8	440	0.99415	=MgF2_Approx(C1,$A8)
9	430	0.99004	0.99010

As can be seen, the function keeps the correct dose, but tracks down the wavelength as necessary.

The following UDF were used:

```
Option Explicit

''''''''''''''''''''''''''''''''''''''''''''''''''''''''''''''''''''''
' Code to approximate the spectra of samples irradiated              '
' by gamma irradiation. These are User Defined Functions             '
' that allow the user to simply calculate the Lorentzian             '
' or Gaussian curves. The benefit of using UDF is that               '
' once the function has been accurately entered, it                  '
' reduces the risk of mistyping the equations elsewhere.             '
' For more information on the parameters listed and used             '
' here, please refer to the relevant section of work.                '
''''''''''''''''''''''''''''''''''''''''''''''''''''''''''''''''''''''

Function MgF2_Approx_With_W2(dbdose As Double, dbWlength As Double)
'This code requires two arguments as listed.
Const dbL1 As Double = 372
Const dbW1 As Double = 29
'The following line is set to 65, but this causes incorrect
'fitting and so has been removed in the following function.
Const dbW2 As Double = 65

Dim dbM1 As Double, dbM2 As Double, dbG1 As Double, dbG2 As Double
```

```
    'define the value of M1 and M2 as a function of total dose
    'nb in VBA log = natural log, not base 10.
    dbM1 = 0.00000148 * Exp(0.6762 * Log(dbdose))
    dbM2 = -0.00467 * Exp(0.000000000342 * Log(dbdose))
    dbG1 = dbM1 * (((dbW1 / 2) ^ 2) / (((dbWlength - dbL1) ^ 2) + ((dbW1 / 2) ^ 2)))
    dbG2 = dbM1 * (((dbW2 / 2) ^ 2) / (((dbWlength - dbL1 + 30) ^ 2) + ((dbW2 / 2) ^
2)))
    MgF2_Approx_With_W2 = 1 - (dbG1 + dbG2)
End Function

Function MgF2_Approx(dbdose As Double, dbWlength As Double)
'This code requires two arguments as listed.
Const dbL1 As Double = 372
Const dbW1 As Double = 29
Dim dbM1 As Double, dbM2 As Double, dbG1 As Double

    'define the value of M1 and M2 as a function of total dose
    'nb in VBA log = natural log, not base 10.
    dbM1 = 0.00000148 * Exp(0.6762 * Log(dbdose))
    'calculate value of Lorentzian
    dbG1 = dbM1 * (((dbW1 / 2) ^ 2) / (((dbWlength - dbL1) ^ 2) + ((dbW1 / 2) ^ 2)))
    'return value of function
    MgF2_Approx = 1 - (dbG1)
End Function

Function BK7_Approx(dbdose As Double, dbWlength As Double)
'This code requires two arguments as listed.
Const dbB1 As Double = 370
Const dbB2 As Double = 640
Dim dbC1 As Double, dbC2 As Double
Dim dbA1 As Double, dbA2 As Double
Dim dbG1 As Double, dbG2 As Double

    'calculate value of A1 and A2 as function of total dose
    dbA1 = 1.014 * Exp(-Exp(13.2 - (1.25 * Log(dbdose))))
    dbA2 = 0.77 * Exp(-Exp(2.48 - (0.17 * Log(dbdose))))
    'calculate value of C1 and C2 as function of total dose
    dbC1 = 14.13 * Log(dbdose)
    dbC2 = 6.87 * Log(dbdose)
    'calculate value of Gaussians
    dbG1 = dbA1 * Exp(-(((dbWlength - dbB1) ^ 2) / (2 * dbC1 ^ 2)))
    dbG2 = dbA2 * Exp(-(((dbWlength - dbB2) ^ 2) / (2 * dbC2 ^ 2)))
    'return value of function
    BK7_Approx = 1 - (dbG1 + dbG2)
End Function

Function BK7_Approx_CutOff(dbdose As Double, dbWlength As Double)
'This code requires two arguments as listed.
'The main difference between this code and BK7_Approx() is
'that this function manually holds the returned value at 0 below
'a cut off range.
Const dbB1 As Double = 370
Const dbB2 As Double = 640
Dim dbC1 As Double, dbC2 As Double
Dim dbA1 As Double, dbA2 As Double
Dim dbG1 As Double, dbG2 As Double
Dim dbCutOffFactor As Double
Dim eWFn As WorksheetFunction
'define the upper and lower value of the correction
'dbUCut = approx wavelength for full transmission
Const dbUCut As Double = 330
'dbLCut = approx wavelength for zero transmission
Const dbLCut As Double = 280
    Set eWFn = Excel.WorksheetFunction

'basic error trap
    If dbdose <= 1 Then MsgBox Title:="ln(1) Error: Function terminating", _
        prompt:="This function uses a value derived from the ln of the dose." & Chr(13)
& "The value of dose must be greater than 1.", _
        Buttons:=vbCritical + vbOKOnly: Exit Function

    'calculate value of A1 and A2 as function of total dose
    dbA1 = 1.014 * Exp(-Exp(13.2 - (1.25 * Log(dbdose))))
    dbA2 = 0.77 * Exp(-Exp(2.48 - (0.17 * Log(dbdose))))
    'calculate value of C1 and C2 as function of total dose
    dbC1 = 14.13 * Log(dbdose)
    dbC2 = 6.87 * Log(dbdose)
```

```
    'calculate value of Gaussians
    dbG1 = dbA1 * Exp(-(((dbWlength - dbB1) ^ 2) / (2 * dbC1 ^ 2)))
    dbG2 = dbA2 * Exp(-(((dbWlength - dbB2) ^ 2) / (2 * dbC2 ^ 2)))
    'calculate cut off correction
    dbCutOffFactor = eWFn.Min(eWFn.Max((dbWlength - dbLCut) / (dbUCut - dbLCut), 0), 1)

    'return value of function
    BK7_Approx_CutOff = (1 - (dbG1 + dbG2)) * dbCutOffFactor
End Function
Sub test()
F2_Approx dbdose:=100000, dbWlength:=800
End Sub


Function F2_Approx(dbdose As Double, dbWlength As Double)
'This code requires two arguments as listed.
Dim eWFn As WorksheetFunction
    Set eWFn = Excel.WorksheetFunction

'The following lines declare the variables used for the
'calculation of the approximation.
Const dbL1 As Double = 328
Const dbL2 As Double = 504
Const dbL3 As Double = 755
Dim dbW1 As Double, dbW2 As Double, dbW3 As Double
Dim dbM1 As Double, dbM2 As Double, dbM3 As Double
Dim dbG1 As Double, dbG2 As Double, dbG3 As Double

    'calculate value of W1, W2 and W3 as function of total dose
    dbW1 = (69 * Log(dbdose)) - 469
    dbW2 = (7.3 * Log(dbdose)) + 312
    dbW3 = (14.8 * Log(dbdose)) + 43

    'calculate value of M1, M2 and M3 as function of total dose
    dbM1 = 0.927 * Exp(-Exp(7.84 - (0.83 * Log(dbdose))))
    dbM2 = 0.31 * Exp(-Exp(29 - (3 * Log(dbdose))))
    dbM3 = 0.363 * Exp(-Exp(9.2 - (0.82 * Log(dbdose))))

    'calculate value of Gaussians G1, G2 and G3
    dbG1 = dbM1 * (((dbW1 / 2) ^ 2) / (((dbWlength - dbL1) ^ 2) + ((dbW1 / 2) ^ 2)))
    dbG2 = dbM2 * (((dbW2 / 2) ^ 2) / (((dbWlength - dbL2) ^ 2) + ((dbW2 / 2) ^ 2)))
    dbG3 = dbM3 * (((dbW3 / 2) ^ 2) / (((dbWlength - dbL3) ^ 2) + ((dbW3 / 2) ^ 2)))

    'return value of function
    F2_Approx = 1 - (dbG1 + dbG2 + dbG3)
End Function

Function F2_Approx_Mod(dbdose As Double, dbWlength As Double)
'This code requires two arguments as listed.
'The following lines are for the cut-off correction
Const dbUCut As Double = 330
Const dbLCut As Double = 300
Dim dbCutOffFactor As Double
Dim eWFn As WorksheetFunction
    Set eWFn = Excel.WorksheetFunction

'The following lines declare the variables used for the
'calculation of the approximation.
Const dbL1 As Double = 328
Const dbL2 As Double = 504
Const dbL3 As Double = 755
Dim dbW1 As Double, dbW2 As Double, dbW3 As Double
Dim dbM1 As Double, dbM2 As Double, dbM3 As Double
Dim dbG1 As Double, dbG2 As Double, dbG3 As Double

    'calculate value of W1, W2 and W3 as function of total dose
    dbW1 = (69 * Log(dbdose)) - 469
    dbW2 = (7.3 * Log(dbdose)) + 312
    dbW3 = (14.8 * Log(dbdose)) + 43

    'calculate value of M1, M2 and M3 as function of total dose
    dbM1 = 0.927 * Exp(-Exp(7.84 - (0.83 * Log(dbdose))))
    dbM2 = 0.19 * Exp(-Exp(35 - (4 * Log(dbdose))))
    'the dbM2 is a manually corrected version to highlight
    'sensitivity
    dbM3 = 0.363 * Exp(-Exp(9.2 - (0.82 * Log(dbdose))))
```

```
    'calculate value of Gaussians G1, G2 and G3
    dbG1 = dbM1 * (((dbW1 / 2) ^ 2) / (((dbWlength - dbL1) ^ 2) + ((dbW1 / 2) ^ 2)))
    dbG2 = dbM2 * (((dbW2 / 2) ^ 2) / (((dbWlength - dbL2) ^ 2) + ((dbW2 / 2) ^ 2)))
    dbG3 = dbM3 * (((dbW3 / 2) ^ 2) / (((dbWlength - dbL3) ^ 2) + ((dbW3 / 2) ^ 2)))

    'calculate cut off correction
    dbCutOffFactor = eWFn.Min(eWFn.Max((dbWlength - dbLCut) / (dbUCut - dbLCut), 0), 1)

    'return value of function
    F2_Approx_Mod = eWFn.Max((1 - (dbG1 + dbG2 + dbG3)) * dbCutOffFactor, 0)
End Function
```

G Initial Data

The data was entered into the system after the attempts to scan the data in had failed. The following tables give the data grouped by material. It should be noted that for some samples, the initial runs did manage to reach a wavelength of 190 nm, and these are shown in some tables.

For those samples measured after the MSSL spectrophotometer light source had become unstable, the data is that from the Harwell PU880 spectrophotometer.

G.1 BK7 glass: 1 to 100 krad

Wavelength	0.5	1	1.5	3	5	10	15	30	50	100
Nm	krad	krad	krad	krad	krad	krad	krad	krad	krad	krad
840	89.88	90.15	90.44	89.50	88.89	88.83	89.31	87.63	88.95	86.09
830	90.21	90.36	90.52	89.63	88.83	88.85	89.40	87.59	88.82	85.94
820	90.08	90.37	90.56	89.63	88.91	88.89	89.30	87.66	88.78	85.79
810	89.99	90.36	90.51	89.70	88.92	88.78	89.22	87.35	88.49	85.36
800	90.02	90.33	90.57	89.60	88.81	88.85	89.23	87.31	88.28	85.00
790	90.01	90.32	90.53	89.70	88.87	88.82	89.06	87.10	88.06	84.49
780	89.97	90.31	90.46	89.72	88.87	88.69	89.04	86.90	87.65	83.93
770	89.98	90.23	90.48	89.78	88.75	88.51	88.90	86.66	87.28	83.23
760	90.02	90.30	90.52	89.50	88.67	88.43	88.67	86.47	86.91	82.45
750	90.09	90.23	90.57	89.73	88.71	88.45	88.58	86.20	86.47	81.70
740	90.03	90.20	90.51	89.67	88.61	88.27	88.46	85.77	85.85	80.72
730	90.05	90.28	90.48	89.61	88.57	88.04	88.27	85.39	85.22	79.53
720	90.01	90.25	90.38	89.56	88.46	87.88	88.02	85.00	84.48	78.39
710	89.98	90.26	90.34	89.47	88.33	87.64	87.73	84.50	83.72	77.11
700	90.02	90.23	90.33	89.46	88.20	87.43	87.46	84.04	82.89	75.65
690	90.01	90.16	90.17	89.22	88.07	87.23	87.15	83.35	81.96	74.18
680	90.00	90.22	90.22	89.19	87.95	86.96	86.79	82.81	81.09	72.71
670	89.79	90.12	90.12	89.12	87.79	86.83	86.46	82.32	80.26	71.17
660	89.79	90.01	90.06	89.03	87.58	86.42	86.02	81.65	79.30	69.69
650	89.76	89.99	89.97	88.88	87.51	86.20	85.77	81.09	78.40	68.27
640	89.73	89.99	89.96	88.94	87.32	86.02	85.44	80.57	77.60	66.99
630	89.77	89.97	89.86	88.72	87.21	85.76	85.21	80.08	76.82	65.76
620	89.72	89.94	89.79	88.64	87.07	85.48	84.88	79.57	76.11	64.64
610	89.73	89.95	89.85	88.61	87.10	85.31	84.75	79.14	75.48	63.60
600	89.73	89.97	89.78	88.56	86.96	85.15	84.41	78.70	74.76	62.62
590	89.72	89.94	89.76	88.54	86.86	85.00	84.14	78.33	74.18	61.63
580	89.67	89.95	89.62	88.39	86.76	84.72	83.92	77.86	73.52	60.66
570	89.69	89.87	89.66	88.45	86.66	84.64	83.72	77.45	72.85	59.61
560	89.71	89.86	89.64	88.38	86.58	84.38	83.45	76.93	72.09	58.47
550	89.69	89.90	89.58	88.31	86.41	84.15	83.09	76.42	71.26	57.21
540	89.66	89.81	89.53	88.19	86.24	83.88	82.76	75.76	70.36	55.87
530	89.69	89.81	89.47	88.12	86.08	83.56	82.35	75.13	69.42	54.45
520	89.65	89.76	89.32	87.95	85.89	83.27	81.88	74.34	68.32	52.94
510	89.64	89.75	89.24	87.84	85.60	82.86	81.43	73.52	67.15	51.19
500	89.49	89.65	89.18	87.72	85.42	82.50	80.91	72.65	65.81	49.38
490	89.45	89.63	89.03	87.59	85.13	82.00	80.26	71.62	64.36	47.40
480	89.41	89.51	88.93	87.31	84.84	81.45	79.64	70.49	62.84	45.34
470	89.37	89.41	88.84	87.15	84.59	80.94	78.96	69.42	61.22	43.18
460	89.29	89.35	88.58	86.95	84.20	80.33	78.18	68.10	59.35	40.86
450	89.32	89.30	88.57	86.77	83.82	79.60	77.29	66.72	57.55	38.57
440	89.18	89.18	88.42	86.53	83.49	79.05	76.50	65.37	55.64	36.17
430	89.14	89.16	88.31	86.30	83.12	78.42	75.63	63.96	53.83	33.96
420	89.12	89.18	88.23	86.10	82.70	77.68	74.71	62.59	51.89	31.82
410	89.01	89.03	88.12	85.93	82.37	77.10	73.85	61.22	50.16	29.85
400	89.00	88.90	87.93	85.69	81.92	76.43	72.99	59.92	48.46	28.06
390	88.98	88.93	87.69	85.52	81.62	75.79	72.29	58.80	47.02	26.46
380	88.79	88.69	87.41	85.00	80.98	75.05	71.47	57.62	45.70	25.18
370	88.60	88.46	87.36	84.86	80.89	74.69	70.82	56.74	44.58	24.06
360	88.21	88.18	87.12	84.54	80.30	74.11	70.34	55.96	43.69	23.14
350	87.55	87.47	86.36	83.93	79.69	73.21	69.37	55.10	42.68	22.32
340	85.84	85.73	84.63	82.07	77.79	71.51	67.61	53.34	41.28	21.37
330	81.40	81.26	80.25	77.64	73.62	67.71	63.89	50.31	38.62	19.76
320	69.02	68.78								
310	43.70	43.74								
300	12.68	12.82								
290	0.71	0.74								
280	0	0								

G.2 BK7 glass: 0.3 to 30 Mrad

Wavelength	150	300	500	1	1.5	3	5	10	15	30
nm	krad	krad	krad	Mrad	Mrad	Mrad	Mrad	Mrad	Mrad	Mrad
840	87.98	82.35	82.75	80.27	75.72	75.01	70.27	70.27	71.01	69.60
830	87.78	81.90	82.13	79.33	74.40	73.72	68.66	68.66	69.25	68.04
820	87.16	81.18	81.18	78.38	72.84	71.84	66.58	66.58	67.22	65.84
810	86.79	80.18	80.00	76.98	71.00	69.81	64.19	64.19	64.74	63.38
800	85.98	79.14	78.72	75.42	68.95	67.31	61.44	61.44	62.01	60.64
790	85.29	78.02	77.17	73.52	66.59	64.55	58.42	58.42	58.91	57.65
780	84.38	76.62	75.45	71.58	63.93	61.62	55.13	55.13	55.51	54.21
770	83.49	75.03	73.47	69.38	61.03	58.32	51.54	51.54	51.89	50.54
760	82.36	73.29	71.21	66.96	57.75	54.70	47.66	47.66	47.86	46.61
750	80.93	71.28	68.77	64.06	54.28	50.77	43.42	43.42	43.59	42.41
740	79.57	69.04	66.02	61.02	50.50	46.68	39.14	39.14	39.26	38.10
730	77.80	66.50	62.90	57.49	46.31	42.12	34.53	34.53	34.58	33.42
720	76.16	64.00	59.96	54.31	42.56	38.12	30.45	30.45	30.44	29.41
710	74.35	61.27	56.68	50.69	38.50	33.86	26.29	26.29	26.26	25.27
700	72.36	58.42	53.27	47.08	34.52	29.79	22.43	22.43	22.35	21.44
690	70.28	55.54	50.01	43.55	30.77	26.02	18.93	18.93	18.84	18.02
680	68.16	52.64	46.68	40.13	27.31	22.55	15.89	15.89	15.78	15.01
670	66.20	49.90	43.51	36.87	24.10	19.50	13.24	13.24	13.10	12.43
660	64.18	47.25	40.69	33.90	21.35	16.88	11.02	11.02	10.91	10.30
650	62.23	44.79	38.04	31.30	18.93	14.67	9.26	9.26	9.14	8.58
640	60.55	42.68	35.65	28.96	16.89	12.82	7.82	7.82	7.70	7.20
630	58.92	40.67	33.56	26.92	15.16	11.29	6.68	6.68	6.56	6.12
620	57.50	38.93	31.76	25.12	13.71	10.00	5.76	5.76	5.65	5.23
610	56.15	37.33	30.05	23.56	12.46	8.95	5.00	5.00	4.91	4.53
600	54.83	35.85	28.49	22.08	11.35	8.01	4.37	4.37	4.27	3.93
590	53.62	34.42	27.06	20.74	10.35	7.17	3.81	3.81	3.72	3.41
580	52.39	33.04	25.62	19.46	9.39	6.41	3.32	3.32	3.23	2.95
570	51.01	31.57	24.17	18.11	8.47	5.69	2.86	2.86	2.77	2.51
560	49.62	30.03	22.72	16.81	7.59	5.00	2.43	2.43	2.35	2.13
550	48.14	28.45	21.25	15.49	6.73	4.35	2.04	2.04	1.97	1.77
540	46.52	26.78	19.70	14.14	5.90	3.72	1.68	1.68	1.62	1.44
530	44.76	25.03	18.12	12.79	5.08	3.14	1.35	1.35	1.31	1.16
520	42.91	23.20	16.50	11.45	4.33	2.59	1.07	1.07	1.03	0.91
510	40.89	21.34	14.87	10.11	3.60	2.10	0.83	0.83	0.80	0.70
500	38.73	19.42	13.26	8.81	2.95	1.67	0.62	0.62	0.60	0.52
490	36.54	17.49	11.66	7.56	2.36	1.29	0.46	0.46	0.45	0.38
480	34.22	15.58	10.08	6.35	1.83	0.96	0.33	0.33	0.31	0.27
470	31.82	13.69	8.59	5.27	1.39	0.70	0.23	0.23	0.22	0.05
460	29.36	11.90	7.20	4.27	1.03	0.50	0	0	0	0
450	26.95	10.21	5.94	3.40	0.74	0.35	0	0	0	0
440	24.54	8.67	4.84	2.67	0.53	0.24	0	0	0	0
430	22.36	7.36	3.91	2.08	0.38	0	0	0	0	0
420	20.32	6.21	3.16	1.63	0.27	0	0	0	0	0
410	18.52	5.29	2.56	1.27	0.16	0	0	0	0	0
400	16.94	4.53	2.09	1.03	0	0	0	0	0	0
390	15.61	3.93	1.75	0.84	0	0	0	0	0	0
380	14.53	3.5	1.51	0.72	0	0	0	0	0	0
370	13.56	3.09	1.27	0.59	0	0	0	0	0	0
360	12.84	2.78	1.09	0.47	0	0	0	0	0	0
350	12.23	2.54	0.98	0.43	0	0	0	0	0	0
340	11.66	2.39	0.90	0.40	0	0	0	0	0	0
330	10.68	2.17	0.81	0.37	0	0	0	0	0	0

G.3 BK7 G18 glass: 1 to 100 krad

Wavelength	0.5	1	1.5	3	5	10	15	30	50	100
nm	krad	krad	krad	krad	krad	krad	krad	krad	krad	krad
840	86.54	86.90	86.62	87.22	88.89	84.00	86.48	86.48	88.54	87.25
830	86.81	87.22	86.67	87.50	88.93	83.98	86.57	86.57	88.86	87.41
820	86.79	87.18	86.84	87.49	89.09	84.21	86.72	86.72	88.87	87.55
810	86.79	87.13	86.77	87.48	88.99	84.09	86.71	86.71	88.92	87.48
800	86.85	87.16	86.74	87.46	88.99	84.11	86.84	86.84	88.98	87.37
790	86.77	87.10	86.80	87.44	89.05	84.22	86.80	86.80	89.07	87.51
780	86.81	87.18	86.82	87.53	89.11	84.19	86.77	86.77	88.96	87.46
770	86.79	87.12	86.83	87.45	89.01	84.20	86.82	86.82	88.95	87.40
760	86.72	87.21	86.76	87.48	89.01	84.13	86.85	86.85	88.89	87.47
750	86.76	87.18	86.92	87.56	89.07	84.31	86.90	86.90	89.05	87.49
740	86.76	87.16	86.87	87.52	89.08	84.20	86.85	86.85	89.03	87.50
730	86.83	87.23	86.88	87.52	89.07	84.19	86.79	86.79	88.93	87.49
720	86.78	87.26	86.85	87.49	89.00	84.22	86.82	86.82	89.03	87.49
710	86.81	87.26	86.83	87.45	89.03	84.19	86.83	86.83	88.95	87.46
700	86.80	87.21	86.83	87.52	89.01	84.25	86.80	86.80	88.98	87.54
690	86.79	87.23	86.74	87.41	88.91	84.16	86.82	86.82	88.85	87.37
680	86.87	87.23	86.69	87.47	88.90	84.14	86.76	86.76	88.88	87.38
670	86.78	87.12	86.74	87.43	88.87	84.25	86.89	86.89	88.93	87.40
660	86.69	87.11	86.68	87.32	88.83	84.06	86.69	86.69	88.82	87.27
650	86.68	87.05	86.69	87.29	88.78	83.96	86.63	86.63	88.67	87.20
640	86.68	87.05	86.71	87.30	88.81	84.04	86.75	86.75	88.74	87.25
630	86.61	87.10	86.58	87.21	88.68	83.95	86.55	86.55	88.70	87.19
620	86.68	86.97	86.55	87.10	88.65	83.90	86.55	86.55	88.60	87.10
610	86.56	86.95	86.54	87.16	88.65	83.92	86.58	86.58	88.53	87.19
600	86.57	86.94	86.43	87.05	88.49	83.92	86.52	86.52	88.47	87.07
590	86.54	86.95	86.42	87.04	88.51	83.88	86.41	86.41	88.42	87.02
580	86.46	86.85	86.33	86.94	88.42	83.76	86.33	86.33	88.29	86.99
570	86.40	86.78	86.30	86.89	88.38	83.81	86.39	86.39	88.31	86.93
560	86.40	86.77	86.24	86.79	88.29	83.70	86.33	86.33	88.28	86.84
550	86.31	86.65	86.16	86.82	88.24	83.57	86.24	86.24	88.28	86.82
540	86.30	86.65	86.04	86.66	88.15	83.56	86.17	86.17	88.11	86.74
530	86.19	86.47	85.97	86.57	88.04	83.51	86.02	86.02	87.96	86.58
520	86.13	86.38	85.82	86.51	87.89	83.33	85.91	85.91	87.85	86.54
510	86.00	86.21	85.75	86.38	87.77	83.22	85.83	85.83	87.73	86.41
500	85.85	86.06	85.56	86.24	87.63	83.09	85.72	85.72	87.62	86.21
490	85.66	85.92	85.42	86.07	87.43	82.94	85.53	85.53	87.48	86.11
480	85.51	85.75	85.21	85.86	87.29	82.66	85.31	85.31	87.28	85.89
470	85.32	85.53	85.06	85.74	87.12	82.50	85.24	85.24	87.07	85.74
460	85.03	85.32	84.80	85.38	86.68	82.50	84.91	84.91	86.76	85.41
450	84.72	84.99	84.37	84.96	86.30	81.79	84.52	84.52	86.34	85.04
440	84.05	84.33	83.79	84.33	85.69	81.18	83.89	83.89	85.75	84.37
430	83.08	83.35	82.87	83.31	84.72	80.20	82.94	82.94	84.69	83.44
420	81.42	81.64	81.13	81.74	82.97	78.61	81.23	81.23	82.91	81.76
410	78.36	78.56	78.03	78.67	79.88	75.70	78.17	78.17	79.82	78.59
400	72.94	73.13	72.73	73.16	74.30	70.43	72.75	72.75	74.25	73.10
390	63.37	63.43	63.02	63.51	64.47	61.15	63.00	63.00	64.35	63.30
380	46.44	46.53	46.07	46.34	47.14	44.63	46.00	46.00	46.87	45.93
370	19.51	19.49	19.32	19.32	19.78	18.66	19.19	19.19	19.46	18.95
360	1.91	1.92	1.82	1.81	1.87	1.77	1.79	1.79	1.81	1.73
350	0	0	0	0	0	0	0	0	0	0

G.4 BK7 G18 glass: 0.3 to 30 Mrad

Wavelength	150	300	500	1	1.5	3	5	10	15	30
nm	krad	krad	krad	Mrad	Mrad	Mrad	Mrad	Mrad	Mrad	Mrad
840	90.23	89.56	89.15	87.28	89.56	90.01	90.01	89.38	89.17	89.96
830	90.58	89.83	89.14	87.60	89.73	90.15	90.33	89.48	89.21	90.10
820	90.50	89.87	89.36	87.46	89.64	90.14	90.31	89.62	89.31	90.19
810	90.50	89.73	89.34	87.63	89.53	90.12	90.25	89.50	89.19	90.05
800	90.58	89.88	89.34	87.46	89.67	90.08	90.36	89.50	89.23	90.12
790	90.46	89.78	89.30	87.54	89.47	90.00	90.23	89.52	89.22	90.08
780	90.47	89.72	89.33	87.55	89.42	90.14	90.21	89.44	89.08	90.05
770	90.33	89.73	89.29	87.45	89.56	90.14	90.28	89.47	89.10	90.07
760	90.43	89.88	89.31	87.49	89.61	90.12	90.36	89.54	89.16	90.12
750	90.36	89.64	89.19	87.39	89.45	90.13	90.16	89.36	89.04	89.94
740	90.26	89.63	89.29	87.40	89.42	90.06	90.17	89.37	89.04	89.91
730	90.24	89.65	89.22	87.46	89.51	90.04	90.14	89.33	88.94	89.97
720	90.30	89.74	89.17	87.40	89.54	90.11	90.26	89.47	89.07	89.96
710	90.21	89.69	89.17	87.41	89.45	90.03	90.09	89.38	88.93	89.95
700	90.20	89.59	89.13	87.42	89.41	90.03	90.09	89.31	88.99	89.85
690	90.17	89.59	89.16	87.34	89.42	89.97	90.08	89.28	88.90	89.77
680	90.19	89.56	89.05	87.35	89.42	90.02	90.08	89.31	88.89	89.76
670	90.06	89.53	89.04	87.32	89.34	89.84	90.06	89.14	88.84	89.72
660	90.11	89.43	89.04	87.25	89.42	89.92	90.01	89.14	88.80	89.65
650	90.05	89.37	88.90	87.19	89.29	89.86	89.97	89.14	88.75	89.61
640	89.90	89.25	89.01	87.21	89.39	89.71	90.01	89.17	88.68	89.40
630	89.88	89.22	88.92	87.16	89.20	89.79	89.89	89.07	88.61	89.37
620	89.86	89.12	88.82	87.16	89.26	89.73	89.77	89.00	88.54	89.36
610	89.82	89.18	88.83	87.10	89.14	89.62	89.79	89.02	88.45	89.34
600	89.67	89.03	88.85	87.12	89.12	89.59	89.68	88.88	88.42	89.15
590	89.62	88.89	88.74	87.03	89.09	89.52	89.70	88.81	88.26	89.08
580	89.54	88.81	88.76	87.08	89.06	89.51	89.61	88.74	88.35	88.95
570	89.34	88.58	88.70	86.98	88.93	89.38	89.45	88.63	88.02	88.80
560	89.26	88.57	88.57	86.83	88.90	89.32	89.34	88.53	87.93	88.64
550	89.16	88.39	88.48	86.79	88.76	89.37	89.26	88.43	87.85	88.55
540	89.03	88.29	88.44	86.69	88.69	89.17	89.11	88.28	87.77	88.48
530	88.91	88.19	88.35	86.63	88.62	89.11	89.12	88.20	87.61	88.23
520	88.73	87.96	88.29	86.54	88.57	88.96	88.96	88.10	87.45	88.07
510	88.64	87.85	88.08	86.44	88.30	88.85	88.81	87.94	87.32	88.02
500	88.47	87.78	87.94	86.25	88.26	88.65	88.73	87.77	87.22	87.79
490	88.38	87.55	87.79	86.10	88.17	88.53	88.56	87.68	87.06	87.70
480	88.31	87.38	87.68	85.92	88.01	88.39	88.45	87.46	86.85	87.51
470	88.06	87.35	87.48	85.76	87.85	88.26	88.26	87.30	86.68	87.37
460	87.55	86.81	87.22	85.44	87.51	87.96	87.83	86.86	86.23	86.91
450	87.15	86.40	86.77	85.04	87.11	87.62	87.51	86.55	85.87	86.44
440	86.49	85.59	86.00	84.41	86.42	86.94	86.85	85.72	85.02	85.53
430	85.20	84.27	85.10	83.39	85.38	85.85	85.72	84.70	83.80	84.09
420	83.05	81.87	83.25	81.57	83.76	84.14	83.75	82.55	81.33	81.60
410	79.02	77.55	80.15	78.42	80.45	80.73	80.26	79.10	79.96	77.04
400	71.93	69.99	74.43	72.72	74.90	75.11	74.02	72.63	69.31	68.85
390	59.30	56.73	64.29	62.58	64.78	64.65	62.99	61.13	55.84	54.79
380	38.73	35.60	46.53	44.96	47.03	46.59	44.06	41.78	34.50	33.07
370	12.18	10.13	18.96	17.91	19.29	18.85	16.51	14.79	9.60	8.60
360	0.65	0.43	1.72	1.55	1.76	1.67	1.28	1.02	0.39	0.27
350	0	0	0	0	0	0	0	0	0	0

G.5 F2 glass: 1 to 100 krad

Wavelength	0.5	1	1.5	3	5	10	15	30	50	100
nm	krad	krad	krad	krad	krad	krad	krad	krad	krad	krad
840	82.52	82.81	81.38	82.18	81.74	78.20	79.21	75.43	73.96	64.34
830	82.75	83.06	81.63	81.98	81.73	78.07	79.13	75.06	73.46	63.35
820	82.72	83	81.63	82.06	81.67	77.94	78.89	74.54	72.88	62.41
810	82.70	82.94	81.45	81.85	81.49	77.77	78.85	74.11	72.08	61.24
800	82.70	82.95	81.53	81.92	81.45	77.54	78.34	73.63	71.34	60.11
790	82.71	82.96	81.53	81.87	81.38	77.39	78.15	73.05	70.70	59.12
780	82.67	82.93	81.39	81.82	81.18	77.16	77.87	72.68	70.03	58.07
770	82.67	82.93	81.35	81.74	81.12	77.03	77.61	72.16	69.40	57.10
760	82.62	82.80	81.35	81.57	80.98	76.85	77.30	71.70	68.78	56.12
750	82.68	82.93	81.38	81.73	80.98	76.75	77.20	71.44	68.29	55.47
740	82.62	82.79	81.30	81.62	80.78	76.61	77.02	71.04	67.77	54.66
730	82.70	82.93	81.32	81.54	80.77	76.43	76.85	70.68	67.29	54.08
720	82.64	82.86	81.28	81.46	80.67	76.34	76.61	70.45	66.99	53.59
710	82.69	82.89	81.24	81.47	80.56	76.20	76.50	70.26	66.66	53.19
700	82.65	82.84	81.27	81.48	80.54	76.15	76.44	70.01	66.38	52.93
690	82.64	82.89	81.25	81.40	80.46	76.01	76.25	69.82	66.19	52.56
680	82.73	82.91	81.20	81.35	80.45	75.95	76.17	69.67	66.02	52.34
670	82.68	82.86	81.15	81.32	80.35	75.87	76.15	69.45	65.89	52.09
660	82.65	82.77	81.12	81.23	80.26	75.70	75.86	69.21	65.53	51.68
650	82.67	82.79	81.04	81.13	80.18	75.59	75.66	68.93	65.11	51.22
640	82.65	82.78	81.06	81.14	80.01	75.37	75.48	68.51	64.63	50.53
630	82.68	82.76	80.91	80.96	79.90	75.14	75.12	68.01	63.85	49.52
620	82.63	82.70	80.80	80.82	79.61	74.74	74.66	67.30	62.85	48.21
610	82.66	82.73	80.74	80.69	79.41	74.35	74.10	66.41	61.60	46.56
600	82.59	82.65	80.68	80.54	79.05	73.92	73.49	65.28	60.08	44.50
590	82.52	82.57	80.62	80.35	78.71	73.33	72.72	63.93	58.25	42.10
580	82.60	82.55	80.43	79.96	78.19	72.55	71.76	62.38	56.10	39.47
570	82.50	82.45	80.26	79.79	77.72	71.75	70.67	60.64	53.81	36.63
560	82.44	82.35	80.05	79.44	77.14	70.84	69.53	58.70	51.34	33.67
550	82.34	82.17	79.83	79.10	76.47	69.85	68.27	56.67	48.70	30.73
540	82.29	82.14	79.72	78.66	75.71	68.72	66.93	54.57	46.06	27.81
530	82.24	81.96	79.38	78.23	74.99	67.60	65.50	52.40	43.41	25.05
520	82.17	81.70	79.14	77.25	74.20	66.32	64.03	50.16	40.73	22.41
510	82.03	81.51	78.79	77.23	73.33	65.15	62.45	47.97	38.07	19.95
500	81.96	81.35	78.57	76.72	72.43	63.79	60.83	45.71	35.46	17.62
490	81.77	81.18	78.17	76.12	71.48	62.39	59.12	43.30	32.79	15.41
480	81.69	80.98	77.83	75.53	70.45	60.93	57.39	40.91	30.18	13.33
470	81.51	80.68	77.44	74.91	69.45	59.42	55.58	38.53	27.56	11.43
460	81.32	80.50	76.95	74.16	68.25	57.76	53.71	36.08	25.04	9.67
450	81.22	80.28	76.56	73.49	67.11	56.19	51.81	33.72	22.69	8.15
440	80.99	79.93	76.08	72.75	65.90	54.57	49.91	31.52	20.53	6.87
430	80.90	79.73	75.71	72.13	64.83	53.08	48.26	29.53	18.67	5.85
420	80.66	79.36	75.26	71.44	63.78	51.72	46.63	27.78	17.08	5.01
410	80.43	79.13	74.90	70.80	62.81	50.35	45.18	26.20	15.73	4.38
400	80.27	78.88	74.43	70.09	61.88	49.13	43.87	24.88	14.60	3.85
390	80.10	78.55	73.89	69.48	60.99	48.11	42.81	23.76	13.64	3.44
380	79.57	78.02	73.07	68.59	60.06	46.94	41.60	22.63	12.81	3.12
370	78.81	77.28	72.37	67.72	59.06	45.89	40.36	21.64	12.01	2.80
360	77.54	76.02	71.08	66.41	57.78	44.56	39.15	20.61	11.19	2.50
350	74.96	73.34	68.30	63.79	55.35	42.48	37.15	19.28	10.39	2.23
340	67.51	66.12	61.35	57.09	49.58	37.81	33.14	16.93	9.02	1.92
330	47.02	45.98	42.70	39.59	34.33	26.12	22.72	11.49	6.09	1.25
320	11.41	11.19								
310	0.11	0.12								
300	0	0								

G.6 F2 glass: 0.3 to 30 Mrad

Wavelength	150	300	500	1	1.5	3	5	10	15	30
nm	krad	krad	krad	Mrad	Mrad	Mrad	Mrad	Mrad	Mrad	Mrad
840	59.35	48.19	54.17	49.84	43.21	41.20	37.52	36.25	35.67	33.80
830	58.20	46.76	53.05	48.28	41.24	39.30	35.63	34.28	33.66	31.90
820	56.20	44.90	51.29	46.50	39.28	37.20	33.59	32.24	31.66	29.82
810	55.28	43.19	49.44	44.58	37.32	35.19	31.62	30.18	29.61	27.86
800	53.85	41.47	47.77	42.86	35.48	33.35	29.72	28.31	27.84	26.01
790	52.49	39.87	46.09	41.14	33.66	31.52	28	26.55	26.07	24.30
780	51.25	38.36	44.56	39.52	32.06	29.90	26.43	24.95	24.46	22.72
770	50.04	37.08	43.13	38.11	30.65	28.46	24.96	23.51	23.10	21.31
760	48.91	35.83	41.88	36.77	29.28	27.16	23.77	22.30	21.84	20.14
750	47.90	34.72	40.69	35.66	28.14	25.99	22.66	21.19	20.73	19.06
740	47.08	33.81	39.71	34.67	27.23	25.10	21.75	20.29	19.88	18.24
730	46.33	33.03	38.87	33.85	26.40	24.30	21	19.56	19.13	17.50
720	45.79	32.46	38.30	33.30	25.89	23.77	20.53	19.07	18.66	17
710	45.37	32.02	37.81	32.84	25.46	23.37	20.14	18.69	18.29	16.63
700	45.04	31.73	37.58	32.54	25.24	23.09	19.90	18.44	18.05	16.42
690	44.73	31.51	37.26	32.38	25.09	22.99	19.78	18.35	17.93	16.28
680	44.51	31.35	37.15	32.28	25.02	22.92	19.71	18.25	17.84	16.20
670	44.27	31.12	36.98	32.14	24.91	22.82	19.61	18.16	17.72	16.08
660	43.90	30.83	36.74	31.93	24.77	22.71	19.46	17.99	17.57	15.91
650	43.37	30.33	36.32	31.55	24.44	22.35	19.11	17.65	17.23	15.56
640	42.66	29.57	35.66	30.88	23.81	21.69	18.48	17.03	16.61	15.01
630	41.49	28.39	34.53	29.83	22.76	20.70	17.50	16.09	15.68	14.11
620	39.97	26.89	33.04	28.36	21.30	19.29	16.17	14.75	14.39	12.87
610	38.09	24.98	31.10	26.43	19.49	17.46	14.49	13.12	12.77	11.35
600	35.78	22.72	28.72	24.10	17.32	15.34	12.52	11.23	10.94	9.63
590	33.14	20.21	26.01	21.49	14.90	13.04	10.47	9.27	9.03	7.86
580	30.29	17.59	23.09	18.72	12.46	10.72	8.44	7.36	7.15	6.13
570	27.26	14.99	20.10	15.91	10.10	8.56	6.56	5.62	5.46	4.59
560	24.27	12.52	17.21	13.28	8.03	6.65	4.96	4.17	4.04	3.34
550	21.35	10.31	14.53	10.92	6.26	5.05	3.67	3.02	2.93	2.35
540	18.64	8.38	12.12	8.86	4.77	3.78	2.67	2.15	2.08	1.64
530	16.16	6.75	10.03	7.12	3.62	2.81	1.92	1.51	1.46	1.12
520	13.87	5.37	8.25	5.66	2.73	2.07	1.37	1.06	1.01	0.77
510	11.81	4.23	6.69	4.50	2.04	1.51	0.98	0.74	0.70	0.52
500	9.96	3.30	5.38	3.52	1.51	1.10	0.69	0.51	0.49	0.36
490	8.33	2.51	4.27	2.70	1.09	0.79	0.48	0.35	0.34	0.24
480	6.25	1.89	3.33	2.03	0.78	0.54	0.32	0.23	0.23	0
470	5.54	1.39	2.55	1.51	0.54	0.37	0.22	0	0	0
460	4.43	1.01	1.91	1.09	0.37	0.25	0	0	0	0
450	3.53	0.72	1.42	0.79	0.26	0	0	0	0	0
440	2.81	0.53	1.07	0.57	0.01	0	0	0	0	0
430	2.27	0.39	0.81	0.33	0	0	0	0	0	0
420	1.86	0.30	0.64	0.26	0	0	0	0	0	0
410	1.56	0.24	0.51	0.23	0	0	0	0	0	0
400	1.34	0.16	0.43	0.01	0	0	0	0	0	0
390	1.17	0	0.37	0	0	0	0	0	0	0
380	1.05	0	0.34	0	0	0	0	0	0	0
370	0.90	0	0.21	0	0	0	0	0	0	0
360	0.75	0	0	0	0	0	0	0	0	0
350	0.64	0	0	0	0	0	0	0	0	0
340	0.57	0	0	0	0	0	0	0	0	0
330	0.34	0	0	0	0	0	0	0	0	0
320										

G.7 F2 G12 glass: 1 to 100 krad

Wavelength	0.5	1	1.5	3	5	10	15	30	50	100
nm	krad	krad	krad	krad	krad	krad	krad	krad	krad	krad
840	81.46	81.60	82.35	83.17	81.64	82.31	82.21	82.64	81.64	82.32
830	81.81	81.83	82.48	83.28	81.70	82.38	82.35	82.95	81.76	82.65
820	81.72	81.81	82.59	83.41	81.81	82.54	82.51	83.06	81.89	82.55
810	81.76	81.77	82.55	83.22	81.82	82.44	82.41	82.87	81.73	82.65
800	81.78	81.81	82.62	83.25	81.85	82.48	82.46	82.96	81.77	82.68
790	81.67	81.77	82.55	83.31	81.74	82.48	82.47	82.93	81.69	82.59
780	81.72	81.73	82.62	83.34	81.76	82.52	82.40	83.01	81.75	82.60
770	81.69	81.80	82.51	83.27	81.76	82.48	82.46	82.94	81.77	82.62
760	81.67	81.76	82.59	83.17	81.71	82.43	82.40	82.84	81.82	82.61
750	81.68	81.73	82.63	83.36	81.79	82.53	82.52	83.04	81.90	82.67
740	81.65	81.72	82.57	83.32	81.79	82.40	82.48	82.89	81.81	82.67
730	81.71	81.77	82.57	83.29	81.73	82.41	82.43	82.96	81.76	82.64
720	81.68	81.76	82.50	83.29	81.74	82.46	82.42	82.94	81.79	82.60
710	81.68	81.75	82.49	83.25	81.71	82.45	82.41	82.91	81.78	82.58
700	81.72	81.79	82.53	83.28	81.72	82.46	82.51	82.93	81.74	82.54
690	81.62	81.80	82.52	83.11	81.65	82.35	82.37	82.83	81.68	82.45
680	81.67	81.69	82.38	83.11	81.66	82.37	82.39	82.76	81.65	82.42
670	81.60	81.60	82.47	83.18	81.66	82.42	82.35	82.80	81.71	82.43
660	81.49	81.57	82.31	83.06	81.52	82.21	82.17	82.67	81.56	82.33
650	81.50	81.56	82.28	82.99	81.49	82.09	82.18	82.66	81.52	82.32
640	81.43	81.52	82.29	82.93	81.53	82.16	82.15	82.68	81.43	82.23
630	81.43	81.46	82.20	82.89	81.40	82.12	82.07	82.62	81.41	82.06
620	81.35	81.48	82.10	82.82	81.25	81.99	82	82.50	81.39	81.98
610	81.35	81.45	82.04	82.77	81.21	81.96	81.99	82.52	81.48	82.01
600	81.30	81.42	82.04	82.77	81.26	81.93	81.92	82.43	81.36	81.98
590	81.27	81.36	82.01	82.66	81.19	81.85	81.88	82.35	81.32	81.98
580	81.20	81.33	81.83	82.51	81.13	81.81	81.76	82.23	81.20	81.85
570	81.10	81.20	81.85	82.56	81.02	81.74	81.72	82.24	81.15	81.76
560	81.01	81.15	81.74	82.48	80.96	81.64	81.63	82.10	81.01	81.73
550	80.89	81.03	81.63	82.35	80.79	81.54	81.48	82.01	80.93	81.57
540	80.80	80.88	81.54	82.20	80.71	81.34	81.43	81.88	80.83	81.46
530	80.64	80.75	81.37	82.07	80.54	81.24	81.27	81.70	80.66	81.25
520	80.57	80.58	81.13	81.87	80.35	81.01	81.05	81.52	80.45	81.01
510	80.21	80.42	80.94	81.60	80.11	80.78	80.85	81.28	80.18	80.88
500	80.06	80.19	80.75	81.29	79.90	80.52	80.58	81.05	79.92	80.57
490	79.65	79.82	80.30	80.95	79.51	80.08	80.24	80.63	79.55	80.12
480	79.19	79.24	79.84	80.49	79.02	79.58	79.66	80.16	78.99	79.58
470	78.45	78.61	79.19	79.79	78.35	78.96	78.97	79.46	78.28	78.78
460	77.36	77.51	77.95	78.69	77.19	77.78	77.95	78.19	76.98	77.59
450	75.71	75.75	76.29	76.87	75.47	76.01	76.10	76.42	75.23	75.60
440	72.85	72.94	73.47	73.97	72.63	73.08	73.11	73.39	72.11	72.43
430	68.19	68.30	68.74	69.27	67.96	68.37	68.43	68.54	67.25	67.27
420	60.75	60.77	61.14	61.55	60.39	60.74	60.79	60.76	59.44	59.14
410	49.30	49.30	49.60	49.98	48.90	49.11	49.09	48.93	47.65	47
400	33.73	33.73	33.96	34.04	33.36	33.45	33.38	33.12	32.04	31.23
390	16.80	16.82	16.86	16.90	16.52	16.52	16.44	16.17	15.53	14.86
380	4.69	4.68	4.63	4.66	4.56	4.53	4.49	4.38	4.14	3.91
370	0.45	0.45	0.45	0.45	0.44	0.43	0.43	0.42	0.41	0.39
360	0	0	0	0	0	0	0	0	0	0

G.8 F2 G12 glass: 0.3 to 30 Mrad

Wavelength	150	300	500	1	1.5	3	5	10	15	30
nm	krad	krad	krad	Mrad	Mrad	Mrad	Mrad	Mrad	Mrad	Mrad
840	83	82.43	83.51	84.56	85.02	84.01	84.17	83.78	84.73	84.46
830	83.19	82.79	83.72	84.62	85.16	84.28	84.19	83.97	84.67	84.58
820	83.11	82.67	83.76	84.52	85.24	84.21	84.26	84.05	84.83	84.56
810	83.26	82.68	83.78	84.60	85.14	84.18	84.24	84.05	84.79	84.61
800	83.07	82.71	83.83	84.48	85.24	84.20	84.27	84.04	84.80	84.55
790	83.11	82.66	83.59	84.51	85.16	84	84.20	83.96	84.73	84.50
780	83.09	82.64	83.75	84.52	85.11	84.06	84.20	83.88	84.60	84.43
770	83.12	82.65	83.71	84.60	85.08	84.11	84.20	83.92	84.63	84.49
760	83.09	82.72	83.67	84.45	85.03	84.11	84.13	83.83	84.56	84.53
750	83.09	82.56	83.64	84.42	85.05	83.97	84.11	83.83	84.49	84.42
740	83.01	82.56	83.64	84.33	84.91	83.98	84.03	83.76	84.43	84.38
730	83.06	82.54	83.58	84.37	84.91	83.98	84.01	83.73	84.48	84.31
720	82.98	82.50	83.72	84.45	84.98	84.04	84.04	83.81	84.53	84.43
710	82.92	82.50	83.54	84.32	84.93	83.95	84.05	83.80	84.38	84.28
700	82.93	82.57	83.56	84.45	84.97	84.02	84.06	83.69	84.40	84.25
690	82.95	82.51	83.65	84.38	84.83	83.86	83.87	83.73	84.36	84.24
680	82.80	82.40	83.56	84.28	84.83	83.83	83.85	83.67	84.31	84.22
670	82.80	82.38	83.59	84.14	84.75	83.73	83.74	83.52	84.28	84.14
660	82.75	82.27	83.44	84.18	84.73	83.63	83.76	83.51	84.19	84.04
650	82.73	82.22	83.49	84.12	84.64	83.63	83.73	83.45	84.07	84.03
640	82.71	82.35	83.28	84.17	84.59	83.49	83.59	83.40	84.05	83.93
630	82.61	82.16	83.34	83.97	84.50	83.46	83.50	83.26	83.98	93.82
620	82.57	82.12	83.25	83.91	84.41	83.47	83.44	83.20	83.87	83.72
610	82.54	82.04	83.17	83.98	84.45	83.36	83.32	83.18	83.78	83.73
600	82.53	82.09	83.24	83.96	84.34	83.29	83.32	83.14	83.81	83.69
590	82.44	82.02	83.14	83.79	84.25	83.26	83.15	83	83.67	83.56
580	82.45	81.98	83.04	83.88	84.22	83.06	83.11	82.83	83.54	83.58
570	82.31	81.85	82.93	83.59	83.91	82.87	82.84	82.67	83.23	83.32
560	82.18	81.70	82.76	83.49	83.80	82.85	82.83	82.52	83.14	83.11
550	82.09	81.65	82.71	83.37	83.73	82.66	82.70	82.38	83.04	82.97
540	81.95	81.46	82.53	83.17	83.53	82.44	82.47	82.26	82.81	82.75
530	81.81	81.23	82.48	83.06	83.28	82.23	82.24	81.98	82.53	82.50
520	81.59	81.07	82.17	82.79	83.12	81.96	81.87	81.60	82.29	82.18
510	81.35	80.77	81.95	82.46	82.76	81.56	81.49	81.24	81.86	81.74
500	81.03	80.35	81.54	82.07	82.24	81.07	80.99	80.73	81.28	81.18
490	80.58	79.92	81.11	81.70	81.67	80.48	80.19	79.87	80.41	80.38
480	79.98	79.33	80.46	80.92	80.83	79.46	79.10	78.76	79.19	79.14
470	79.10	78.28	79.55	79.87	79.49	78.06	77.47	77.01	77.56	77.39
460	77.69	76.67	77.86	78.16	77.33	75.66	74.88	74.27	74.73	74.54
450	75.67	74.26	75.65	75.54	74.15	72.22	71.03	70.29	70.59	70.46
440	72.14	70.45	71.87	71.51	69.27	67.02	65.14	64.17	64.39	64.12
430	66.84	64.56	65.95	65.17	61.77	59.06	56.63	55.33	55.43	55.15
420	58.28	55.44	56.77	55.57	51.01	47.91	44.90	43.36	43.29	42.94
410	45.95	42.67	43.84	42.15	36.87	33.65	30.46	28.91	28.67	28.34
400	30.07	26.91	27.86	26.19	21.20	18.52	15.88	14.67	14.48	14.20
390	13.99	11.89	12.44	11.25	8.16	6.72	5.33	4.77	4.66	4.53
380	3.57	2.89	3.07	2.69	1.76	1.42	1.09	0.98	0.95	0.93
370	0.37	0.32	0.35	0.32	0.26	0.25	0.23	0.23	0.23	0.23
360	0	0	0	0	0	0	0	0	0	0

G.9 Sapphire - Merck: 1 to 100 krad

Wavelength	0.5	1	1.5	3	5	10	15	30	50	100
nm	krad	krad	krad	krad	krad	krad	krad	krad	krad	krad
840	84.47	84.17			83.93	82.94	83.56	84.83	84.25	84.09
830	84.72	84.44			83.94	83.09	83.56	84.87	84.31	84.13
820	84.65	84.43			84.08	83.18	83.74	84.86	84.38	84.16
810	84.64	84.39			83.98	83.08	83.63	84.89	84.36	84.06
800	84.59	84.37			84.01	83.03	83.55	84.78	84.33	84.12
790	84.54	84.27			83.97	83.12	83.53	84.69	84.33	84.05
780	84.55	84.28			83.87	82.92	83.57	84.61	84.28	84.05
770	84.62	84.22			83.87	82.98	83.44	84.50	84.19	83.99
760	84.64	84.14			83.84	82.93	83.39	84.59	84.11	83.89
750	84.65	84.25			83.93	82.97	83.48	84.59	84.20	84.01
740	84.56	84.23			83.89	82.94	83.34	84.59	84.30	83.98
730	84.72	84.36			83.89	82.98	83.31	84.51	84.05	83.91
720	84.66	84.29			83.83	82.93	83.25	84.51	83.94	83.82
710	84.63	84.30			83.76	82.87	83.15	84.39	83.84	83.76
700	84.61	84.23			83.70	82.87	83.03	84.23	83.75	83.70
690	84.66	84.19			83.59	82.68	82.89	84.08	83.62	83.47
680	84.58	84.12			83.51	82.68	82.82	83.93	83.52	83.42
670	84.55	84.02			83.47	82.60	82.71	83.81	83.50	83.38
660	84.49	83.99			83.35	82.48	82.59	83.62	83.29	83.22
650	84.47	83.92			83.26	82.42	82.49	83.52	83.24	83.20
640	84.41	83.87			83.26	82.32	82.46	83.40	83.20	83.17
630	84.48	83.85			83.10	82.28	82.40	83.31	83.11	83.02
620	84.33	83.77			83.07	82.17	82.35	83.15	82.96	82.91
610	84.25	83.60			82.97	82.17	82.15	83.11	82.86	82.89
600	84.06	83.45			82.69	81.86	81.99	82.81	82.68	82.62
590	83.92	83.29			82.48	81.67	81.77	82.62	82.45	82.44
580	83.68	83.08			82.20	81.32	81.42	82.19	82.14	82.06
570	83.46	82.80			81.95	81.13	81.18	82.04	81.90	81.89
560	83.33	82.64			81.61	80.83	80.88	81.67	81.50	81.60
550	83.17	82.43			81.33	80.57	80.62	81.39	81.26	81.34
540	83	82.32			81.10	80.26	80.27	81	80.87	81.12
530	82.88	82.21			80.78	79.96	79.93	80.65	80.47	80.79
520	82.82	82.06			80.40	79.52	79.55	80.18	79.96	80.45
510	82.70	81.88			80.08	79.20	79.02	79.69	79.43	80.08
500	82.52	81.73			79.64	78.73	78.45	79.06	78.78	79.58
490	82.48	81.53			79.20	78.18	77.89	78.40	78.10	79.05
480	82.40	81.40			78.71	77.75	77.34	77.73	77.48	78.55
470	82.41	81.38			78.53	77.49	76.90	77.25	76.93	78.13
460	82.45	81.36			78.28	77.11	76.42	76.68	76.31	77.67
450	82.61	81.51			78.11	77.02	76.01	76.36	75.89	77.37
440	82.62	81.45			78.05	76.84	75.76	76.14	75.51	77.10
430	82.59	81.53			77.96	76.72	75.65	75.95	75.35	76.92
420	82.62	81.46			77.81	76.67	75.48	75.84	75.24	76.84
410	82.63	81.45			77.83	76.56	75.37	75.63	75.08	76.77
400	82.54	81.42			77.73	76.46	75.24	75.55	74.99	76.64
390	82.69	81.49			77.88	76.59	75.30	75.72	75.20	76.64
380	82.73	81.45			77.77	76.40	75.23	75.56	75.22	76.47
370	82.77	81.58			77.96	76.62	75.34	75.81	75.52	76.70
360	82.57	81.49			78.10	76.60	75.42	75.93	75.51	76.76
350	82.67	81.61			78.13	76.51	75.29	75.81	75.60	76.54
340	82.57	81.57			77.84	76.40	75.16	75.84	75.75	76.54
330	82.51	81.56			78.23	76.59	75.38	76.01	75.99	76.57
320	82.17	81.19								
310	81.66	80.46								
300	80.94	80.16								
290	81.07	80.11								
280	80.24	79.07								
270	78.89	77.27								
260	76.63	74.26								
250	75.23	72.56								
240	74.68	72.02								
230	63.56	60.70								
220	8.25	7.69								
210	0.57	0.56								
200	0.75	0.69								
190	1.84	1.67								

G.10 Sapphire - Merck: 0.3 to 30 Mrad

Wavelength	150	300	500	1	1.5	3	5	10	15	30
nm	krad	krad	krad	Mrad	Mrad	Mrad	Mrad	Mrad	Mrad	Mrad
840	83.01	83.27	85.80	85.29	85.24	85.72	85.78	85.55	85.60	85.48
830	83.34	83.53	86.09	85.43	85.34	85.78	86	85.58	85.77	85.65
820	83.20	83.58	86.08	85.35	85.41	85.82	85.93	85.58	85.78	85.63
810	83.14	83.47	85.94	85.30	85.31	85.64	85.85	85.60	85.68	85.58
800	83.02	83.34	85.92	85.31	85.37	85.71	85.75	85.63	85.58	85.39
790	82.94	83.29	85.77	85.06	85.28	85.60	85.66	85.46	85.35	85.35
780	82.97	83.29	85.76	85.07	85.22	85.54	85.55	85.39	85.25	85.17
770	83	83.24	85.79	84.97	85.28	85.71	85.46	85.40	85.38	85.10
760	82.99	83.23	85.73	84.92	85.21	85.53	85.54	85.30	85.27	85.03
750	82.82	83.14	85.55	84.86	85.03	85.41	85.37	85.22	85.21	84.90
740	82.75	83.12	85.50	84.94	85.06	85.34	85.34	85.13	85.17	84.99
730	82.70	82.97	85.38	84.86	85.02	85.28	85.30	85.03	85.09	84.81
720	82.64	82.96	85.48	84.84	84.97	85.32	85.24	85.14	85.10	84.83
710	82.57	82.88	85.30	84.72	84.83	85.26	85.17	84.92	85.02	84.67
700	82.55	82.82	85.24	84.61	84.85	85.20	85.01	84.80	84.89	84.59
690	82.39	82.76	85.04	84.43	84.71	85.02	84.94	84.69	84.74	84.33
680	82.21	82.65	84.95	84.27	84.64	85.02	84.82	84.67	84.63	84.19
670	82.15	82.57	84.66	84.08	84.45	84.91	84.58	84.58	84.41	84.03
660	82.02	82.47	84.67	84.02	84.38	84.75	84.52	84.52	84.31	83.86
650	81.93	82.44	84.52	83.92	84.34	84.70	84.52	84.41	84.25	83.71
640	81.88	82.35	84.44	83.81	84.27	84.59	84.36	84.29	84.08	83.67
630	81.74	82.27	84.36	83.64	84.17	84.58	84.24	84.22	84	83.47
620	81.64	82.25	84.23	83.48	84.06	84.40	84.14	84.17	83.86	83.31
610	81.60	82.10	84.06	83.40	83.97	84.27	84.01	84.01	83.76	83.18
600	81.43	81.93	83.83	83.20	83.77	84.22	83.76	83.81	83.53	82.90
590	81.22	81.77	83.59	82.98	83.57	83.91	83.58	83.53	83.32	82.54
580	81.06	81.67	83.43	82.74	83.26	83.70	83.34	83.25	83.06	82.21
570	80.70	81.30	82.97	82.32	82.86	83.23	82.81	82.78	82.56	81.67
560	80.38	80.99	82.58	81.96	82.55	82.86	82.54	82.51	82.16	81.21
550	80.13	80.74	82.31	81.63	82.35	82.56	82.29	82.20	81.86	80.70
540	79.82	80.49	81.88	81.31	82.04	82.21	81.89	81.81	81.46	80.22
530	79.46	80.18	81.50	80.93	81.69	81.87	81.52	81.41	81.16	79.64
520	79.08	79.85	80.93	80.36	81.38	81.49	81.12	81.02	80.58	79.01
510	78.56	79.33	80.29	79.84	80.96	81.11	80.60	80.47	80.09	78.28
500	77.97	78.80	79.63	79.16	80.47	80.61	80.03	79.91	79.53	77.48
490	77.37	78.34	78.92	78.37	79.92	80.02	79.47	79.17	78.91	76.68
480	76.79	77.80	78.16	77.84	79.41	79.47	78.97	78.55	78.32	75.87
470	76.32	77.33	77.53	77.22	79.11	79.10	78.40	78.18	77.86	75.27
460	75.82	76.87	77.05	76.67	78.77	78.74	77.94	77.67	77.42	74.58
450	75.54	76.63	76.51	76.43	78.61	78.49	77.65	77.34	77.09	74.14
440	75.21	76.31	76.15	76.06	78.50	78.38	77.34	77.01	76.84	73.69
430	75.04	75.98	75.93	75.87	78.47	78.27	77.17	76.76	76.54	73.36
420	74.95	75.93	75.74	75.64	78.24	78.16	76.98	76.64	76.36	73.18
410	74.90	75.91	75.51	75.59	78.11	78.01	76.75	76.40	76.18	73.08
400	74.85	75.81	75.56	75.54	78.04	77.84	76.84	76.48	76.14	73.04
390	74.88	75.78	75.47	75.52	77.86	77.74	76.54	76.34	76.11	72.99
380	74.91	75.91	75.62	75.57	77.65	77.58	76.79	76.56	76.18	73.25
370	75.10	75.87	75.82	75.71	77.27	77.42	76.78	76.51	76.18	73.39
360	75.20	75.87	75.87	75.10	77.19	77.27	76.73	76.56	76.46	73.74
350	75.20	76.07	75.85	76.22	76.62	76.78	76.59	76.28	76.30	73.75
340	75.42	76.09	76.15	76.37	76.53	76.97	76.62	76.58	76.42	74.23
330	75.35	76.20	76.32	76.73	76.43	76.53	76.74	76.55	76.58	74.45
320										

G.11 Sapphire - Union Carbide: 1 krad to 30 Mrad

Wavelength	0.5	1	15	30	500	1	15	30
nm	krad	krad	krad	krad	krad	Mrad	Mrad	Mrad
840	80.64	80.18	81.74	81.51	81.61	84.28	82.70	82.81
830	80.91	80.46	81.68	81.66	81.71	84.60	82.90	82.87
820	80.86	80.35	81.70	81.76	81.70	84.46	82.81	82.84
810	80.84	80.43	81.62	81.61	81.75	84.36	82.83	82.66
800	80.87	80.36	81.52	81.62	81.71	84.50	82.78	82.62
790	80.84	80.26	81.49	81.44	81.58	84.45	82.66	82.53
780	80.74	80.22	81.40	81.45	81.51	84.33	82.56	82.37
770	80.78	80.22	81.30	81.50	81.59	84.33	82.57	82.29
760	80.80	80.16	81.30	81.40	81.67	84.28	82.46	82.27
750	80.78	80.25	81.24	81.41	81.54	84.17	82.39	82.17
740	80.80	80.19	81.17	81.36	81.70	84.17	82.43	82.20
730	80.80	80.32	81.12	81.21	81.68	84.17	82.32	82.19
720	80.84	80.28	81.05	81.20	81.71	84.12	82.29	82.25
710	80.79	80.24	80.96	81.13	81.70	84.07	82.19	82.14
700	80.81	80.30	80.92	81.13	81.59	83.99	82.16	82.03
690	80.80	80.21	80.77	80.90	81.48	84.06	82.04	81.90
680	80.82	80.19	80.66	80.79	81.45	83.95	81.90	81.79
670	80.76	80.19	80.58	80.68	81.35	83.89	81.87	81.57
660	80.77	80.12	80.45	80.62	81.33	83.86	81.70	81.48
650	80.73	80.04	80.36	81.46	81.27	83.89	81.71	81.40
640	80.68	79.93	80.27	80.42	81.25	83.73	81.53	81.30
630	80.65	79.97	80.19	80.27	81.07	83.68	81.41	81.12
620	80.56	79.90	79.97	80.11	81.03	83.65	81.30	80.98
610	80.51	79.79	79.80	79.92	81.03	83.56	81.10	80.79
600	80.40	79.68	79.55	79.68	80.97	83.31	80.89	80.64
590	80.22	79.51	79.21	79.38	80.69	83.10	80.68	80.47
580	80.03	79.32	78.81	79.03	80.57	82.92	80.40	80.10
570	79.82	79.06	78.53	78.70	80.26	82.56	79.96	79.66
560	79.67	78.88	78.08	78.31	80.02	82.37	79.61	79.31
550	79.52	78.66	77.75	78	79.93	82.17	79.32	79.05
540	79.50	78.62	77.42	77.69	79.74	82.01	78.93	78.77
530	79.51	78.52	77.03	77.25	79.71	81.84	78.54	78.47
520	79.39	78.47	76.53	76.84	79.58	81.65	78.33	78.13
510	79.38	78.32	76.09	76.40	79.43	81.56	77.83	77.69
500	79.25	78.16	75.47	75.87	79.27	81.21	77.43	77.31
490	79.15	77.85	74.84	75.32	79.05	80.96	76.87	76.76
480	79.01	77.67	74.10	74.74	78.92	80.70	76.35	76.31
470	78.91	77.41	73.41	74.18	78.71	80.51	75.94	75.79
460	78.70	77.24	72.70	73.44	78.40	80.06	75.35	75.23
450	78.63	77.05	71.89	72.79	78.34	79.72	74.66	74.71
440	78.25	76.66	71.01	72.09	78.16	79.34	74.15	74.15
430	78.08	76.27	70.33	71.45	77.79	78.95	73.57	73.46
420	77.82	75.99	69.65	70.84	77.56	78.53	72.92	72.90
410	77.64	75.77	69.09	70.39	77.31	78.16	72.50	72.56
400	77.48	75.62	68.85	70.15	77.21	78.14	72.31	72.39
390	77.59	75.82	69.01	70.25	77.29	78.07	72.51	72.38
380	77.73	75.98	69.31	70.63	77.49	78.36	72.83	72.80
370	77.99	76.17	69.96	71.24	77.62	78.74	73.35	73.30
360	78.14	76.43	70.54	71.71	77.78	79.14	73.77	73.83
350	78.25	76.74	71.18	72.05	77.39	79.02	74.03	74.04
340	78.31	76.82	71.54	72.53	77.34	79.28	74.45	74.43
330	78.28	76.88	72.13	72.75	77.21	79.41	74.98	74.96
320	78.28	76.98						
310	77.91	78						
300	77.47	77.34						
290	77.40	77.20						
280	76.22	76.19						
270	73.91	73.96						
260	69.01	69.90						
250	58.39	61.77						
240	43.61	49.93						
230	32.46	39.95						
220	26.97	34.39						
210	23.72	30.80						
200	19.39	25.46						
190	10.05	13.05						

G.12 Sapphire - CMS Hemlite: 1 krad to 30 Mrad

Wavelength	0.5	1	15	30	500	1	15	30
nm	krad	krad	krad	krad	krad	Mrad	Mrad	Mrad
840	79.84	79.52	79.85	80.35	81.77	82.78	81.98	81.38
830	79.96	79.65	79.94	80.38	81.73	82.94	82.15	81.45
820	80.10	79.68	80.09	80.38	81.90	82.87	82.17	81.59
810	80.19	79.71	80.14	80.54	82.11	83.04	82.15	81.60
800	80.04	79.69	80.13	80.58	81.94	83.03	82.23	81.59
790	79.80	79.52	80.04	80.36	81.65	82.73	82.03	81.57
780	79.90	79.60	80.11	80.49	81.73	82.82	81.96	81.52
770	79.90	79.55	80.04	80.46	81.72	82.75	82.08	81.52
760	79.86	79.55	80.12	80.41	81.81	82.69	82.02	81.58
750	79.94	79.56	80.20	80.57	81.86	82.84	82.06	81.50
740	79.92	79.63	80.19	80.41	81.72	82.76	81.96	81.45
730	79.95	79.60	80.15	80.48	81.65	82.72	82.01	81.46
720	80.04	79.67	80.22	80.60	81.93	82.86	82.10	81.56
710	79.96	79.62	80.22	80.53	81.80	82.81	82	81.53
700	79.96	79.72	80.11	80.61	81.88	82.89	82.08	81.59
690	79.94	79.68	80.13	80.47	81.77	82.79	81.98	81.45
680	79.89	79.64	80.16	80.32	81.65	82.72	82.01	81.52
670	79.79	79.49	80.18	80.26	81.53	82.70	81.97	81.47
660	79.74	79.49	80.04	80.20	81.62	82.59	81.98	81.56
650	79.75	79.52	80.04	80.15	81.48	82.54	81.95	81.51
640	79.71	79.44	80.05	80.16	81.41	82.48	81.88	81.47
630	79.68	79.45	79.96	80.10	81.39	82.43	81.88	81.45
620	79.61	79.41	79.94	79.97	81.30	82.32	81.85	81.43
610	79.55	79.36	79.94	79.91	81.25	82.24	81.85	81.44
600	79.58	79.38	79.86	79.91	81.30	82.35	81.91	81.47
590	79.57	79.35	79.86	79.91	81.23	82.24	81.79	81.36
580	79.58	79.36	79.82	79.81	81.29	82.32	81.86	81.40
570	79.52	79.30	79.83	79.80	81.12	82.07	81.70	81.23
560	79.52	79.27	79.80	79.77	81.09	82.06	81.68	81.24
550	79.49	79.28	79.77	79.77	81.10	82.16	81.74	81.33
540	79.53	79.30	79.75	79.72	80.99	82.04	81.63	81.27
530	79.49	79.24	79.75	79.68	80.97	82.06	81.70	81.25
520	79.47	79.25	79.75	79.55	80.88	81.95	81.71	81.26
510	79.42	79.18	79.63	79.55	80.87	81.90	81.61	81.18
500	79.44	79.06	79.56	79.45	80.77	81.79	81.52	81.16
490	79.41	78.97	79.49	79.35	80.67	81.69	81.52	81.14
480	79.35	79	79.46	79.24	80.63	81.69	81.48	91.07
470	79.27	79.96	79.47	79.22	80.67	81.69	81.48	81.07
460	79.25	78.88	79.39	79.16	80.57	81.58	81.30	80.96
450	79.17	78.92	79.38	79.10	80.49	81.48	81.34	81.04
440	78.92	78.65	79.16	78.91	80.36	81.41	81.25	80.79
430	78.78	78.53	78.94	78.66	80.10	81.16	80.97	80.62
420	78.52	78.17	78.62	78.41	79.75	80.77	80.76	80.33
410	78.20	77.98	78.34	78.07	79.40	80.40	80.54	80.11
400	78.10	77.87	78.23	77.88	79.29	80.40	80.36	80.02
390	78.19	77.96	78.24	77.90	79.32	80.42	80.30	80.02
380	78.30	78.02	78.40	78.04	79.46	80.54	80.40	80.04
370	78.28	77.97	78.21	78.05	79.52	80.45	80.30	79.99
360	78.22	77.79	78.02	77.74	78.89	79.94	80	79.46
350	78.17	77.61	76.81	76.73	78.19	79.06	78.93	78.53
340	77.72	77.04	74.90	75.23	76.90	77.62	77.89	77.28
330	77.45	76.35	73.19	73.33	75.05	75.78	76.37	75.89
320	76.86	75.84						
310	76.46	75.82						
300	75.67	74.96						
290	75.46	75						
280	74.98	74.50						
270	74.62	74.13						
260	73.55	72.83						
250	72.61	71.64						
240	72.05	70.98						
230	66.16	65.33						
220	37.88	37.60						
210	6.60	6.66						
200	3.41	3.39						
190	9.17	9.21						

G.13 Sapphire - CMS Hemex: 1 krad to 30 Mrad

Wavelength	0.5	1	15	30	500	1	15	30
nm	krad	krad	krad	krad	krad	Mrad	Mrad	Mrad
840	79.78	79.79	79.34	79.18	81.46	82.15	80.94	80.91
830	79.72	79.71	79.61	79.52	81.48	82.09	81.30	80.96
820	79.51	79.48	79.65	79.58	81.63	82	81.27	80.98
810	79.41	79.36	79.49	79.36	81.53	81.95	81.09	80.96
800	79.55	79.52	79.53	79.22	81.59	82.04	81.07	81.01
790	79.45	79.41	79.63	79.41	81.48	81.80	81.07	81.02
780	79.38	79.25	79.52	79.37	81.47	81.76	81	80.94
770	79.41	79.35	79.55	79.23	81.49	81.90	81.08	80.98
760	79.32	79.24	79.55	79.37	81.51	81.87	81.16	80.98
750	79.46	79.36	79.62	79.38	81.44	81.93	81.03	80.88
740	79.43	79.33	79.65	79.48	81.52	91.79	81.02	80.87
730	79.66	79.59	79.65	79.41	81.53	81.95	81.08	80.95
720	79.57	79.52	79.66	79.46	81.52	81.91	81.21	81.01
710	79.58	79.59	79.71	79.49	81.51	81.94	81.06	81.01
700	79.58	79.50	79.64	79.53	81.57	81.98	81.12	80.93
690	79.52	79.44	79.62	79.40	81.49	81.80	81.05	80.96
680	79.50	79.39	79.60	79.34	81.50	81.83	81.08	81.03
670	79.40	79.28	79.61	79.23	81.49	81.77	81.01	80.93
660	79.32	79.22	79.54	79.17	81.51	81.73	81.02	81.04
650	79.32	79.21	79.49	79.14	81.48	81.76	81.04	80.99
640	79.25	79.19	79.53	79.16	81.42	81.65	80.99	81.02
630	79.24	79.19	79.47	79.13	81.40	81.60	80.98	80.95
620	79.24	79.10	79.46	79.03	81.44	81.57	80.90	81.01
610	79.13	79.08	79.51	79.05	81.37	81.51	81	80.99
600	79.24	79.18	79.52	79.08	81.42	81.59	80.98	81.07
590	79.25	79.14	79.50	79.06	81.39	81.52	80.90	80.96
580	79.29	79.19	79.43	78.99	81.48	81.67	81	81.04
570	79.17	79.12	79.49	79.05	81.34	81.59	80.82	80.88
560	79.21	79.14	79.44	78.99	81.34	81.51	80.85	80.82
550	79.16	79.08	79.49	78.96	81.38	81.49	80.88	80.96
540	79.14	79.14	79.43	78.97	81.36	81.45	80.79	80.82
530	79.07	79.03	79.37	78.90	81.37	81.39	80.85	80.87
520	79.07	79.02	79.32	78.83	81.26	81.34	80.71	80.83
510	79.07	78.99	79.28	78.81	81.24	81.22	80.75	80.85
500	79	78.88	79.30	78.75	81.20	81.24	80.74	80.81
490	79	78.81	79.23	78.61	81.13	81.13	80.70	80.84
480	78.88	78.81	79.12	78.62	81.16	81.16	80.66	80.71
470	78.82	78.74	79.16	78.59	81.14	81.18	80.73	80.73
460	78.74	78.72	79.12	78.47	81.05	81.05	80.54	80.62
450	78.81	78.71	79.05	78.50	81.06	81.01	80.55	80.55
440	78.74	78.56	78.95	78.36	81.05	80.93	80.47	80.62
430	78.58	78.50	78.96	78.27	80.96	80.85	80.43	80.56
420	78.47	78.38	78.78	78.24	80.82	80.80	80.38	80.37
410	78.39	78.24	78.76	78.03	80.62	80.57	80.11	80.36
400	78.23	78.13	78.55	77.89	80.63	80.49	80.10	80.23
390	78.27	78.16	78.68	77.98	80.49	80.38	80.05	80.14
380	78.18	78.11	78.43	77.78	80.65	80.43	79.89	80.19
370	78.07	77.97	78.35	77.70	80.49	80.33	79.85	79.96
360	77.94	77.85	78.30	77.49	80.24	80.07	79.77	79.71
350	77.96	77.74	77.95	77.45	79.80	79.83	79.36	79.39
340	77.62	77.47	77.49	76.98	79.58	79.57	78.86	79.02
330	77.56	77.12	77.28	76.39	79.31	79.36	78.41	78.57
320	77.14	76.81						
310	77.04	76.84						
300	76.42	76.15						
290	76.50	76.20						
280	75.82	75.76						
270	75.60	75.56						
260	74.85	74.67						
250	74.21	73.79						
240	73.85	73.31						
230	70.32	69.89						
220	42.76	42.58						
210	6.58	6.37						
200	2.99	2.93						
190	9.41	9.57						

G.14 Magnesium Fluoride - Merck: 1 to 100 krad

Wavelength	0.5	1	1.5	3	5	10	15	30	50	100
nm	krad	krad	krad	krad	krad	krad	krad	krad	krad	krad
840	93.32	93.01			91.61	88.76	91.53	92.69	92.11	92.02
830	93.65	93.28			91.58	88.84	91.33	92.64	92.05	92.09
820	93.51	93.23			91.70	88.98	91.50	92.85	92.24	92.19
810	93.53	93.24			91.69	88.90	91.37	92.73	92.16	92.19
800	93.46	93.18			91.84	88.89	91.31	92.73	92.16	92.21
790	93.38	93.19			91.65	88.89	91.39	92.79	92.18	92.22
780	93.55	93.20			91.74	88.89	91.46	92.79	92.16	92.23
770	93.42	93.19			91.78	89	91.35	92.75	92.11	92.29
760	93.45	93.15			91.71	88.93	91.31	92.69	92.13	92.17
750	93.46	93.21			91.86	89.06	91.50	92.89	92.25	92.42
740	93.49	93.25			91.86	89.06	91.47	92.84	92.24	92.32
730	93.60	93.31			91.91	89.11	91.44	92.83	92.35	92.36
720	93.61	93.30			91.88	89.07	91.46	92.83	92.37	92.36
710	93.68	93.37			91.86	89.10	91.44	92.85	92.39	92.39
700	93.68	93.31			92.03	89.14	91.43	92.87	92.47	92.41
690	93.56	93.40			91.88	89.06	91.41	92.77	92.27	92.37
680	93.53	93.35			91.86	89.06	91.35	92.73	92.26	92.39
670	93.43	93.24			91.91	89.03	91.31	92.76	92.17	92.44
660	93.32	93.27			91.85	88.95	91.27	92.72	92.07	92.36
650	93.33	93.30			91.86	88.94	91.25	92.73	92.07	92.38
640	93.35	93.27			91.82	88.95	91.20	92.81	92.18	92.41
630	93.35	93.27			91.84	88.98	91.20	92.72	92.01	92.35
620	93.29	93.22			91.75	88.95	91.14	92.70	91.97	92.31
610	93.30	93.26			91.78	89.01	91.11	92.65	91.96	92.41
600	93.30	93.20			91.78	88.95	91.08	92.63	91.93	92.27
590	93.32	93.18			91.75	88.97	91.09	92.65	91.98	92.30
580	93.39	93.16			91.73	88.93	91.05	92.58	91.85	92.16
570	93.25	93.17			91.77	89.01	91.11	92.65	91.94	92.22
560	93.33	93.15			91.78	88.93	91.06	92.61	91.86	92.23
550	93.24	93.18			91.71	88.95	91	92.51	91.83	92.24
540	93.30	93.23			91.72	88.92	91	92.57	91.86	92.23
530	93.26	93.27			91.70	88.84	90.94	92.54	91.80	92.18
520	93.27	93.21			91.69	88.79	90.89	92.55	91.68	92.10
510	93.18	93.19			91.70	88.81	90.88	92.44	91.71	92.13
500	93.19	93.19			91.69	88.84	90.84	92.49	91.68	92.11
490	93.16	93.15			91.69	88.83	90.78	92.36	91.61	92.07
480	93.13	93.16			91.66	88.76	90.75	92.32	91.57	92.03
470	93.10	93.10			91.72	88.80	90.75	92.40	91.62	92.07
460	93.06	93			91.63	88.70	90.59	92.38	91.56	92.06
450	93.08	93.12			91.72	88.60	90.63	92.30	91.56	91.97
440	93.04	93.05			91.61	88.68	90.56	92.16	91.48	91.93
430	92.94	93.05			91.71	88.60	90.56	92.22	91.56	91.96
420	93.01	92.99			91.60	88.62	90.45	92.15	91.59	91.97
410	92.90	92.91			91.51	88.57	90.38	92.05	91.38	91.94
400	92.88	92.90			91.51	88.45	90.32	91.95	91.30	91.77
390	92.86	92.97			91.58	88.32	90.03	91.89	91.24	91.78
380	92.82	92.79			91.12	88.13	89.84	91.47	90.85	91.33
370	92.73	92.63			91.09	87.95	89.77	91.47	90.83	91.30
360	92.77	92.72			91.11	88.21	89.97	91.49	90.83	91.51
350	92.95	92.94			91.30	88.25	90.01	91.67	91.11	91.46
340	92.76	92.69			91.32	88.22	89.86	91.53	90.94	91.70
330	92.74	92.78			91.32	88.38	89.97	91.72	90.94	91.80
320	92.57	92.50								
310	92.31	91.91								
300	91.92	91.38								
290	91.75	91.28								
280	91.24	90.46								
270	90.85	89.66								
260	90.17	88.81								
250	89.76	88.35								
240	90.15	88.89								
230	90.34	89.32								
220	90.02	89.43								
210	90	89.32								
200	88.33	87.53								
190	87.22	86.62								

G.15 Magnesium Fluoride - Merck: 0.3 to 30 Mrad

Wavelength	150	300	500	1	1.5	3	5	10	15	30
nm	krad	krad	krad	Mrad	Mrad	Mrad	Mrad	Mrad	Mrad	Mrad
840	90.10	91.38	94.81	94.30	93.87	92.89	93.12	93.43	94.93	95.07
830	90.40	91.67	94.84	94.62	94.04	93.09	93.15	93.58	95.23	95.32
820	90.34	91.66	95.10	94.65	93.97	92.98	93.21	93.77	95.23	95.39
810	90.33	91.69	94.99	94.73	94.11	93.05	93.21	93.68	95.20	95.33
800	90.36	91.59	94.98	94.60	94.02	93.03	93.10	93.71	95.11	95.30
790	90.36	91.55	94.87	94.71	93.90	92.99	93.05	93.63	95.06	95.18
780	90.39	91.51	94.79	94.53	93.91	93.03	92.96	93.65	95	95.16
770	90.38	91.53	94.79	94.64	93.93	93.08	93.01	93.68	95.15	95.26
760	90.41	91.68	94.87	94.53	94.02	93.13	93	93.71	95.20	95.23
750	90.30	91.49	94.87	94.47	94.03	93.01	93.02	93.58	94.98	95.22
740	90.31	91.53	94.88	94.51	93.91	93.05	93.07	93.59	95	95.28
730	90.25	91.54	94.87	94.43	94.07	93.07	93.05	93.63	95.09	95.25
720	90.34	91.57	95.05	94.64	94.19	93.15	93.20	93.68	95.19	95.28
710	90.30	91.60	94.96	94.59	94.08	93.05	93.16	93.70	95.09	95.28
700	90.30	91.62	94.98	94.60	94.11	93.21	93.21	93.68	95.14	95.29
690	90.31	91.56	94.83	94.59	93.98	93.13	93.10	93.70	95.12	95.33
680	90.29	91.52	94.89	94.60	93.96	93.15	93.04	93.68	95.14	95.18
670	90.23	91.51	94.73	94.68	93.91	93.12	92.88	93.65	95.10	95.23
660	90.31	91.42	94.71	94.64	93.84	93.08	92.89	93.71	95.09	95.12
650	90.23	91.44	94.74	94.70	93.85	93.10	92.93	93.61	95.10	95.10
640	90.33	91.48	94.66	94.53	93.81	93.27	92.88	93.65	95.07	95.15
630	90.23	91.43	94.67	94.54	93.79	93.13	92.79	93.59	95.06	95.07
620	90.23	91.31	94.59	94.54	93.74	93.08	92.85	93.63	95.02	95.09
610	90.20	91.40	94.66	94.47	93.84	93.18	92.88	93.64	95.01	95.14
600	90.30	91.35	94.56	94.52	93.74	93.07	92.84	93.54	95.07	94.98
590	90.20	91.35	94.59	94.52	93.75	93.02	92.85	93.62	95	94.96
580	90.24	91.31	94.60	94.47	93.70	93.06	92.91	93.65	94.99	94.94
570	90.22	91.31	94.47	94.44	93.62	93.01	92.76	93.41	94.82	94.85
560	90.17	91.31	94.39	94.35	93.61	93.04	92.71	93.35	94.89	94.80
550	90.12	91.24	94.40	94.40	93.69	93.05	92.69	93.49	94.81	94.79
540	90.05	91.19	94.38	94.30	93.50	92.96	92.68	93.42	94.85	94.79
530	90.04	91.23	94.38	94.42	93.44	92.93	92.71	93.42	94.87	94.82
520	90.11	91.17	94.31	94.37	93.41	92.92	92.60	93.36	94.69	94.73
510	90	91.13	94.24	94.36	93.48	93.04	92.61	93.35	94.81	94.76
500	90.01	91.05	94.24	94.33	93.45	92.97	92.58	93.41	94.82	94.81
490	89.94	90.94	94.32	94.24	93.41	93.07	92.55	93.38	94.71	94.76
480	90.01	91.04	94.27	94.33	93.37	93.01	92.55	93.33	94.79	94.72
470	90	91.01	94.20	94.42	93.42	93.05	92.65	93.52	94.81	94.67
460	89.90	90.94	94.04	94.15	93.30	92.98	92.47	93.19	94.68	94.52
450	89.89	90.91	94.15	94.28	93.32	92.88	92.49	93.29	94.58	94.49
440	89.83	90.80	94.09	94.22	93.33	93.01	92.40	93.07	94.46	94.23
430	89.73	90.84	94.03	94.21	93.19	92.91	92.25	92.90	94.19	93.74
420	89.75	90.67	93.88	94.21	93.13	92.68	91.97	92.68	93.77	93.15
410	89.75	90.75	93.85	93.96	93	92.50	91.80	92.11	93.16	92.28
400	89.54	90.65	93.88	93.99	92.97	92.47	91.44	91.75	92.80	91.58
390	89.37	90.50	93.59	93.74	92.60	92.16	90.94	90.85	91.61	89.97
380	89.08	90.10	93.16	93.56	92.07	91.25	89.20	87.86	87.88	84.41
370	88.88	89.79	92.93	93.17	91.43	90.29	87.44	84.86	84.28	79.19
360	88.77	89.97	93.22	93.35	91.85	90.99	88.71	86.62	86.31	82.54
350	89.11	90.22	93.25	93.48	92.40	91.66	90.50	90.06	90.64	88.75
340	89.10	90.56	93.76	93.76	92.81	92.36	91.71	91.92	92.86	92.38
330	88.79	90.07	93.62	93.88	92.95	92.33	91.66	92.27	93.07	92.66
320										

G.16 Magnesium Fluoride - Roynon Howes: 1 krad to 30 Mrad

Wavelength	0.5	1	15	30	500	1
nm	krad	krad	krad	krad	krad	Mrad
840	90.39	90.99	89.23	91.17	91.88	92.05
830	90.69	91.24	89.34	91.27	92.06	92.11
820	90.58	91.21	89.48	91.29	92.19	92.01
810	90.71	91.14	89.34	91.33	92.16	92.14
800	90.61	91.10	89.36	91.28	92.22	92.10
790	90.62	91.01	89.38	91.42	92.10	92.02
780	90.56	91.04	89.31	91.42	91.99	92.05
770	90.59	91.01	89.34	91.46	92.21	92.16
760	90.57	91.10	89.28	91.43	92.25	91.98
750	90.67	91.05	89.55	91.48	92.05	92.06
740	90.64	91.13	89.47	91.50	92.05	92.04
730	90.79	91.24	89.50	91.50	92.11	92.12
720	90.75	91.25	89.59	91.50	92.19	92.16
710	90.77	91.28	89.56	91.62	92.14	92.06
700	90.78	91.33	89.57	91.55	92.12	92.05
690	90.78	91.29	89.56	91.53	92.12	92.03
680	90.80	91.18	89.45	91.58	92.16	92.13
670	90.83	91.11	89.48	91.60	92.03	91.99
660	90.70	91.05	89.31	91.53	92.11	92.02
650	90.69	91.08	89.33	91.55	92.05	92.02
640	90.69	91.05	89.37	91.55	92.01	91.97
630	90.83	91.13	89.31	91.53	92.07	91.96
620	90.73	91	89.25	91.53	92	91.89
610	90.70	90.95	89.19	91.51	92	91.88
600	90.70	91	89.24	91.52	92.07	91.92
590	90.78	91.06	89.26	91.53	92.05	91.88
580	90.72	91.02	89.19	91.44	92.13	91.94
570	90.71	91.03	89.34	91.50	91.92	91.80
560	90.73	91.02	89.26	91.45	91.93	91.77
550	90.69	90.99	89.23	91.50	91.93	91.83
540	90.75	91	89.17	91.50	91.86	91.75
530	90.73	91	89.18	91.49	91.93	91.75
520	90.70	91.04	89.18	91.44	91.87	91.67
510	90.77	90.92	89.07	91.45	91.91	91.69
500	90.75	90.89	89.09	91.46	91.95	91.71
490	90.65	90.86	89.05	91.39	91.93	91.64
480	90.66	90.84	88.98	91.35	91.87	91.68
470	90.66	90.79	89.03	91.48	92.04	91.71
460	90.63	90.80	88.99	91.36	91.76	91.50
450	90.67	90.78	89	91.42	91.82	91.56
440	90.53	90.81	89.03	91.41	91.93	91.64
430	90.59	90.67	88.96	91.37	91.83	91.62
420	90.58	90.78	88.93	91.46	91.71	91.52
410	90.52	90.70	88.99	91.37	91.67	91.49
400	90.50	90.67	88.82	91.32	91.63	91.49
390	90.58	90.72	88.95	91.44	91.49	91.25
380	90.52	90.63	88.71	91.16	91.45	91.30
370	90.41	90.55	88.82	91.27	91.47	91.18
360	90.25	90.52	88.83	91.39	91.52	91.35
350	90.49	90.59	88.79	91.49	91.28	91.11
340	90.31	90.47	88.76	91.18	91.55	91.25
330	90.40	90.78	89	91.46	91.45	91.40
320	90.22	90.39				
310	90.16	90.15				
300	89.83	89.65				
290	89.97	90.01				
280	89.76	89.68				
270	89.62	89.60				
260	89.34	89.32				
250	88.95	89.20				
240	89.18	89.23				
230	88.93	89				
220	88.62	88.61				
210	88.39	88.40				
200	86.70	86.83				
190	85.92	86.05				

G.17 Magnesium Fluoride - Carl Zeiss: 1 krad to 30 Mrad

Wavelength	0.5	1	15	30	500	1	15	30
nm	krad	krad	krad	krad	krad	Mrad	Mrad	Mrad
840	87.87	88.82	87.59	88.92	91.28	92.12	93.09	92.35
830	88.36	89.07	87.65	89.05	91.33	92.32	93.16	92.46
820	88.20	89.10	87.80	89.18	91.35	92.33	93.25	92.47
810	88.23	89.03	87.73	88.97	91.31	92.41	93.15	92.57
800	88.26	89.04	87.72	88.90	91.20	92.22	93.23	92.47
790	88.23	89.04	87.66	88.93	91.19	92.15	93.07	92.41
780	88.28	89.07	87.63	88.89	91.06	92	92.99	92.43
770	88.25	89.09	87.67	88.83	91.13	92.13	93.05	92.54
760	88.29	89.03	87.73	88.80	91.22	92.18	93.08	92.46
750	88.33	89.05	87.79	88.95	91.14	92	93.01	92.48
740	88.31	89	87.77	88.97	91.22	92.14	93.08	92.54
730	88.47	89.23	87.83	89.06	91.15	92.24	93.15	92.46
720	88.43	89.22	87.86	89.06	91.24	92.25	93.18	92.55
710	88.48	89.20	87.91	89.15	91.33	92.27	93.08	92.47
700	88.43	89.15	87.87	89.19	91.25	92.29	93.18	92.48
690	88.50	89.26	87.80	88.97	91.24	92.08	93.04	92.50
680	88.59	89.30	87.65	88.85	91.11	92.08	93.05	92.46
670	88.46	89.24	87.57	88.82	90.94	91.87	92.90	92.44
660	88.43	89.25	87.59	88.80	90.93	91.93	92.89	92.49
650	88.49	89.26	87.52	88.70	90.98	91.91	92.89	92.47
640	88.45	89.24	87.52	88.65	90.88	91.75	92.80	92.46
630	88.42	89.28	87.41	88.63	90.81	91.85	92.85	92.41
620	88.47	89.29	87.41	88.59	90.80	91.74	92.83	92.39
610	88.45	89.23	87.37	88.59	90.75	91.85	92.76	92.41
600	88.50	89.33	87.52	88.67	90.89	91.77	92.82	92.35
590	88.48	89.36	87.54	88.59	90.89	91.69	92.78	92.36
580	88.53	89.31	87.48	88.48	90.84	91.82	92.77	92.40
570	88.56	89.36	87.48	88.55	90.78	91.61	92.71	92.25
560	88.60	89.30	87.43	88.53	90.64	91.60	92.65	92.27
550	88.45	89.34	87.45	88.52	90.72	91.61	92.68	92.35
540	88.53	89.32	87.41	88.51	90.61	91.57	92.62	92.22
530	88.59	89.36	87.37	88.48	90.66	91.58	92.69	92.24
520	88.56	89.38	87.33	88.46	90.58	91.56	92.51	92.20
510	88.59	89.32	87.27	88.43	90.59	91.55	92.63	92.20
500	88.59	89.36	87.34	88.37	90.55	91.46	92.61	92.22
490	88.54	89.35	87.18	88.26	90.50	91.46	92.59	92.22
480	88.55	89.39	87.16	88.23	90.34	91.35	92.58	92.19
470	88.62	89.36	87.26	88.30	90.56	91.47	92.58	92.20
460	88.53	89.28	87.12	88.26	90.39	91.31	92.44	92.04
450	88.60	89.37	87.16	88.22	90.42	91.34	92.55	91.99
440	88.56	89.27	87.12	88.15	90.36	91.33	92.36	91.90
430	88.56	89.30	87.19	88.07	90.44	91.25	92.23	91.60
420	88.59	89.32	87.09	88.15	90.36	91.19	91.97	91.10
410	88.58	89.25	87.11	88.09	90.20	91.05	91.54	90.55
400	88.51	89.22	87	87.88	90.05	90.96	91.24	90.01
390	88.54	89.34	86.87	87.80	89.93	90.88	90.72	89.03
380	88.49	89.20	86.38	87.23	89.68	90.61	88.66	85.55
370	88.42	89.06	86.30	87.18	89.45	90.48	86.66	81.90
360	88.25	89.03	86.58	87.30	89.65	90.73	88.04	84.10
350	88.42	89.18	86.79	87.66	89.78	90.75	90.27	88.20
340	88.42	89.04	86.93	87.68	90.11	91.13	91.51	90.38
330	88.51	89.14	87.06	87.81	90.22	91.22	91.71	90.56
320	88.39	89.02						
310	88.40	88.75						
300	87.68	88.18						
290	87.78	88.27						
280	87.48	87.33						
270	87.06	86.72						
260	86.42	85.86						
250	86.11	85.49						
240	86.52	86.05						
230	86.60	86.60						
220	86.66	86.83						
210	86.80	86.84						
200	85.59	85.57						
190	84.78	84.87						

9 References

1 Billington, D.S. and Crawford, J.H., *Radiation Damage in Solids*, Oxford University Press, 1961

2 Much, R., Lumb, D., Cropper, M.S., Hunt, R., Mason, K.O., Cordova, F.A., Sasseen, T., Ho, C., Priedhorsky, W., Jamar, C., and Antonello,E., *The Optical/UV Monitor on the X-ray Multi-Mirror Mission*, Proc. Ultraviolet Astrophysics Beyond the IUE, ESA SP-413, p 815, 1999

3 Mason, K.O., Breevald, A., Much, R., Carter, M., Cordova, F.A., Cropper, M.S., Fordham, J., Huckle, H., Ho, C., Kawakami, H., Kennea, J., Kennedy, T., Mittaz, J., Pandel, D., Priedhorsky, W.C., Sasseen, T., Shirey, R., Smith, P., and Vreux, J.-M., *The XMM-Newton Optical/UV Monitor Telescope*, A&A **365**, p L36-L44, 2001

4 Cropper, M., *Technical Requirements Specification for the XMMOM*, **XMM-OM/MSSL**, SP-0009.01, 1991

5 Fordham, J.L.A., Bone, D.A., et al., in Proc. ESA Symposium on Photon Detectors for Space Instrumentation, ESA SP-356, p 103, 1992

6 *The Planetary Report*, editor C. Anderson, **13**, number 6, 1993.

7 Bailey, J.V., *Biomedical Results of Apollo*, editor Johnston, R.S., Dietlein, L.F. and Berry, C.A., section II, **2**, NASA, 1975

8 Friebele, E.J. and Gingerich, M.E., *Photobleaching Effects in Optical Fibre Waveguides*, Applied Optics, **20**, p 3448, 1981

9 Musikant, S. and Malloy, W.J., *Environments Hostile to Optical Materials in Low Earth Orbit*, in Optical Surfaces Resistant to Severe Environments, SPIE **1330**, p 119, 1990

10 European Space Agency, The Particle and Ultraviolet Radiation Testing of Space Materials, ESA **PSS-01-706**, Issue 1, 1983

11 Barré, H., Nye, H. and Janin, G., *An Overview of the XMM Observatory System*, ESA Bulletin **100** , 1999

12 Evans, H.D.R., *XMM Radiation Analysis – Dec 14 Launch*, ESA Memo ref: esa/estec/tos-ema/99-112/he, 1999

13 Pellicori, S.F., Russell, E.E. and Watts, L.A., *Radiation Induced Transmission Loss in Optical Materials*, Applied Optics **18**, p 2618, 1979

14 Schott Glass Co, *General Glass Catalogue*, p1066

15 CRC Handbook of Chemistry and Physics, editor D.R. Lide, 72nd edition, CRC Press, Boston, 1991

16 Eisberg, R, and Resnick, R., *Quantum Physics of Atoms, Molecules, Solids, Nuclei and Particles*, John Wiley and Sons, 2nd edition, 1985

17 Martin, A. and Harbison, S.A., *An Introduction to Radiation Protection*, Chapman and Hall Ltd., 3rd edition, 1986

18 Shapiro, J., *Radiation Protection for Scientists and Physicians*, Harvard University Press, 3rd edition, 1986

19 Griscom, D.L., Friebele, E.J., Long, K.J, and Fleming, J.W., Fundamental Defect Centres in Glass: Electron Spin Resonance and Optical Absorption Studies of Irradiated Phosphor Doped Silica Glass and Optical Fibres, J. Applied Physics, **54**, p 3743, 1983

20 Kakuta, T. and Yaki, H., *Irradiation Tests of Electronic Components and Materials*, 3rd International Workshop on Future Electron Devices, RDA/FED, Tokyo, 1986

21 Johnson, R.T., A Survey of Ageing of Electronics with Application to Nuclear Power Plant Instrumentation, IEEE Transactions on Nuclear Science, **30**, p 4538, 1983

22Levy, P.W., Overview of Nuclear Radiation Processes: Phenomenological Features of Radiation Damage in Crystals and Glasses, in Radiation Effects in Optical Materials, Editor P.W. Levy, Proc. SPIE **541**, p 2, 1985

23 Holmes-Siedle, A. and Adams, L., *Handbook of Radiation Effects*, Oxford University Press, p 241, 1993

24 Overeijnder, H., Szymonski, M., Haring, A. and de Vries, A.E., *Energy Distribution of Atoms Sputtered from Alkali Halides by 540 eV Electrons*, Rad. Effects, **36**, p 63, 1978

25 Evans, B.D., Comas, J. and Malmberg, P.R., *Coloration Induced in MgO by MeV $^{20}Ne^{+}$ Bombardment*, Phys. Rev., **B6**, p 2453, 1972

26 Pfeffer, R. L., *Damage center formation in SiO2 thin films by fast electron irradiation*, J. Applied Physics, **57**, p 5176, 1985

27 Arnold, G.W. and Compton, W.D., Phys. Rev., **116**, p 802, 1959

28 Griscom, D.L., Proc. N. J. Kreidl Honorary Symp., J. Non-Cryst. Solids,

29 Williams, R.T., *Nature of Defects and Defect Generation in Optical Crystals*, in Radiation Effects in Optical Materials, Editor P.W. Levy, Proc. SPIE **541**, p 25, 1985.

30 Gorlich, P., Karras, H. and Kotitz, G., *On the Coloration Layer in Deuteron-Irradiated LiF Crystals*, Phys. Stat. Sol. (a), **3**, p 1629, 1963

31 Tsuboi, T., Kato, R. and Nakagawa, M., *Irradiation-Induced VUV Absorption in MgF_2 Crystals*, J. Phys. Soc. Japan, **25**, p 645, 1968

32 Facey, O.E. and Sibley, W.A., *Optical Absorption and Luminescence of Irradiated MgF_2*, Phys. Rev., **186**, p 926, 1969.

33 Blunt, R.F. and Cohen, M.I., *Irradiation-Induced Color Centers in Magnesium Fluoride*, Phys. Rev., **153**, p 1031, 1967.

34 Fuchs, R., *Theory of the Beta Band in Alkali Halide Crystals*, Phys. Rev., **111**, p 387, 1958

35 Griscom, D.L., *Nature of Defects and Defect Generation in Optical Glasses*, in Radiation Effects in Optical Materials, Editor P.W. Levy, Proc. SPIE **541** p 38, 1985

36 Sibley, W.A. and Facey, O.E., *Color Centers in MgF_2*, Phys. Rev., **174**, p 1076, 1968

37 Sibley, W.A. Nelson, C.M. and Crawford, J.H., *Effect of Plastic Deformation on the Colorability of "Pure" and "Doped" KCl Crystals*, Phys. Rev., **139**, A1328, 1965

38 Facey, O.E., Lewis, D.L. and Sibley, W.A., *Electron and Neutron Damage in MgF_2 Crystals*, Phys. Stat. Sol., **32**, p 831, 1969

39 Townsend, P.D., Browning, R., Garlant, D.J., Kelly, J.C., Mahjoobi, A., Michael, A.J. and Saidoh, M., *Sputtering Patterns and Defect Formation in Alkali Halides*, Radiat. Effects **30**, p 55, 1976

40 Zachariasen, W.H., *The Atomic Arrangement in Glass*, J. Am. Chem. Soc., **54**, p 3841, 1932

41 Ehrt, D. and Vogel, W., *Radiation effects in glasses*, Nucl. Inst. and Meth. in Phys., **B65**, p 1, 1992

42 Mitchell, E.W.J. and Paige, E.G.S., *Research Notes: On the Formation of Colour Centres in Quartz*, Proc. Physical Society, **B 67**, Issue 3, p 262, 1954

43 Stapelbroek, M., Griscom, D.L., Friebele, E.J. and Sigel Jr., G.H., J. Non-Cryst. Solids, **32**, p 313, 1979

44 Palma, G.E. and Gagosz, R.M., J. Phys. Chem. Solids, **33**, p 177, 1972

45 Andreav, A.Ts., Borkina, G.Yu., Bubnov, M., Voitsekhovskii, V., Dainov, E.M., Kotov, V.M. and Pryakhina, T.A., *Influence of Gamma Irradiation the Temperature Dependence of the Optical Losses in Quartz Glass Polymer Fibre Waveguides*, Sov. J. Quant. Elec., **11**, p 1095, 1981

46 Friebele, K.J, Schultz, P.C. and Gingerich, M.E., *Compositional Effects on the Radiation Response of Ge-Doped Silica Core Optical Fibre Waveguides*, App. Optics, **19**, p 2910, 1980

47 Bellis, J.G., *The Transmission Efficiency of the Fibre Optic Taper Used in the MIC Detector*, XMM Technical Document, p 1, 1992

48 Blue, M.D. and Roberts, D.W., *Effects of Space Exposure on Optical Filters*, App. Optics, **31**, p 5299, 1992

49 Nicoletta, C.A. and Eubanks, A.G., Effect of Simulated Space Radiation on Selected Optical Materials, App. Optics, **11**, p 1365, 1972

50 Grillot, P.N. and Rosenberg, W.J., *Proton Radiation Damage in Optical Filter Glass* App. Optics, **28**, p 4473, 1989

51 Daly, E.J., *XMM Radiation Environment*, XMM OM Expt. Engineering Mtg., ESTEC, 1991

52 Cole Smith, L., Becher, J., Fowler, W.B. and Flemming, K., *Proton Induced Noise in Digicons*, NASA Technical Paper **1852**, 1981

53 Danner, R., Charged Particle Induced Background Expected on XMM, ESTEC Working Paper No. **1674**, 1992

54 Draft Copy of Section 11, *The Radiation Design Handbook, Issue 1*, ESA **PSS-01-609**, 1987

55 Marker, A.J., Hayden, J.S. and Speit, B., *Radiation Resistant Optical Glasses*, in Reflective and Refractive Optical Materials for Earth and Space Applications, Editor(s): Riedl, M.J.; Hale, R.R., and Parsonage, T.B., SPIE **1485**, p 160, 1991

56 Malitson, I.H., Dodge, M.J. and Gonshery, M., *Radiation Induced Instability in Refractive Properties of Some Optical Glasses*, Opt. Soc. America, Ann. Meet., p 1583, 1965

57 Becher, J., Kernell, R.L., Reft, C.S. and Smith, L.C., *Radiation Effects Studies for the High Resolution Spectrograph*, NASA Technical Report **PTR-80-2**, 1980

58 DataFit v8.0.32, Copyright © 1995-2002 Oakdale Engineering, Oakdale, USA, (http://www.curvefitting.com/)

59 Bowers, R. and Deeming, T, *Atomic Properties of Matter from Astrophysics I: Stars*, Jones and Bartlett Publishers, Inc. 1984